SEISMOTECTONICS AND SEISMIC HAZARD IN AREAS OF DIFFERING CRUSTAL DEFORMATION RATES

IAN G MAIN

B.Sc. (St Andrews)

M.Sc. (Durham)

DOCTOR OF PHILOSOPHY

UNIVERSITY OF EDINBURGH

1985

I, Ian Main, declare that this thesis was entirely my own composition and that, except where expressly stated to the contrary, the work described herein was completely carried out and written by myself.

.....

ABSTRACT

Expressions for crustal deformation as evidenced by seismic moment release or slip rates are derived from a Weibull distribution and Gumbel's third distribution of extreme values in earthquake magnitudes. These are compared with the tectonically observed values, as are the maximum magnitudes obtained by the statistical studies with those inferred from maximum fault areas. Both types of distribution exhibit a good match between the seismic and tectonic crustal deformation in the following areas: The tectonically complex Eastern Mediterranean; Southern California; The New Madrid Seismic zone. All of these regions have apparent bimodal distributions of earthquake magnitude, with a particularly good match in the New Madrid zone between the tectonic slip rates and fault areas and the seismicity distribution on two characteristic families of faults. By contrast the mainland UK has a seismicity which can only account for a small fraction of the known tectonic movement, exactly as one might expect for a regime of slow elastic rebound following glacial unloading.

A new frequency-magnitude distribution is derived from Information theory. Its number density is $n(m)=c.\exp\langle-\lambda_1 m-\lambda_2 M_o(m)\rangle$, where $\lambda_1=b\ln(10)$ and b is the Gutenberg-Richter 'b-value'. $M_o(m)$ is the moment-magnitude relation. By analogy with statistical mechanics b can be related to a geometric similarity dimension D by $b\approx 2D$, thereby explaining the observation $0<b<1.5$ as corresponding to the release of strain energy in a finite volume, $D<3$. This distribution fits the Mediterranean data better than the Weibull form, and predicts a repeat of the 1857 earthquake in Southern California ($M_w>7.9$) 156 years after this date on average, with a range considering errors of 87-281 years. This compares well with some results from trenching across the fault (once every 163 years, but from 55-275 years). The method could be used

in areas where the slip rate is known but direct trenching is impossible and to define a time constant to indicate when a seismic gap is likely to become reactivated.

Source parameters are derived for Greek earthquakes from teleseismic recordings of surface waves (M_s>5.5) and local P waves (1.8<M_L<4.5) in order to further evaluate the seismic hazard and to test some of the assumptions of the Information theory distribution. Typical stress drops of the smaller events (1-10 bars) scale vary well with the larger events (7-12 bars), representing dimensional self-similarity of the seismic process in Central Greece over an energy ratio of 1:10,000 (!). A calibration procedure for the seismic moments of the larger events shows that ignoring the effect of orientation of the seismic source only increases the standard deviation of these moments from 25% to 40%.

A detailed study of Aegean seismotectonics is undertaken. The moment-magnitude relation $\log(M_o) = A+BM_s$, with A = 10.97(.63), B = 1.21(.11) is found from surface wave studies (A in SI units and uncertainties are in brackets). By contrast the available body wave moments are shown to be too low by a factor of two or three in this area. The tectonic and seismic slip rates are compared for (a) the spreading Aegean basin and (b) the sinking subduction slab of the Hellenic arc. The Aegean activity can be explained by mostly seismic gravitational collapse, whilst the seismic activity of the sinking slab is only a small fraction of that expected from its known slip rate. The latter activity may be more due to the internal buckling of the slab due to thermal expansion or mantle phase changes than to stick-slip sliding at its boundaries. A characteristic peak in the magnitude distribution at $M_s \approx 7$ can be related to a block-like earth structure of a characteristic size similar to the known seismogenic depth in the

spreading Aegean crust. This macroscopic quantum effect is similar to the behaviour observed in the New Madrid zone, and may be a fairly common feature of seismogenic zones.

The reasonable agreement throughout between the tectonic and seismogenic slip rates show that the methods used have an important role to play in investigating other second-order effects of plate tectonics, as well as being testament to a surprising degree of stationarity of the seismic process in some areas. However, practical results also emerge in the form of quantititive estimates of seismic hazard in areas of greatly differing crustal deformation rates.

ACKNOWLEDGEMENTS

I should like to express my appreciation to Dr Chris Browitt of the British Geological Survey and Prof Ken Creer of Edinburgh University for their support towards the realisation of this work. I am also most particularly grateful to Dr Paul Burton, my supervisor at BGS, for his strong support in all my research efforts in the last few years, and for all his useful advice, discussions and comments on the present text.

No one really works completely on their own in research any more, and I am particularly grateful to the following people for their specific help with various parts of this project: Graham Neilson, for specific contributions mentioned in the text, and for always having an open door; Bob McGonigle and Charlie Fyfe, for assistance with various aspects of the computational side of the work; Colin MacBeth, for passing on his knowledge and a computer program on surface waves; Maureen Ritchie, for teaching me how to drive the routine analysis of the VOLNET data and helping with some aspects of the Greek literature search. General discussions with all of the above mentioned people, as well as with my fellow students - Andrew McDonald, Graham Roberts, Sheila Peacock and Alan Logan - and most other members of the Global Seismology Research Group, proved most helpful in many day-to-day problems.

I am also grateful for generous assistance from abroad: to Dr John Anderson, of the Scripps Institute, San Diego for information on the tectonic model and for some comments on aspects of Chapter 3; and to Dr Arch Johnstone, of the Tennessee Earthquake Information Centre, for providing the data on the New Madrid seismic zone. Prof Antoni Correig (Barcelona), Prof Pietro Cosentino (Palermo), Dr Frank Horvath (Budapest) and Dr Xavier Le Pichon (Paris) generously gave permission to reproduce some of their figures in the text.

Pat Condon, Alan Logan, Bob McGonigle, Colin MacBeth, and Graham Neilson all helped at a late stage of proofing by providing a 'second eye'. Finally, I should like to thank Jan Fraser for typing the thesis, and the Natural Environment Research Council for providing financial support for a project which I have very much enjoyed carrying out.

CONTENTS

"Science is a very human form of knowledge. We are always at the brink of the known, we always feel forward for what is to be hoped. Every judgement in science stands on the egde of error, and is personal. Science is a tribute to what we can know although we are fallible ..... We have to touch people".

The Ascent of Man

Jacob Bronowski

INTRODUCTION

Seismotectonics and seismic hazard

As its name implies 'seismotectonics' refers to the study of the relationship between tectonic activity over geological time scales and earthquake (seismic) activity in more recent epochs (historical or instrumental). On the other hand the 'seismic hazard' is a numerical estimate of the probability of occurrence of earthquakes of varying magnitudes and resultant ground motions which are caused by this underlying process. Seismology in the past has been a useful indicator of the boundaries of the earth's plates - such as the 'Ring of Fire' circling the Pacific, and in delineating the Benioff zones where old ocean floor is subducted for recycling in the earth's convective engine - the primary driving force behind all plate tectonic motion. In this thesis the relationship between tectonic activity and resulting earthquakes will be investigated in more detail, and in particular for many regions of the world where plate tectonics does not fully explain the activity. The intention of this work is not to challenge the basic concept, but rather to investigate possible second order effects such as the reactivation of old lines of weakness within otherwise fairly rigid plates, or the effects of irregular geometry at the plate boundaries.

One of the prime methods of looking at this problem is to consider the slip rate over geological time. The slip rate in areas at plate boundaries is usually well known from magnetic anomalies on the ocean floor, and several faults along plate boundaries or within plates have now also been investigated to give a measurement of this important geological parameter. In Chapter 1 various methods of estimating a seismogenic slip rate from the

current earthquake frequency magnitude distribution from recent earthquake catalogues are reviewed, and in Chapter 2 two of these methods are used to compare slip rates from long-term geological processes with the current earthquake activity represented by the catalogues.

In Chapter 3 a completely new approach to the seismic hazard problem of combining the implications of short-term earthquake catalogues with long-term geological slip rates is developed using Shannon's (1948) Information theory. The slip rate here is used as a direct constraint on the earthquake size distribution in order to make this distribution consistent with both the long-term tectonic activity and the short-term seismic effects. This is an improvement on earlier methods which were indirect. This allows a great improvement in any subsequent estimation of the 'seismic hazard', here quantified as the probability of occurrence of different magnitudes in the potential source zone. 'Seismic risk' is a much more specific measure of the danger posed by earthquakes to a particular building or facility which may include a valuation of the structure's worth. In the whole of this thesis one of the most important products is the quantification of seismic hazard by the average repeat time of earthquakes of a given magnitude, with the advantage over some previous studies that these estimates are also consistent with the long-term crustal deformation expressed by the slip rate and are specified within well defined error bounds.

Another application of the earthquake distribution developed in Chapter 3 is in evaluating 'long-term earthquake recurrence intervals', by using the average repeat time of the largest magnitudes. By applying the slip rate method to compare this time constant with the time elapsed since the last major event, the

areas of the earth currently most at risk from catastrophic earthquakes can be identified, and limited resources can be concentrated on the areas most likely to bear fruit in the ongoing search for a reliable method of short term earthquake prediction. The most directly applicable results of the methods to be described, however, are in terms of their influence on hard decisions on earthquake zoning, building design codes, earthquake engineering and insurance levels.

In the final two chapters the Aegean area is investigated in some detail as a case study. In Chapter 4 source parameters such as seismic moment, magnitude, slip, fault area, stress drop and strain drop are derived for several earthquakes and these are used to test some of the assumptions of the distribution developed in Chapter 3. In the final chapter the problem of the tectonic stretching of the Aegean sea is investigated in detail, an area whose activity has yet to be fully explained by plate tectonics or any other current theory.

Glossary of notation used in this thesis

The following are the main parameters of the thesis. There should be no confusion between fault area and the A parameter of the moment-magnitude relation in any given context. Another aspect of the nomenclature of this thesis is that 'seismic moment' is often abbreviated to 'moment'. This should not cause confusion with the ordinary concept of a moment in the sense of a couple applied to a swinging door, for example, because there are no references to this use of the word in the thesis. Other parameters will be defined as they crop up in the text, but this list should be consulted if no explanation is given. On some diagrams the computer graphics produced no subscripts, e.g. mb for m_b, but it should be obvious where these would be appropriate.

N.B. References to equations are sometimes abbreviated by omitting the qualifer 'equation'. Thus, for example (3.2) refers to equation (3.2).

m_b : body wave magnitude

M_s : surface wave magnitude

M_L : Richter's local magnitude

M_w : Kanamori's seismic moment magnitude

m : symbol used in theoretical treatment for M_w or an unspecified magnitude

M_o : seismic moment

μ : rigidity modulus

ρ : density

A,V : fault area, volume containing deformation

a or r,L or ℓ,W or w: fault radius, length, width

$s,\dot{s}$: average fault slip, slip rate

$\Delta\sigma$: stress drop

Δe : strain drop

$\dot{e}$: strain rate

A,B: parameters of the decadic moment-magnitude relation

α,β: " exponential "

(also P, S wave velocities respectively)

ω : maximum limiting magnitude

$M_{o\omega}$: " moment

N : cumulative frequency (usually normalised to annual unit times)

n : number density "

F : discrete frequency "

P : cumulative probability "

p : probability density "

b,b' : decadic, exponential Gutenberg-Richter b-value

(ω,u,λ) : parameters of the Weibull/Gumbel's third distribution

ε : covariance error matrix for the Weibull distribution

(λ_1,λ_2) : parameters of the new distribution developed in Chapter 3 (N.B. $\lambda_1 = b'$)

m_c : lower limiting magnitude, or completeness threshold

m_T : magnitude associated with average repeat time T

N_T : total no. of events per unit time in a complete earthquake catalogue

ν : power of fault length distribution ℓ^{ν}

D : fractal dimension

ϕ_F, δ, λ : fault plane solution (azimuth, dip and rake)

$\hat{f}$, $\hat{n}$: unit vectors parallel and perpendicular to the slip direction

Ω : spectral density

Ω_o : long period spectral density

f_c : corner frequency

$\Psi_{\phi\theta}$: radiation pattern

f, ω, T : wave frequency, angular frequency and period

h : focal depth

γ, γ' : attenuation parameter per km or per degree

R : source station distance

Units of measurement

In much of the geophysical literature c.g.s. units are used as units of measurement. In order to give the reader a comparison with the SI units used throughout this thesis (unless otherwise stated) a conversion summary is given below:

		SI	c.g.s.
Seismic Moment	M_o	1Nm	10^7 dyne cm
Stress drop	$\Delta\sigma$	$1 Nm^{-2}$	10 dynes cm^{-2}
	(1 bar = 10^5 Nm^{-2} = 10^6 MPa)		
Rigidity modulus	μ	$1 Nm^{-2}$	10 dynes cm^{-2}
Energy	E	1J	10^7 ergs
Density	ρ	1kg m^{-3}	10^{-3} gcm^{-3}
Moment-magnitude relation		A = 1	A = 8

(i.e. A(SI) = A(cgs) - 7)

CHAPTER 1

Existing theory and practice in earthquake recurrence statistics

1.1 Introduction

Earthquake recurrence statistics are important for two reasons. The first is that they quantify the seismic hazard due to a broad range of event sizes. It may be, for example, that the tectonic stress which causes earthquakes is released primarily in several small events, or perhaps (actually much more commonly) in rarer large events. Earthquake recurrence statistics quantify effects such as this through the frequency magnitude distribution, which can then be combined with knowledge of attenuation of seismic energy and local site effects to produce an estimate of the hazard (as annual probabilities of occurrence of acceleration, velocity, displacement, or intensity for example). Thus practical decisions can be made on building design criteria to mitigate the inevitable recurrence of these events.

The second reason for examining recurrence statistics is in evaluating long term recurrence intervals of specific large events which are known to have occurred previously. This can be done directly by combining the average repeat time of a characteristic earthquake, which can be found by geological and geomorphological investigation of surface trends, or less accurately by extrapolation of usually short term frequency magnitude statistics, with an estimate of the characteristic magnitude and the date of the last occurrence, using the concept of a 'seismic gap'. For example the southern section of the San Andreas fault in California last ruptured in a great earthquake in 1857. No large events have

occurred along this break since then, leaving a 'gap' in the linear trend of the seismicity along this fault near Los Angeles. The average repeat time found from trenching across the fault in some peaty sediments is about 163 years, which means that for a normal distribution of repeat times, the cumulative probability of a large event having occurred will reach 50% by the year 2020.

This chapter will summarise the different theoretical forms used for the frequency magnitude distribution, and show how geological information from slip rates on faults can be used to tighten up the extrapolation of recurrence statistics in areas where there is no direct evidence from trenching studies.

1.2 Curvature in the log-linear seismicity distribution and an associated limiting maximum magnitude

The most commonly applied description of seismicity in terms of the relative frequency of occurrence of different sizes of earthquake is the Gutenberg-Richter law (e.g. Richter, 1958; Esteva, 1968)

$$\log N (x \geq m) = a - bm. \qquad (1.1)$$

N is the number of times a magnitude m.is equalled or exceeded in a unit time interval and b is a constant which usually varies in the range of $0.5 < b < 1.5$. Some examples of a line fit to cumulative frequency data N(m) are given in fig 1.1 for different seismic zones, showing up variation in the b-value by the different slopes on the log-linear graph.

Although this law is widely used in hazard estimation it does have some serious drawbacks. For example if the seismic energy E_s (in Joules) is related to magnitude by

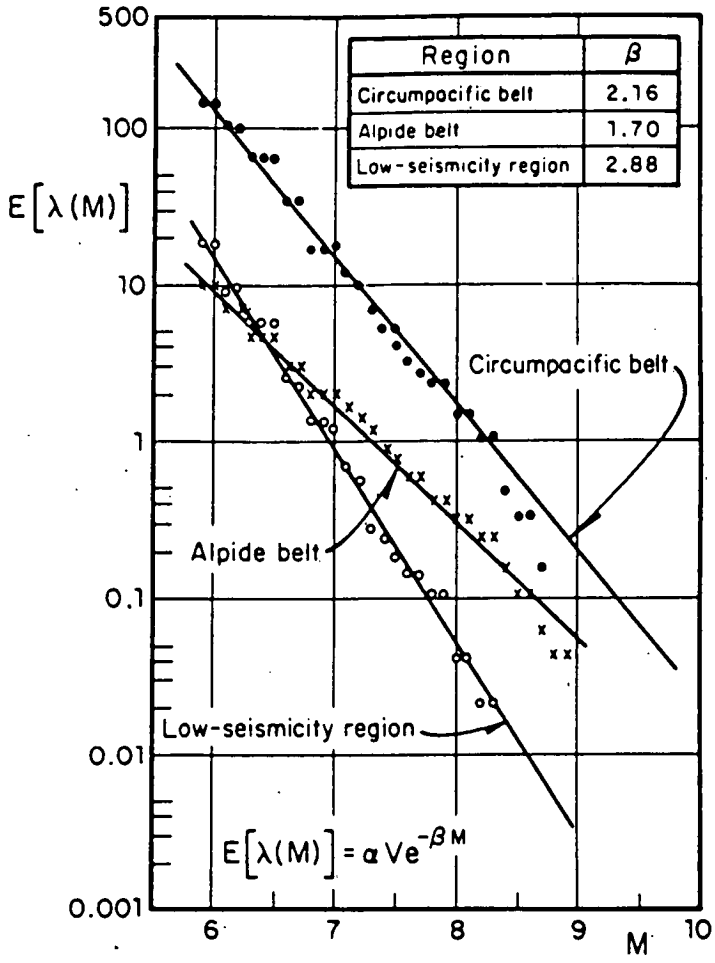

Figure 1.1 An example of a log-linear frequency magnitude plot due to Esteva (1968). $E[\lambda(M)]$ corresponds to N of equation (1.1) and $\beta = b\ln 10$ here. The lines drawn through the data represent a least squares fit assuming the log-linear Gutenberg-Richter law. The b-values corresponding to β are 0.94, 0.74 and 1.25 respectively, showing the kind of range this parameter takes in different regions. The curvature above M=8 could be due to instrumental saturation.

$$E_s(m) = 10^{4.8+1.5m} , \qquad (1.2)$$

Richter (1958) then the energy released in the magnitude range (m,∞) is an integral over this range

$$E_s = \int_m^\infty E_s(m)\, n(m)\, dm , \qquad (1.3)$$

where $n(m) = -dN/dm$ is the number density function of (1.1). From (1.1) and (1.2) it can be shown that this integral is infinite for $b < 1.5$ (Knopoff & Kagan, 1977 and section 1.7), which means that there must be a cut-off magnitude ω before $m \to \infty$ to avoid this absurdity. This limiting maximum magnitude is a reflection of the finite breaking strength of the earth's crust, and the finite extent of the source zone.

The limiting magnitude has a further consequence. Because the interval (ω, ∞) now has no events $(N(\omega) = 0)$, the cumulative frequency just below ω is also significantly reduced compared to (1.1) for the same density distribution, giving rise to an associated curvature in the log-linear plot at high magnitudes (Båth, 1981a). An example of this curvature is given in fig 1.2 from Cosentino and Luzio (1976). (The curvature at high magnitudes in fig 1.1 may be due to saturation in the magnitude scale discussed in the following section). The investigation of the precise form of the relationship between the limiting magnitude and this curvature, using added information from seismotectonic studies, is one of the prime objectives of this thesis. This is important because the tectonic activity which generates earthquakes - and the resulting seismic hazard - is usually dominated by the very largest events, which occur in the range most sensitive to the

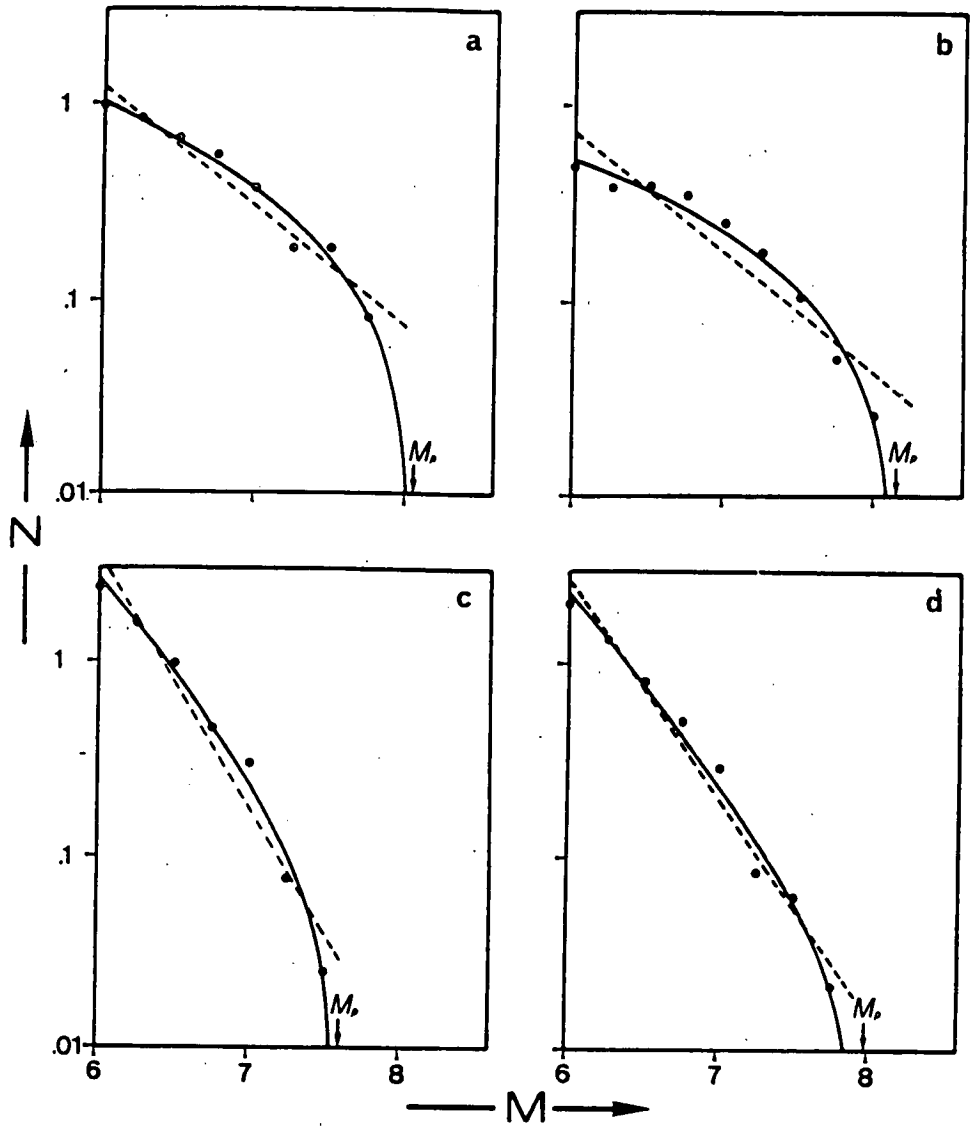

Figure 1.2 Examples of frequency magnitude distributions which are not linear on the standard log-linear plot, after Cosentino and Luzio (1976). The regions analysed are (a) New Zealand, (b) Burma arc, (c) Mid-Atlantic Ridge and (d) The Indian Ocean. The curvature shown here cannot be due to the instrumental saturation discussed in section 1.2, because this predominantly affects magnitudes M_s above 8.0. (For a further discussion of the line fit used, see section 1.3). M_p in their notation corresponds to ω used throughout this thesis for a maximum magnitude. It is obvious that the dashed lines representing fits to equation (1.1) are an inadequate description of the seismicity.

form of this curvature.

1.3 Saturation of the magnitude scale and a definition of the seismic moment magnitude

All instrumental magnitude scales suffer from saturation at high magnitudes. As earthquakes increase in size more energy shifts towards the D.C. (or infinite period) end of the ground motion - the direct movement on the fault itself (Howell, 1981). However, all instruments for recording earthquakes have response characteristics which sample only a limited range of the seismic energy spectrum about their natural frequency f_o, or equivalent period T_o. For the surface wave magnitude scale M_s this natural period is about 20s and for the body wave scale m_b it is about 1s. These magnitude scales cannot pick up increases in energy release in frequency ranges outside the natural bandwidth of the seismographs. So as larger and larger events with longer and longer fault lengths and associated natural periods are picked up a point is reached where an event, say twice as large in terms of energy as a previous one, produces no detected increase in the measured magnitude. For M_s this saturation occurs on average at approximately 8.0, which led Kanamori (1977, 1978) to propose an unsaturated magnitude scale called the "seismic moment magnitude", M_w, which extrapolates M_s beyond this onset.

The seismic moment M_o is perhaps the best currently available measure of the size of an event. It is defined by the equation

$$M_o = \mu A s = (\mu/\bar{\sigma})\Delta W \ , \qquad (1.4)$$

where μ is the rigidity modulus, A is the fault area, s is the average slip on the fault, $\bar{\sigma}$ is the average stress level during the earthquake, and ΔW is the change in strain energy. Thus the seismic moment can be easily related to various source parameters. The seismic moment magnitude M_w is then defined by

$$M_w = (\log_{10} M_o - A)/B \quad ,$$

$$\text{or } M_o = 10^{A+BM_w} \quad , \qquad (1.5)$$

$$\text{or } M_o = e^{\alpha+\beta M_w} \quad ,$$

where B = 3/2 follows from Kanamori and Anderson's (1975) theoretical considerations on fault geometry as well as from empirical fits to available data. The most recent work on this conversion from seismic moment, M_o, to seismic moment magnitude, M_w, indicates the following values for A and related stress drops $\Delta\sigma$:

see equation 1.2.

Interplate events	A = 9.1	$\Delta\sigma$ = 30 Bars
Intraplate events	A = 8.7	$\Delta\sigma$ = 76 Bars
Average value	A = 8.85	$\Delta\sigma$ = 52 Bars
California	A = 8.83	$\Delta\sigma$ = 50 Bars

from Singh and Havskov (1980), where A is appropriate for M_o in SI units. The seismic moment of an individual event can be estimated from geological field evidence, the area of the aftershock distribution or from the seismological record of an event - particularly the longer periods. Methods of determining

the seismic moment from various phases of a seismogram will be described in Chapter 4.

1.4 Examples of different empirical and theoretical frequency-magnitude distributions

The Gutenberg-Richter relation (1.1) has already been discussed. In many cases this is found to be an adequate description of the seismicity of a region, although we should be wary of linear extrapolation beyond the observed magnitude range because of possible curvature introduced by a limiting magnitude ω. In particular Chinnery and North (1975) found that, when global seismicity statistics were corrected for the effects of instrumental saturation of the magnitude scale, equation (1.1) held right up to the largest events. Even a small extrapolation beyond the observed magnitude range implies the occurrence of an event of $M_o = 10^{24}$ Nm (about M_w 9.9!) on average once every 50 years or so. This really massive scale of seismic energy release would require some rethinking of plate tectonic models and could have the consequence of a considerable excitation of the Chandler wobble.

On a more local scale fig 1.2 shows that (1.1) is often an inadequate description of the seismicity. However its density distribution may be retained and restricted to a range bounded by a maximum magnitude ω. The density distribution becomes

$$\begin{aligned} n(m) &= p\, e^{-b'm} && m \leq \omega \\ &= 0 && m > \omega \ , \end{aligned} \qquad (1.6)$$

where $b' = b \ln 10$, $p = b' 10^a$. The cumulative frequency $N(x>m)$ is then equal to the integral of $n(m)$ over the magnitude

range (m,ω), which is

$$N(x>m) = \frac{e^{-b'm} - e^{-b'\omega}}{e^{-b'u} - e^{-b'\omega}} \quad . \tag{1.7}$$

This relation is called the truncated Gutenberg-Richter law, and was used in the fit to the data of fig 1.2.

A theoretical generalisation of this density distribution is due to Caputo (1976, 1977). Starting with a basic distribution of fault lengths (ℓ) and stress drops ($\Delta\sigma$) of

$$n(\ell)\, d\ell \propto \ell^{-\nu}\, d\ell \tag{1.8}$$
$$n(\Delta\sigma)\, d\Delta\sigma \propto \Delta\sigma^{\alpha-1}\, d\Delta\sigma \quad ,$$

he derived a distribution

$$n(m) = p\, e^{-b'm} - q \quad , \tag{1.9}$$

where $q = p\, e^{-b'\omega}$, and p,q,b' can be related to constants specifying the distribution of fault lengths and stress drops, and to maximum and minimum values of these parameters. The form of this density distribution is that it is log-linear up to a magnitude m_2 say, and then curves asymptotically to zero occurrence at $m = \omega$. As $\omega \to \infty$, $q \to 0$ and (1.9) reduces to (1.6).

An empirical distribution which also has this asymptotic form is the Weibull (1951) distribution,

$$N(x>m) = \left\{(\omega-m)/(\omega-u)\right\}^{1/\lambda} \quad . \tag{1.10}$$

Note that in both (1.7) and (1.10) $N(u) = 1$, so u is the

characteristic earthquake for unit time (if N is normalised to unit time intervals). The difference between this form and that of (1.9) is that the distribution (1.10) is curved over the entire magnitude range below ω. The parameter λ is a measure of this curvature. Jenkinson (1955) showed that $0 < \lambda < 1$ and that as $\lambda \to 0$ the log-linear curve straightens to the form of (1.1). Thus high λ values correspond to a greater degree of curvature. The behaviour of this distribution is further analysed in Chapter 2.

A new frequency magnitude relation is proposed in Chapter 3 on the basis of using Information theory to directly incorporate additional knowledge of the seismic moment release rate $\dot{M}_o$ into the seismicity distribution. The form of its density distribution is

$$n(m) = p\, e^{-b'm}\, e^{-\lambda_2 M_o(m)} , \qquad (1.11)$$

where $M_o(m)$ is given by the seismic moment-magnitude relation (1.5). This model comes in between the behaviour of (1.6) and (1.9), curving down less drastically just below ω than Caputo's model.

The shapes of the distributions outlined in this section are given in fig 1.3, by way of a summary and reference for future discussion.

1.5 Extreme value distributions

Two of the main problems in the evaluation of seismic hazard from a catalogue of earthquakes are (a) the incompleteness of reporting of events and (b) the occurrence of non-independent aftershock sequences. The former could be due to the threshold of detectable

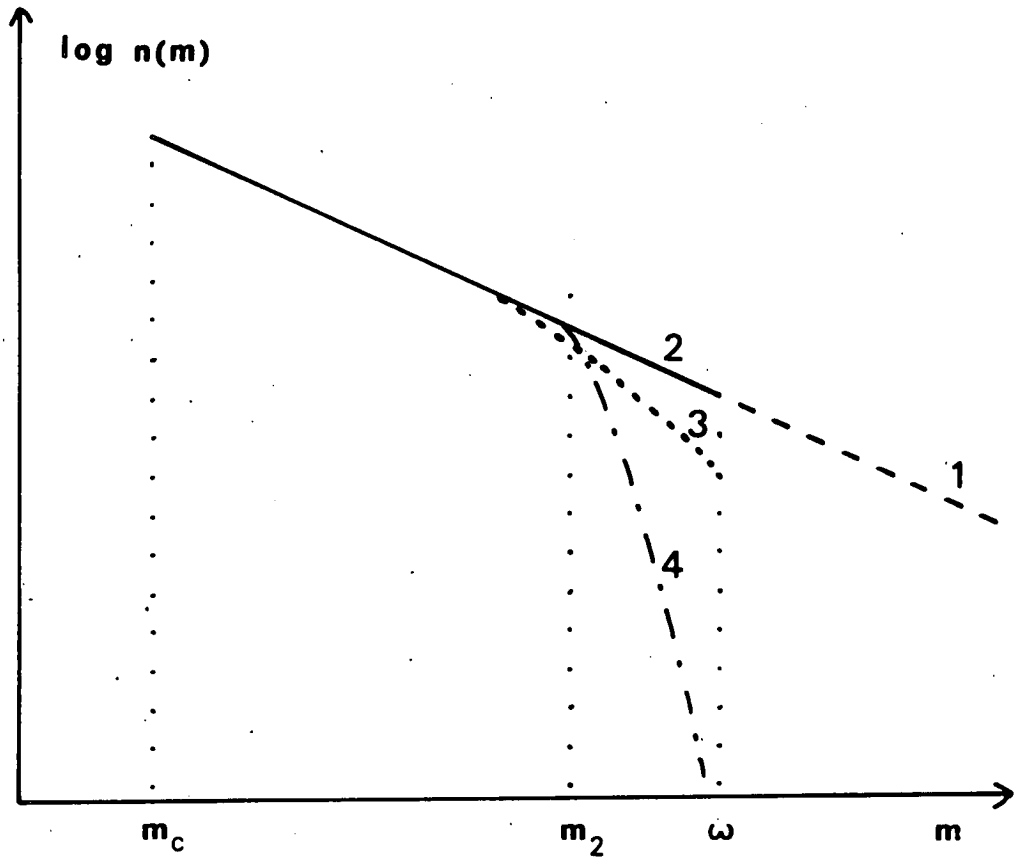

Figure 1.3 Comparison between seismicity models. The models shown in increasing order of complexity are:- 1 The Gutenberg-Richter law; 2 A truncated form of 1, due to Cosentino and Luzio (1976); 3 The Information theory model derived in Chapter 3; and 4 Caputo's model (1976). The Weibull distribution is similar to 4 except that it is also curved below m_2. 3 tends simply to 2 if the parameter λ_2 in equation (1.11) is zero. Caputo's version differs from 3 in having (a) a sudden departure from log-linearity at m_2 rather than more gradually, and (b) an asymptotic limit ω at $n(\omega) = 0$ rather than at finite n.

excitation of modern instruments or to a sparsely populated area around the source in historical times and the latter complicates the Poissonian assumption made below. One method of lessening the impact of both of these problems is to use only the extreme values - that is only the largest event in any unit time interval - as a basis for evaluating the hazard. We can be much more confident that this subset will be complete, and since it samples the tail of the initial frequency distribution the method should enhance the effects of a limiting magnitude and any associated curvature. The procedure also effectively eliminates the smaller aftershocks. The main drawback of the method is that much of the information available to us from smaller events is simply thrown away.

Consider a Poisson process of independent events

$$P(i) = \frac{N^i e^{-N}}{i!} , \qquad (1.12)$$

where P(i) is the probability that i large earthquakes occur during a given unit time, and N is the mean number of large earthquakes per unit time. For our purposes N is given simply by the cumulative frequency distribution normalised to unit time. For the extreme value process we wish i = 0, so that no events greater than (say) m_j occur in each unit time interval j containing a total of N_j events. m_j is the largest event or the 'extreme value' in the j^{th} sample of unit time.

Thus, for i = 0, $N^i = 1$ and $i! = 1$, so

$$P(x \leq m) = \exp\{-N(x > m)\} . \qquad (1.13)$$

A type I distribution of extreme values has an initial distribution N given by (1.1), and a type III distribution has N given by the Weibull distribution (1.10) so that, for the latter case

$$P(x \leq m) = \exp\left[-\{(\omega-m)/(\omega-u)\}^{1/\lambda}\right] \quad . \qquad (1.14)$$

This form is analysed in greater detail in Chapter 2. A detailed description of the theory is given by Jenkinson (1955) and Gumbel (1958). The form (1.14) has been used in order to predict global maximum magnitudes by Yegulalp and Kuo (1974) and by Makropoulos (1978) and Burton (1979) in order to quantitatively evaluate seismic hazard.

1.6 Quantitative assessment of earthquake hazard

The assessment of earthquake hazard involves

(a) The probability of a large earthquake occurring in a potential source zone.

(b) Reduction in ground shaking with distance by geometric spreading and attenuation effects.

(c) Local site conditions.

The first of these can be quantified through the observed frequency distribution of earthquake magnitudes in a potential source zone, using the methods outlined in the previous two sections. Most results of studies such as this are produced in the form of a mathematical return period defined by

$$T(m) = 1/N(m) \quad , \qquad (1.15)$$

for the annual cumulative frequency distribution N or

$$T(m) = \frac{1}{1 - P(m)} , \qquad (1.16)$$

where P is the annual non-exceedence probability given by (1.14). This term 'return period' can be misleading, since the event is not expected to recur at regular intervals. Because of this it is known there is a significant random component to any series of events (indeed this is the justification for assuming a Poisson process in section 1.4) and the term 'average repeat time' is preferred for the remainder of this thesis. However, since in many cases the instrumental catalogue of events is of much shorter length in time (≈80 years) than the average repeat time of the largest events (≈160 years in Southern California), it is very important to quantify errors of extrapolation beyond this range. This uncertainty may be reduced on extension of the catalogue to historical times (Ambraseys, 1971), or by geological slip rates incorporated by the methods described in the next section and in Chapters 2 and 3.

The second process (b) reduces the effect of ground shaking with distance, although it is known that longer periods attenuate less quickly than shorter ones, so that tall buildings may be at risk quite far from the source (Nuttli, 1979). It is obvious that more work needs to be done on attenuation effects to quantify effects like these, particularly with strong motion instruments placed near likely source areas.

Finally, and in many cases most importantly, the effects of local site conditions should be considered. Most of those who have browsed the literature have been struck by photographs showing wildly differing levels of damage within a small area. Buildings

which are almost perfectly intact can stand beside areas of almost total devastation (e.g. see Walker, 1982 p8). One of the earlier systematic investigations into the effects of a large earthquake (Lawson et al, 1908) showed up a very good correlation between site geology and intensity of damage for the 1906 earthquake in San Franscisco. Most of the extensive damage was confined to areas built on unconsolidated pleistocene sands and alluvium, with buildings on the intrusive basalts or the Franciscan series of sandstones and cherts suffering less markedly. Other site conditions which complicate matters even further are due to the possible amplification effects of topography and the local geological profile.

To account for the first two conditions Algermissen and Perkins (1976) (see fig 1.4) used local relations for the relationship between magnitude, distance and ground shaking parameters such as ground acceleration and velocity - combined with annual probabilities of earthquake occurrence - in order to produce a contour map of the earthquake hazard. The approach uses the extreme value theory of Gumbel (1958) to evaluate contours for the maximum, or peak accelerations and velocities. Because of the smaller degree of attenuation in the Central and Eastern U.S., the potential seismic hazard is similar in some areas of Tennessee to that only a few hundred km from the San Andreas fault, despite the much lower frequency of occurrence of large events in the east! This surprising conclusion is partly due to the greater competence of mid-plate crust compared to that near a deforming plate boundary. A greater quantitative understanding of more local site effects resulting from strong motion studies near large events should improve maps such as fig 1.4 on a local scale as more data

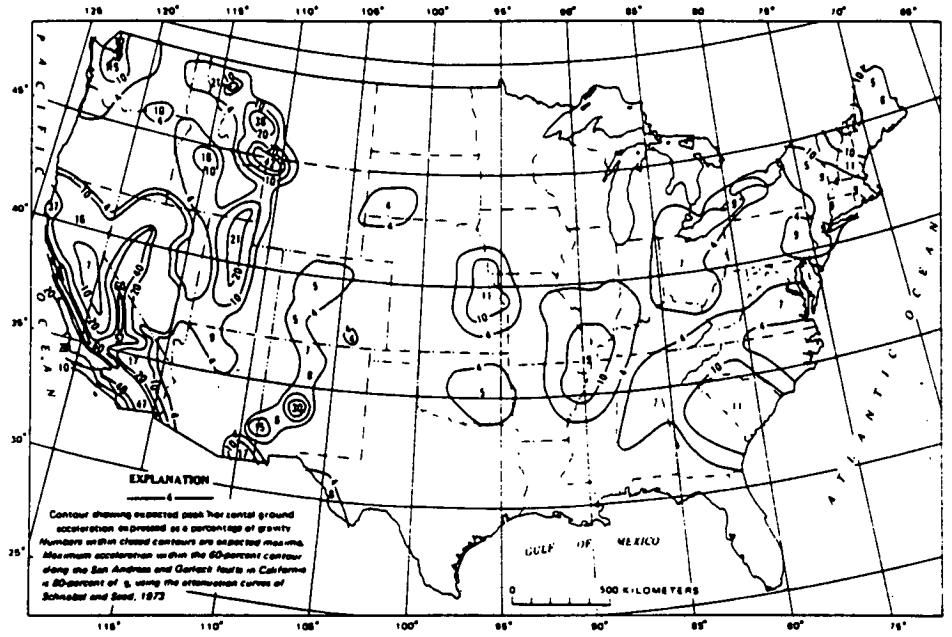

a. Map showing maximum levels of peak horizontal ground acceleration at rock sites in the United States in a 50-year period, (Algermissen and Perkins, 1976). There is a 90% chance that the contoured values of acceleration will not be exceeded within a 50-year period. The map reflects the relative frequency of occurrence of earthquakes in the eastern and western United States.

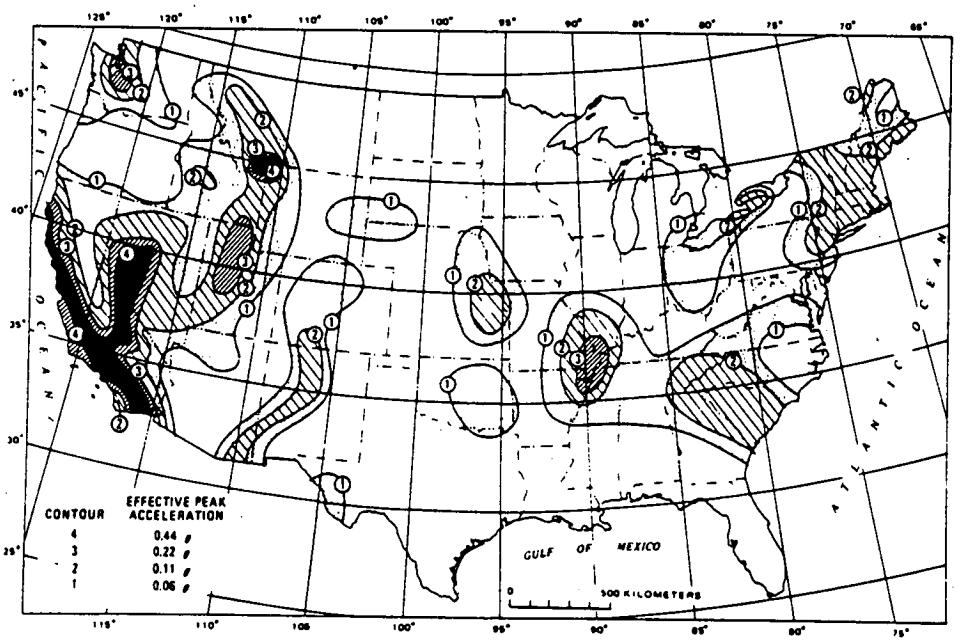

b. Preliminary seismic zones proposed by the Applied Technology Council (1978). Contours connect areas having equal values of effective peak acceleration. Site-specific studies are recommended for zone 4.

Figure 1.4 Two examples of contoured hazard maps taken from Hays (1984).

become available. The importance of maps such as these is in forming the basis for decisions made on building design codes in order to mitigate against the hazard posed by earthquakes to life and property.

The scope of the present study is confined to the evaluation of the probabilities of occurrence of earthquakes of varying size in likely source zones, although it is hoped that this section has emphasised the importance of other geophysical effects, together with some of the practical aspects of the eventual use to which studies such as this one may be put.

1.7 The incorporation of crustal deformation into earthquake recurrence statistics

In seeking to extrapolate beyond the era of instrumentation (tens of years) many studies use the subjective approach of an Intensity scale of damage (say the Modified Mercalli Scale) to extend the earthquake catalogue to hundreds and even thousands of years (Ambraseys, 1971). However fig 1.5 from Main (1980) shows that any empirical attempt to correlate intensity scales with the concept of a magnitude is subject to very large scatter. Intensity of damage to buildings is simply not the same thing as ground motion measured on a seismograph. Fortunately, in many cases there is a third source of information on the right time scale (thousands to tens of thousands of years). This is the geological and geophysical observation of crustal deformation rates (slip or strain), which will henceforth be incorporated into the parameter

$$\dot{M}_o = \mu A \dot{s}$$

$$\dot{M}_o = 2.5\ \mu V \dot{e} \quad . \tag{1.17}$$

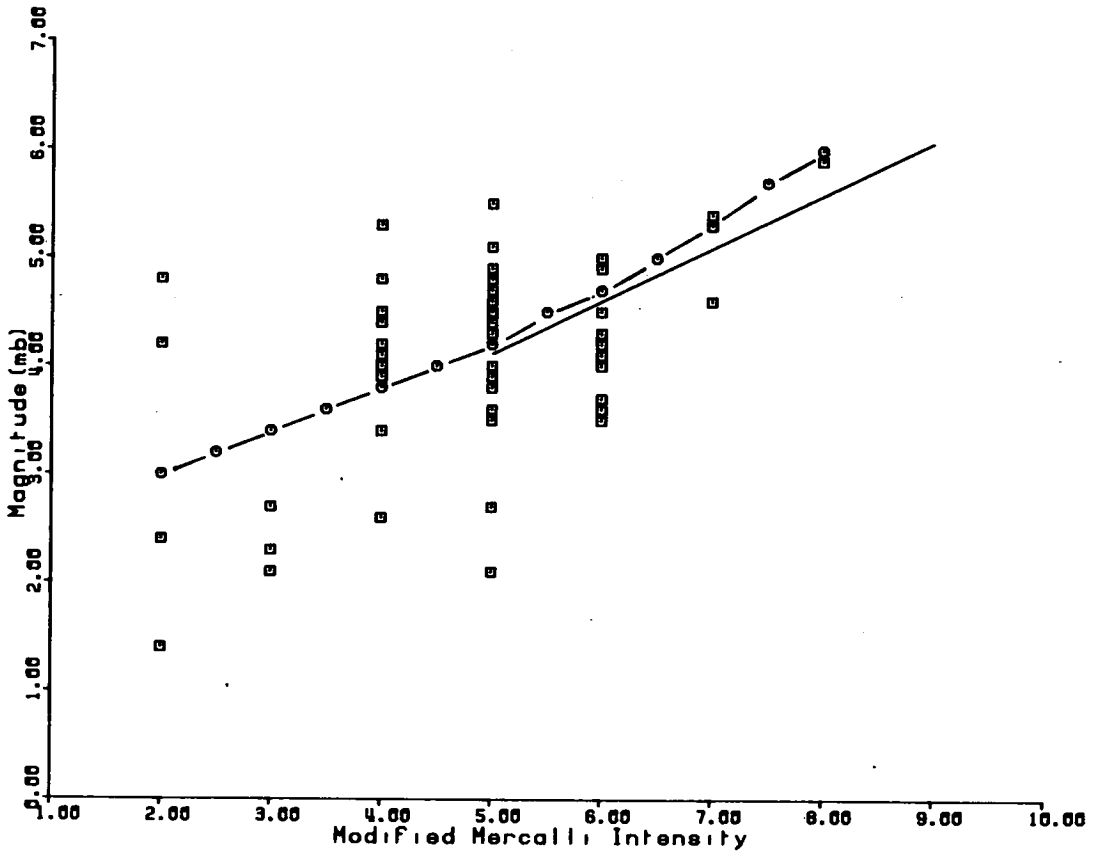

Figure 1.5 Intensity–magnitude relations after Nuttli (1979) (broken line) and Street and Lacroix (1979) (solid line) compared to recent data for the Central and Eastern United States. These data, cross symbols, on felt and damaging earthquakes, are extracted from regional Catalogues of the International Seismological Centre, Newbury, for the period January 1968 to June 1977.

The seismic moment release rate, $\dot{M}_o$, is proportional to the slip rate $\dot{s}$ along a fault of area A, or to the strain rate $\dot{e}$ in a deforming volume V for a more complicated area (Papastamatiou, 1980). The maximum potential seismic moment, say $M_{o\omega}$, can also be related to evidence of previous large-scale breaks and depths of the seismogenic layer via

$$M_o = CV\,\Delta\sigma \;:\; M_{o\omega} = CV_{max}\,\Delta\sigma = C'\,A_{max}^{3/2}\,\Delta\sigma\,, \qquad (1.18)$$

where C is a constant which is defined by the fault type and $\Delta\sigma$ is the stress drop (Kanamori and Anderson, 1975). For example a circular fault has C = 16/7 and $V = a^3$, where a is the radius. The maximum focal volume V_{max} can then be related to the maximum fault area by $A_{max} = \pi a^2$, $V_{max} = 4/3\ \pi\ a^3$ in this case. Combining this equation with (1.5) as in section 2.1 allows estimation of the limiting magnitude ω from the field observation of maximum fault areas and comparison with the extrapolation from the short term recurrence statistics.

The seismic moment release rate $\dot{M}_o$ can also be compared with the discrete sum of seismic moments ΣM_o in unit time interval from a catalogue which contains magnitudes by using (1.5) on every entry in the catalogue, as in Davies and Brune (1971). Alternatively the parameters of the continuous empirical line fit can be used by integrating annual occurrence densities multiplied by M_o. Anderson (1979) did this for the truncated Gutenberg-Richter relation as follows.

He used

$$\dot{M}_o = \int_o^{M_{o\omega}} M_o \, n(M_o) \, dM_o \quad , \tag{1.19}$$

and changed the variable from seismic moment to magnitude using (1.5) because in practice nearly all of the available catalogues consist of magnitudes at the present time. Thus

$$\dot{M}_o = \int_{-\infty}^{\omega} e^{\alpha+\beta m} \, n(m) \, dm \quad , \tag{1.20}$$

where $\alpha = A \ln 10$ and $\beta = B \ln 10$. Using (1.6) to define $n(m)$ gives

$$\dot{M}_o = e^{\alpha + \beta\omega} \frac{e^{-b'\omega}}{(\beta - b')} \quad , \tag{1.21}$$

$$\text{or } \dot{M}_o = \frac{M_{o\omega} \, 10^{-b\omega}}{(B-b) \ln 10} \quad .$$

Thus the seismic moment release rate is expressed as a fraction of the maximum which could be released in any one event. It is interesting to note that, since $B = 3/2$ (Kanamori and Anderson, 1975) the b-value is confined theoretically by the denominator to $b < 3/2$ in order to preserve finite, positive $\dot{M}_o$.

The preceeding outline has shown how two parameters of the seismicity distribution - the moment release rate $\dot{M}_o$ and the maximum magnitude ω - can be compared with those observed over geological time scales and for more recently recorded events. This gives a test of the stationarity of an earthquake catalogue based on a short term instrumental catalogue against long-term

effects.

Finally, in a few areas of the world, and notably in Southern California (Sieh, 1978) some basic spadework through faults can reveal direct evidence of previous events. By radiocarbon dating of charcoal deposited in the very recent holocene sediment a table of interoccurrence times can be built up and compared with extrapolations of recurrence curves as a further test. For example table (1.1) is taken from Anderson and Luco (1983), who used (1.5) and the time-predictable and slip-predictable models of Shimazaki and Nakata (1980) to estimate the magnitudes of the events found at Pallet Creek by Sieh. Currently this area is a very prominent and useful area of research in quaternary geology. Hopefully such studies will soon extend to several areas of the globe where faults break the surface to give seismologists a direct measurement of average repeat times for long-term earthquake prediction.

1.8 Summary

This chapter has introduced some of the basic theory and observation of earthquake recurrence statistics which were available at the start of the project, and has shown where the new developments described in the following two chapters fit into the overall picture. It has been shown that the linear Gutenberg-Richter law is often an inadequate description of seismic recurrence statistics on a local level, and some empirical and theoretical distributions which account for the observed curvature to a limiting maximum magnitude have been outlined. Further, the chapter has shown how two important geological parameters - the seismic moment release rate (which is proportional to the slip

Table 1.1 Pallet Creek Events: Estimates of magnitude (M_S) from the interoccurrence times of Sieh (1978) and the time- and slip-predictable model of Shimazaki and Nakata (1980). The table is taken from Anderson and Luco (1983), and the region analysed is the San Andreas fault in Southern California.

	Time Predictable Model			Slip Predictable Model		
Est. event year	Waiting Time to next event (years)	Inferred slip in event (m)	Magnitude	Waiting time from prior event (years)	Inferred slip in event (m)	Magnitude
1857	> 125	> 4.6	> 7.81	112	4.1	7.74
1745	112	4.1	7.74	275	10.2	8.26
1470	275	10.2	8.26	225	8.3	8.15
1245	225	8.3	8.15	55	2.0	7.33
1190	55	2.0	7.33	225	8.3	8.15
965	225	8.3	8.15	105	3.9	7.71
860	105	3.9	7.71	195	7.2	8.06
665	195	7.2	8.06	120	4.4	7.78
545	120	4.4	7.78	?	?	?

rate) and the maximum fault area - can be related to the observed integral of seismic moment under the curve and the maximum magnitude respectively. The potential use of studies such as this is shown in the areas of long-term earthquake warning via an evaluation of the average repeat time and in probabilistic evaluation of contoured maps of likely levels of ground shaking. The former should help identify areas currently most at risk for detailed prediction studies (thereby optimising the distribution of limited resources) and the latter is essential for hazard mitigation by building design codes and earthquake insurance. In a wider geophysical context, the present study is also useful, for example, in investigating the details of various tectonic processes via the slip rate and the seismic moment.

In the next chapter, the concept of an integral of the seismic moment over the magnitude range is generalised by using the empirical Weibull distribution and Gumbel's third distribution of extreme values. From this it is hoped to obtain better estimates of the seismic hazard, and to compare the present-day seismicity with the longer term geological processes in several different tectonic zones.

CHAPTER 2

The application of the Weibull distribution and its related extreme value distribution to four diverse tectonic zones

2.1 Introduction

The previous chapter has shown the link between the maximum magnitude and curvature in the log-linear frequency magnitude distribution. Such curvature has been observed in laboratory models by Burridge and Knopoff (1967) and King (1975), and also in a theoretical model by Kuznetsova et al (1981), which considered the effect of inhomogeneities along a fault. Furthermore this behaviour is commonly observed in seismicity distributions around the world - for example by Botti et al (1980) in the Western Alps, Burton et al (1982, 1984) in Turkey, Makjanic (1982) in Yugoslavia, Makropoulos (1978) in Greece as well as by Consentino and Luzio (1976) (fig 1.2) and later in this chapter. There is also experimental evidence that the distribution of microfracture events in stressed San Marco gabbro shows curvature asymptotic to a maximum size at low frequencies (Scholz, 1968). Even volcanic seismicity shows this characteristic curve to a limiting magnitude. Qamar et al (1983) showed this retrospectively for the seismicity preceeding the eruption of Mount St. Helens in 1980 on 18 May. The curve at high magnitudes indicated a characteristic source dimension of about 3km, compared to a volume of earthquake foci of (3x3x6) km^3 from hypocentral studies.

Analogous curved distributions have been observed elsewhere in nature, for example in the yield strength and fatigue life of steel (Weibull, 1951), and are commonly used in meteorological analysis

(Jenkinson, 1955). The Weibull distribution can be usefully extended to preferentially analyse the largest events associated with curvature because of its simple form (see section 1.5). The largest events in this case consist of a subset of the frequency distribution - namely the largest (extreme) value in any unit time interval.

In this chapter the Weibull distribution (1.10) and Gumbel's third extreme value distribution (1.14) are chosen as empirical approximations to the recurrence statistics, and the maximum fault dimensions and slip rates inferred from curve fits to empirical earthquake data are compared with those observed geologically, in order to see if the short term earthquake catalogues are actually compatible with long term effects. This is very important for greater understanding of the relationship between seismicity and tectonic effects, and as a check on any extrapolations from the recurrence statistics for quantitative hazard estimation. For example a good match also implies that the commonly held assumption of the stationarity of earthquake - generating processes is actually valid.

The relationship between the maximum magnitude and source dimension, V has been discussed in the previous chapter, and can be summarised by a combination of (1.5) and (1.18)

$$\omega = \frac{\log_{10}\{C\ V\ \Delta\sigma\} - A(\Delta\sigma)}{B}\ , \qquad (2.1)$$

where

$C = 16/17$, $V = a^3$ for a circular fault of radius a, and

$C = \pi/2$, $V = W^2L$ for a strike-slip fault of length L and width W.

For a dip-slip fault $C = \pi(\lambda+2\mu)/[4(\lambda+\mu)]$, $V = W^2L$, although no distinction has yet been made between normal and thrust models (Kanamori and Anderson, 1975). λ and μ are the Lamé constants here. C is a constant, $\Delta\sigma$ is the typical stress drop, $A(\Delta\sigma)$, B, are given by the magnitude-moment relation. The second seismotectonic property - the rate of release of seismic moment - requires a modification of Anderson's (1979) theory to account for curvature described by the Weibull distribution. This is carried out in the next section, and the models developed are applied to four diverse tectonic zones later in the chapter.

2.2 Models of crustal deformation rates from (I) the Weibull distribution and (II) Gumbel's third distribution of extreme values

The measure of crustal deformation is taken to be the rate of release of seismic moment ($\dot{M}_o$). This can be related to slip rates ($\dot{s}$) on individual faults, or strain rates ($\dot{e}$) over a more diffuse area by the equation (1.17).

Two models are used to estimate the rate of crustal deformation, following (I) from the cumulative frequency of occurrence (which will be called the whole process here) and (II) from the extreme value probabilities (a part process). The descriptions 'whole' or 'part' depend on whether the whole catalogue is used or not.

2.2.1 Model I An average value for the rate of release of seismic moment is given by integration over the range $(0, M_{o\omega})$ where $M_{o\omega}$ is the largest moment which might be released in a single event for a particular region. This is equivalent to integrating over the magnitude range $(-\infty, \omega)$.

Putting the Weibull density distribution from (1.10) into

(1.20) gives

$$\dot{\bar{M}}_o = \int_{-\infty}^{\omega} e^{\alpha+\beta m}\, k\, \frac{(\omega - m)^{k-1}}{(\omega - u)^k}\, dm \quad , \tag{2.2}$$

where $k = 1/\lambda$. Then

$$\dot{\bar{M}}_o = \frac{k\, e^{\alpha}}{(\omega - u)^k} \int_{-\infty}^{\omega} e^{\beta m}\, (\omega - m)^{k-1}\, dm \quad . \tag{2.3}$$

Let $x = \omega - m$ be a dummy variable, so that $dx = -dm$ and $\int_0^{\infty} = -\int_{\infty}^{0}$ gives

$$\dot{\bar{M}}_o = \frac{k\, e^{\alpha+\beta\omega}}{(\omega - u)^k} \int_0^{\infty} e^{-\beta x}\, x^{k-1}\, dx \quad . \tag{2.4}$$

Letting $t = \beta x$, $dt = \beta dx$ gives

$$\dot{\bar{M}}_o = \frac{k\, e^{\alpha+\beta\omega}}{\{\beta(\omega-u)\}^k} \int_0^{\infty} e^{-t} t^{k-1}\, dt \quad . \tag{2.5}$$

The integral is now a gamma function $\Gamma(k)$, and using $\Gamma(k+1) = k\Gamma(k)$ and $M_{o\omega} = e^{\alpha+\beta\omega}$ from the moment-magnitude relation gives

$$\dot{\bar{M}}_o = \frac{M_{o\omega}\, \Gamma(k+1)}{\{\beta\, (\omega-u)\}^k} \quad . \tag{2.6}$$

Thus $\dot{\bar{M}}_o$ is expressed as a function of (α, β) - the parameters of the seismic moment-magnitude relation, and $(\omega, u, \lambda = 1/k)$ - the three parameters of the Weibull distribution.

2.2.2 Model II Forming a probabilistic expectation value for the

extreme value case gives

$$\langle \dot{M}_o \rangle = \int_o^{M^{o\omega}} M_o p(M_o)\, dM_o \quad , \tag{2.7}$$

where $P(X<M_o) = \int_o^{M_o} p(X)\, dX$ is the extreme value distribution following from the normalised probability density p. Replacing p with the density distribution of (1.13), which is given by

$$p = \frac{d}{dm}\left\{e^{-N(m)}\right\} = e^{-N(m)} \frac{-dN(m)}{dm} = e^{-N(m)}\, n(m) \tag{2.8}$$

gives, on conversion to magnitude by (1.5)

$$\langle \dot{M}_o \rangle = \int_{-\infty}^{\omega} e^{\alpha+\beta m} e^{-N(m)} n(m)\, dm \quad . \tag{2.9}$$

Note that this equation is similar to (1.20) except for the extreme value probability term $P(m)=e^{-N(m)}$ inside the integral. Thus (2.9) is also the average value of the moment release rate produced by the extreme values alone, and $\langle \dot{M}_o \rangle$ will therefore always be <u>less</u> than $\dot{M}_o$ of Model I.

Letting $x = e^{-N(m)}$; $dx = e^{-N(m)} n(m)\, dm$ in (2.9) gives

$$\langle \dot{M}_o \rangle = \int_o^1 e^{\alpha+\beta m(x)}\, dx \quad . \tag{2.10}$$

Using (1.14) to define m(x) gives

$$\langle \dot{M}_o \rangle = M_{o\omega} \int_0^1 \exp \{\beta(u-\omega) (-\ell n\ x)^{\lambda}\}\ dx \quad , \tag{2.11}$$

where x is a dummy variable. For a limiting maximum magnitude $0 < \lambda < 1$, and $\omega > u$, so the integral is always less than one, and once more $\langle \dot{M}_o \rangle$ is expressed as a fraction of the maximum seismic moment which may be released in any one event. The integral was solved in the present work by a numerical algorithm due to Gill and Miller (1972) which uses third order finite-difference formulae and produces error estimates.

In evaluating parameters of the distribution (1.14) the unit time interval must sometimes be taken to be i years rather than annually in order to reduce problems associated with intervals devoid of any recorded events. If this is the case then u and λ are also appropriate for a unit time of i years, and conversion to annual rates, i = 1, can be done via

$$\langle \dot{M}_o \rangle_i = i \langle \dot{M}_o \rangle_1 \quad , \tag{2.12}$$

where $\langle \dot{M}_o \rangle_i$ is the seismic moment released per i years.

Thus (2.6) and (2.11) define the rate of release of seismic moment in terms of the statistically determined parameters (ω, u, λ) - the link to the physical process of strain or slip rates being represented by the terms $M_{o\omega}$ and β.

2.2.3 Uncertainties in $\bar{\dot{M}}_o$ and $\langle \dot{M}_o \rangle$ Because (ω, u, λ) are subject to (often large) statistical error in the curve fit to empirical data allowance must be made for this in predictions of $\dot{M}_o$. This can be done by the equation

$$\delta(\langle\dot{M}_o\rangle, \bar{\dot{M}}_o) = \left\{\sum_{i=1}^{3}\sum_{j=1}^{3} \frac{\partial^2(\langle\dot{M}_o\rangle, \bar{\dot{M}}_o)}{\partial p_i\, \partial p_j}\, \sigma_{ij}^2\right\}^{\frac{1}{2}}, \tag{2.13}$$

which represents a complete covariance error in $\langle\dot{M}_o\rangle$ and $\bar{\dot{M}}_o$ respectively. $p_{i,j}$ takes on values (ω, u, λ) in turn and σ_{ij} is the statistically determined covariance error in these parameters. The covariance matrix ε is defined by

$$\varepsilon = \begin{Bmatrix} \sigma_\omega^2 & \sigma_{\omega u}^2 & \sigma_{\omega\lambda}^2 \\ \sigma_{u\omega}^2 & \sigma_u^2 & \sigma_{u\lambda}^2 \\ \sigma_{\lambda\omega}^2 & \sigma_{\lambda u}^2 & \sigma_\lambda^2 \end{Bmatrix}, \tag{2.14}$$

as in Burton (1979). This is the most complete method of allowing for error, because in general the parameters ω and λ are dependent on each other. A large ω leads to less curvature (lower λ) and vice versa. This manifests itself in a negative contribution from $\sigma_{\omega\lambda}^2$, or a reduction in the overall error assigned when compared to the variance method (i.e. a sum only of the positive diagonal elements σ_i^2).

From (2.6) it can be shown by partial differentiation that

$$\begin{aligned} \frac{\partial\bar{\dot{M}}_o}{\partial\omega} &= \beta\bar{\dot{M}}_o - \frac{\partial\bar{\dot{M}}_o}{\partial u} \\ \frac{\partial\bar{\dot{M}}_o}{\partial u} &= \frac{\bar{\dot{M}}_o\, k}{(\omega-u)} \\ \frac{\partial\bar{\dot{M}}_o}{\partial k} &= \bar{\dot{M}}_o\,\{1 - \ell n[\beta(\omega-u)]\} \end{aligned} \tag{2.15}$$

$$\frac{\partial \bar{\dot{M}}_o}{\partial \lambda} = \frac{\partial \bar{\dot{M}}_o}{\partial k} \left\{\frac{-1}{\lambda^2}\right\} \quad ,$$

and, if $f(x) = \exp\{\beta(u-\omega)\ (-\ell n\ x)^{\lambda}\}$ in (2.11)

$$\frac{\partial \langle \dot{M}_o \rangle}{\partial \omega} = \beta \langle \dot{M}_o \rangle - \frac{\partial \langle \dot{M}_o \rangle}{\partial u}$$

$$\frac{\partial \langle \dot{M}_o \rangle}{\partial u} = \beta M_{o\omega} \int_o^1 f(x)\ (-\ell n\ x)^{\lambda}\, dx \qquad (2.16)$$

$$\frac{\partial \langle \dot{M}_o \rangle}{\partial \lambda} = \beta(u-\omega)\ M_{o\omega} \int_o^1 f(x)\ (-\ell n\ x)^{\lambda}\ \ell n\ (-\ell n\ x)\, dx \quad .$$

Note that the formulae for $\partial \dot{M}_o / \partial \omega$ are similar in form.

Appendix 1 contains a program MOMENT-FF2 which was developed to calculate $\dot{M}_o$, $\partial \dot{M}_o / \partial \omega$, $\partial \dot{M}_o / \partial u$, $\partial \dot{M}_o / \partial \lambda$ and hence $\delta \dot{M}_o$ from (ω, u, λ), ε and (α, β) using both models.

2.3 Application of Models I and II to four tectonic zones

Having developed the theory of evaluating $\dot{M}_o(\omega, u, \lambda, \alpha, \beta) \pm \delta \dot{M}_o$ in the previous section its application to four tectonic zones can now be considered. As an introduction the basic data culled from an earthquake catalogue (of epicentres, times, depths and magnitudes) are now described.

In the extreme value case the largest event m_i in each unit time interval i is extracted and then this subset is ranked in ascending size m_i, i=1, n. The magnitudes are then assigned a plotting point probability given by Gringorten (1963)

$$P(m_i) = (i - 0.44)/(n + 0.12) \quad , \qquad (2.17)$$

where n is the total number of time intervals. A curve of the form (1.14) can then be fitted to this data set (m_i, P_i).

The frequency case is simpler, and involves mere counting of the number of magnitudes in the range $(m_j-\delta/2, m_j+\delta/2)$, where typically $\delta = 0.1$. (Magnitudes are usually quoted to one decimal place). This gives what will be called a 'discrete frequency' F_j. The cumulative frequency $N_j = \sum_{i=j}^{m} F_i$ is then just a sum of these terms above a chosen magnitude, giving a data set (m_j, N_j).

The computer programme which was used to find (ω, u, λ) also evaluates the covariance error matrix ε, which includes an allowance for the uncertainty in magnitude. In this section this uncertainty is estimated as $\delta m_i = \pm 0.5$. The curve fit was carried out by using a non-linear least squares algorithm developed initially by Marquardt (1963), and translated into FORTRAN for general application by Bevington (1969, p 237). It has been applied to extreme value analysis of seismic hazards by Burton (1978, 1979), by Makropoulos (1978) and been updated by Bob McGonigle (1982, pers. comm.). This latter version of the program was modified (RISK-FF7, see Appendix 1) for the whole process cumulative frequency fit specifically required in the present work.

Empirical curve fits were then performed for four diverse tectonic regions: (a) the Central and Eastern Mediterranean, (b) the New Madrid seismic zone, (c) Southern Californa, and (d) the Mainland U.K. $\dot{M}_o$ (ω,u,λ,A,B) can then be compared with geological and geophysical observation. Figs 2.1 - 2.3 are epicentral plots for regions a-c and figs 2.4 and 2.5 show the completeness

histograms. The curve fits to cumulative frequency data are given in figs 2.6, 2.7 and 2.8, and are summarised in table 2.1, while the extreme value fits are represented in figs 2.9, 2.10 and 2.11 and are summarised in table 2.2. The predictions of magnitudes associated with average repeat times T as defined in equations (1.15) and (1.16) for (a) the whole process cumulative frequency analysis and (b) the part process extreme value approach are given in tables 2.3 and 2.4. Each area is now discussed separately.

2.3 (a) The Central and Eastern Mediterranean (32°-48°N, 4°-36°E) North (1977) tabulates seismic moment values for this area of diffuse, plate boundary seismicity. From his table 4 the total seismic moment released in this area for the period 1943 through 1971 was 70×10^{19} Nm or a rate $\dot{M}_o = 24 \times 10^{18}$ Nm yr^{-1}. A more complete picture from 1963-1970 (his table 1) gives a rate 46×10^{18} Nm yr^{-1}, which may be regarded as a minimum value.

A seismicity map of the area concerned is given in fig 2.1 and an excellent summary of the complex geo-tectonic setting is given in Horvath and Berckhemer (1982). The histograms of fig 2.4 show that the catalogue used (Burton, 1978) is complete for the time range analysed (1943-1971) above magnitude 4.5. The range (3.6, 4.5) is not complete - as can be inferred from the sudden jump in the number of events reported on introduction of the WWSSN network in 1963. Fig 2.6 shows the Weibull fit and fig 2.9 the extreme value curve fit. The parameters and covariance errors (which include an allowance for ± 0.5 uncertainty in the magnitude measurement) can be seen in tables 2.1 and 2.2. Note that in some cases the actual values of (ω, u, λ) for N and P differ slightly as predicted by Makjanic (1980), who attempted to allow for this by

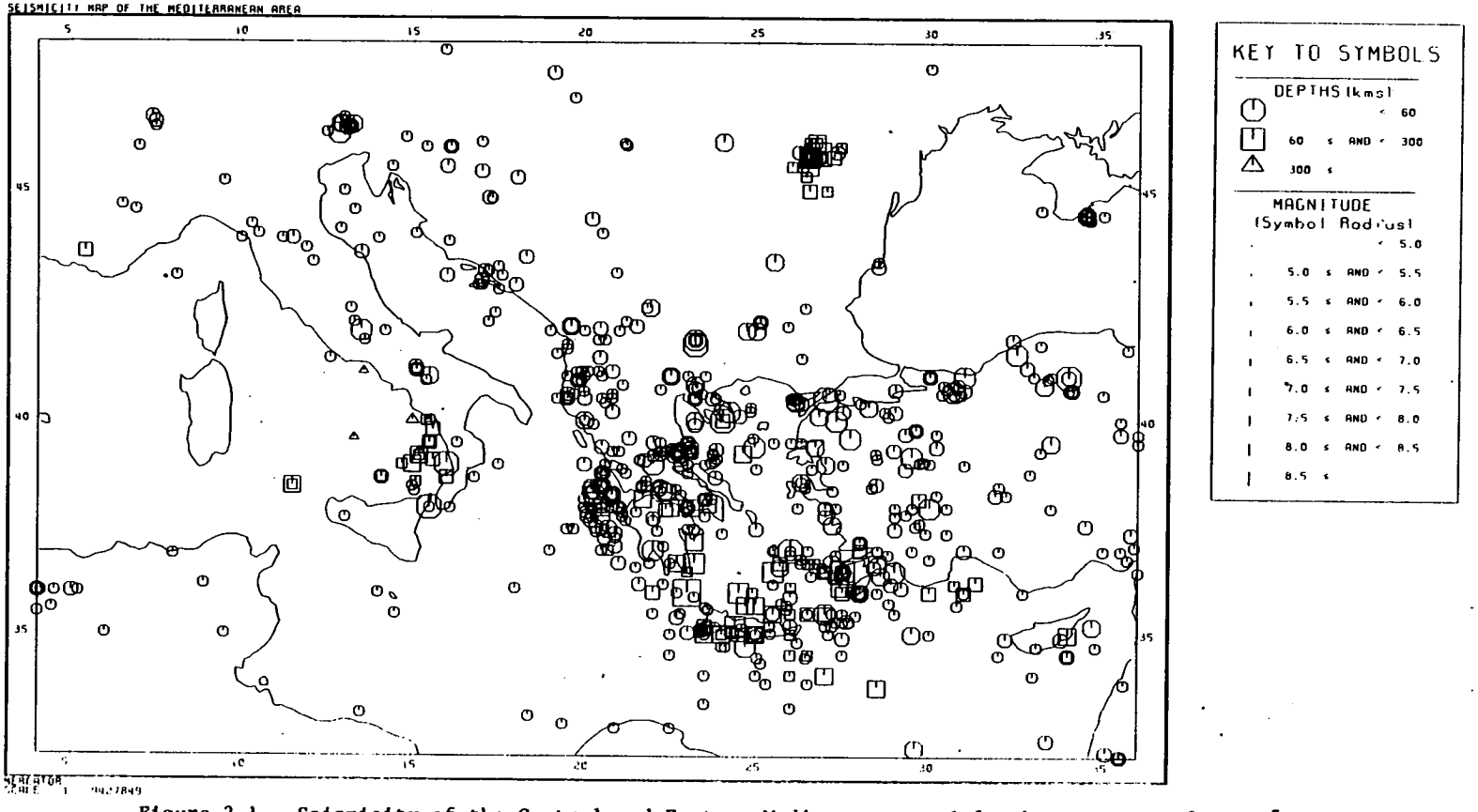

Figure 2.1 Seismicity of the Central and Eastern Mediterranean. Only those events of $M_S > 5$ are shown for economy of plotting. The tectonic interaction is composed of a collision between Africa and Eurasia, with seismic energy being released mainly along the arcuate trend of the Hellenic arc south and west of Greece and the Aegean sea.

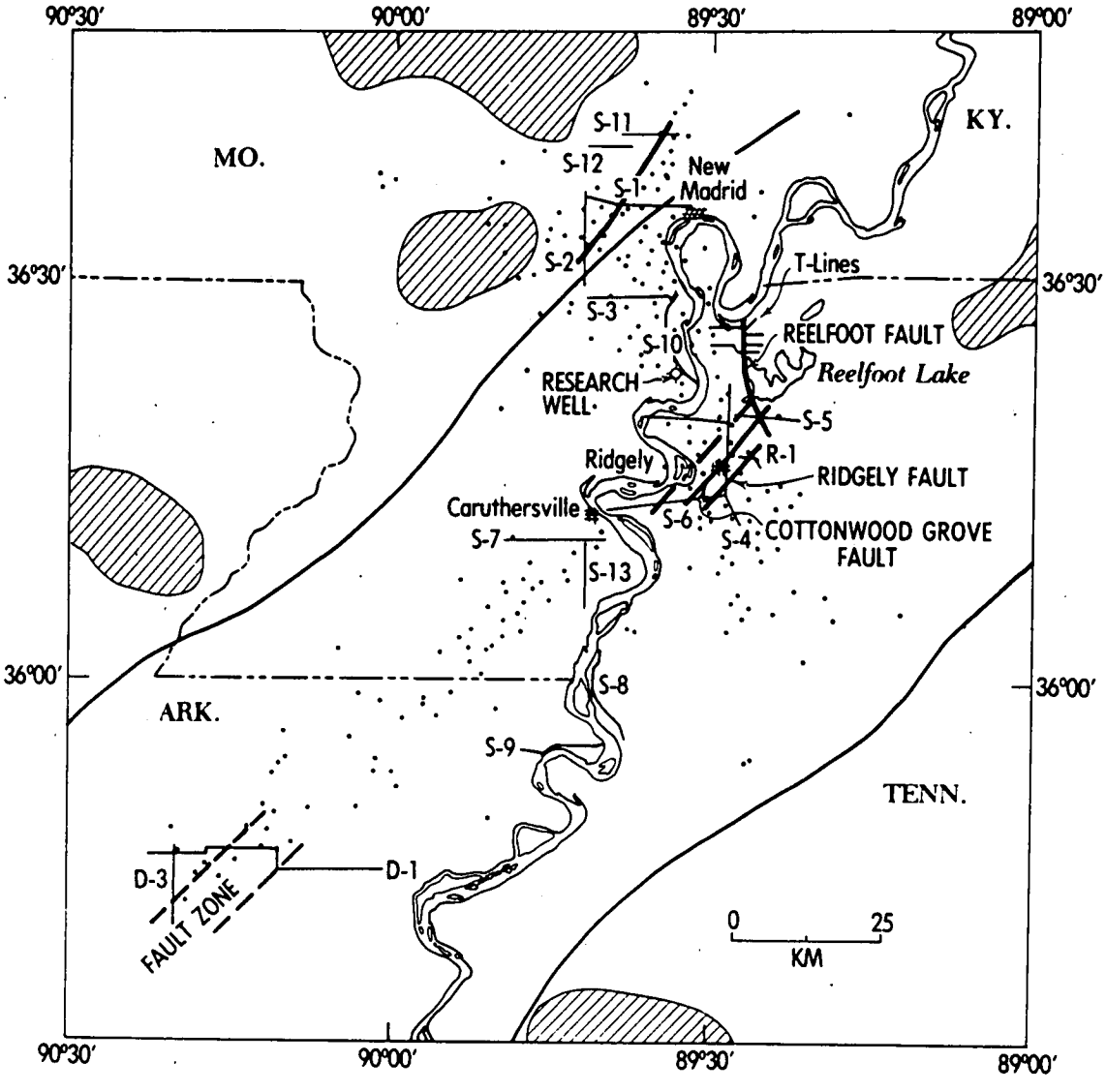

Figure 2.2 Tectonic setting of the area around the New Madrid seismic zone (after Zoback et al (1980)), showing microearthquake epicentres (dots), locations of seismic profiles (eg. S-7) and principle faults inferred from the data. The continuous heavy black lines are rift boundaries, and igneous plutons are represented by the hatched areas. There are three main seismicity trends: (1) a 100 km long stretch running SW-NE from the SW corner, (2) a section running SSE-NNW at the terminus of (1), and (3) the smallest trend SW-NE near New Madrid. Copyright 1980 by the American Association for the Advancement of Science.

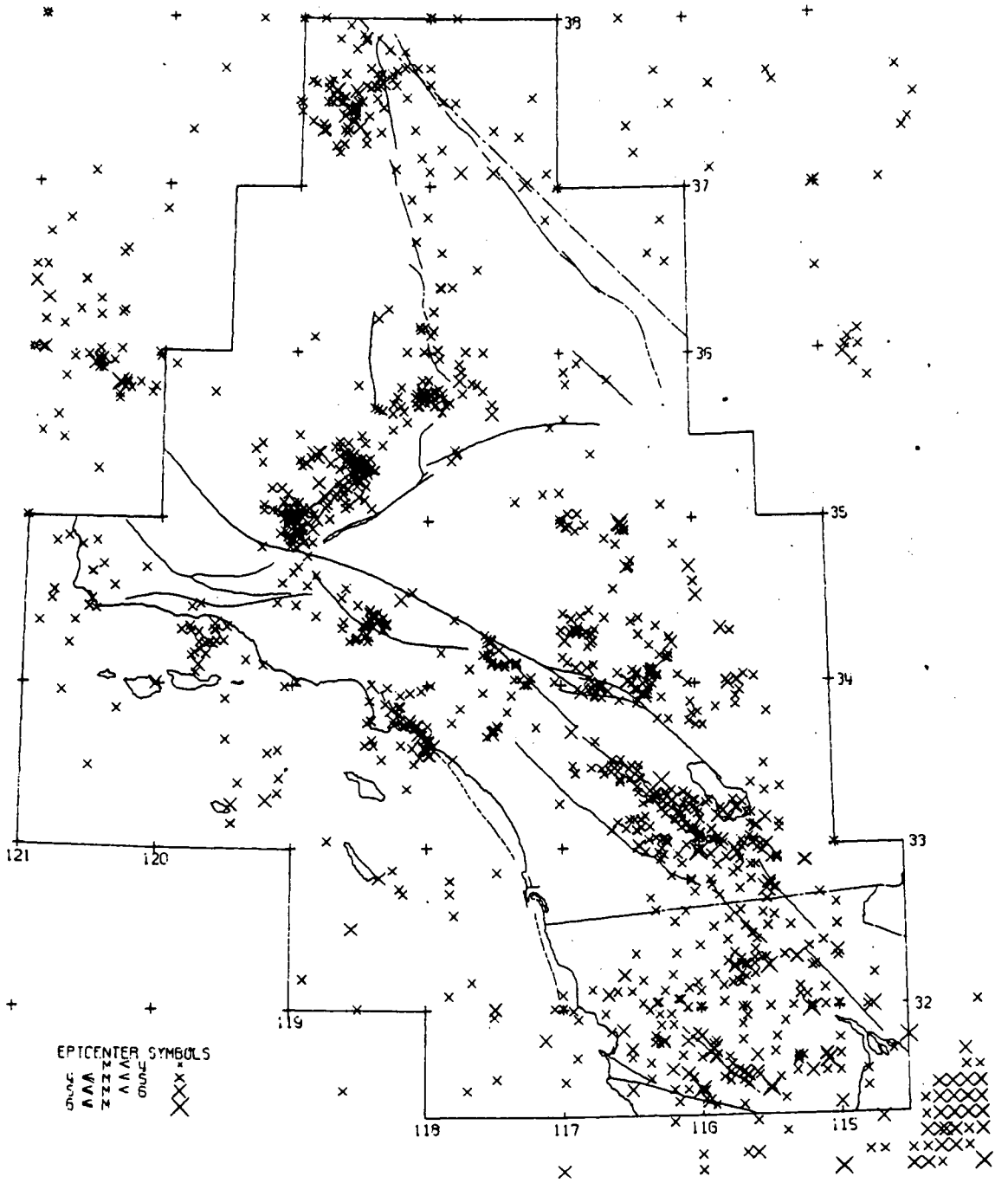

1932 THROUGH 1972, EVENTS EQUAL OR GREATER THAN MAGNITUDE-4

Figure 2.3 Seismicity and main surface fault breaks for Southern California (after Hileman et al 1973). The quiet zone on the line of the fault between (120°W, 35.5°N) and (117.5°W, 34.2°N) last ruptured in 1857 (Fort Tejon) with an estimated magnitude of 8.25 or greater (Sieh, 1978).

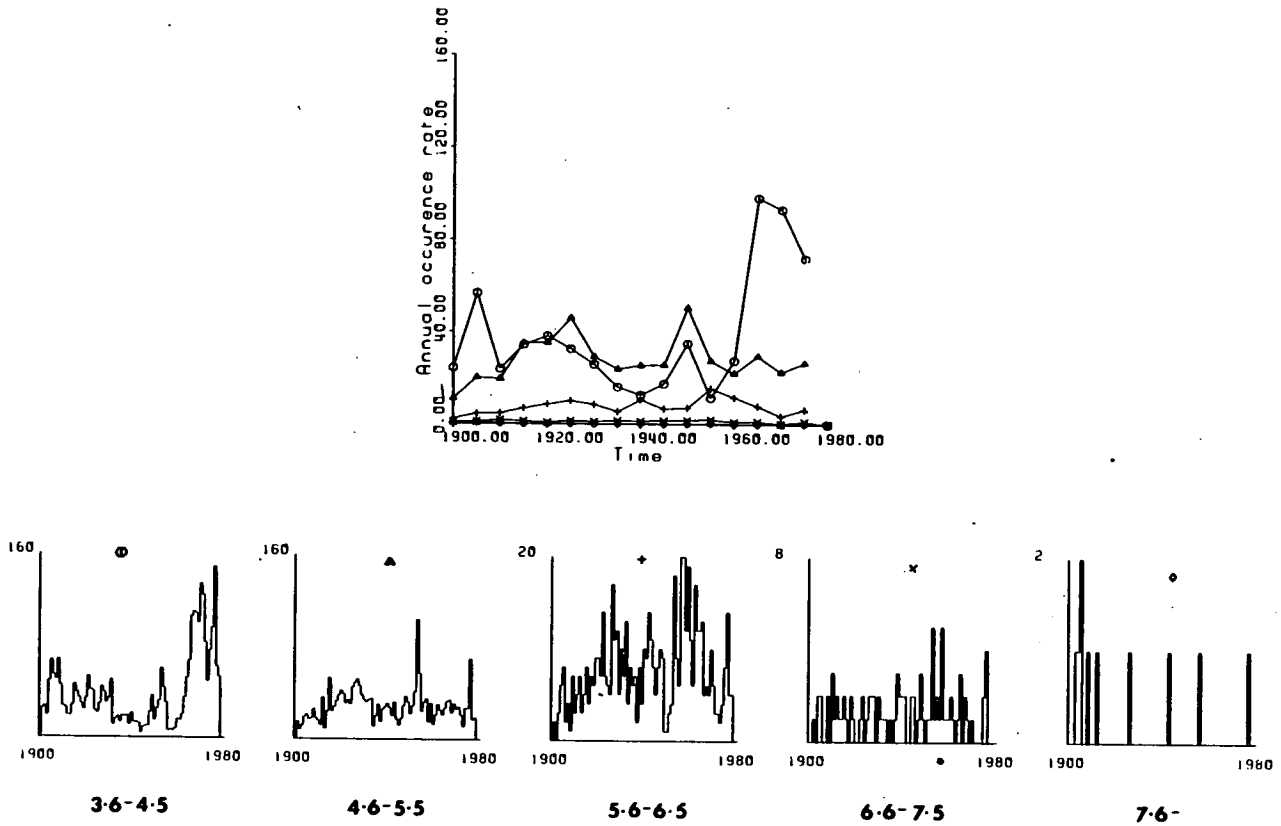

Figure 2.4 Completeness testing for the Mediterranean catalogue. The lower diagrams show the annual frequency of occurrence of events in the magnitude ranges indicated, with 5-yearly averages plotted on the upper figure. The roughly constant frequency of events in the range (4.6, 5.5) since 1920 or so, compared to the sudden jump in the range (3.6, 4.5) around 1963 indicates that the former is complete for the time span analysed (1943-1971), if we assume a reasonably stationary process.

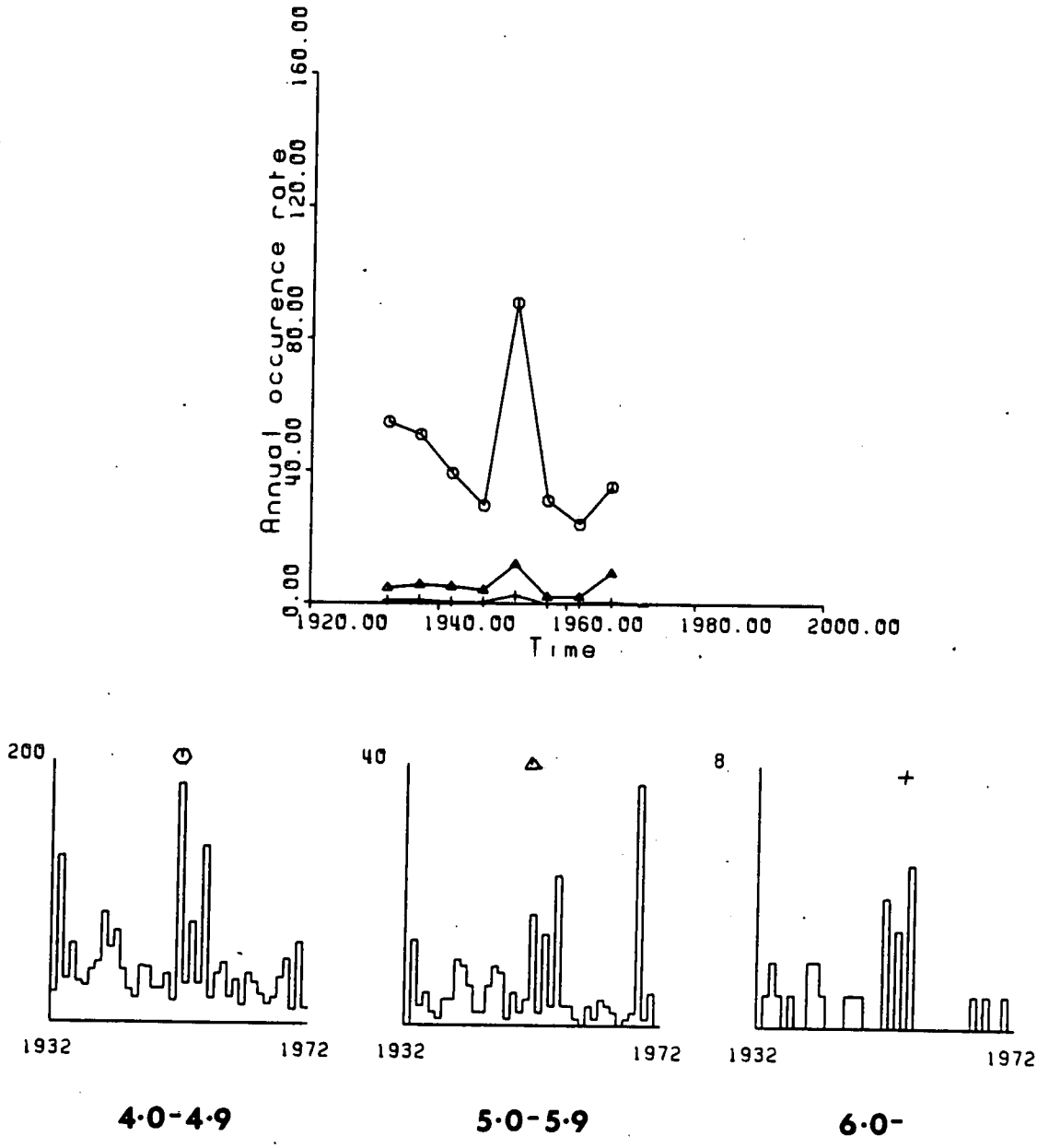

Figure 2.5 Completeness testing for the Southern Californian catalogue. As in fig 2.4 the roughly constant frequency of events in (4.0, 4.9) since 1932 indicates a completeness threshold of 4.0 for this time period.

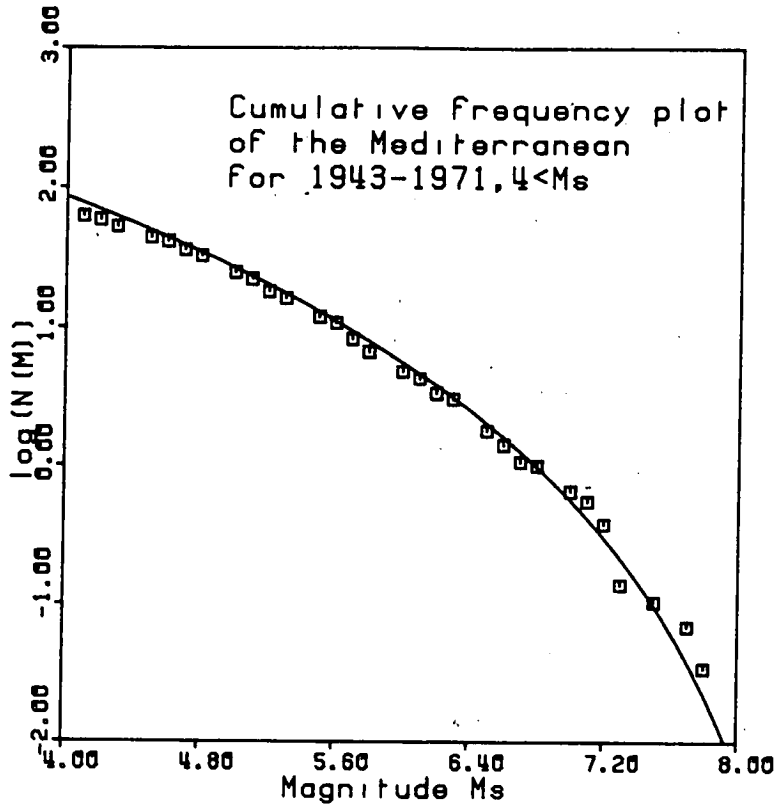

Figure 2.6 Weibull curve fitted to the Mediterranean data. The curved cumulative frequency distribution N(m) as in equation (1.10) is compared with the data. A straight line would obviously not be applicable to this area on a log-linear plot such as this.

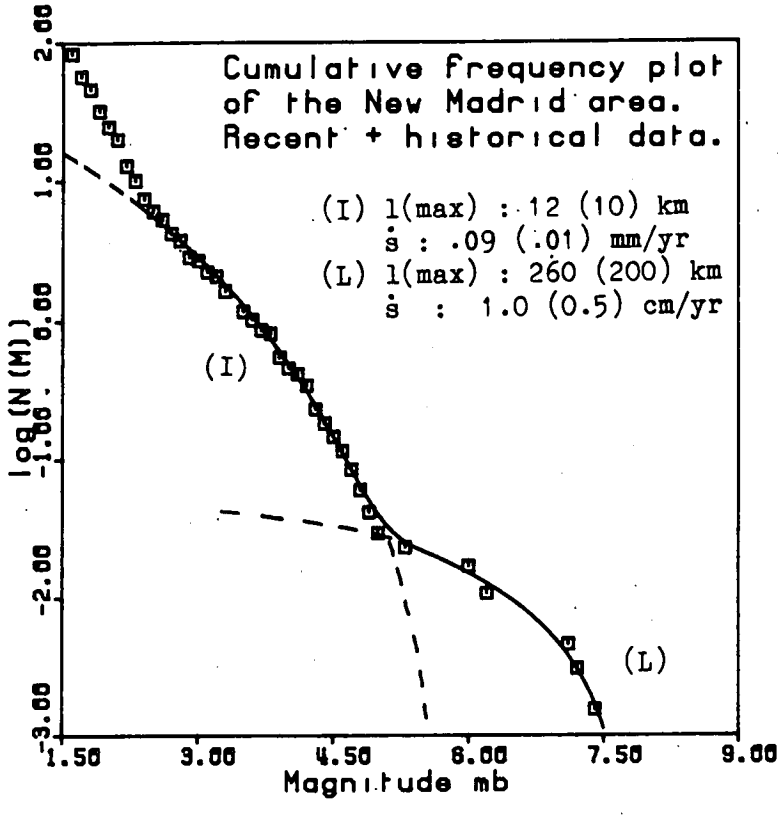

Figure 2.7 Weibull line fit to the New Madrid data. This data set was supplied by Johnstone (1981), and contains historical and recent microearthquake data, joined at magnitude 3.5 m_b. A superposition of two distributions (of 'Large' - (L) and 'intermediate' events (I)) is compatible with field observation of two characteristic orders of slip rates and maximum fault lengths. This can be seen by comparing the fault lengths l(max) and slip rates $\dot{s}$ inferred from the parameters of the Weibull fit (ω, $\dot{M}_o$) with those observed (in parentheses). The slip rates inferred for (I) mean that about ten of the smaller subsidiary faults are required to account for the total. About five can be seen on fig 2.2 and further reflection surveys may find others.

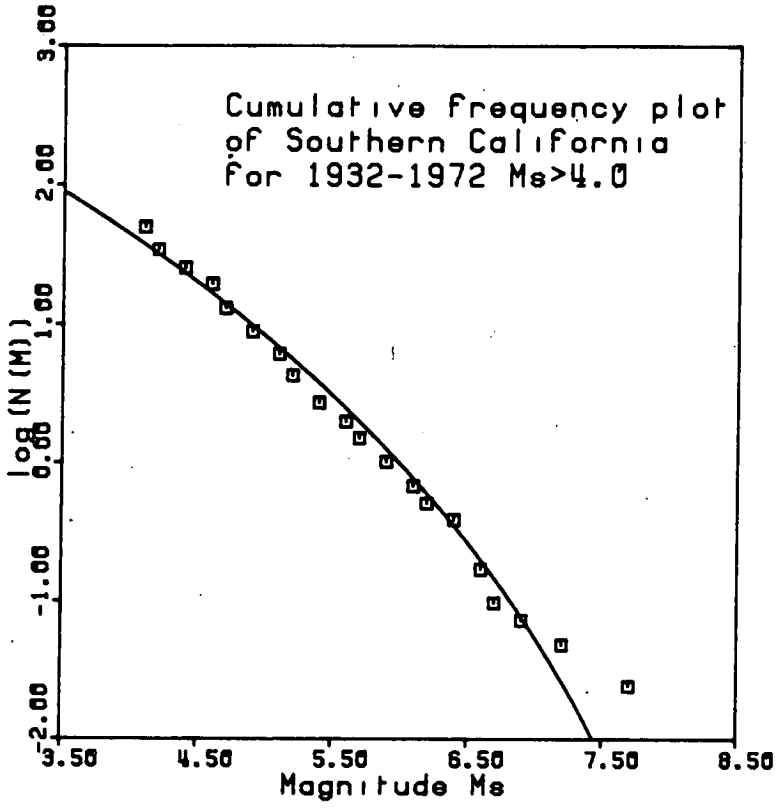

Figure 2.8 Weibull line fit to the Southern Californian data. In this case the line fit seriously underestimates the occurrence rate of the largest events which have occurred. A line fit of the form (1.1) would in this case give a better fit at these magnitudes, but again there seems to be some evidence of a bimodal distribution, the ranges meeting at $M_s \approx 6.7$ or so.

Figure 2.9 Gumbel's third distribution of extreme values fit to the Mediterranean extreme value data.

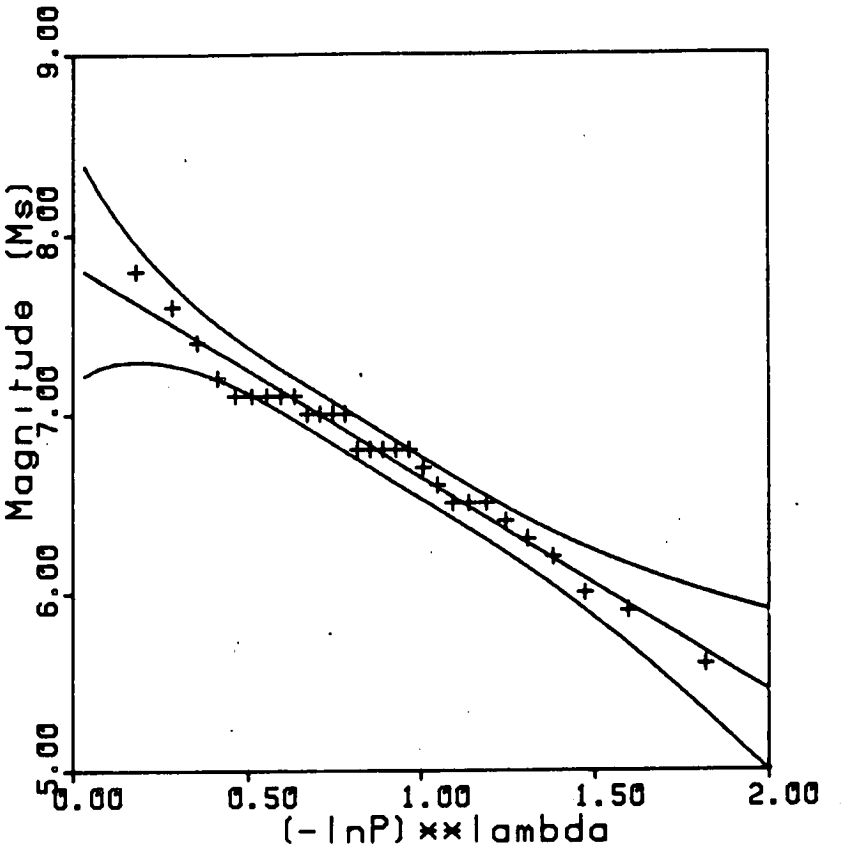

(a) M_s vs $(-\ln P)^{\lambda}$ plots as a straight line (the λ parameter - the indicator of curvature being incorporated into the x axis). It can clearly be seen that ω is the intercept on the y axis and u is defined where x = 1. The covariance error matrix, which includes an estimate of magnitude uncertainty, leads to the confidence limits drawn.

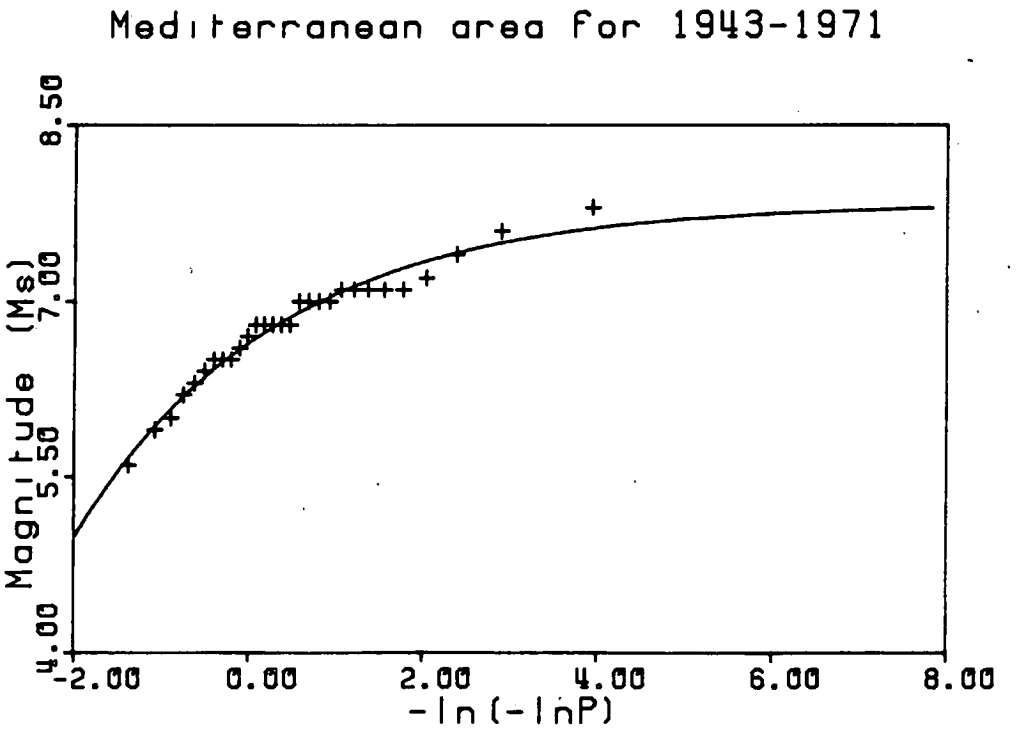

(b) M_s vs $\{-\ln(-\ln P)\}$. This choice of x axis illustrates the effect of curvature in the cumulative frequency distribution $N = -\ln P$. Annual extreme values are used in both diagrams to define the plotting point probability P defined in section 1.5.

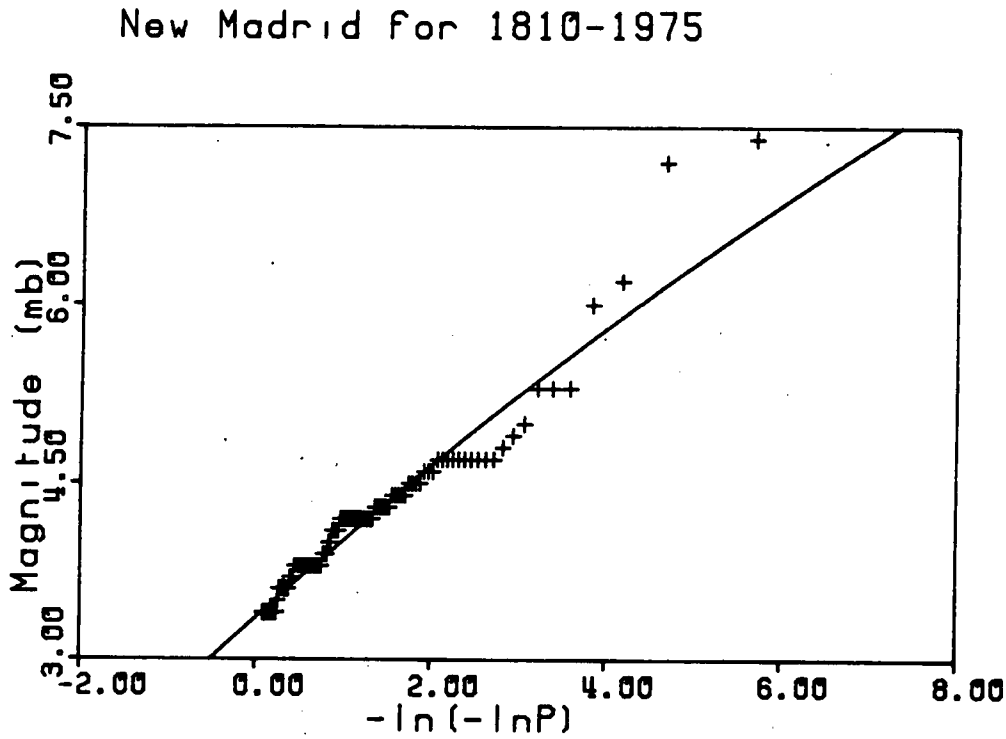

Figure 2.10 Gumbel's third distribution of extreme values fit to the New Madrid extreme value data. The solid theoretical line is effectively straight. Because of the superposition evident in fig 2.7 the line fit is not a good description of the seismicity. Again annual extremes were used.

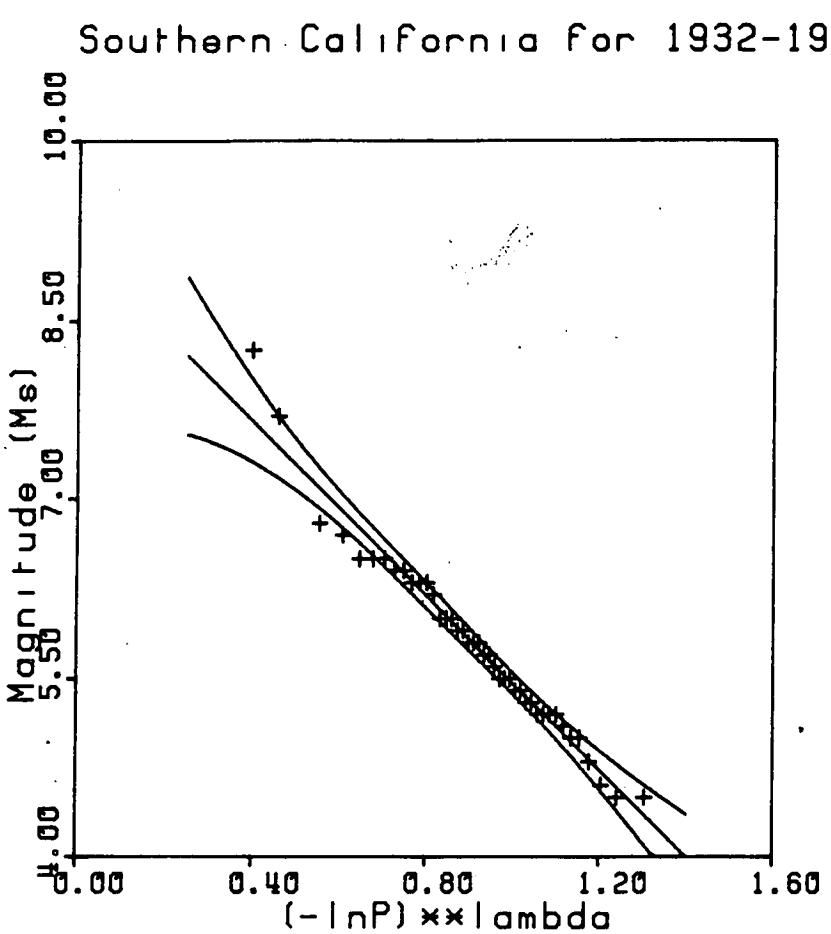

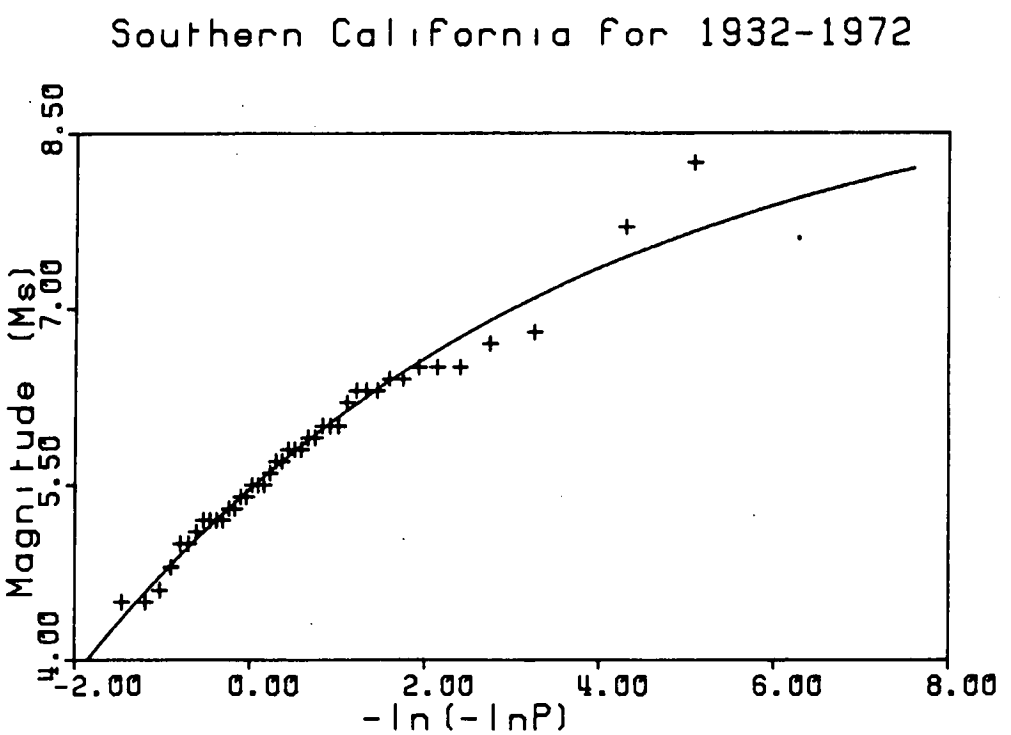

Figure 2.11 Gumbel's third distribution of extreme values fit to the Southern Californian extreme value data. Again the occurrence of the largest extremes are underestimated and bimodal curvature is a possibility. Annual extreme values are used to plot the data.

Table 2.1

Moment release rates predicted by cumulative frequency curve fits to $N(m) = \{(\omega-m)/(\omega-u)\}^{1/\lambda}$ (Model I and figs 2.6-2.8)

Area+	Parameters (ω, u, λ)	Covariance error matrix ε			Local values for A, B	$\bar{\dot{M}}_o$ (ω,u,λ,A,B) $\times 10^{18}$ Nm yr^{-1}	$\dot{M}_o$ Observed or estimated $\times 10^{18}$ Nm yr^{-1}
(a)	(8.16, 6.80, 0.251) M_s	0.855	-0.031	- 0.119			
		-0.031	0.018	0.008	9.0 1.5	87 + 110	≥46
		-0.119	0.008	0.018		- 49	
(b) Range (5.0, 7.5)	(7.81, -23.5, 0.680) m_b*	1.43	71.1	- 0.752			
		71.1	4179.0	-42.5	8.58 1.5	1.2 + 12	≈ 0.6
		-0.752	-42.5	0.437		- 1.1	
(b) Range (2.5, 5.0)	(5.61, 3.63, 0.263) m_b*	1.000	-0.084	- 0.154			
		-0.084	0.019	0.015	8.58 1.5	4.0 + 23.6	≈ 10^{-4} -10^{-2}
		-0.154	0.015	0.025		- 3.4 ($\times 10^{-4}$)	
(c)	(9.26, 6.00, 0.126) M_s/M_L	9.45	-0.304	- 0.340			
		-0.304	0.026	0.012	8.83 1.5	8.3 + 86.9	≈ 16
		-0.340	0.012	0.012		- 7.6	

* Refer to text for m_b/M_s conversion

+ Areas are: (a) the Central and Eastern Mediterranean, (b) the New Madrid seismic zone, and (c) Southern California

Table 2.2

Moment release rates predicted by extreme value curve fits to $P(m) = \exp\{-(\omega-m)/(\omega-u)\}^{1/\lambda}$ (Model II and figs 2.9-2.11)

Area[+]	Parameters (ω, u, λ)	Covariance error matrix ε			Local values for A, B		$\dot{M}_o$ (ω,u,λ,A,B) x 10^{18} Nm yr^{-1}	$\dot{M}_o$ Observed or estimated x 10^{18} Nm yr^{-1}
(a)	(7.84, 6.64, 0.435) M_s	0.484	-0.044	-0.200	9.0	1.5	44 + 26 - 16	>46
		-0.044	0.014	0.021				
		-0.200	0.021	0.093				
(b) Range (3.0, 7.5)	(19.4, 3.36, 0.042) m_b*	1123.	2.54	-3.20	8.58	1.5	-	≈ 0.6
		2.54	0.013	-0.007				
		-3.20	-0.007	0.009				
(c)	(9.11, 5.46, 0.182) M_s/M_L	3.700	-0.063	-0.219	8.83	1.5	8.5 + 16.3 - 5.6	≈ 16
		-0.063	0.008	0.004				
		-0.219	0.004	0.013				
(d)	(5.46, 4.58, 0.590) m_b*	0.190	-0.026	-0.134	8.7	1.5	2.2 + 1.0 $(x10^{-3})^{0.7}$	≈ 34 $(x10^{-3})$
		-0.026	0.015	0.026				
		-0.134	0.026	0.113				

* Refer to text for m_b/M_s conversion

+ Areas are: (a) the Central and Eastern Mediterranean, (b) the New Madrid seismic zone, (c) Southern California, and (d) Mainland U.K.

Table 2.3

Magnitudes m_T associated with average repeat time $T = 1/N$ for N a Weibull distribution (equation 1.10)

T yrs	(a) Mediterranean M_s		(b) New Madrid $m_b < 5$		(b) New Madrid $m_b > 5$		(c) Southern California M_s/M_L	
2.0	7.02	(0.136)*	3.96	(0.142)	-	-	6.27	(0.151)
5.0	7.25	(0.166)	4.31	(0.137)	-	-	6.60	(0.153)
10.0	7.40	(0.208)	4.53	(0.142)	1.28	(4.525)	6.82	(0.181)
20.0	7.52	(0.258)	4.71	(0.168)	3.73	(1.423)	7.03	(0.234)
50.0	7.65	(0.330)	4.90	(0.232)	5.62	(0.257)	7.27	(0.329)
100.0	7.73	(0.385)	5.02	(0.291)	6.44	(0.322)	7.44	(0.413)
200.0	7.80	(0.438)	5.12	(0.353)	6.96	(0.265)	7.59	(0.504)

* All uncertainties inferred from the covariance matrix ε are quoted in brackets. To derive this uncertainty a magnitude measuring error of $\pm$ 0.5 is assumed, and an expression similar to (2.13) is used for $m_T = m(N)$, $N = 1/T$ via (1.10)

Table 2.4

Magnitudes m_T associated with average repeat times $T = 1/(1-P)$ for P as defined by Gumbel's third distribution (equation 1.14)

T (yrs)	(a) Mediterranean M_s		(c) Southern California M_s or M_L		(d) Mainland U.K. m_b	
2.0	6.82	(0.121)*	5.70	(0.093)	-	-
5.0	7.22	(0.126)	6.34	(0.110)	-	-
10.0	7.39	(0.169)	6.69	(0.122)	4.62	(0.122)
20.0	7.51	(0.234)	6.99	(0.152)	4.98	(0.113)
50.0	7.62	(0.324)	7.32	(0.223)	5.20	(0.156)
100.0	7.68	(0.387)	7.53	(0.293)	5.29	(0.209)
200.0	7.72	(0.443)	7.72	(0.373)	5.35	(0.260)

* All uncertainties inferred from the covariance matrix ε are quoted in brackets. To derive this uncertainty a magnitude measuring error of = $\pm$ 0.5, and an expression similar to (2.13) is used for $m_T = m(P)$, $P = 1 - 1/T$ via (1.14).

generalising (1.13) to P = exp {-const.N}. (The underlying reason for this observed discrepency is that the seismic process is not a purely random one).

To convert to moment release rates refer to North's table 4 again, where an average stress drop for an earthquake occurring in the area of interest is 38 bars. This implies that A = 9.0 using Singh and Havskov's (1980) formulation for SI units, and with B = 3/2 leads to a good linear fit to North's (1974) fig 4, right up to the highest magnitudes. This last point indicates that there appears to be no instrumental saturation effect for this catalogue, because this would show up on the graph as curvature asymptotic to a saturation magnitude.

Both predictions of the short term moment release rates from models I and II agree with the observed value $M_o \geq 46 \times 10^{18}$ Nm yr^{-1} to within a factor two or so, which is in both cases within the expected uncertainty. This consistency, where a reasonable error in (ω, u, λ) exists, and some knowledge of a local stress drop or A value is available, shows that the model proposed is quantitatively adequate well within the limits of statistical uncertainty.

Further inspection of this uncertainty shows the following relative effects of the three Gumbel parameters:

$$\frac{\partial \langle \dot{M}_o \rangle}{\partial \omega} \Big/ \frac{\partial \langle \dot{M}_o \rangle}{\partial u} \Big/ \frac{\partial \langle \dot{M}_o \rangle}{\partial \lambda} = 1.3 \;/\; 1 \;/\; 1.8$$

$$\frac{\partial \langle \dot{M}_o \rangle}{\partial \omega} \sigma_\omega \Big/ \frac{\partial \langle \dot{M}_o \rangle}{\partial u} \sigma_u \Big/ \frac{\partial \langle \dot{M}_o \rangle}{\partial \lambda} \sigma_\lambda = 7.7 \;/\; 1 \;/\; 4.7 \quad .$$

This result shows that u is the best-determined parameter and that ω and λ have a dominant effect on the total variance uncertainty in $\langle \dot{M}_o \rangle$ in this case. This effect is tempered by their interdependence already discussed above, and highlights the need to include the off-diagonal elements of the complete covariance error matrix in any attempt to quantity an error in $\langle \dot{M}_o \rangle$.

Finally, note from the tables that the error in $\langle \dot{M}_o \rangle$ is less than that for $\bar{\dot{M}}_o$ (60% compared with 126%). This is compatible with the fact that the largest events are usually more accurately recorded, and that these events dominate in the determination of $\dot{M}_o$.

The comments of the last three paragraphs were also found to apply qualitatively to the following areas of study, the actual values being quoted in this subsection for illustration only.

2.3 (b) The New Madrid seismic zone (35°-37°N, 89°-90.5°W)

This area of mid-plate seismicity has received much attention in recent years for reasons both practical and theoretical. Zoback et al (1980) summarised the available geological and geophysical data, and concluded that the area consists of three main seismic trends (see fig 2.2), set in a reactivated graben structure. Why the seismicity should largely follow the axis of the graben is not clear.

Practical interest is stimulated by the possibility of a repeat of the 1811-1812 sequence of major events (7.1 - 7.4 m_b) in an area of relatively low seismic attenuation and high population density, and theoretical interest comes from the break-down of the classical theory of rigid plate tectonics. These

events are unusual in that they have occurred in an area which is otherwise relatively quiet in terms of moderate seismicity, and their very existence suggests that the American plate may be far from rigid. Because the seismicity trends are situated in a zone primarily of EW compression (Zoback and Zoback, 1980) right lateral strike slip motion might be expected along the trends (1) and (3) of fig 2.2 and thrust on section (2). Russ (1981) showed that this is borne out to a large extent by the few fault plane solutions available, and that section (2) may result from reactivated dip-slip faulting. Together with Schilt and Reilinger (1981), he also indicates that such evidence as there is favours 5 mm yr^{-1} of uplift occurring in and around the northern part of the active zone. There is some evidence that some of this motion is taken up by aseismic creep since earthquakes in Schilt and Reilinger (1981) did not produce enough movement to account for all of the uplift detected in a later levelling survey.

The catalogues analysed are described by Nuttli (1979) and Johnston (1981) quoting m_b values inferred from macroseismic intensities and recent data on small earthquakes, so there are no problems associated with instrumental saturation. All events from Johnston's (1981) data set for $m_b > 2.5$ were included in the analysis. The most successful curve fit came from considering the ranges (2.5, 5.0) and (5.0, 7.5) separately as in fig 2.7, which plots the superposition of these two separate distributions. There may also be a third component in the range of (1.6, 2.5). This superposition can also be seen in the extreme value case (fig 2.10), but due to the scarcity of data in the higher portion the two ranges cannot be separated. In this case the curve fit is effectively straight, even though systematic bimodal curvature is

evident from the figure. For this reason no realistic $\langle \dot{M}_o \rangle$ could be obtained with the impossibly high value of ω obtained in table 2.2.

In arriving at the entries in table 2.1 for $\dot{M}_o$ the magnitude conversions

$$M_s = 1.59\ m_b - 3.97 \qquad 6.5 < M_s < 8.0 \qquad (2.18)$$

$$M_s = 1.93\ m_b - 4.8 \qquad 4.0 < M_s < 6.0\ , \qquad (2.19)$$

from results summarised in Marshall (1970) were used to match the ranges above and below magnitude 5.0 respectively. There is some evidence that the stress drops in this area are relatively high, so a value $\Delta\sigma$ = 100 bars was chosen to estimate A for the region via Singh and Havskov's (1980) formulation. Considering the large error involved in converting from epicentral Intensities I_o to m_b (see fig 1.5) and then to M_s it is not surprising that the final error quoted in $\dot{M}_o$ is as high as a factor 10 or so.

In fig 2.7 for the range $m_b > 5.0$ the largest events ($m_b > 7$) were moved to positions consistent with average repeat times of 650 years (Russ, 1981). This gave agreement within a factor 2 with the estimated moment release rate from three fault areas modelled as one fault 20 km deep (Nuttli and Herrmann, 1978) by 200 km long moving at 0.5 mm yr^{-1}, if $\mu = 3 \times 10^{10}$ Nm^{-2}. The value of ω calculated from (2.1) for the geological data, with L = 100 km, W = 20 km and $\Delta\sigma$ = 100 bars is given by a strike slip model and turns out to be $M_w = 8.14$, or $m_b = 7.6$ from (2.18). This is in good agreement with the value found statistically of $m_b = 7.8 \pm 1.2$, and the historical magnitudes (7.1 - 7.4 m_b).

For the magnitude range (2.5, 5.0), using a circular fault

model the maximum fault area $A_{max} = \pi a^2$ (for $\omega = 5.6$) was found to be 150km^2 which implies L≈12 km and $\dot{s} \approx 9 \times 10^{-2}$ mm yr^{-1}. This typical movement on what are supposed to be a collection of several subsidiary faults compares favourably with that observed on one such fault (1.2×10^{-2} mm yr^{-1} and fault length 10 km from Zoback et al (1980) on the Cottonwood Grove fault if it is noted that there are at least five other such faults in fig 2.2). It can be seen that the seismicity represented by the range (2.5, 5.0) contributes only a minor fraction of the stress release.

The conclusion here is that bumps in the cumulative frequency distribution have been numerically related to the superposition of two different characteristic orders of observed faulting, i.e. both parameters established by the statistical curve fit, $\{A_{max}(\omega), \dot{M}_o(\omega,u,\lambda,A,B)\}$, or more simply $\{L, \dot{s}\}$ agree within their error with those inferred from geological and geophysical evidence. It appears difficult to suggest any other reasons for the shape of the curve which would match the tectonic information so well by chance.

2.3 (c) Southern California (31°-38°N, 114.5°-121°W)

This well-researched area of high seismicity on a plate boundary is very different from the previous example. It includes the site of the 1952 Kern Co event and the 1971 San Fernando earthquake, as well as the 400 km long 'locked zone' which previously ruptured in 1857 with an estimated magnitude of 8.25 M_s or greater and an average repeat time of 163 years (Sieh, 1978).

The catalogue used was that of Hileman, Allen and Nordquist (1973), whose publication also gives excellent maps of the seismicity and the tectonic setting (e.g. see fig 2.3). The analysis of fig 2.5 shows that for the period concerned (1932-1972)

magnitudes (M_s or M_L) above 4.0 or so are completely reported.

Anderson (1979) indicates a moment release rate of 12 x 10^{18} Nm yr^{-1} for a 500 km long fault, but the catalogue analysed in the present work contains a 650 km stretch of the San Andreas fault and its offshoots, so $\dot{M}_o$ = 16 x 10^{18} Nm yr^{-1} may be more appropriate. These figures assume a depth of the brittle zone of 15 km and $\mu \approx 3$ x 10^{10} Nm^{-2}, with a slip rate from plate tectonic constraints of 5.5 cm yr^{-1}. Since the slip rate on surface faults is of the order 1 - 3.7 cm yr^{-1} the deformation must take place in a broad zone around the main fault trend.

Fitting the Weibull distribution to the data proved to be unsuccessful above magnitude 6.7 (fig 2.8). The curve fit seems to follow curvature apparent in the range (4.0, 6.7) and seriously underestimates the occurrence of the highest magnitudes. It may be that the activity above 6.7 is a separate characteristic distribution as in the New Madrid area, but with only three or four data points this cannot be tested from the current catalogue. Singh and Havskov (1980) give A = 8.83 for this area, which implies a moment release rate of the right order only at the expense of allowing a value for ω of 9.3 - one magnitude higher than Sieh's deterministic estimate.

Hanks, Hileman and Thatcher (1975) indicate that M_o for the Kern Co (1952) event was 2 x 10^{20} Nm and M_s = 7.7. Using A = 8.83 gives M_w = 7.65, so there are no grounds for supposing instrumental saturation is important, since this is the largest event in the catalogue.

The extreme value curve fit (fig 2.11) gives a similar value for ω, but u is significantly different (even considering its error). Curvature does seem to be enhanced by this method (higher

value for λ) but once more there is a poor fit at the highest magnitudes and the possibility of two separate curved distributions is evident. The data point for M_s = 8.25 is inferred from Sieh's (1978) estimates of M_s and the average repeat time T, with T = 1/(1-P). As in sections (a) and (b) the moment release rates inferred from the curve fit are in agreement with those observed within a factor less than the estimated uncertainty (a factor 2 compared with 3 or 4) but in this case it is evident that the parameters of the curve fit may be significantly improved upon.

2.3 (d) United Kingdom mainland

This area of relatively low intraplate seismicity differs from the New Madrid area in that no catastrophic events are documented in historical times. Burton (1981) analysed this area in terms of the third distribution of extreme values and produced the (ω, u, λ) set in table 2.2(d). The unit time for this set was 6 years. The m_b/M_s relation (2.19) is thought appropriate because of the typical range of events in terms of magnitude.

Using (1.5) and the values of ω, B given in table 2.2(d) gives $M_{o\omega}$ = 2.0 x 10^{17} Nm for A = 8.7 for an intraplate area, and if this is modelled as a circular fault via (1.18) the maximum fault area would be 350 km^2 for a corresponding typical stress drop of 76 bars. Since $\langle \dot{M}_o \rangle = 2.2 \times 10^{15}$ Nm yr^{-1} from table 2.2(d) and assuming $\mu = 3 \times 10^{10}$ Nm^{-2}, a typical seismogenic fault movement of 0.2 mm yr^{-1} is expected.

Unfortunately there is very little direct tectonic information as yet on U.K. seismicity. However, King's (1980) results showed that the fault area for the Carlisle event of 26th December 1979 was of the order 40 km^2 for an event of 5.0 m_b. Very little

information exists on contemporary fault slip rates, although there is some evidence of surface movement directly following glacial unloading (Sissons and Cornish, 1982). The thrust mechanism of the Carlisle event (King, 1980), and the strike-slip solution for the Kintail earthquake swarm of 1974 (Assumcao, 1981) are both compatible with compressive tectonics.

King (1980) assumes $\Delta\sigma$ = 30 bars might be appropriate for earthquakes in the U.K. In this case A = 9.1, $M_{o\omega}$ = 5.13 x 10^{17} Nm, the maximum fault area = 1200 km^2, $\dot{s}$ = 0.06 mm yr^{-1}. King's results are consistent in themselves, but if $\Delta\sigma$ = 30 bars, fault planes with areas an order of magnitude greater than those which have been observed so far might be expected. A more realistic picture might be to interpret the maximum fault area as representing a sum of several smaller faults of the order of tens of km^2, moving at rates around 0.1 mm yr^{-1}. This speculative interpretation is compatible with the spread of U.K. seismicity around small, localised centres such as at Comrie and in pockets in the North West of England and South Wales, and the absence of catastrophic events in historical time such as in the New Madrid area.

A deterministic estimate of the movement between the sinking South of England and the relative uplift consistent with glacial unloading of the North of England and Scotland is 1.5 mm yr^{-1} (Rossiter, 1972). If the depth of the U.K. seismogenic zone is taken to be 5 km from the depth distribution of U.K. earthquakes (Neilson, 1982, pers. comm.), and its length is modelled as of the order 200 km from the width of the mainland, then the maximum fault area is 1000 km^2 and $\dot{M}_o \approx 3.4 \times 10^{16}$ Nm yr^{-1}. This area favours King's choice of $\Delta\sigma$ and comparison of the values of $\dot{M}_o$ and

$\langle \dot{M}_o \rangle$ in table 2.2 indicate that over 90% of the observed movement occurs aseismically. This is exactly what might be expected from elastic rebound of the crust following glacial unloading.

2.4 Discussion of Results

In most cases where moment release rates were available the distributions N and P successfully modelled both the observed curvature at high magnitudes and the predicted moment release rates from models I and II. The exceptions tended to be in areas where there was evidence that the distribution was bimodal - being most striking in the New Madrid area (fig 2.10). It is unfortunate that in most cases there are insufficient data to separate the two distributions.

The Weibull and (more obviously) the extreme value fits both seem to underestimate the occurrence of the largest events (especially if superposition of two characteristic fault sizes is present). Allowing for the uncertainty of the curve fit the moment release rates inferred from models I and II are in general compatible with field observation, although the match between ω from the curve fit and a deterministic estimate $\omega(A,B,\Delta\sigma,V,C)$ from (2.1) is not always good. This exceedence of a deterministic ω (in almost every case) is also related to the poor fit to (and systematic underestimation of) recurrence statistics at the highest magnitudes seen in the figures. Perhaps it is not strictly meaningful to compare the two estimates of the maximum magnitude (from the curve fit and the deterministic value from known fault areas) in any case, since ω from the curve fit is defined as the maximum magnitude ever, for $T = \infty$, and as such must include values greater than those previously observed in a short time span (even

via the deterministic estimation). By definition then the statistical value of ω is an overestimate, and this leads to a compensating underestimation of the hazard from large events below this value in the curve fit.

The tables 2.1 and 2.2 show some small differences between (ω, u, λ) found from the cumulative frequency and extreme value data for the Mediterranean area. u is pretty much the same (within σ_u) but ω is smaller (with corresponding higher λ) to reflect the tighter curve found by using extreme values. This might be expected because the extreme values are naturally chosen at larger magnitudes - where curvature is more likely. To some extent this discrepency would lessen as the sample time increased, and eventually the values should coalesce at $T = \infty$.

The differences between the two approaches can also be seen by comparing the predictions of m_T in tables 2.3 and 2.4. The Weibull curve fit to the cumulative frequency data gives slightly higher values for m_T in the Mediterranean and in Southern California. From this comparison of (ω, u, λ) and m_T it can be concluded that the basic assumptions to derive the extreme value distribution (1.14) do not seem to hold for these two data sets. For example there is no infinite sample of events, and at least some of the earthquakes are causally related (especially, say, the aftershocks of the 1952 Kern Co event in Southern California).

Consistent underestimation of the probability of occurrence of largest events in the catalogue is also strongly indicative of an auto-correlation error between the value of ω and the probability of occurrence of smaller magnitudes. This is inherent in both curve fits. This will be illustrated more fully in the next chapter when discrete frequency statistics are considered

(fig 3.2).

Another serious theoretical drawback of the distribution used is that $n(\omega) = 0$. For a cyclic input and release of strain energy $n(\omega)$ might be expected to take some non-zero value, implying a repeat time $T = 1/N(m)$ which is not infinite as $m \to \omega$.

However, despite these qualifications it can be seen that careful quantitative comparison of $\dot{M}_o \pm \delta\dot{M}_o$ can be used as a method of distinguishing areas where the curve fit is indeed applicable at the highest magnitudes. Incorporation of better deterministic values for the maximum magnitude (from seismicity trends or geological zoning), and geological estimates of their average repeat times could also improve the quality of the curve fit at these magnitudes.

Typical uncertainties in $\dot{M}_o$ were found to be a factor of 2-4 or so, with the extreme value estimates giving slightly lower uncertainties, and agreement within this range with observed moment release from (i) a short term catalogue for an internal consistency check in the Mediterranean and (ii) long term geological estimates in Southern California indicates that this approach may be usefully applied in several other seismic zones of the world.

2.5 Recent developments

Since the work for this chapter was completed and published (see inclusion Main and Burton, 1984a) some new observations have come to light which are relevant and consistent with the interpretation of the results of this chapter. The first concerns Sieh's (1978) estimate of the surface wave magnitude of the 1857, Southern California, earthquake. He estimated $M_s > 8\frac{1}{4}$, because the macroseismic effects of the 1857 event exceeded those of the 1906,

San Francisco earthquake, and this latter event had been assigned an instrumental magnitude of $8\frac{1}{4}$. Abe and Noguchi (1983) have now confirmed an observation by Neilson (1983, pers. comm.) that this was due to an overestimation of about 0.5 magnitude units on the latter event, because of incorrect damping constants being used on seismograms from the very early 1900s.

This confirmed some suspicions aroused in section (2.3(c)) by looking at the curve fits around the data point associated with Sieh's work in Southern California. This point should have been at T = 163 years, $M_s = 7\frac{3}{4}$, rather than $M_s = 8\frac{1}{4}$, which would have brought it within the covariance error bounds of the extreme value curve fit shown on fig 2.11.

The second point is that several other examples of the bimodal distribution observed in the New Madrid area have now been observed around the world: Båth (1981b) observed a strikingly similar shape to that of fig 2.7 in Turkish recurrence statistics, and attributed this to the predominence of aftershock sequences in the earthquake catalogue. (This interpretation would also hold for the New Madrid area if aftershocks can take place away from the main fault plane.); Singh et al (1983) found similar behaviour in Mexico, but did not suggest a cause; Schwartz and Coppersmith (1984) explain a bimodal distribution in the frequency-magnitude statistics of the Wasatch zone (including geologically estimated data points similar to Sieh (1978)) in terms of two separate characteristic fault lengths in the area. The discussion on New Madrid in this chapter goes one step further than this latter reference in considering slip rates also; a further example from Southern California with a slightly different interpretation will be given in the next chapter.

All of these observations of characteristic bimodal

distributions are consistent with so-called 'Asperity models' (e.g. Aki, 1984), which lead to a predominence of a few characteristic earthquake sizes, reflected as a few bumps on the frequency magnitude distribution. The idea is that, just as some rocks can be broken down into similar-sized elementary blocks by jointing, so can larger scale fractures such as faults by bends and inhomogeneities, and subsequent concentration of stress around these so-called 'asperities'.

This macroscopic quantisation of earth materials into characteristic lengths seems to apply to various scales of rock fracture (Sadovskii et al, 1982): from clast sizes (mm) in rock samples, through 1 m joints to 100 m blocks for small earthquakes, 10 km lengths in the Intermediate magnitude range of New Madrid, for example, and the 100 km length of the dominant fault in the same area. The results of many other more recent empirical observations are therefore in agreement with the results obtained in this chapter, and their interpretation is consistent with the quantitative attempts made here to explain their qualitative and quantitative form.

2.6 . Summary

First of all several examples of the relationship between a physical maximum magnitude and curvature in the cumulative frequency magnitude distribution were discussed, and a formal relationship between maximum fault area and a deterministic maximum magnitude was given. Two new theoretical models were then developed to extend Anderson's (1979) model of crustal deformation to the Weibull distribution and Gumbel's third distribution of extreme values, including in both cases an estimate of the error.

These two models were then applied to four diverse tectonic

zones, with interesting results. In particular the New Madrid seismic zone shows two distinct curves which can be related within a factor two or so to two sets of geological and geophysical observations of characteristic maximum fault areas and slip rates. Superposition of many such (curved) characteristic distributions may explain the observed linearity of the global frequency/seismic moment distribution observed by Chinnery and North (1975). All estimates of ω are consistent with geological estimation within their errors (which turn out to be of the order of factor 3 or 4), but the geological estimates of fault area often imply that ω found by these statistical methods is larger than the deterministic value based on fault areas. Even though a large statistical error in ω allows for this, this systematic difference, which leads directly to an underestimation of the actual occurrence rates of large magnitudes just below ω in the curve fit, represents a consistent autocorrelation effect in the method. Of course the statistically determined value of ω would in general be expected to approach the deterministic value from above as longer catalogue time spans are considered and so a statistical ω larger than the deterministic value is logical. However if this causes a consistent underestimation of the hazard (ie the probability of occurrence) of events which are known to have occurred then this autocorrelation becomes significant. Despite this qualification the method could usefully be applied to several areas of the world in studies similar to the present one.

To summarise, this <u>empirical</u> method is reasonably good for evaluating moment release rates (and modelling the observed curvature) but is not always successful when comparing the statistical maximum magnitude with a deterministic value obtained

from a maximum fault area. This subsequently led to the development of a completely new approach which includes these two pieces of information automatically, by a direct method which will be discussed in the next chapter. This avoids any dichotomy, for example, of comparing the statistical quantity ω with a deterministic maximum fault area, by effectively merging the short-term statistical magnitude data with long-term geological data which are dominated by the large events near ω.

CHAPTER 3

A new frequency magnitude distribution

3.1 Introduction

The previous chapter has shown how the choice of an empirical distribution can lead to systematic differences between the earthquake data and the curve or line fit. It seems that a Weibull distribution consistently underestimates the average repeat times of large events and the statistically determined ω exceeds a deterministic estimate of the maximum magnitude from geological evidence, although in some cases this could be due to overestimation of the largest catalogue magnitudes. In another study Anderson and Luco (1983) concluded that Caputo's distribution (equation 1.9) does not fit the data of table 1.1 as well as a truncated exponential (equations 1.6 or 1.7). However there are areas of the world where a truncated exponential also does not describe the seismicity (for example see fig 3.2 for the Mediterranean catalogue).

A further problem is introduced by the possibility of superposition of characteristic fault sizes highlighted by the previous chapter's results for the New Madrid seismic zone. The aim of this chapter is to develop a method of avoiding the problems inherent in the somewhat arbitrary choice of a given empirical distribution, and which also allows for possible superposition in estimating the repeat times of the great events which are longer than the historical or instrumental catalogue. The aim is to develop a joint distribution which combines the information from (a) the earthquake catalogue (instrumental and

historical) and (b) the geological record in a way which involves a minimum of assumptions. Thus the recurrence rates and associated average repeat times of large earthquakes can be estimated without having to extrapolate blindly from a short term catalogue. Once again it is the geological record and the information represented by the slip rate and the observed seismogenic fault area which is the crucial addition to the seismicity statistics.

One natural method of combining the data from a short term catalogue of events and the long term geological observation in an unbiased way is to use the principles of Information theory. This method accepts that knowledge of the system is incomplete and chooses an estimate (or inference) of the distribution which is the least biased with respect to this ignorance. Of course there are an infinite number of distributions which are consistent with an underdetermined problem such as earthquake recurrence statistics. Information theory picks only the most likely form consistent with the limited knowledge of the system, usually expressed in terms of an average observation of one or more of the parameters which can be measured. To do this involves maximising an entropy function which quantifies the information content and is subject only to the constraints which are put in, i.e. the information which is available. Even if this distribution requires subsequent modification with increasing knowledge of the system it remains the best <u>contemporary</u> solution to the problem (Jaynes, 1957).

3.2 The earthquake frequency-magnitude distribution from Information theory

3.2.1 Derivation of the distribution

Information theory is applicable in a wide class of problems where the average value of a physical parameter can be estimated even though it may deviate significantly from this value from time to time. Its methods have been shown to be methematically identical to, but are more general than those of statistical mechanics (Jaynes, 1957). Berrill and Davis (1980) have previously applied it to the earthquake frequency-magnitude distribution to derive the truncated Gutenberg-Richter law of equations (1.6) and (1.7) for historical earthquake catalogues. In this section their results are extended by the direct inclusion of the long-term average strain energy release through the seismic moment release rate.

Consider the continuous range of magnitudes (m_c, ω), where ω is the maximum magnitude consistent with the finite breaking strain of the earth and the finite dimensions of the source zone, and m_c is an arbitrarily chosen lower bound. m_c may be physically determined by the minimum dimension which will support seismic rupture, as well as by other physical constraints such as stress drop and friction along the fault, but in practice will usually be the lower bound of complete reporting of events.

For this magnitude range a probability function must be picked in a way which avoids a biased choice, but is consistent with currently available knowledge. This is similar to the common problem in statistics of devising some method of sampling that avoids bias. Shannon (1948) showed that there is a unique, unambiguous criterion for the "amount of uncertainty" represented

by such a probability distribution. Shannon proved that the only quantity which is positive, which increases with increasing uncertainty, and is additive for independent sources of uncertainty is

$$S(p) = -\int_{m_c}^{\omega} p(m)\, \ln\{p(m)\}dm \ , \qquad (3.1)$$

where p(m) is the probability density function of magnitudes in this case (Berrill and Davis, 1980). Jaynes (1957) demonstrated that the thermodynamic entropy was mathematically equivalent to Shannon's definition, which can also be called the 'Information theory entropy'. In this section a distribution p is sought by maximising S (for minimum ignorance or uncertainty, maximum information content) subject to the constraints

$$\int_{m_c}^{\omega} p(m)dm = 1 \ , \qquad (3.2)$$

$$\int_{m_c}^{\omega} m\, p(m)dm = \langle m \rangle \ , \qquad (3.3)$$

$$\int_{m_c}^{\omega} M_o(m)\, p(m)dm = \langle M_o \rangle \ , \qquad (3.4)$$

where $M_o(m)$ is given by the moment-magnitude relation (1.5).

$\langle m \rangle$ and $\langle M_o \rangle$, respectively the average magnitude and moment per event in the range (m_c, ω), are the two pieces of information which are available about the system. In this case the

expectation value and the mean value are equivalent, so to avoid confusion later on the notation here sticks with $\langle m \rangle$ etc to comply with the first definition in (3.3). $\langle m \rangle \pm \sigma_{\langle m \rangle}$ is evaluated simply from the earthquake catalogue once m_c is specified (see Appendix 1, MAXENT-FF1 for a computer program; σ is a standard error in the mean) and $\langle M_o \rangle \pm \sigma_{\langle M_o \rangle}$ may be inferred from a catalogue of moments where this is available, from geological or geophysical evidence of long-term fault movement, or from current plate tectonic models. Note that $\langle M_o \rangle$ is proportional to the average release of seismic strain energy via (1.4). The quantity normally accessible is $\dot{M}_o$ - the rate of release of seismic moment, but this is related quite simply to $\langle M_o \rangle$ by $\langle M_o \rangle = \dot{M}_o / N_T$, where N_T is the total number of events in the catalogue per unit time.

The method of Lagrangian undetermined multipliers applied to these four equations (Appendix 2A) gives

$$p(m) = \exp\{-\lambda_1 m - \lambda_2 M_o(m)\}/Z \ , \tag{3.5}$$

where Z is given by

$$Z = \int_{m_c}^{\omega} \exp\{-\lambda_1 m - \lambda_2 M_o(m)\} dm \ . \tag{3.6}$$

Z is the function which is necessary in order that (3.5) satisfies the normalisation criterion (3.2).

It is easy to show (Appendix 2B) that

$$\langle m \rangle = -d\{\ell n(Z)\}/d\lambda_1 \tag{3.7}$$

$$\langle M_o \rangle = -d\{\ell n(Z)\}/d\lambda_2 \ .$$

In principle, equations (3.7) could be solved and the distribution uniquely specified in terms of the three variables $\langle m \rangle$, $\langle M_o \rangle$, ω, once m_c has been chosen. Unfortunately this must be done numerically because (3.7) has no analytical solution. The method that was applied here involves an iteration procedure from starting values of λ_1 and λ_2, using a third order finite-difference formula due to Gill and Miller (1972) to evaluate the complicated integrals $\langle m \rangle$ and $\langle M_o \rangle$ (see Appendix 1, the program is called MAXENT-FF2).

The cumulative form of the probability distribution is defined by

$$P(x>m) = \int_m^\omega p(x)dx = N(x>m)/N_T \ , \qquad (3.8)$$

if N is the cumulative frequency distribution. The number density $n(m) = -dN(x>m)/dm$ is then given by $n = N_T p$, or

$$n(m)dm = C \exp\{-\lambda_1 m - \lambda_2 M_o(m)\}dm \ , \qquad (3.9)$$

where $C = N_T/Z$, and $M_o(m)$ is given by (1.5).

It will be noted that $\langle m \rangle$, $\langle M_o \rangle$, Z and N_T all depend on the range chosen (m_c, ω), but are most sensitively dependent on m_c. For the purpose of the present type of work this will not matter if (a) the terms λ_1 and λ_2 are reasonably constant independent of the choice of m_c, and (b), proper normalisation is carried out by using (3.2) and (3.8). It is obvious that (a) can only be effected by considering a range of events where we are sure the catalogue is complete, and (b) is taken care of by the terms Z and N_T which

will vary according to the choice of m_c. It will also be shown that the relative independence of λ_1 with respect to m_c is due to a constant similarity dimension in the fault geometry in the following sections. This criterion is equivalent to what will be called dimensional (geometric) self-similarity.

3.2.2 A physical model from statistical mechanics

In order to interpret (3.9) a physical model of a fault is now considered and the methods of statistical mechanics are applied to its localised elements. These elements may be as small as the lattice constant of the predominant crystal, or may be related to inhomogeneities such as joints or bedding planes. In the following it is assumed that the elemental areas A_o are small enough to warrant a continuous approach.

Consider an arbitrary two dimensional area $A \approx \ell^2$ which ruptures during an event on the fault plane A_{max} (fig 3.1). Assuming a constant strain drop (so that the model is geometrically self similar and therefore can be scaled up or down without altering this dimensionless quantity) the fault slip $s \propto \ell$, so that $M_o \propto \ell^3$ from (1.4).

If an energy level E is characterised by the symbol r, and can be filled in g ways then the discrete frequency F of state transition by statistical mechanics is given by

$$F_r = g_r \exp\{-\lambda_2' (E_r - E_{r'})\} . \qquad (3.10)$$

$\Delta W = (E_r - E_{r'})$ in this case is the change in strain energy which is proportional to M_o via (1.4), and λ_2' depends on the average energy $\langle E \rangle$. In thermodynamics $\langle E \rangle = kT$ for example. The

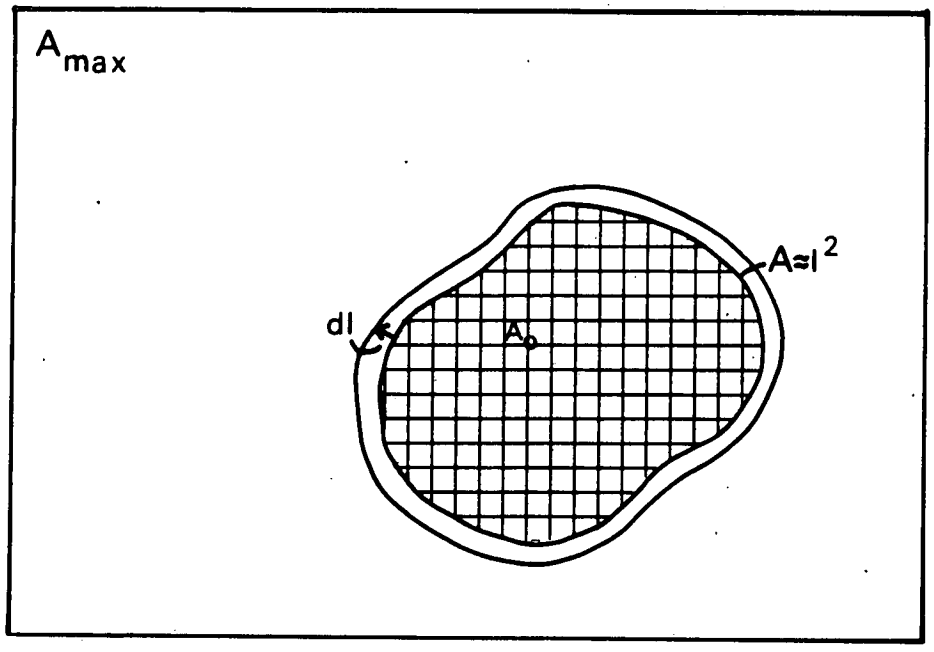

Figure 3.1 A two dimensional geometric fault model. The area A can fit into A_{max} in A_{max}/A ways. A_o represents the physical lower limit to seismic energy release and depends on the spacing of inhomogeneities in the earth. The density of degenerate states, if A_o is assumed to be very small and $A = \ell^2$, is

$$d(\ell)d\ell = \{A_{max}/\ell^2\} - \{A_{max}/(\ell + d\ell)^2\} = 2A_{max}/\ell^3 d\ell.$$

degeneracy g is given by a simple geometric constraint on $M_o(\ell)$. On a planar fault as in fig 3.1, $g(\ell) = A_{max}/A(\ell)$ so that, for the continuous case, the density $d(\ell)$ of degenerate states is given by

$$d(\ell)d\ell = g(\ell)-g(\ell+d\ell) = (2A_{max}/\ell^3)d\ell \ , \qquad (3.11)$$

after binomial expansion and ignoring terms in $d\ell^2$ and higher.

This can be compared with Caputo's (1976) postulate

$$d(\ell) \propto \ell^{-\nu} \ . \qquad (3.12)$$

In a planar fault of two dimensions (say D=2), $\nu=3$ by comparing (3.11) and (3.12) and so

$$D = \nu - 1 \ , \qquad (3.13)$$

in this case. However, it can be seen by induction that this holds for any value of the dimension D and the power of the length density distribution ν. This concept of dimension will be discussed more fully later.

Meanwhile the variable in (3.11) is converted from length to moment using $M_o \propto \ell^3$; $dM_o \propto \ell^2 d\ell$

$$\begin{aligned} d(M_o)\ dM_o &= d(\ell)d\ell \\ &\propto M_o^{-(\nu+2)/3} dM_o \ , \end{aligned} \qquad (3.14)$$

and then to magnitude via (1.5)

$$d(m)\,dm = d(M_o)\,dM_o$$

$$\propto \exp\{(\alpha+\beta m)\,(\frac{1-\nu}{3})\}\,dm\ . \qquad (3.15)$$

If $d(m) \propto e^{-b'm}$ then

$$b' = \beta\,(\frac{\nu-1}{3}) \quad \text{or} \quad b = B\,(\frac{\nu-1}{3})\ . \qquad (3.16)$$

The continuous number density $n(\ell)$ is then given by a combination of the geometric term with a Boltzmann exponential

$$n(\ell)d\ell = d(\ell)d\ell\,\exp(-\lambda_2 M_o(\ell))\ , \qquad (3.17)$$

where $\lambda_2 M_o = \lambda_2' \Delta W$ from (1.4), or

$$n(m)\,dm = \text{const.}\ e^{-b'm} e^{-\lambda_2 M_o(m)} dm\ . \qquad (3.18)$$

This form is identical to (3.9) if $\lambda_1 = b' = b \ln 10$.

Thus the distribution (3.9) can be interpreted as a Boltzmann distribution of possible energy transitions in a stressed zone, multipled by a geometric factor which is directly related to the dimension of the source zone and is represented by the familiar b-value.

3.2.3 A note on fractal dimension

By combining (3.13) and (3.16) an interesting result is obtained

$$b = \frac{B\,D}{3} \approx D/2\ , \qquad (3.19)$$

if $B \approx 3/2$. Thus the dimensions of the source zone of 1, 2, 3 correspond to b-values of $\frac{1}{2}$, 1, $1\frac{1}{2}$ which covers both the empirically observed range (section 1.2) and the permissible range for finite energy release (section 1.7, equation 1.21). Thus the observation that $b < 3/2$ is a consequence both of a finite energy density, and of the release of that energy in a cracked surface which can fill (at most) a volume (D=3). This combination of ideas enhances the statistical mechanical interpretation of the previous section.

It is interesting to note that data on Californian fault breaks at the surface indicate that $\nu = 2.5$ (Caputo, 1982). This would imply $b = 0.75$, in good agreement with theoretical models developed by Petrov (1981), where $b = 0.75$ results from random statistical fluctuations in microcrack density and Vere-Jones (1976) where $b = 0.75$ results from a critical branching model. The non-integer D implies by analogy with the normal concept of density, a density distribution of fault lengths which has a fractal (ie non-integer) dimension ($D=\nu-1=1.5$ in this example). The fractal dimension of the fault geometry may be modelled by (a) irregularities along the main fault break or (b), scattered smaller replicas of the original fault (see Mandelbrot, 1982). Caputo's (1982) value for ν only accounts for (b) because only surface breaks are considered, which may explain why the b value predicted from ν under-estimates the empirical value for b of 0.87 (Epstein and Lomnitz, 1966) and 0.89 ± 0.03 (this chapter, section 3.3.2).

3.2.4 Uncertainties in the distribution and its predictions

The distribution (3.9) represents the most likely form of the frequency magnitude relation consistent with $\langle m \rangle$ and $\langle M_o \rangle$. These

two parameters have associated uncertainties which are independent, and can be related to the uncertainties in λ_1 and λ_2 by the solution of a series of four equations for the propagation of standard errors of the form, for example

$$\sigma^2_{\langle m\rangle} = \left\{\frac{\partial\langle m\rangle}{\partial\lambda_1}\right\}^2 \sigma^2_{\lambda_1} + \left\{\frac{\partial\langle m\rangle}{\partial\lambda_2}\right\}^2 \sigma^2_{\lambda_2} + \left\{\frac{\partial\langle m\rangle}{\partial\lambda_1}\right\}\left\{\frac{\partial\langle m\rangle}{\partial\lambda_2}\right\} \sigma^2_{\lambda_1\lambda_2} + \left\{\frac{\partial\langle m\rangle}{\partial\lambda_2}\right\}\left\{\frac{\partial\langle m\rangle}{\partial\lambda_1}\right\} \sigma^2_{\lambda_2\lambda_1} \quad .$$

These four similar equations in $\sigma^2_{\langle m\rangle}$, $\sigma^2_{\langle M_o\rangle}$, $\sigma^2_{\langle mM_o\rangle}$, $\sigma^2_{\langle M_o m\rangle}$ can be reduced to a matrix form as

$$\begin{Bmatrix} a^2 & b^2 & ab & ba \\ b^2 & c^2 & bc & cb \\ ab & bc & ac & b^2 \\ ba & cb & b^2 & ca \end{Bmatrix} \begin{Bmatrix} \sigma^2_{\lambda_1} \\ \sigma^2_{\lambda_2} \\ \sigma^2_{\lambda_1\lambda_2} \\ \sigma^2_{\lambda_2\lambda_1} \end{Bmatrix} = \begin{Bmatrix} \sigma^2_{\langle m\rangle} \\ \sigma^2_{\langle M_o\rangle} \\ 0 \\ 0 \end{Bmatrix} , \qquad (3.20)$$

where $$a = \frac{\partial\langle m\rangle}{\partial\lambda_1} = \langle m\rangle^2 - \langle m^2\rangle \quad ,$$

$$b = \frac{\partial\langle m\rangle}{\partial\lambda_2} = \frac{\partial\langle M_o\rangle}{\partial\lambda_1} = \langle m\rangle\langle M_o\rangle - \langle mM_o\rangle \quad ,$$

$$c = \frac{\partial\langle M_o\rangle}{\partial\lambda_2} = \langle M_o\rangle^2 - \langle M_o^2\rangle \quad ,$$

follow from differentiating (3.3) and (3.4). At this point note that $\dot{M}_o = \langle M_o\rangle \dot{N}_T$ is a function of the slip rate, whereas $\langle m\rangle$

depends only on the individual magnitudes in the catalogue. $\dot{M}_o$ varies hardly at all with changing m_c because it is dominated by the larger events but $\langle m \rangle$ varies dramatically. Therefore $\langle M_o \rangle$ and $\langle m \rangle$ are essentially independent variables, which is why it has been assumed that $\sigma_{\langle m\, M_o \rangle} = \sigma_{\langle M_o m \rangle} = 0$ in (3.20). This equation can be simplified slightly by subtracting the bottom row from the third to give

$$(ac - b^2)\, \sigma^2_{\lambda_1\lambda_2} - (b^2 - ac)\, \sigma^2_{\lambda_2\lambda_1} = 0 \quad , \tag{3.21}$$

or, since $ac - b^2$ is not in general zero

$$\sigma^2_{\lambda_1\lambda_2} = \sigma^2_{\lambda_2\lambda_1} \, . \tag{3.22}$$

Thus a simpler problem remains:

$$\begin{Bmatrix} a^2 & b^2 & 2ab \\ b^2 & c^2 & 2bc \\ ab & bc & ac+b^2 \end{Bmatrix} \begin{Bmatrix} \sigma^2_{\lambda_1} \\ \sigma^2_{\lambda_2} \\ \sigma^2_{\lambda_1\lambda_2} \end{Bmatrix} = \begin{Bmatrix} \sigma_{\langle m \rangle} \\ \sigma_{\langle M_o \rangle} \\ 0 \end{Bmatrix} . \tag{3.23}$$

This equation was solved by diagonalising the 3 x 3 matrix and back-substitution, using very high precision to avoid rounding error. (The program MAXENT-FF3 in Appendix 1 does this job).

The contribution to errors in the cumulative frequency distribution N are then added up. These are: the covariance terms in λ_1 and λ_2 which depend on uncertainties in the moment release rate $\dot{M}_o$ and a standard error in $\langle m \rangle$; fluctuations in N_T as seen in the completeness graphs in Chapter 2; a measuring uncertainty in the magnitude ω; a variable A parameter to quantify uncertainties

in the moment-magnitude relation. The latter criterion is necessary since eventually the distribution (3.9) (which is cast in terms of M_w) will be compared with empirical data (in M_s or M_L). The form of the propagation of errors equation in a quantity $N(\langle m\rangle, \langle M_o\rangle, N_T, \omega, A)$ is

$$\delta N^2 = \left\{\frac{\partial N}{\partial \langle m\rangle}\right\}^2 \sigma^2_{\langle m\rangle} + \left\{\frac{\partial N}{\partial \langle M_o\rangle}\right\}^2 \sigma^2_{\langle M_o\rangle} + \left\{\frac{\partial N}{\partial N_T}\right\}^2 \sigma^2_{N_T}$$

$$+ \left\{\frac{\partial N}{\partial \omega}\right\}^2 \sigma^2_{\omega} + \left\{\frac{\partial N}{\partial A}\right\}^2 \sigma^2_{A},$$

but it is necessary to recast the uncertainties in the parameters $\langle m\rangle$ and $\langle M_o\rangle$ in terms of λ_1 and λ_2 because there is no analytical form for $\partial N/\partial\langle m\rangle$ and $\partial N/\partial\langle M_o\rangle$. This requires the addition of the covariance terms in λ_1 and λ_2. Formally the final uncertainty in N is taken to be

$$\delta N^2 = \left\{\frac{\partial N}{\partial \lambda_1}\right\}^2 \sigma^2_{\lambda_1} + \left\{\frac{\partial N}{\partial \lambda_2}\right\}^2 \sigma_{\lambda_2} + \left\{\frac{\partial N}{\partial \lambda_1}\right\}\left\{\frac{\partial N}{\partial \lambda_2}\right\} 2\sigma^2_{\lambda_1\lambda_2}$$

$$+ \left\{\frac{\partial N}{\partial N_T}\right\}^2 \sigma^2_{N_T} + \left\{\frac{\partial N}{\partial \omega}\right\}^2 \sigma^2_{\omega} + \left\{\frac{\partial N}{\partial A}\right\}^2 \sigma^2_{A}. \qquad (3.24)$$

Errors in $T(m) = 1/N(m)$ can also be allowed for via $\delta T/T = -\delta N/N^2$. (MAXENT-FF5 (Appendix 5) evaluates average repeat times and errors from (3.24), given m). A similar equation to (3.24), with N replaced throughout by m_T holds for the error in m_T, which is solved for by MAXENT-FF4 (Appendix 1) for different values of T, given (3.9).

3.3 Application of the distribution

In order to test the validity of the approach developed in this chapter, two regions were chosen for analysis - the requirements being that the catalogue was large enough for reasonable statistical treatment of discrete frequencies

$$F(m) = \int_{m-\delta m/2}^{m+\delta m/2} n(m)\, dm \quad , \tag{3.25}$$

and the availability of reasonable data on $\dot{M}_o$. Thus the catalogue for the Central and Eastern Mediterranean was chosen for an inspection of the properties of the distribution as an internal consistency check, and the catalogue for Southern California as a test of the primary objective of this thesis - the direct incorporation of seismotectonic deformation rates into earthquake hazard evaluation.

3.3.1 The Central and Eastern Mediterranean

Since the method and the particular programs which were used for each step have been outlined in section 3.2, and a description of the earthquake catalogue and moment release rates were given in the previous chapter, only the results are presented in this and the following section.

Figure 3.2 (which was drawn by MAXENT-G in Appendix 1) shows the theoretical line (expressed in terms of M_w via (1.5)) for $m_c = 4.75$ compared to discrete frequency data (M_s). The dotted line corresponds to a Weibull curve fit. It can be seen at a glance that the distribution (3.9) fits the data better than the Weibull curve, which consistently overestimates the occurrence of

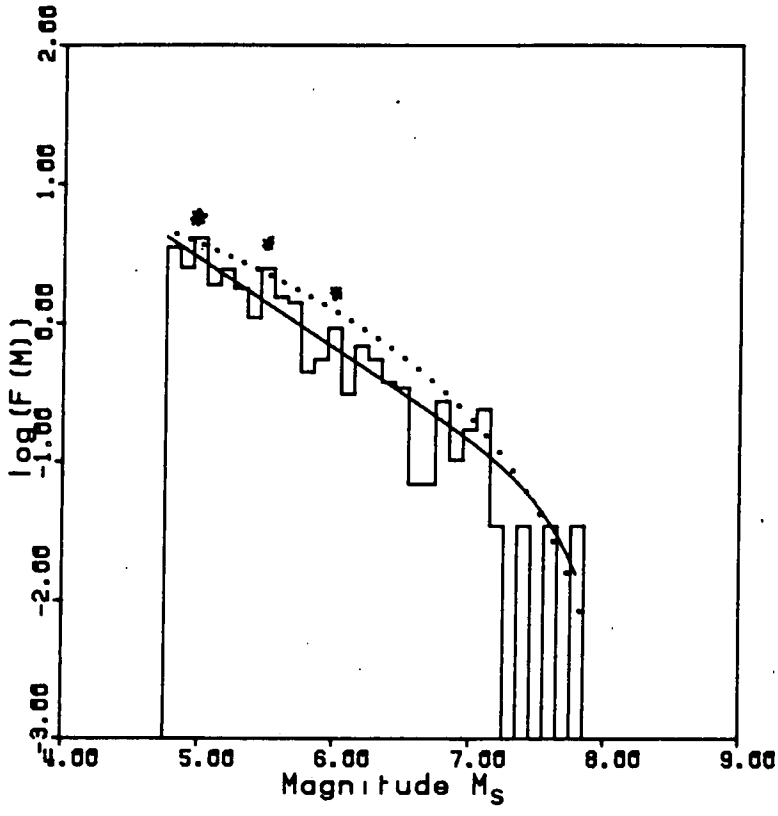

Figure 3.2 Discrete frequency plot of earthquake magnitudes for the Central and Eastern Mediterranean. Discrete frequency-magnitude data (m_i, F_i) are compared with the theoretical distribution (3.9) (solid line). A summary of the parameters of this distribution is given in tables 3.1 and 3.2, for a lower completeness threshold m_c = 4.75. An extrapolation of the straight line portion of the distribution (a truncated exponential) overestimates the occurrence of the highest magnitudes. The autocorrelation error of the Weibull fit (dotted line) is evident in the middle range. The good agreement between the theoretical (M_w) line and the empirical data (M_s) indicates internal consistency of the method. M_w is defined here as the unsaturated M_s scale. The points marked (*) indicate reader bias towards the points (5.0, 5.5, 6.0), a reflection of the accuracy of earlier instruments (±0.5).

the middle range of magnitudes. On the other hand a truncated exponential would extrapolate the straight line portion and overestimate the occurrence of the highest magnitudes. In general terms the Information theory distribution seems to combine the best features of both empirical distributions.

Another advantage that the distribution (3.9) has is that the line is always directly compatible with the best estimates of ω and $\dot{M}_o$ because these constraints are actually fed in to the distribution. Empirical line fits can only be consistent with these best estimates within certain error bounds. The figure shows one aspect of the magnitude uncertainty quite clearly - namely the consistent overestimation of $\frac{1}{2}$-magnitude intervals due to a magnitude uncertainty of ± 0.5, particularly in the early years of seismology. The good agreement of the theoretical line (M_w) and the empirical data (M_s) indicates that the values of A and B discussed in Chapter 2 are valid within the error bounds of the method, expressed here by δA.

Figure 3.3 shows the cumulative frequency fit with error bounds. $\sigma_{<m>}$ and σ_{N_T} are given by standard errors on their means. The bounds also include a possible error in the moment-magnitude parameter A of ± 0.2 from inspection of North (1974), in ω of ± 0.3 as a typical magnitude uncertainty and an arbitrary allowance for 50% uncertainty in $\dot{M}_o$. The uncertainty in A quantifies the error due to the necessity of comparing a theoretical line (M_w) with the data (M_s). Note that despite the possibility of superposition (above and below $M_s \approx 7$) the distribution fits the data well within the given error bounds. This agreement between data from a catalogue with magnitudes and moment release rates measured from the same seismograms and a theoretical distribution based on making

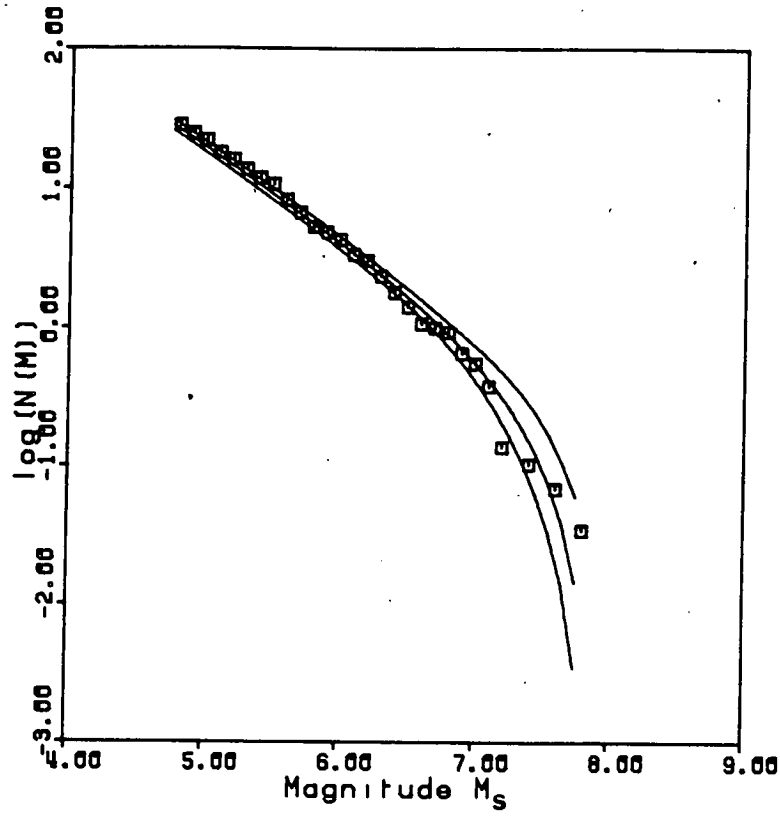

Figure 3.3 Cumulative frequency plot of earthquake magnitudes for the Central and Eastern Mediterranean. Cumulative frequency data (m_i, N_i) are compared to the theoretical distribution (3.9) and its error bounds. Despite the possibility of two earthquake populations (above and below magnitude 7) the line fits well considering the errors.

the best use of limited knowledge otherwise indicates that the method is indeed internally consistent. This internal consistency - or self-consistency - is an important check on the validity of the distribution (3.9).

Table 3.1 summarises the effect of altering m_c on the parameters and uncertainties. Since magnitude is normally quoted to one decimal point ($\delta m = 0.1$ in (3.25)) m_c was chosen as $4.5 + \delta m I/2$, where I is integral. (Chapter 2 showed that the catalogue was complete above magnitude 4.5). The table shows that b stays reasonably constant with increasing m_c (within its error), although there is a tendency both for b and σ_b to increase with m_c. This systematic trend is offset by a tendency for λ_2 to decrease, and the resulting negative contribution to the error from the covariance term $\sigma^2_{\lambda_1\lambda_2}$.

The predictions of $m_T(\sigma_{m_T})$ which follow are given in table 3.2. It can be seen that all of the entries for given T are virtually identical, thus backing up the assumption of self-similarity which is important in the assumption of a constant strain drop as well as for the fractal interpretation of the b-value in section 3.2.

This discussion has shown that the distribution (3.9) is better than some of the alternatives, not only in the quantitative sense of fitting the empirical data better, but doing so in a manner which is directly consistent with the available knowledge of the seismotectonics of the area. An added bonus is that, despite the possible superposition of two seismicity distributions and the use of M_w for the theoretical line, the occurrence of the largest magnitudes (M_s) is matched well by the overall line.

Table 3.1 Variation in b and λ_2 with changing m_c for the Central and Eastern Mediterranean *

m_c	b^+ (σ_b)	λ_2 (σ_{λ_2}) x 10^{-20} $(Nm)^{-1}$	($\sigma^2_{\lambda_1\lambda_2}$)
4.45	0.59 (0.03)	0.36 (0.43)	(-0.025)
4.55	0.59 (0.03)	0.38 (0.46)	(-0.031)
4.65	0.63 (0.04)	0.40 (0.40)	(-0.029)
4.75	0.64 (0.04)	0.24 (0.39)	(-0.032)
4.85	0.66 (0.05)	0.22 (0.41)	(-0.039)
4.95	0.71 (0.06)	0.14 (0.39)	(-0.041)
5.05	0.66 (0.07)	0.23 (0.45)	(-0.059)

* ω is a constant at 7.85 ± 0.3, with

$\dot{M}_o$ = 8 ± 4 x 10^{19} Nm yr^{-1}

A = 9.0 ± 0.2, B = 1.5

+ $b = \lambda_1 \log_{10} e$; $\sigma_b = \sigma_{\lambda_1} \log_{10} e$

Table 3.2

Variation in $m_T(\sigma_{m_T})$ with changing m_c for the Central and Eastern Mediterranean

T in yrs \ m_c	4.45		4.55		4.65		4.75		4.85		4.95		5.05	
1	6.78	(0.07)*	6.77	(0.08)	6.75	(0.08)	6.75	(0.08)	6.73	(0.09)	6.69	(0.09)	6.72	(0.10)
2	7.09	(0.08)	7.05	(0.08)	7.04	(0.07)	7.04	(0.07)	7.02	(0.08)	7.00	(0.08)	7.02	(0.08)
5	7.32	(0.22)	7.31	(0.22)	7.32	(0.18)	7.33	(0.17)	7.32	(0.16)	7.31	(0.13)	7.31	(0.15)
10	7.46	(0.41)	7.46	(0.42)	7.48	(0.36)	7.49	(0.35)	7.48	(0.34)	7.50	(0.30)	7.48	(0.34)
20	7.58	(0.65)	7.57	(0.66)	7.60	(0.60)	7.61	(0.58)	7.61	(0.57)	7.63	(0.52)	7.60	(0.58)
50	7.69	(0.99)	7.68	(1.02)	7.71	(0.92)	7.72	(0.89)	7.72	(0.90)	7.74	(0.82)	7.72	(0.94)
100	7.75	(1.24)	7.74	(1.28)	7.77	(1.13)	7.77	(1.09)	7.78	(1.10)	7.79	(0.99)	7.77	(1.17)
200	7.79	(1.44)	7.79	(1.51)	7.80	(1.30)	7.81	(1.24)	7.81	(1.26)	7.82	(1.11)	7.81	(1.33)

* Uncertainties in m_T result from an equation similar to (3.24) with N replaced throughout by m_T

3.3.2 Southern California

The previous section checked for self-consistency of the method with contemporary data and compared the Information theory distribution with some commonly used empirical methods. In this section the aim is to test one of the primary objectives of this thesis - the direct incorporation of crustal deformation rates derived from data on a geological time span via the terms $\dot{M}_o$ and N_T, with a view to extrapolating beyond historical and instrumental time scales. Previously this has been done only indirectly by comparing moment predictions from extrapolation of line fits to contemporary data with quaternary evidence of fault movement. Examples are Anderson (1979) for the (linear) truncated Gutenberg-Richter law and Main and Burton (1984) (i.e. the results of Chapter 2) for the more general (curved) type III Weibull frequency distribution and its extreme value equivalent.

The area under study here has been subject to occasional major shocks, the last being in 1857 along the currently locked aseismic portion of the San Andreas fault. Sieh (1978) has shown that shocks of this order of magnitude repeat on average every $T = 163 \pm 27$ years, where the uncertainty is a standard error in the mean. The repeat time has varied from 55 - 275 years between the 9 events regarded as proven without reasonable doubt.

Sieh estimated the size of this event as $M_s > 8.25$, by comparison of macroseismic effects with those for the instrumentally recorded 1906 San Francisco earthquake. Singh and Havskov (1980) find that $A = 15.83$, $B = 1.5$ is most appropriate for Southern California in (1.5), and Anderson (1979) gives M_o for the 1857 event as 9×10^{20} Nm from the extent of the surface break and fault slip. These two data imply that $M_w = 8.1$ - showing

that the $M_o - M_w$ relation cannot account for the relatively high M_s value of the 1906 event.

Neilson (1983, oral communication) suggested that this was almost certainly due to incorrect gains being used on early seismograms, a view later confirmed in detail by Abe and Noguchi (1983). Their corrected magnitude for the San Francisco earthquake is about 7.8 (M_s) and since the macroseismic data indicate that the 1857 event in Southern California was larger, it might be expected that $M_s > 7.8$. (Both models in table 3.3 satisfy this criterion).

If an average slip rate at the 1857 fault break of 3.2 cm yr^{-1} is assumed and $s = \dot{s}t$ in (1.4) then an average magnitude $\bar{m} \approx 8.05 \pm 0.15$ M_w is found for appropriate values of t from Sieh's table of recurrence times (see table 3.3, model (b)). The slip rate is consistent within ±0.5 cm yr^{-1} with (a) the creep rate over four years in Central California -3.2 cm yr^{-1} (Lisowski and Prescott, 1981) (b) 4½ m of slip repeated every 163 years for approx 2000 yrs - 2.8 cm yr^{-1} (Sieh, 1978) and (c) geologically estimated slip rates on the San Andreas fault - 3.7 cm yr^{-1} (Anderson, 1979, table 1). This good agreement over different time scales also lends support to the stationarity hypothesis. A higher value for the relative plate motion across the San Andreas transform of 5.5 cm yr^{-1} indicates that a significant amount of movement occurs in a broad deformation zone around the main fault. The calculated value of $\bar{m}$ results from locally appropriate values of A (15.83) and B (1.5), $\mu \approx 3 \times 10^{10}$ Nm^{-2}, length L = 400 Km (Sieh, 1978) and depth 15 Km (Anderson, 1979). Table 3.3 summarises this speculative slip predictable model and compares it with the model of Anderson and Luco (1983), since some of the input parameters and assumptions are slightly different - for example the choice of the

Table 3.3 Comparison of the slip-predictable+ models of (a) Anderson and Luco (1983) and (b) this chapter

	Times t between events in years*	Model (a) (M_s)	Model (b) (M_w)
	112	7.74	7.96
	275	8.26	8.22
	225	8.15	8.17
	55	7.33	7.73
	225	8.15	8.17
	105	7.71	7.95
	195	8.06	8.12
	120	7.78	7.98
Average	163.4	7.8975	8.0375
Standard deviation	72.2	0.3119	0.1663

* From Sieh (1978)
+ Shimazaki and Nakata (1980)

moment-magnitude relationship.

The results of this table can be summarised by assuming that a reasonable estimate of the size of future events in this area is a magnitude greater than or equal to $\bar{m} - \delta\bar{m}$. Thus the point (m_i, N_i) can be included in the cumulative frequency graph of (7.90, 1/163) since $\bar{m} = 8.05$, $\delta\bar{m} = 0.15$; $N = 1/T$, $T = 163$ yrs (see fig 3.5).

Table 3.4 summarises the input and output parameters of the solution to the distribution (3.9) for this area from (a) the earthquake catalogue and (b) a plate tectonic model of the area. These results are plotted graphically in figs 3.4 and 3.5 for comparison with frequency magnitude data from the catalogue and the geologically inferred point. Table 3.5 gives the magnitudes m_T associated with average repeat times T in the area defined by the extent of the earthquake catalogue (see fig 2.3). A final result is that the long-term prediction of the occurrence interval for the largest events ($M_w > 7.9$) is once every 156 years, and considering the errors in the model the range is 87 - 281 years. This agrees very well with Sieh's observation of an average repeat time of 163 years, but varying within a range of 55-275 years (table 3.3).

Combining this average repeat time with the knowledge that the last great event ruptured the fault at Pallet Creek in 1857, a recurrence of this catastrophic event might be expected (on average) in 2013. Thus for a normal distribution of recurrence times the cumulative probability of Southern California being hit by a great earthquake will have reached 50% by this date.

3.4 Discussion of results

The first conclusion from figs 3.2-3.5 is that the distribution

Table 3.4 Summary of Input and Output parameters of the solution for the parameters of equation (3.9) for Southern Californian data.

(a) From the Earthquake catalogue 1932-1972 (Hileman et al, 1973)

m_c : 4.25
$\langle m \rangle$: 4.738 (0.014)
N_T : 25.512 (4.368) per year

(b) From a tectonic model (Anderson, 1979; Singh & Havskov, 1980; Sieh, 1978)

μ	:	3×10^5 bars	(30%)		
l	:	670 Km		A	: 8.83 (0.20)
l_{max}	:	400 Km	(25%)		
$\Delta\sigma_{max}$	:	70 bars	(30%)	$\dot{M}_o$	: 16 (8) $\times 10^{18}$ N m yr^{-1}
W	:	15 Km	(30%)		
$\dot{s}$	:	5.5 cm yr^{-1}	(20%)	ω	: 8.4 (0.3)
$\Delta\sigma$	:	50 bars	(40%)		

(c) Output parameters

λ_1 (σ_{λ_1}) : 2.041 (0.061)
λ_2 (σ_{λ_2}) : 0.040 (0.078)
($\sigma^2_{\lambda_1\lambda_2}$) : (-0.00207)

l is the length of the seismic zone studied.

W is the fault width.

l_{max} is the maximum length of possible fault break constrained by present bends and inhomogeneities. The assumption is that the northern boundary is constrained by the creeping segment of the San Andreas fault and the southern boundary by the termination of the quiescent zone where the deformation zone branches out and becomes more complex.

$\sigma^2_{\lambda_1}$, $\sigma^2_{\lambda_2}$, $\sigma^2_{\lambda_1\lambda_2}$ represents the covariance error resulting from equivalent uncertainties in $\langle m \rangle$ and $\langle M_o \rangle$, with $\sigma^2_{\langle mM_o \rangle} = 0$ due to independence.

A is correct for S.I. units.

All uncertainties are given in brackets.

Table 3.5

Magnitudes m_T associated with average repeat times T in years for Southern California

T	m_T	(σ_{m_T})
1	5.831	(0.089)
2	6.165	(0.092)
5	6.597	(0.096)
10	6.912	(0.098)
20	7.208	(0.098)
50	7.556	(0.099)
100	7.777	(0.128)
200	7.960	(0.213)

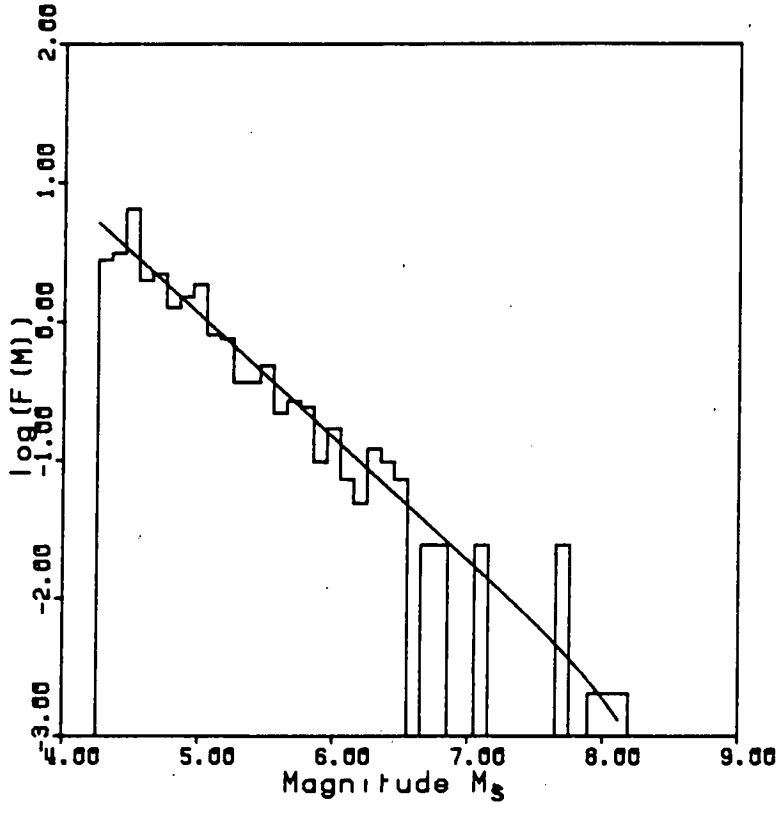

Figure 3.4 Discrete frequency plot of earthquake magnitudes for Southern California. Discrete frequency data (m_i, F_i) are compared with the theoretical distribution (3.9) (solid line). A summary of the parameters of the distribution is given in tables 3.3 and 3.4, for a completeness threshold $m_c = 4.25$. The point at magnitude 8.05 ± 0.15 is evaluated from the slip predictable model of table 3.3(b). Note once again the overestimation of half-magnitude intervals (4.5, 5.0, 5.5 etc) due to magnitude uncertainty in the early years of the catalogue. There is only a slight curve down at the highest magnitudes, in this case due to the small value of the curvature parameter λ_2. The actual data are a combination of local, surface and moment-magnitudes, with the theoretical solid line worked out for M_w.

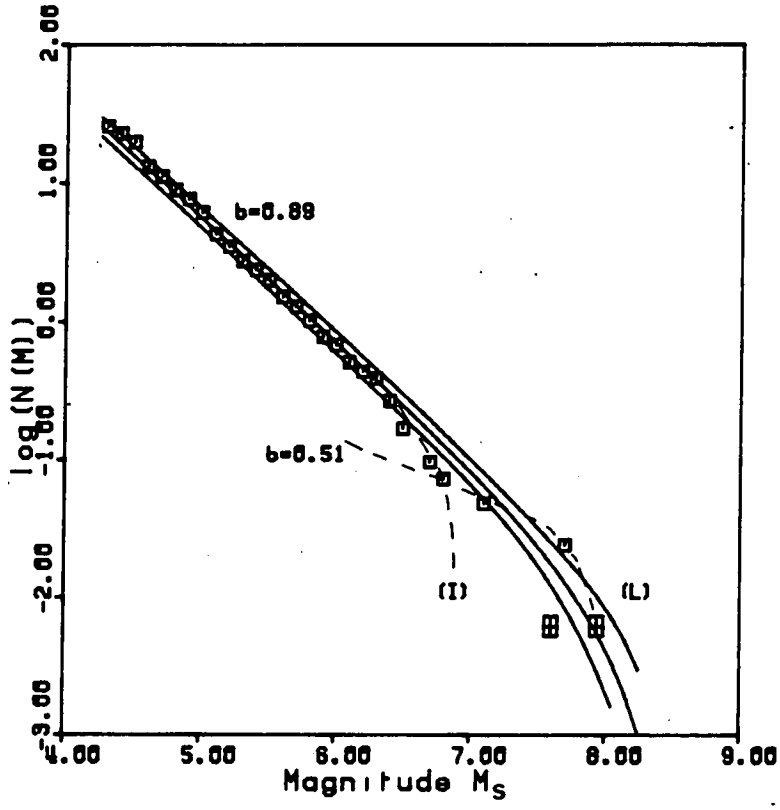

Figure 3.5 Cumulative frequency plot for Southern California. Cumulative frequency-magnitude data (m_i, N_i) are compared to the theoretical distribution (3.9) and its error bounds. Despite the possibility of superposition (of (I) - intermediate and (L) - large earthquakes) the extrapolation fits the M_w data from model (b) of table 3.3. Anderson and Luco's model (a) seems to underestimate the tectonic hazard, even considering error bounds. (Model (a) is the box at M_w 7.6, Model (b) the box at M_w 7.9). The largest events are consistent with a b-value of 0.51, which corresponds to a dimension of 1, and is consistent with the interpretation of the San Andreas fault system as the transform boundary between two thin plates.

developed in this chapter fits the data from the earthquake catalogue and the known seismic moment release rate well within its given error bounds. This is true both for $\dot{M}_o$ estimated from seismograms which were recorded within the time span of a shortened Mediterranean catalogue, and for a long-term estimate from tectonic slip rates in Southern California. Equation (3.9) certainly fits the Mediterranean data better than the forms of a truncated exponential or a Weibull distribution. In Southern California λ_2 is very small so a truncated exponential would probably be adequate here. However the extra information on $\dot{M}_o$ at long periods reduced the error at longer average repeat times compared to using only $\lambda_1 \pm \sigma_{\lambda_1}$ - via the negative covariance term $\sigma_{\lambda_1\lambda_2}$ - so even in the second example there is an improvement over existing methods.

Both examples show good correlation between the theoretical (M_w) lines and the empirical (M_s) data, thereby providing a consistency check on the values of A and B chosen. Another general point to notice on both cumulative frequency diagrams and in table 3.1 is the reasonably constant slope of the theoretical line (i.e. the b-value) and empirical data over two or three magnitude units above m_c. Since $b \approx 2D$ this represents self-similarity (i.e. a constant similarity dimension D) over a scale of about 1:10,000! (since 1 magnitude corresponds to a factor 30 or so increase in energy).

Where the assumption of self-similarity does begin to break down is at the highest magnitudes, where both graphs show possible superposition effects. In particular fig 3.5 shows a marked break in slope at magnitude 6.6 M_s, from b = 0.89 to b = 0.51, corresponding to a sudden reduction in the similarity dimension D from about 2 to about 1. This may be due to the finite width of

the fault zone, which reduces the geometric degree of freedom from two to one for magnitudes above 6.6 M_S, and is probably related to the seismogenic depth of about 15km. Scholz (1982) discussed a model of this type and its effect on scaling laws for large earthquakes, and this figure appears to be in tentative agreement with his L-model (scaling according to L-length rather than W-width as previously considered in Kanamori and Anderson (1975).

However, the parameter λ_2 in both cases allows a fit to this difficult part of the graph in a manner which is directly consistent with the geological information. Three possible types of behaviour can be imagined at the high magnitudes: $\lambda_2 = 0$ corresponds to a truncated exponential; λ_2 positive to a downward curve at higher magnitudes; and λ_2 negative to a curve upwards. This feature of a curve up may be useful in some areas where there is a bimodal distribution with an anomalously high proportion of large events, such as in Mexico (Singh et al, 1983). The main strength of the approach in this chapter is that the behaviour of the distribution as average repeat times beyond the instrumental scale are investigated is biased by as few assumptions as possible - these being directly consistent with the information put in. Here $\dot{M}_o$ has been chosen as appropriate, but in other areas an energy release rate $\dot{E}$, a known recurrence time from historical data on large events (Dong et al, 1984), or a combination of several sources of information may be used. It is even possible to imagine a time-dependent distribution which combines several observations of earthquake precursors, since at present no one precursor seems to be reliable on its own (Rikitake, 1976).

The method could, for the present, be usefully applied in many areas of the world where historical data are unreliable or

unavailable, especially as tectonic models become increasingly sophisticated with satellite and laser ranging studies. In conjunction with the concept of a seismic gap (McCann et al, 1979), the average repeat time inferred for the largest events by this method could be used as a less arbitrary guide to the areas of the world currently most at risk from catastrophic events. (In this reference a seismic gap was deemed to exist after an arbitrary time of 30 years since the last catastrophic event).

3.5 Summary

A new frequency magnitude distribution was developed from the principles of Information theory, thereby allowing direct incorporation of the geological data on the slip rate and the maximum fault area. The form of the distribution can be interpreted as the combination of two terms representing a) the geometry (dimension) of the source zone and b) a Boltzmann distribution of possible strain-energy transitions. This interpretation comes from a statistical mechanical treatment of fault elements, which is mathematically very similar to the Information theory treatment.

The geometrical dependence can be further broken down to relate the b-value to the (fractal) dimension D of the cracked source medium. As in Aki (1981), it turns out that $b \approx D/2$, explaining the range of observed b-values $0.5 < b < 1.5$ as being limited by corresponding dimensions $1 < D < 3$ and a finite energy density. The self-similarity required for this interpretation holds in two examples over a surprisingly large energy range (1:10,000!) but breaks down at the very highest magnitudes where superposition is evident.

An internal consistency check on the Mediterranean catalogue of magnitudes and seismic moments showed that the distribution combines the best features of the truncated exponential and Weibull line fits, with the added advantage that the distribution is automatically consistent with the slip rate and the maximum fault area. The information represented by the latter can also compensate for possible superposition at high magnitudes, since the total moment release rate is dominated by the largest events. Because of this slightly more confidence can be had in extrapolations beyond catalogue time scales for earthquake hazard studies.

The Californian catalogue gives an extrapolation which is consistent with a model developed from Sieh's table of occurrence times, and incidentally showed that the magnitude of the instrumentally recorded San Franscisco earthquake (1906) was too high by about half a magnitude unit. The long-term prediction of average repeat times for the largest events in Southern California by this method is once every 156 years, with a range 87-281 years, and this compares well with the results obtained by Sieh on direct trenching into the San Andreas fault (163 years, with a range 55-275 years).

This method could be used on global catalogues using plate tectonic models and the concept of a seismic gap to identify those regions of the earth currently most at risk (in a probabilistic sense) from catatrophic earthquakes. This would seem to be less arbitrary than the '30 years rule' which originally defined a seismic gap as existing 30 years after the last big event.

The really important point to emerge from this chapter is that, although the distribution developed does fit the empirical

data better than two other commonly used forms it is not just another theoretical curiousity, but by definition is the best that can be done with the currently limited knowledge of the earthquake process. Any subsequent improvements will require a better understanding of the latter, for example the validity of the assumption of stationarity and dimensional self-similarity. In the following chapter the aim is to investigate some of these assumptions in more detail for one particular tectonic province - the Aegean.

CHAPTER 4

A seismotectonic analysis of the Aegean area I: Source parameters

4.1 Introduction

In the last two chapters two different models of seismic moment release were developed and tested in up to four areas where a suitable, homogeneous earthquake magnitude catalogue was available. At this point it was decided that a more detailed investigation of one particular area of interest was necessary in order to develop some of the subtleties of the method. One natural advantage of such a case study is that the treatment of the data could be made more consistent and yield a more convincing overview of the whole method.

The area of the so-called 'Aegean plate' around Greece was chosen as suitable for such a detailed study for the following reasons:-

1) The complex seismicity and underlying tectonics of the area are an interesting puzzle which a detailed investigation of slip rates determined from seismicity studies may help solve.
2) In a European context, the area affected contains most of the significant seismic energy release (even in a global context Greek seismicity accounts for about 2% of the total).
3) The availability of a homogeneous earthquake catalogue going back to 1900.
4) The availability of extensive digital data on small earthquakes.

The main aims of the remainder of this thesis are (a) to further investigate the validity of the distribution (3.9) and some

assumptions behind it and (b) to test a tectonic model for the Aegean against the data on seismic moment release in the Greek area. The latter requires the derivation of seismic moments for large events, and the former a detailed investigation of the source parameters over a broad range of events down to the level of small earthquakes. First a brief summary of the results culled from an extensive literature search is presented, and then the extraction of seismic moment and other parameters from Rayleigh waves (for events $M_S > 5.5$) and P waves (for the small earthquakes with $M_L \approx 3$) is discussed. The results obtained will be used in an analysis of Aegean seismotectonics and seismic hazard in the final chapter, using the methods derived in the previous chapters.

4.2 Results of literature search: Source parameters

4.2.1 Introduction

Some hundreds of references relevant to Greek seismicity and tectonics were consulted in order to evaluate the reliability of the various tectonic models and to look for available data on source parameters. The references had already been compiled as part of the wider Volos project (Burton et al, in prep), and those consulted are listed in Appendix 3. The tectonic model will be discussed in the following chapter, but the available source parameters of Aegean earthquakes are now considered in a few subsections.

4.2.2 Earthquake magnitude catalogues

The most homogeneous catalogue for Greek seismicity is that of Makropoulos (1978), published more widely in Makropoulos and Burton

(1981). After considering other catalogues Båth (1983) concluded that 'this catalogue is apparently the most homogeneous one in existence for this area, with all parameters recalculated or re-examined'. The catalogue now covers the period 1901-1981, including 613 events for the period 1917-63 which were relocated using first arrival data from the International Seismological Summary. Consistent surface wave magnitudes were assigned mainly using readings from the Swedish network at Uppsala. The authors conclude that the catalogue is complete for magnitudes above 5.5 M_s for the period since 1918 or so, and above 4.7 since the introduction of the WWSSN (World-wide standard station) network in 1963.

Another catalogue which will be used is the result of recordings from a seismograph network called VOLNET (Volos network) which was set up by Paul Burton and others in a joint project (BGS and Athens University) to investigate: (a) the details of the tectonic stretching within the Aegean 'plate' behind the Hellenic arc; (b) the most probable seismotectonic model for the Volos-Almiros-Atalanti region in eastern Greece; and (c) seismic hazard combined with engineering geological studies of the latter region. For our purposes the Aegean plate includes the Greek mainland as well as the Aegean sea and the western edge of Turkey. The area covered by the network is illustrated in fig 4.1 (from the frontispiece of the VOLNET station bulletin). Although designed amongst other aims to investigate the detail of a forked seismicity trend identified in Makropoulos and Burton (1981), the network also picks up data further south on the actively stretching Gulf of Corinth. If any significant large events do occur this network should give very accurate hypocentre locations and assist the

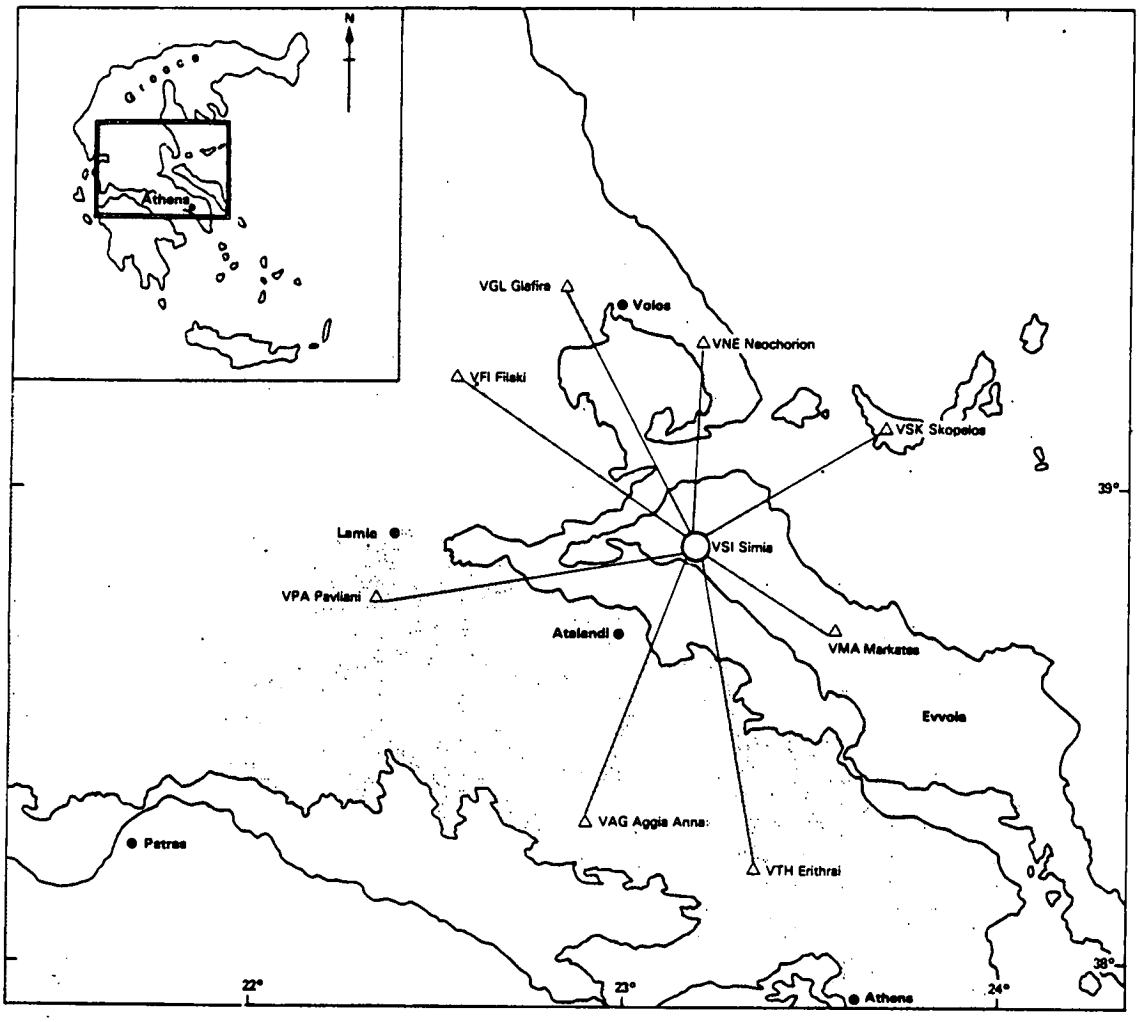

Figure 4.1 The VOLNET array of seismometers in location, Central Greece. This diagram is reproduced from the BGS VOLNET bulletins. The network is discussed in Burton et al (in prep).

matching of major earthquake sites with known faults.

VOLNET began operation in Jan 1983, the field observations on magnetic tape being used to produce arrival times, local magnitudes, hypocentral locations and digital velocity seismograms on magnetic tape. A magnitude range of 1.8-4.5 M_L is covered, although catalogue completeness is difficult to assess. Station bulletins are available from Jan 1983 to present from the Global Seismology Research Group of the British Geological Survey in Edinburgh. A small sample of the VOLNET data for epicentres spread throughout mainland Greece and the Aegean sea was supplied for the present work for the purpose of determining earthquake focal properties from earthquake spectra.

Between them, these two catalogues provide homogeneous data for a time span 1901 to present, over a magnitude range 1.8 M_L - 7.0 M_S. This represents an ideal data set to test the assumptions of self-similarity in the interpretation of the previous chapter as well as other aspects of the distribution (3.9).

4.2.3 Seismic moments

With the advent of the World Digital Seismograph Network (WDSN) and the International Deployment of Accelerometers (IDA) it has been possible to evaluate the centroid-moment tensor solutions from P-waves for earthquakes of magnitudes 5.3 M_s and over ($M_o > 10^{17}$ Nm). Dziewonski and others have published these results from P-wave data for the period since Jan 1982 in various editions of Physics of the Earth and Planetary interiors. The most recent at the time of writing is Dziewonski et al (1984), which contains events up to Mar 1984 and references to all the appropriate earlier

papers.

So far only scalar seismic moments have been discussed, but the digital data allow investigation of the orientation of the source and possible dilatation effects through the use of a 3x3 tensor moment. Dziewonski et al (1984) also summarise their results in terms of a scalar moment and a fault plane solution. Table 4.1 contains all of these seismic moments for the area of Makropoulos and Burton's (1981) Greek catalogue (18°-30°E, 33°-43°N) for the time period Jan 1982 through Mar 1984.

North's (1977) work on hand-digitised surface waves for M_S > 5.5 for the period 1963-1971 on long period WWSSN records for Mediterranean events has already been discussed. These results were used in Chapter 2 to estimate a moment release rate for the area covered by fig 2.1. The relevant portion of data for the present area of interest was extracted and is summarised in table 4.2.

Table 4.3 contains a few seismic moments from miscellaneous intensive studies of particular events, including one from field observation only.

The data of these three tables show that two major gaps in the seismic moment record of large events in the area existed before the present work was undertaken. These were the period 1972-1978 and prior to 1963. The period 1979-1981 does have some solutions, but the coverage is less complete than North's results. (Even North's data set omitted earthquakes as large as 6.1 M_S where severe multipathing effects were observed on the seismograph records). It is not yet possible to evaluate the completeness of the catalogue of Dziewonski and others, although it is fairly certain that the digital processing should cover nearly all of the

Table 4.1 Seismic moments Jan 1982-Mar 1984[x]

Date Day Mo Yr	Time H m secs	Lat °N	Lon °E	Depth km	M_o $x10^{17}$Nm	M_s	m_b
18 01 82	19 27 32.9	39.84	24.46	9.0	93.8	6.9[+]	-
17 08	22 22 29.8	33.70	22.90	23.4	39.8	6.6[+]	-
16 11	23 41 28.8	40.12	19.35	10.4	3.20	5.5	5.6*
17 01 83	12 41 44.7	38.13	20.38	10.1	235.0	7.0	6.1*
19 03	21 41 49.0	34.75	24.89	65.0	3.33	-	5.7*
23 03	23 51 15.8	37.92	20.48	32.7	22.3	6.2	5.8*
05 07	12 01 32.6	40.45	27.01	27.9	17.7	6.1	5.7*
06 08	15 44 00.6	39.85	24.56	10.1	117.0	7.0	6.2*
27 09	23 59 40.1	36.97	27.70	170.3	1.41	-	5.5*
11 02 84	08 02 54.8	38.11	21.86	15.0	3.32	5.4	5.4*

x These data are taken from Dziewonski et al (1984) and references therein.

+ From the International Seismological Centre (ISC) bulletins. The rest are not yet published at the time of writing.

* M_{s_z} and m_b from the monthly listings of the Preliminary Determination of epicentres. U.S.G.S.

Table 4.2. Seismic moments for large Greek earthquakes 1963-1971.*

Date			Time			Lat	Lon	Dep	M_o	M_s
Year	Mo	Day	Hr	m	s	N	E	km	10^{17}Nm	
1963	Sep	18	16	58	13	40.71	29.02	48	27.0	6.3
1963	Dec	16	13	47	57	36.97	20.96	15	4.8	5.8
1964	Apr	11	16	0	43	40.30	24.83	33	3.2	5.6
1964	Apr	29	4	21	5	39.25	23.72	20	2.2	5.5
1964	Jul	17	2	34	26	38.05	23.63	155	22.0	6.0
1964	Oct	6	14	31	23	40.30	28.23	34	180.0	7.0
1965	Mar	9	17	57	54	39.34	23.82	18	17.0	6.3
1965	Mar	31	9	47	26	38.38	22.26	45	190.0	6.6
1965	Apr	5	3	12	54	37.75	22.00	34	15.0	6.0
1965	Apr	9	23	57	2	35.06	24.31	39	25.0	6.1
1965	Apr	27	14	9	5	35.63	23.53	37	19.0	5.5
1965	Jul	6	3	18	42	38.37	22.40	18	42.0	6.4
1965	Nov	28	5	26	5	36.12	27.43	73	7.7	5.6
1965	Dec	20	0	8	16	40.21	24.82	33	5.3	6.0
1966	Feb	5	2	1	45	39.10	21.74	16	23.0	6.2
1966	May	9	0	42	53	34.43	26.44	13	13.0	5.9
1966	Oct	29	2	39	24	38.90	21.10	1	7.8	5.8
1967	Mar	4	17	58	9	39.25	24.60	60	91.0	6.8
1967	May	1	7	9	3	39.60	21.29	34	23.0	6.2
1967	Nov	30	7	23	50	41.41	20.44	21	150.0	6.5
1968	Feb	19	22	45	42	39.40	24.94	7	670.0	7.2
1968	May	30	17	40	26	35.45	27.88	27	12.0	5.9
1968	Dec	5	7	52	11	36.60	26.92	31	18.0	5.6
1969	Jan	14	23	12	6	36.11	29.19	22	53.0	5.9
1969	Mar	3	0	59	10	40.09	27.50	6	7.3	5.9
1969	Mar	23	21	8	42	39.14	28.48	9	9.1	5.9
1969	Mar	25	13	21	34	39.25	28.44	37	18.0	5.8
1969	Mar	28	1	48	29	38.55	28.46	4	120.0	6.4
1969	Jun	12	15	13	30	34.43	25.04	22	19.0	6.2
1969	Jul	8	8	9	13	37.50	20.31	30	4.1	5.8
1969	Oct	13	1	2	30	39.78	20.59	27	3.4	5.7
1970	Apr	8	13	50	28	38.34	22.56	23	31.0	6.2
1970	Apr	23	9	1	26	39.13	28.65	28	3.8	5.4
1970	Aug	19	2	1	51	41.08	19.77	21	7.2	5.3

* M_o evaluated by surface waves by North(1977), and all other data from the catalogue of Makropoulos and Burton(1981).

Table 4.3 Miscellaneous seismic moments and stress drops

Date			Time			Lat	Lon	Dep	M_o	$\Delta\sigma$	M_s
Day	Mo	Yr	Hr	m	secs	°N	°E	km	$x10^{17}$Nm	bars	
18	03	53	19	06	16.0	40.20	27.52	8	770.0	65[1]	7.4*
23	05	78	23	34	11.4	40.73	23.24	0	5.6[2]	12[2]	5.9
20	06	78	20	03	21.4	40.78	23.24	3	52.0[2]	12[2]	6.6
24	02	81	20	53	38.4	38.22	22.93	33	72.8[3]	10[4]	7.0
25	02	81	02	35	53.3	38.12	23.14	33	16.8[3]	8[4]	6.7
04	03	81	21	58	05.9	38.20	23.28	29	9.7[3]	7[4]	6.5

1 From surface faulting (Ambraseys, 1970)

2 From P-waves and aftershock areas (Soufleris et al, 1982)

3 From P-waves (Jackson et al, 1982)

4 From P- and S-waves (Kim et al, 1984)

* From Makropoulos and Burton (1981), an updated version.

events down to M_S 5.3.

Obviously we are still a long way from having a complete, homogeneous catalogue of seismic moments for Greece and the Aegean. However, when the results of this chapter for the period 1972-1978 (i.e. table 4.4) are added to tables 4.1, 4.2 and 4.3 over half of the events of magnitudes $M_S > 5.3$ since 1963 will have had seismic moments assigned to them. This magnitude range has been completely reported since the advent of the WWSSN network in 1963 (see fig 2.4).

4.2.4 Fault plane solutions

Having identified the gap in the moment record of 1972-1978 attention was concentrated on finding fault plane solutions for the events in this range for $M_S > 5.5$, because these were required to evaluate the medium response at a later stage. (A listing of these events is given in table 4.4.) The plan was to complement North's work and produce a homogeneous catalogue of seismic moments for the time period 1963-1978. Although most of the available fault plane solutions were collected in the literature search, table 4.5 only lists those events which will be analysed later in this chapter.

Fig 4.2 illustrates what the symbols ϕ_F, δ and λ represent as descriptors of the orientation of the fault plane and the direction of slip; ϕ_F is the strike of the fault, δ is the dip of the fault and λ is the rake or direction of slip. λ is positive for a reverse fault and negative for a normal fault. $\delta = 90^\circ$, $\lambda = \pm 90^\circ$ corresponds to a dip-slip fault, and $\lambda = 0^\circ$ to a strike slip fault. If ϕ_A is the source-station azimuth, then $\phi = \phi_A - \phi_F$ in fig 4.2.

The events to be evaluated in section 4.3 have been given

Table 4.4 Seismic moments 1972-1978+

List of all events greater than 5.5 M_s in the Greek catalogue* for the time period 1972-1978.

Year	Date	Time H m s	Lat. °N	Long. °E	Dep. km	M_o x10^{17}Nm	M_s	Event Code
1972	May 4	21 39 57	35.15	23.56	13	75.86	6.4	C
1972	Sep 13	4 13 19	37.96	22.38	75	30.90	6.2	F
1972	Sep 17	14 7 15	38.35	20.27	33	66.07	5.9	G
1973	Nov 4	15 52 12	38.87	20.54	13	6.03	5.9	H
1973	Nov 29	10 57 44	35.18	23.81	37	6.03	5.9	I
1975	Jan 8	19 32 34	38.24	22.65	26	2.95	5.7	L
1975	Mar 17	5 35 17	40.48	26.08	18	7.54	5.8	K
1975	Mar 27	5 15 7	40.45	26.12	15	128.82	6.7	B
1975	Apr 4	5 16 16	38.11	21.98	56	4.68	5.7	M
1975	Sep 22	0 44 56	35.20	26.26	55	8.51	5.7	N
1976	Jan 18	15 10 28	38.81	20.51	5	5.50	5.7	O
1976	May 11	16 59 48	37.56	20.35	33	-	6.3	D
1977	Sep 11	23 19 23	35.05	23.03	33	39.81	6.2	E
1977	Nov 28	2 59 10	36.05	27.76	85	7.08	5.9	J
1978	Jan 29	10 23 44	35.18	25.94	33	2.48	5.7	P
1978	Mar 7	22 33 46	34.66	25.50	33	5.40	5.7	Q
1978	Jun 20	20 3 29	40.75	23.41	15	72.44	6.6	A

+Evaluated later in this chapter

*Makropoulos and Burton (1981)

Table 4.4a. List of digitised seismograms and epicentral distances.

These are the 120 or so seismograms used in the actual evaluation of Mo. Another 80 were digitised but found unsuitable for analysis for various reasons (such as interference from other events, poor signal/noise ratios).

Station	Code	Epicentral dist in degrees
Event A		
Blacksburg,Va,US	BLA	75.8
Matsushiro,Japan	MAT	82.6
College,Alaska,US	COL	74.5
La Plata,Argentina	LPA	106.0
Chiang Mai,Thailand	CHG	67.2
Kodaikanal,India	KOD	56.4
Kap Tobin,Greenland	KTG	37.6
Nairobi,Kenya	NAI	43.5
New Delhi,India	NDI	45.2
Event B		
Arequipa,Peru	ARE	106.2
Blacksburg,Va,US	BLA	77.6
Chiang Mai,Thailand	CHG	65.2
College,Alaska,US	COL	74.9
Davao,Phillipines	DAV	92.6
La Plata,Argentina	LPA	107.6
Matsushiro,Japan	MAT	81.3
Mundaring,Australia	MUN	109.9
New Delhi,India	NDI	43.2
Windhoek,Namibia	WIN	63.2
Event C		
Addis Ababa,Ethiopia	AAE	29.5
Arequipa,Peru	ARE	103.3
Blacksburg,Va,US	BLA	79.2
Chiang Mai,Thailand	CHG	67.7
College,Alaska,US	COL	80.1
Godhavn,Greenland	GDH	53.1
Kingsbay,Spitsbergen	KBS	44.2
Mundaring,Australia	MUN	109.5
Natal,South Africa	NAT	68.0
New Delhi,India	NDI	45.6
San Juan,Puerto Rico	SJG	79.6

Table 4.4a(cont.)

Station	Code	Epicentral dist in degrees
Event E		
Arequipa,Peru	ARE	102.9
Blacksburg,Va,US	BLA	79.0
College,Alaska,US	COL	80.2
Corvalis,Oregon,US	COR	95.1
Grahamstown,S Africa	GRM	68.0
La Plata,Argentina	LPA	102.7
Kap Tobin,Greenland	KTG	42.8
Godhavn,Greenland	GDH	53.0
Event F		
Nairobi,Kenya	NAI	41.2
Kap Tobin,Greenland	KTG	39.9
New Delhi,India	NDI	46.2
College,Alaska,US	COL	77.2
Matsushiro,Japan	MAT	85.1
Natal,South Africa	NAT	68.3
Chiang Mai,Thailand	CHG	68.3
Addis Ababa,Ethiopia	AAE	32.4
Kevo,Finland	KEV	32.0
Blacksburg,Va,US	BLA	76.7
Shiraz,Iran	SHI	26.3
Event G		
College,Alaska,US	COL	76.7
Eskdalemuir,Scotland	ESK	23.2
Godhavn,Greenland	GDH	49.1
Kevo,Finland	KEV	31.7
Kap Tobin,Greenland	KTG	38.9
Nairobi,Kenya	NAI	42.3
New Delhi,India	NDI	47.8
San Juan,Puerto Rico	SJG	76.3
Weston,Massachusetts,US	WES	66.5
Event H		
Kingsbay,Spitsbergen	KBS	40.3
Kevo,Finland	KEV	31.1
Kap Tobin,Greenland	KTG	38.5
New Delhi,India	NDI	47.5
Poona,India	POO	50.2
Porto,Portugal	PTO	22.4
Quetta,Pakistan	QUE	38.9

Table 4.4a (cont.)

Station	Code	Epicentral dist in degrees
Event I		
Addis Ababa,Ethiopia	AAE	29.4
Eskdalemuir,Scotland	ESK	27.4
Kevo,Finland	KEV	34.7
Kap Tobin,Greenland	KTG	42.9
New Delhi,India	NDI	45.3
Porto,Portugal	PTO	26.1
Quetta,Pakistan	QUE	36.4
Event J		
Addis Ababa,Ethiopia	AAE	28.7
Eskdalemuir,Scotland	ESK	28.6
Kevo,Finland	KEV	33.8
Kingsbay,Spitzbergen	KBS	43.5
Kongsberg,Norway	KON	26.4
Nairobi,Kenya	NAI	38.1
Event K		
Addis Ababa,Ethiopia	AAE	33.3
Eskdalemuir,Scotland	ESK	24.4
Godhavn,Greenland	GDH	49.2
Kingsbay,Spitzbergen	KBS	38.9
Shiraz,Iran	SHI	24.1
Kevo,Finland	KEV	29.4
Quetta,Pakistan	QUE	34.6
Event L		
Addis Ababa,Ethiopia	AAE	32.5
Eskdalemuir,Scotland	ESK	24.4
Kingsbay,Spitsbergen	KBS	41.0
Nairobi,Kenya	NAI	41.4
Quetta,Pakistan	QUE	37.2
Copenhagen,Denmark	COP	18.8
Event M		
Godhavn,Greenland	GDH	49.3
Kevo,Finland	KEV	29.4
Nairobi,Kenya	NAI	42.7
New Delhi,India	NDI	43.1
Porto,Portugal	PTO	26.2
Quetta,Pakistan	QUE	34.6

Table 4.4a (cont.)

Station	Code	Epicentral dist in degrees
Event N		
Addis Ababa,Ethiopia	AAE	28.4
Camp Century,Greenland	CCG	55.4
Eskdalemuir,Scotland	ESK	28.6
Kongsberg,Norway	KON	26.8
Kabul,Afghanistan	KBL	34.9
Nairobi,Kenya	NAI	37.6
New Delhi,India	NDI	43.4
Poona,India	POO	45.1
Porto,Portugal	PTO	27.9
Quetta,Pakistan	QUE	34.4
Event O		
Eskdalemuir,Scotland	ESK	22.9
Kevo,Finland	KEV	31.2
Kabul,Afghanistan	KBL	38.8
Nairobi,Kenya	NAI	42.6
New Delhi,India	NDI	47.6
Quetta,Pakistan	QUE	38.9
Event P		
Addis Ababa,Ethiopia	AAE	28.5
Kevo,Finland	KEV	34.6
Kingsbay,Spitsbergen	KBS	44.2
Nairobi,Kenya	NAI	37.6
Quetta,Pakistan	QUE	34.7
Shiraz,Iran	SHI	23.1
Event Q		
Addis Ababa,Ethiopia	AAE	28.2
Eskdalemuir,Scotland	ESK	28.6
Kevo,Finland	KEV	35.2
Kingsbay,Spitsbergen	KBS	44.7
Nairobi,Kenya	NAI	37.3
Kongsberg,Norway	KON	27.1

Table 4.5 Fault plane solutions

For explanation of symbols see fig 4.2. The solutions actually used later are underlined.

Ref	McKenzie (1978) (unless indexed otherwise)			Drakopoulos & Delibasis* (1982)			
Event Codex	ϕ_F	δ	λ	ϕ_F	δ	Θ_p	λ
A	278	46	-70^{++}	106	26	5	-11
B	41	60	-45				
C	106	86	+90	138	82	78	+81
D				128	72	68	-77
E				94	36	14	+24
F	48	74	+20	52	80	46	+47
G	150	76	+90	33	86	20^{+}	+20
H	135	40	+90	142	82	82	+90
I	139	82	+90	121	72	67	-75
J				152	62	59	+76
K							
L				99	78	67	+70
M	46	54	-90	103	60	40**	-47
N	180	44	+40	176	66	40	+44
O				154	76	50	-52
P							
Q							

* This reference quotes the plunge Θ_p, which is related to λ by $\lambda = -\sin^{-1}\{\sin \Theta_p / \sin \delta\}$

\+ On checking this solution severe doubts were formed on its validity

** A severe difference in polarity observation and interpretation is evident for this event between the two references

++ From Soufleris and Stewart (1981)

x These codes refer to the events listed in table 4.4

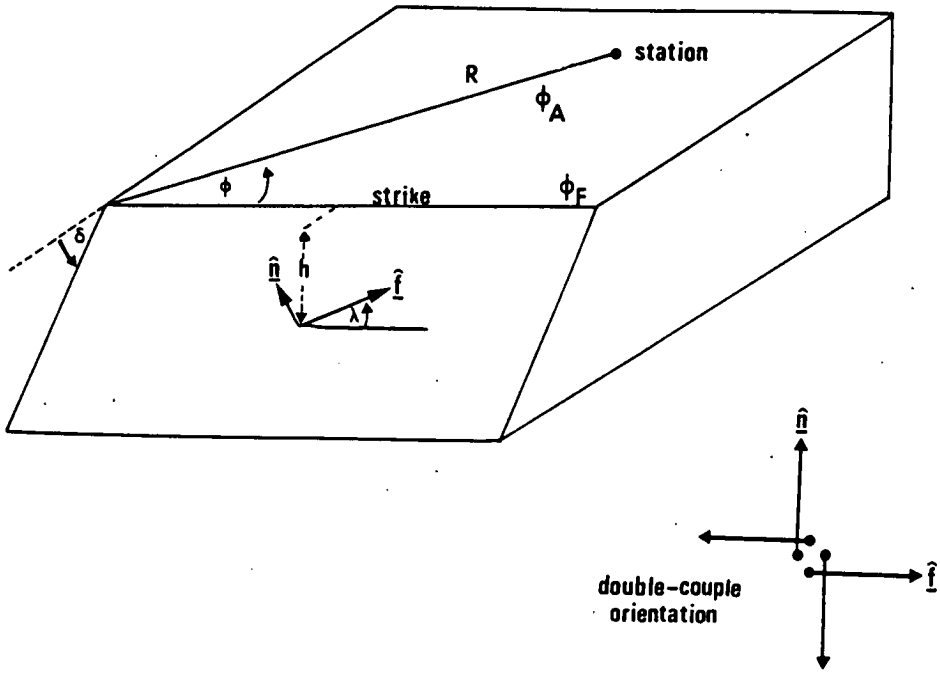

Figure 4.2 Orientation of the seismic source. Strike ϕ_F; dip δ; rake λ; epicentral distance R; source-station azimuth ϕ_A. $\hat{f}$ is the unit vector along the slip direction, and $\hat{n}$ a unit vector normal to the fault plane. The magnitude of the double couple whose orientation is described in the subsidiary diagram is equal to M_o.

codes A-Q and are listed in tables 4.4 and 4.5 in (roughly) decreasing order of magnitudes to allow quick reference in the main text. Of all the fault plane solutions listed in table 4.5 only events G and M differ significantly between the two main source references. An inspection of the polarity diagrams for these events in Drakopoulos and Delibasis (1982) led to the decision to use McKenzie's (1978) solution for both these events because of the better fit to the polarity data. Otherwise the former's solution were used because the actual value for λ can be inferred directly from this reference (McKenzie does not quote λ), and because of the reasonable agreement otherwise between the two sets of results. The solutions which will actually be used later are underlined in the table for clarity.

4.2.5 Other source parameters

P-wave data can be inverted to give the source area as well as the total seismic moment by using the theory outlined in section 4.4. Fault area can also be independently estimated by the extent of the distribution of aftershocks (e.g. North, 1977), although this may lead in general to an overestimate if the activity triggers stress adjustment outside the initial fault plane.

By using equations (1.4) and (1.18) the slip s or the stress drop $\Delta\sigma$ can be evaluated once the fault area and the seismic moment are available, although uncertainties add at every stage. In order to investigate properties of geometric self-similarity essential to the geometric interpretation of the b value in the previous chapter the best parameter to evaluate is probably the stress drop, because of its obvious dimensional scaling properties. Stress drops of very large and very small events can be compared because the

parameter is a force normalised to unit area. Table 4.3 also collects the available data on stress drops for events in the area of interest. From its length it can be seen that not much is known about this area in terms of these parameters.

However, both the Thessaloniki, 1978 and the Corinth, 1981 sequences of events had fairly low stress drops in the range 7-12 bars, and these events could be thought of as typical of the stretching (normal faulted) part of the Aegean 'plate'. Higher values for the reverse faulting associated with possible subduction under this plate might be expected, since the average value of the stress drop in the Eastern Mediterranean as a whole is 38 bars (section 3.2(a)). However it should be borne in mind that the two values of stress drops quoted have been estimated by different methods.

4.3 Seismic moments from surface waves

4.3.1 Introduction

The aim of this section was to plug the gap in knowledge of seismic moments at the time the project started - (1972-1978 inc.) in order to produce a homogeneous set of seismic moments for the time period 1963-present. North (1977) had already published his results from surface wave studies for the period (1963-1971 inc.), and so the method used in this section runs in close parallel to that study, particularly to the more detailed description given in an earlier Ph.D. Thesis (North, 1973). The results of this section (table 4.4), when added to those of North (table 4.2) should form a reasonably homogeneous data set for the period (1963-1978).

4.3.2 Theory

The theory of surface waves is very complex, but in the present work the derivation of amplitudes at a given azimuth and distance was carried out by use of a computer programme from Douglas et al (1972). A general overview of the method is given in Aki and Richards (1980), Chapter 7. For this reason only a brief outline will be given here, and attention will be further restricted to Rayleigh waves by only considering the vertical component of ground motion.

Seismic Rayleigh waves are transmitted along the free surface of an elastic solid from the earthquake source, and differ from Love waves in that they ideally only produce motion in a vertical plane. Surface waves have two main advantages over body waves in extracting seismic moment at the source:- (a) they suffer less degradation due to inhomogeneities than body waves, because of their longer wavelengths and (b) their signal/noise ratio at teleseismic distances is greater at longer periods because surface wave geometrical spreading is two dimensional, whereas body wave geometrical spreading is three dimensional. The main disadvantage is that the periods of interest (10-200s) are too high to observe any corner frequency (at about 3-6s for these events). This explains why North (1977) had to use the distribution of aftershocks to estimate fault area.

The real component of the spectral content of a Rayleigh wave Ω can be expressed by

$$\Omega(\omega) = M_o S_T(\omega)\, S_F(\omega;\, \phi)\, M_Z(\omega;\, \phi;\, h;\, s_j;\, \alpha_\ell,\, \beta_\ell,\, \rho_\ell,\, t_\ell)$$
$$R^{-\frac{1}{2}}\, D(\omega)\, I(\omega), \qquad (4.1)$$

where M_o for our purposes is the size of the double couple at the source - i.e. the seismic moment, and the other parameters are as follows:

$S_T(\omega)$	:	Source time function
$S_F(\omega)$	:	Source finiteness function
$M_Z(\omega)$	:	Medium response for a plane layered structure
$R^{-\frac{1}{2}}$	:	Geometric spreading
$D(\omega)$	:	Attenuation
$I(\omega)$	:	Instrument response
$\alpha_\ell, \beta_\ell, \rho_\ell, t_\ell$	:	Earth model: P velocity, S velocity, density and thickness respectively of the ℓ^{th} layer
ϕ	:	Source station azimuth (see fig. 4.2)
h	:	Depth of source
s_j	:	Orientation parameters of the source

s_j depends on $\hat{f}$ and $\hat{n}$ as defined in fig 4.2 and on α_s, β_s - the velocities in the source layer. The form of s_j and the detailed matrix algebra required to correct for the layering of the earth are described in Haskell (1964). Thus $M_o S_T S_F$ describe the source, M_Z the effect of the layered medium, $R^{-\frac{1}{2}}D$ the reduction in amplitude with distance and I the effect of the instrument.

Fig 4.3 shows an example of a source finiteness function for a strike-slip earthquake with rupture length L, rupture velocity $V_R \approx 0.7\beta$ following MacBeth's (1983) calculations of S_F. The range of interest here is the magnitude range (5.6 - 6.7 M_s), or a rupture length L of about 10-40 km after using Wyss's (1979) relationship

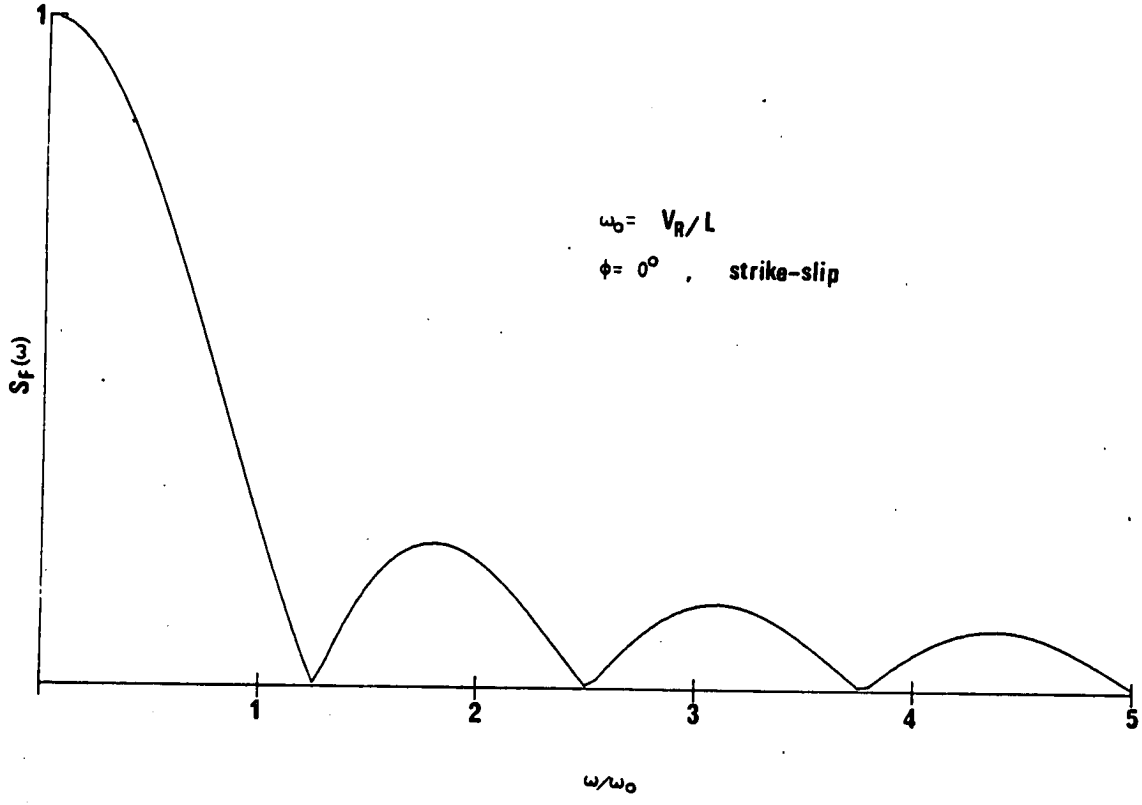

Figure 4.3 Source finiteness function for a strike-slip earthquake with rupture length L, rupture velocity V_R at an azimuth of 0° (from MacBeth, 1983).

$$M_s = \log (A \text{ in } \text{km}^2) + 4.15 \qquad M > 5.6 \ , \tag{4.2}$$

and A = LW, L ≈ 2W (A is fault area and W is fault width). Thus $\omega_o = V_R/L$ is in the range 0.20 - 0.05 Hz, or equivalently in periods 0.8 - 3.2 sec for a typical velocity V_R of 3 km s^{-1}.

Like North (1977) this study concentrates on periods T of 30s - 70s, so the source finiteness has practically no effect on the spectrum ($S_F \approx 1$). Most importantly these considerations show that no spectral 'holes' can be caused by the nodes of the plot on fig 4.3, since the frequencies of interest $\omega = 2\pi/T$ are all much less than ω_o. ($\omega/\omega_o \ll 1$ in fig 4.3).

The source time function that was used was a simple exponential ramp in time of the form:

$$S_T(t) = 1 - e^{-\omega_T t} \qquad t \geq 0 \ ,$$

$$\text{or } S_T(\omega) = \frac{1}{\omega\{1 + (\frac{\omega}{\omega_T})^2\}^{\frac{1}{2}}} \ , \tag{4.3}$$

in the frequency domain.

The correction for geometrical spreading $R^{\frac{1}{2}}$ can also be written as $(E \sin \Delta)^{\frac{1}{2}}$ where E is the radius of the earth in km and Δ is the angular separation of source and receiver. The other distance correction is attenuation

$$D(\omega; R) = \exp\{-\gamma(\omega)R\} = \exp\{-\gamma'(\omega)\Delta\} \ . \tag{4.4}$$

Attenuation correction was effected by using the empirical parameter γ (the attenuation coefficient) rather than the specific

attenuation parameter (normally denoted Q) because only the corrected amplitude at R = 0 is of interest in the present work.

4.3.3 Data reduction

The basic data are recorded on long period (20s) seismograms of the World Wide Standard Station Network and are available on 70mm film chips in the BGS microfilm library like the example in fig 4.4a, which is the record of event A (20th June Thessalonika) at the American station whose WWSSN code is BLA (i.e. Blacksburg in Virginia, U.S.). It can be seen at a glance from this figure that most of the long period energy recorded at a station is indeed in the surface wave at these teleseismic distances, because of the greater reduction and dissipation of body wave energy with distance.

(a) Time window of surface wave

The first step was to choose the time interval (t_1,t_2) to be digitised, and this was done initially with reference to a time window corresponding to an approximate group velocity window (U_{min}, U_{max}) of 2.5 - 4.0 km s^{-1} via

$$t_1 = \frac{R}{U_{max}} < (t - t_o) < \frac{R}{U_{min}} = t_2 \ , \qquad (4.5)$$

where R is the source station distance and t_o is the time the earthquake occurred. Some justification for this procedure is given in fig 4.5, from Correig et al (1982) which plots group velocities against wave periods for Europe. The period range of interest (30-70s) is easily within the range of (U_{min}, U_{max}) on this dispersion diagram.

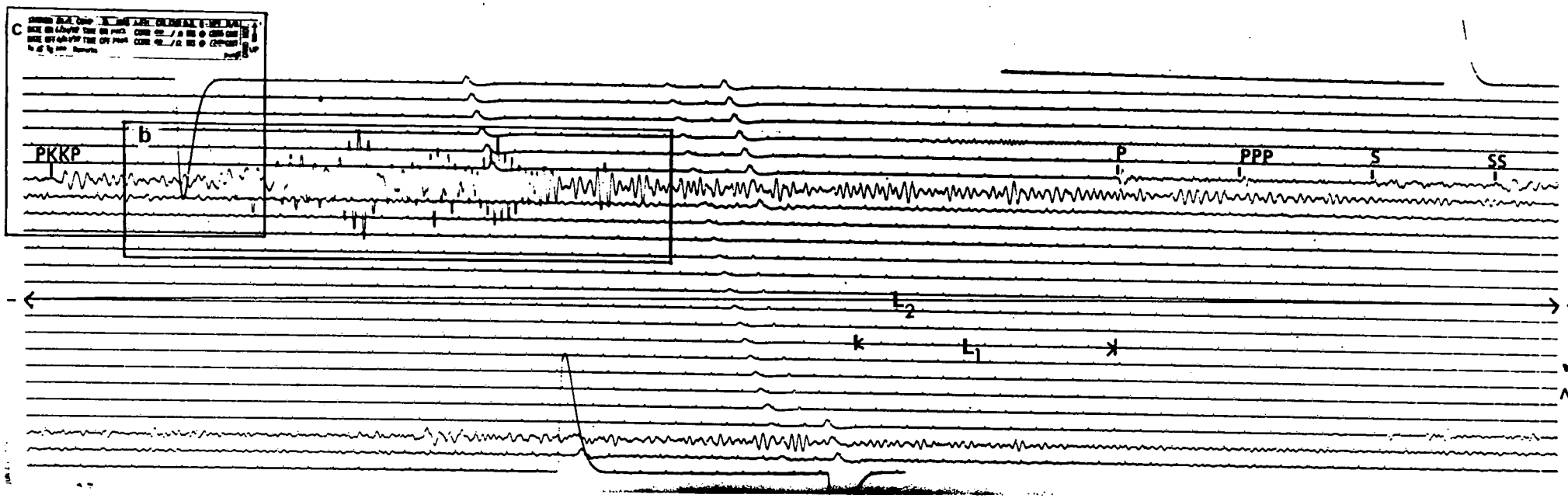

Figure 4.4a WWSSN long, period record. This example is of event A. The header information is in the top left hand corner, and directly under this in the calibration pulse. The event of interest is in the top half of the seismogram. Measurements of L_1, L_2, and L_3 are used to scale the trace to the original ground motion and correct for the traverse of the recording pen across the recording drum (see text). Sections indicated by boxes (b) and (c) are enlagred in the following figures. Various body wave phases were located with the assistance of Graham Neilson. A second event lower down the seismogram occurred NW of the Kurile islands. The station BLA (Blacksburg, Virginia) is in the north eastern U.S., so the azimuthal path across the Atlantic, but is still (just) predominantly continental.

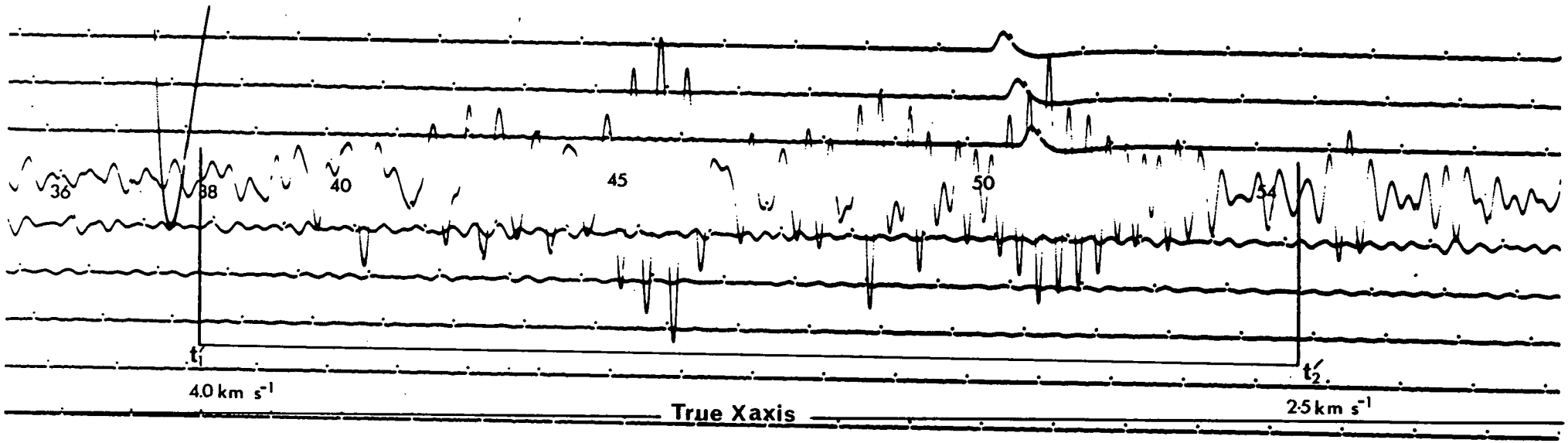

Figure 4.4b Surface wave energy. The true x-axis is shown, as is the time window (t_1', t_2') which was digitised in this case. In this example this matched the group velocity window (t_1, t_2) from 4.0 and 2.5 km s^{-1} but this was not always the case. Note that the late arrival due to multipathing at about 55s was not digitised.

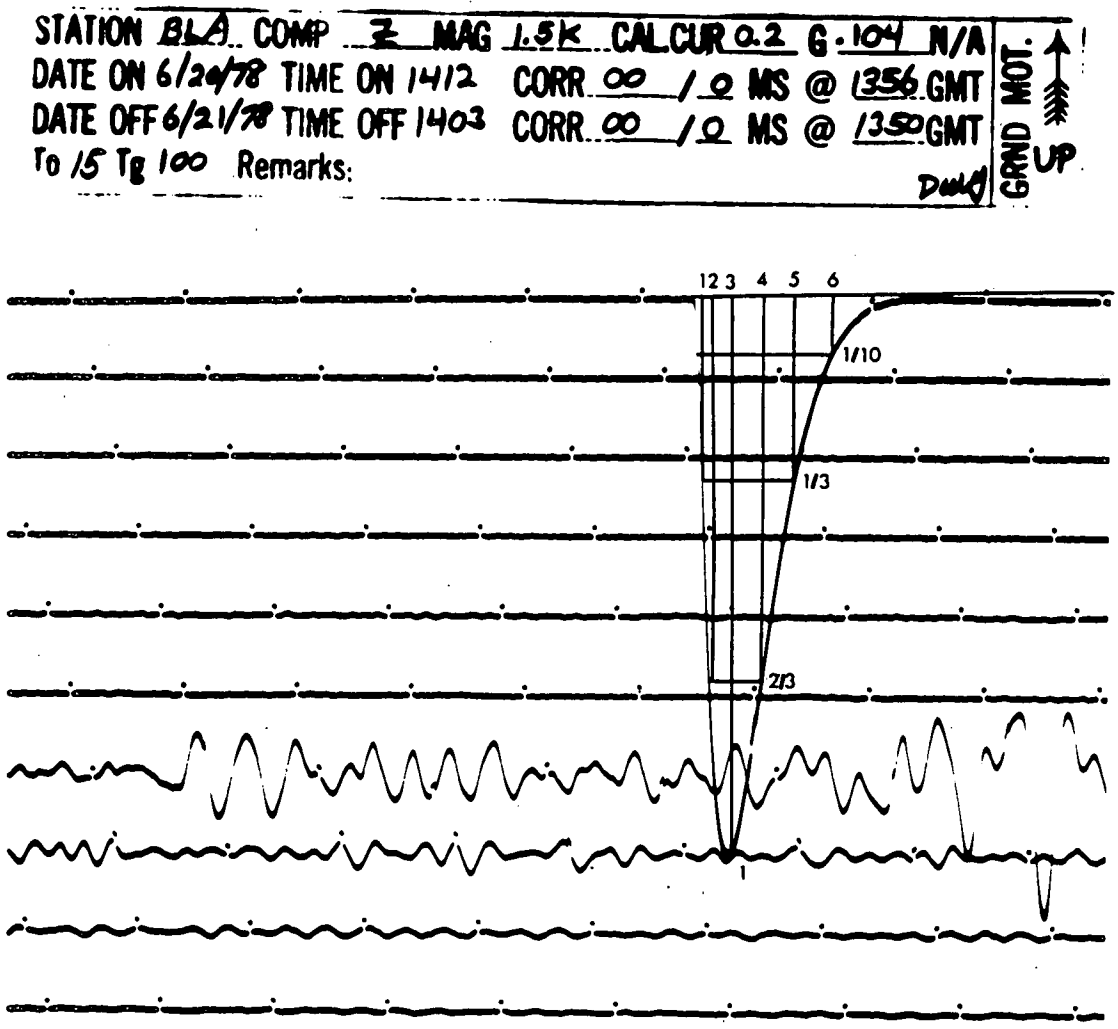

Figure 4.4c Calibration pulse and Header.
The header information contains the date, station name, recording component and time (GMT) to identify the event, as well as calibration parameters MAG (amplification factor) CALCUR (Calibration current) and G (Galvanometer constant). Points (P_i, Q_i) at factors 1, 2/3, 1/3, 1/10 of the maximum amplitude A_o are used together with G and CALCUR to describe the instrument response I(t) or I(ω) after reference to a library of known pulses and their responses.

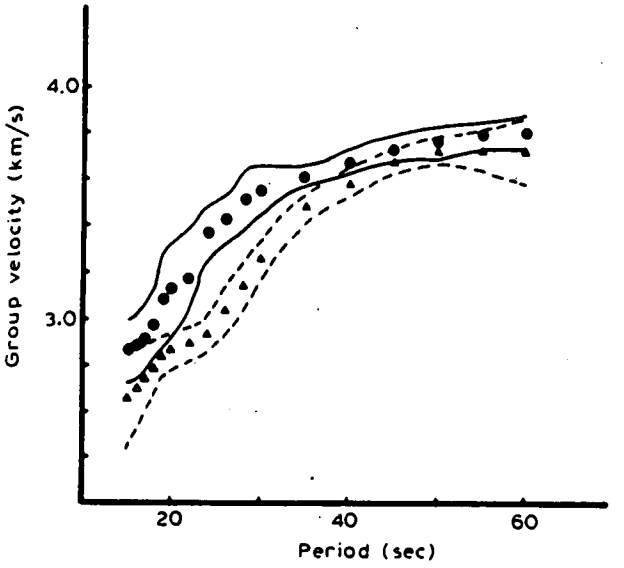

Figure 4.5 European dispersion characteristics. Observed group velocities for Western Europe (circles) and Southeastern Europe (triangles). Continuous and dashed lines represent standard deviations (after Correig et al, 1982).

Having calculated (t_1,t_2), the microfilm chip was copied onto two A3 sheets and the seismogram inspected to see how well these times matched an estimate of the time window defined by the arrival of long period energy and the signal duration picked by eye. Usually t_1 was found to be correct if taken to the nearest minute, but t_2 often included later arrivals caused by lateral refraction off inhomogeneities (for example see fig 4.4b). These refractions can be spotted because they have longer periods in a general trend of decreasing T with respect to t, and often look very similar to earlier arrivals. Such refractions are inevitable because almost all paths from Greece to stations above 20° away contain continent/ocean boundaries. Using (t_1, t_2) as a guide, and inspecting the seismogram for effects such as multipathing, defines (t_1', t_2') the time window to be digitised on fig 4.4b. Further discussion of the choice of time window and dispersion characteristics is given in Appendix 4.

(b) Digitisation of seismogram

Having copied a record of the whole chip onto an approximate size 1.20 x 0.40 m (the approximate size of the original), the portion including (t_1', t_2') was placed on a Hewlett-Packard digitising table. The surface wave in this interval was then traced relative to the horizontal edge of the original record, the X, Y coordinates being noted by the digitiser 5 times every second (real time). In order to smooth this record and prepare the resultant time series for Fourier analysis the data set was interpolated to give (X_i', Y_i') at unit intervals ΔX of 0.5 mm, which corresponds to about $\Delta t = 1.6$ seconds on the seismogram's time scale. This digitisation interval is more than adequate to avoid aliasing during Fourier analysis at the periods of interest (30-70s), because the Nyquist frequency

$(\frac{1}{2\Delta t})$ is 312 m Hz or an equivalent period of 3.2 seconds. The accuracy of the digitisation was then tested by plotting this interpolated record and overlaying this on the original on a light table.

In order to set the scale a measurement of the length between 10 minute markers (say L_1) and a measurement of the total horizontal length of the record (L_2) was noted, together with a note of the amplification factor of the recording instrument (MAG) (fig 4.4c). The real length of one of the original records is standardised at 910 mm, so finally

$$X_i'' = X_i' \times \frac{600}{L_1} \quad \text{in secs} \ ,$$

$$Y_i'' = Y_i' \times \frac{910}{L_2} \times \frac{1000}{MAG} \quad \text{in microns} \ .$$

The factor 1000 converts Y'' to microns from the mm units of Y', and X', L_1, L_2 are in mm. The final output file contains a set of times defined by X_1'' and $\Delta X''$, where $X_i'' = X_1 + (i-1)\ \Delta X$ and a string of amplitudes Y_i'', i = 1, N where N is the number of digitised points.

In addition to this procedure, a correction for pen traverse (of L_3 mm per cycle) across the drum at an angle Θ was included to correct for true vertical amplitude via

$$Y_i' = Y_i' + X_i' \tan\theta \ ; \quad \theta = \tan^{-1}(L_3/L_2) \ .$$

(X_i'', Y_i'') have now been corrected to an equally spaced series of amplitudes in time on the same scale as the ground motion.

(c) Instrument calibration and response

This was carried out following a procedure and FORTRAN program outlined in Espinosa et al (1962, 1965) and discussed in detail in Burton (1973), Appendix C. The method is quick and accounts adequately for variations in instrument response between WWSSN stations.

Each calibration pulse (as shown in Fig 4.4c) is characterised on the digitising table by noting points (P_i, Q_i) $i = 1,6$ relative to (P_o, Q_o), the onset of the pulse. The maximum amplitude of the pulse is A_o and the points at $1/3\ A_o$, $2/3\ A_o$, A_o are noted on the increasing part of the pulse ($i = 1,3$) and then $2/3 \cdot A_o$, $1/3\ A_o$, $1/10\ A_o$ ($i = 4,6$) on the decreasing half of the cycle. After correcting these for the drum roll Θ and the scaling factors as outlined in the previous section the calibration current (CALCUR) and the galvanometer constant (G) were noted. The instrument response was then characterised by

$$I(\omega) = f\{\text{CALCUR}, G, (P_i, Q_i)_{i=1,6}\} \quad ,$$

and matched to a library of known instrument calibration pulse shapes to choose the one closest to this set of parameters.

This method is not perfect, but is very quick to apply to the 200 or so seismograms which were digitised. It is much better than assuming a theoretical shape of the instrument response, because unfortunately, WWSSN turns out to be not as 'standard' in this respect as one might expect (Burton, 1973, Appendix C).

The instrument correction can then be done (in the frequency domain) by a simple division, to give an instrument corrected spectrum

$$\Omega_{OBS}(\omega) = \Omega(\omega)/I(\omega) \ .$$

(d) Time series analysis

The data is now in the form of a string of N amplitude terms Y_i'' at equal time intervals $\Delta t \approx 1.6s$ - i.e. a time series. The Fourier transform of a continuous function Y(t) is

$$F(\omega) = \int_{-\infty}^{\infty} Y(t)\, e^{-i\omega t}\, dt \ , \qquad (4.6)$$

which must be replaced for computing purposes by a discrete series transform with coefficients

$$F_j(f_j) = \Delta t \sum_{k=0}^{N} Y_i''\, e^{-2\pi i f_j k \Delta t} \ , \qquad (4.7)$$

where F_j assumes discrete values at the frequencies f_j, and the highest frequency is the Nyquist frequency - $1/(2/\Delta t)$. F_j are in general complex, so real and imaginary parts can be considered separately,

$$\Omega_j(f_j) = \text{mod}\ (F_j) \ ,$$

$$\phi_j(f_j) = \arg\ (F_j) \ . \qquad (4.8)$$

For evaluating M_o, only the real part Ω is required. The Ω_j are then smoothed by a Gaussian filter over 5 neighbouring points. The computer program TSAP, developed and listed in Burton and Blamey (1972) and in Burton (1973), was used to produce $\Omega_j(f_j)$, and to correct for the instrument effect by the method outlined in

the previous section.

Fig 4.6 gives an example of the program output, showing the steps described above. It begins with a digitised seismogram (fig 4.6a) which is first corrected for any secular trends. A discrete Fourier transform is then performed (fig 4.6b), and the best instrument response compared with the calibration constants (P_i,Q_i) is plotted (fig 4.6c). The amplitudes Ω are then divided by I to get the instrument-corrected spectrum Ω_{OBS} in micron secs (fig 4.6d), which is plotted on log-log paper.

(e) The medium response

This, the most complicated step, was performed by producing synthetic spectra by the method of Douglas et al (1972) for M_o = 1Nm, using a computer program called BIGE provided by A. Douglas. The forms of S_F and S_T have already been discussed, and these were also incorporated in the program.

The parameters of table 4.6 (α_ℓ, β_ℓ, ρ_ℓ, t_ℓ) were used for the earth model, with the source parameters (h, ϕ, δ, λ, α_s, β_s) of tables 4.4, 4.5 and 4.6 to give the medium response

$$M_Z(\omega;\ \phi;\ h;\ s_j(\alpha_s,\ \beta_s,\ \delta,\ \lambda);\ \alpha_\ell,\ \beta_\ell,\ \rho_\ell,\ t_\ell)$$

The earth models were reduced to the top 5 layers for a predominantly continental path (table 4.6a) or the top 6 (including the water layer) for a predominantly oceanic path (table 4.6b). This was done to reduce computing time because the lower layers (below a depth of 350 km) had a negligible effect on the Rayleigh spectrum at periods of 30-70s on several trial runs.

The program actually used is listed in MacBeth (1983), Appendix D2, which is a modified version of BIGE and computes a

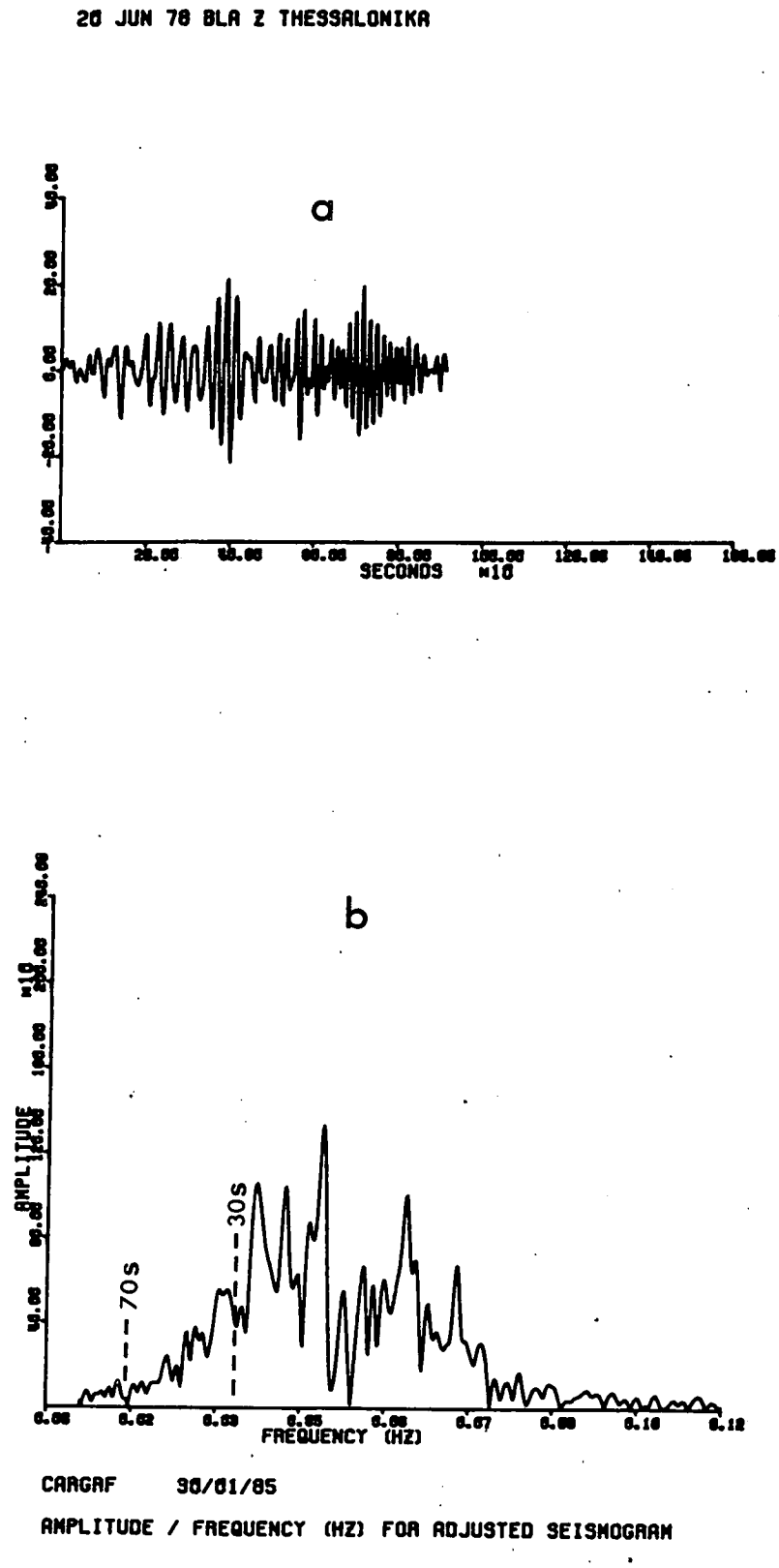

Figure 4.6 Time series analysis and instrument correction. (a) original seismogram; (b) Fourier transform of seismogram - $\Omega(\omega)$; (c) Instrument reponse $I(\omega)$; (d) Ω/I - instrument corrected spectrum. The period range 30-70s is shown. Most of the spectrum below 0.02 Hz ad above 0.09 Hz is probably noise.

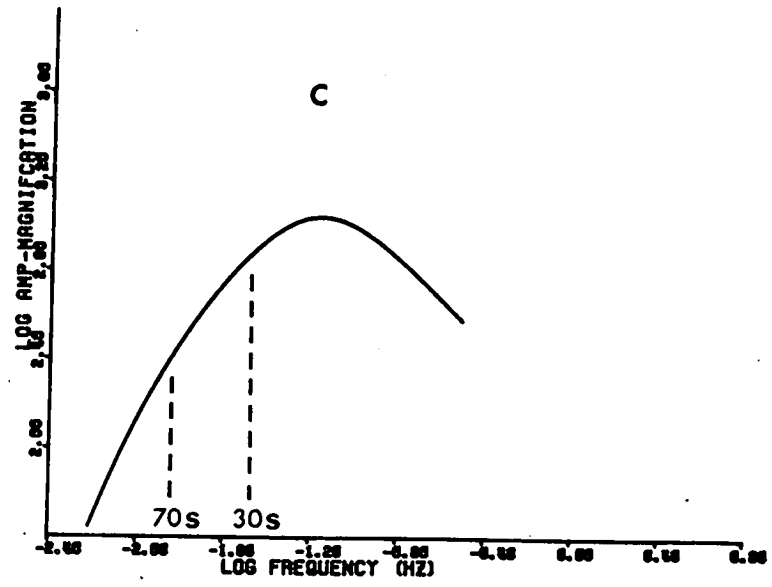

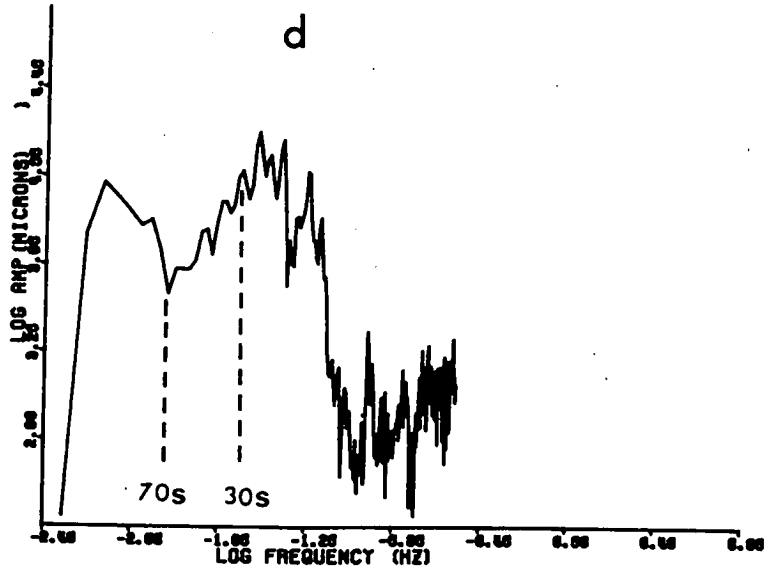

Figure 4.6 (cont.)

Table 4.6 Earth model*

(a) Crust-upper mantle structure for continent

Depth (km)	Thickness (km)	β(km/sec)	α(km/sec)	ρ(g/cm^3)
0	10	3.49	6.05	2.75
10	20	3.67	6.35	2.85
30	20	3.85	7.05	3.08
50	65	4.65	8.17	3.45
115	250	4.30	8.35	3.54
365	85	4.75	8.80	3.65
450	200	5.30	9.80	3.98
650	400	6.20	11.15	4.43
1050	240	6.48	11.78	4.63
1290	∞	6.62	12.02	4.71

(b) Crust-upper mantle structure for ocean

Depth (km)	Thickness (km)	β(km/sec)	α(km/sec)	ρ(g/cm^3)
0	4	0.00	1.52	1.03
4	1	1.00	2.10	2.10
5	5	3.70	6.41	3.07
10	50	4.65	8.10	3.40
60	150	4.15	7.60	3.40
210	240	4.75	8.80	3.65
450	200	5.30	9.80	3.98
650	400	6.20	11.15	4.43
1050	240	6.48	11.78	4.63
1290	∞	6.62	12.02	4.71

* After Knopoff and Chang (1977)

theoretical spectrum

$$\Omega_{TH} = M_o\, S_T(\omega)\, S_F(\omega;\, \phi)\, M_Z(\omega)\, R^{-\frac{1}{2}} = \Omega/DI \quad ,$$

for M_o = 1Nm, R = 1 km. Ω_{TH} is the theoretical amplitude for an event with source parameters (h, ϕ, δ, λ) in a layered medium (α_ℓ, β_ℓ, ρ_ℓ, t_ℓ) for unit seismic moment at unit distance. The actual amplitude Ω_{OBS} after time series analysis and instrument correction is

$$\Omega_{OBS} = \Omega/I = M_o\, S_T(\omega)\, S_F(\omega,\phi)\, M_Z(\omega)\, R^{-\frac{1}{2}}\, D(\omega) \quad .$$

So the actual seismic moment is evaluated by simple proportion.

$$M_o = \frac{\Omega_{OBS}}{\Omega_{TH}} \left(\frac{R}{1}\right)^{\frac{1}{2}} \exp(\gamma R) \times 1\text{Nm} \quad . \qquad (4.9)$$

(f) Distance correction

At this stage Ω_{OBS} and Ω_{TH} in (4.9) have been calculated, leaving only a correction for geometric spreading and attenuation of $R^{\frac{1}{2}} \exp(\gamma R)$ or $(E \sin \Delta)^{\frac{1}{2}} \exp(\gamma' \Delta)$ in terms of the epicentral distance Δ in degrees. Values of γ' per degree are listed in table 4.7, which was obtained by linear interpolation of values quoted by North (1973) from studies by Anderson et al (1965) and Tsai and Aki (1970).

First of all the digital output from TSAP ($\Omega_{OBS}(f_j)$) was reduced to seven readings at frequencies $f_i = f_o + (i-1)\Delta f$; i=1,7 with f_o = 10 mHz, Δf = 2.5 mHz, since f_j was slightly different for each event-station pair. This frequency range reduces the data to

Table 4.7 Attenuation: $e^{-\gamma R}$ or $e^{-\gamma' \Delta}$

(a) $D(\omega) = e^{-\gamma R}$ after Tsai and Aki (1970) for $20 < T < 45$ and Anderson et al (1965) otherwise, for R in km. T is the period of the surface wave.

(For a complete discussion see North (1973) p46.)

T(s)	20-45	50	60	70	80	90	100
$\gamma(10^{-6}/km)$	150	125	105	80	70	60	50

(b) $D(\omega) = e^{-\gamma' \Delta}$. Interpolating the above linearly at intervals of 2.5 m Hz gives the following values of γ' in terms of Δ in degrees. $f = 1/T$.

f(mHz)	30	27.5	25	22.5	20	17.5	15	12.5	10
$\gamma'(10^{-3}/^{\circ})$	16.7	16.7	16.7	16.7	13.9	12.0	10.3	7.8	5.5

the time period 30-70s. Then the parameter

$$A(r) = \frac{\Omega_{OBS}\ (f_i,\ \Delta_j)}{\Omega_{TH}\ (f_i)}\quad (E \sin \Delta_k)^{\frac{1}{2}}\ ,$$

for the k^{th} station at the i^{th} frequency was plotted on graphs such as fig 4.7a. Since this parameter is equal to $M_o \exp(-\gamma R)$ from (4.9), the intercept on the Y axis on fig 4.7a is simply M_{oi} - the seismic moment for the i^{th} frequency. This intercept was found for each frequency f_i by calculating a centroid $(\bar{\Delta}_i,\ \bar{A}_i)$ and applying the equation

$$\log A_{ik} = \log M_{oi} - \gamma_i' \Delta_k \log(e)\ ,$$

for given values of γ_i'. Values of Δ_k are given in table 4.4a for the 120 or so seismograms actually used in the determination of the final values of M_o obtained in table 4.4.

Finally, the seismic moment was evaluated by taking a geometric mean of the seven values of the M_o at frequencies between 30 and 70s.

$$\log\ (M_o) = \frac{\sum_{i=1}^{7} \log(M_{oi})}{7}\ .$$

This procedure could be applied to all the events with fault plane solutions, and was therefore used to produce all of the seismic moments listed in table 4.4, with the exception of event D - which was not analysed at all because of interference by an earlier event

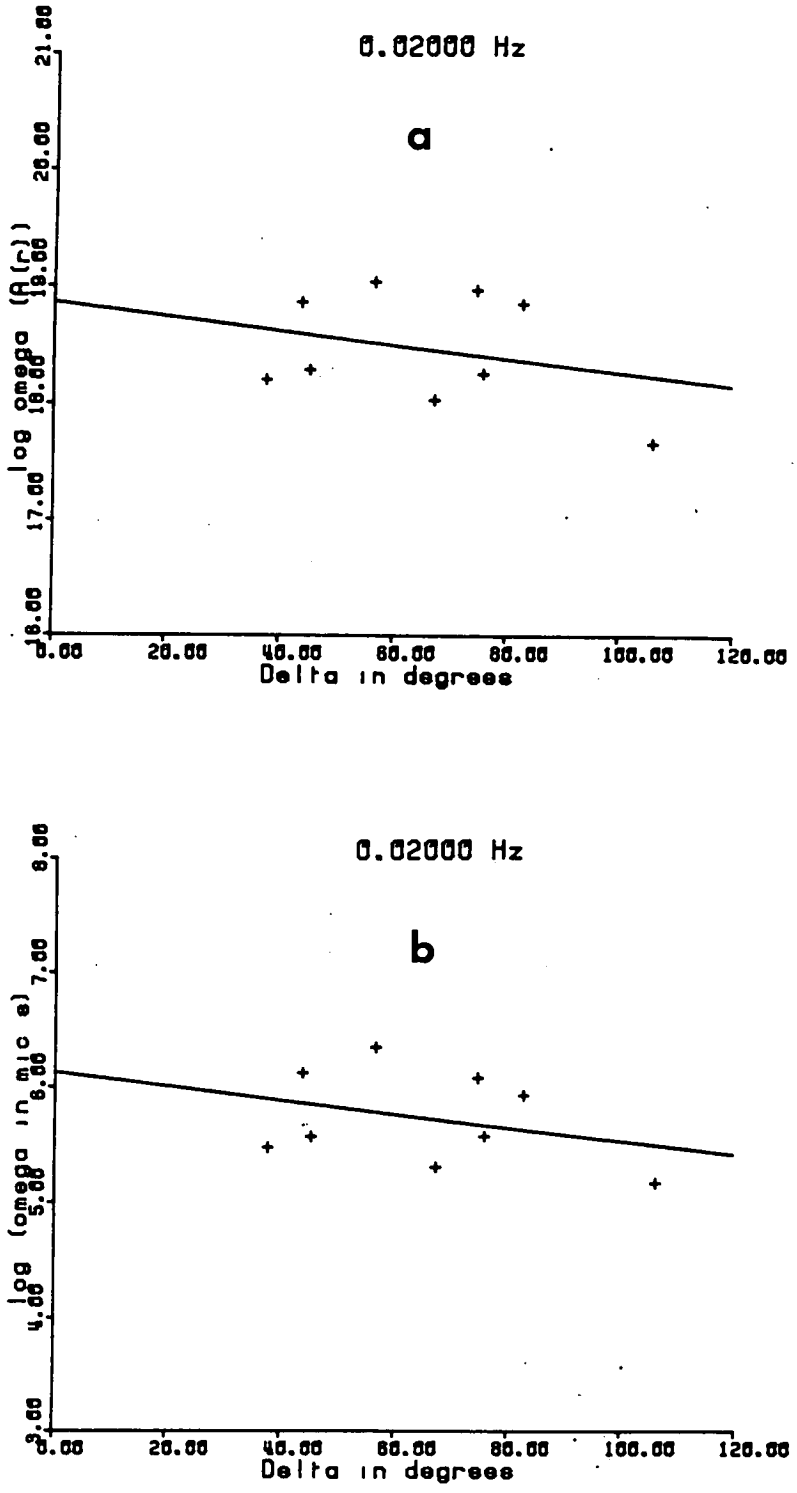

Figure 4.7 Attenuation corrections.

(a) correction of $\Omega_{OBS}R^{\frac{1}{2}}/\Omega_{TH}$ by using the value of $\gamma'(\omega)$ in table 4.7.
(b) a similar correction on $\Omega_{OBS}R^{\frac{1}{2}}$ for the same event (Event A).

on the record, and events K, P, Q - which had no fault plane solutions in the literature and were treated separately.

(g) Moment calibration for events K, P, Q

This subsection began with an inquiry into how much the fault plane solution really affects the eventual value of M_o - given that most of the data are chosen at azimuths near the antinodes of the radiation pattern. This happens naturally since most of the data at nodal points have very low signal to noise ratios, and so are not used.

First of all consider fig 4.7b, which misses out the medium response calculation, and then corrects for attenuation as in the last section with a y axis parameter

$$Y_{ik} = \Omega_{OBS}\ (f_i,\ \Delta_k)\ (E \sin \Delta)^{\frac{1}{2}} .$$

The intercept on the y axis Y_{oi} was then averaged over the same seven frequencies as in the previous section.

$$\log\ (Y_o) = \frac{\sum_{i=1}^{7} \log\ (Y_{oi})}{7} .$$

Fig 4.8 plots log M_o vs log Y_o, which can be fitted by least squares straight line with the equation

$$\log M_o = a + b \log Y_o , \qquad (4.10a)$$

with a = 13.003 ± 0.383, b = 0.965 ± 0.071 for M_o in Nm and Y_o in micron seconds. Within the accuracy of this line fit, this represents a straight proportionality relationship, with b = 1

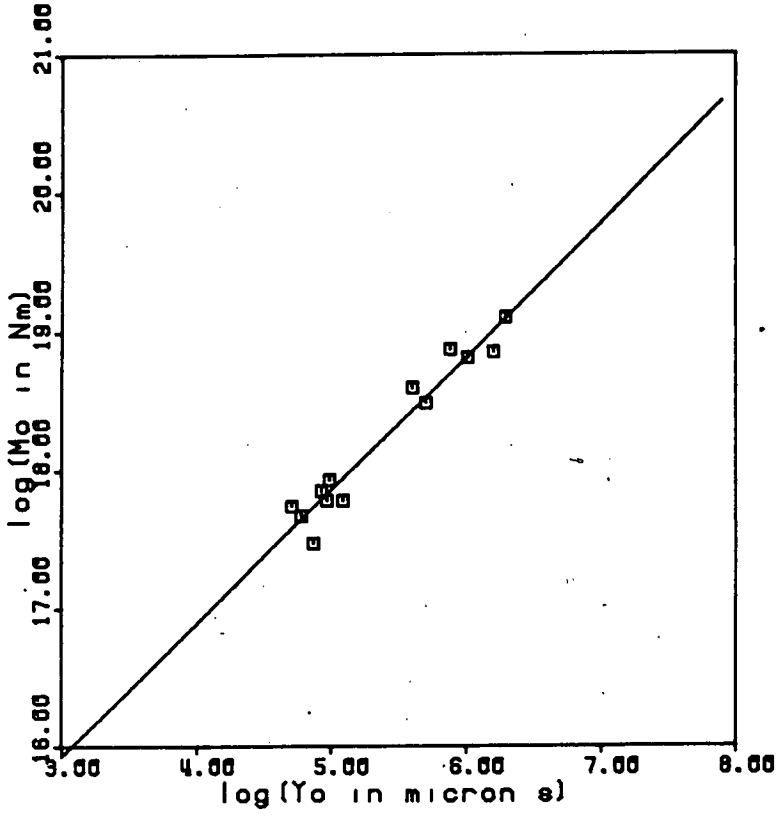

Figure 4.8 Moment calibration. A plot of M_o vs Y_o as defined in the text section 4.3.3(g). The line is fit by least squares to the data in table 4.8, with gradient 0.965 ± 0.071 and intercept 13.033 ± 0.383.

Table 4.8 Calibration of M_o vs Y_o : the data

These values are quoted as logarithms to the base ten, and plotted on fig 4.8. Y_o as defined in section 4.3.3(g) is in micron s and M_o is in Nm. Standard deviations of Y_o and M_o are given in brackets.

Event code	log Y_o	log M_o
A	6.20 (0.10)	18.86 (0.07)
B	6.29 (0.17)	19.11 (0.18)
C	5.88 (0.21)	18.88 (0.08)
E	5.60 (0.06)	18.60 (0.15)
F	5.70 (0.12)	18.49 (0.08)
G	6.01 (0.07)	18.82 (0.14)
H	4.97 (0.11)	17.78 (0.11)
I	5.09 (0.15)	17.78 (0.07)
J	4.93 (0.12)	17.85 (0.04)
L	4.87 (0.11)	17.47 (0.11)
M	4.78 (0.15)	17.67 (0.10)
N	4.99 (0.14)	17.93 (0.10)
O	4.71 (0.10)	17.74 (0.09)
K	5.02 (0.09)	
P	4.52 (0.15)	
Q	4.87 (0.11)	

$$M_o = k\, Y_o \quad . \qquad (4.10b)$$

$k = 10^a = 1.08 \times 10^{19}$ N/s. Thus Y_o was found for events K, P, Q and converted to the values M_o listed in tables 4.4 and 4.8 by using this calibration equation (4.10b).

It is obvious from comparing fig 4.7a and 4.7b that the fault plane solution for event A has little effect on the observed amplitudes in this case. That this is true generally is borne out by the good fit to the data in fig 4.8. However the listing of M_o vs Y_o in table 4.8 does show that the values of log M_o are in general better constrained by their standard deviations (typically ± 0.10) than log Y_o (typically ± 0.15) showing that inclusion of the fault plane solution has (on average) led to a slightly better solution.

4.3.4 Discussion of results

At first glance table 4.4 seems scant reward for many hours of digitising and computer processing. However this is a complete list of all the seismic moments for events of magnitude greater than 5.5 M_s for the period 1972-1978, with only one exception for event D.

One interesting result did emerge concerning the effect of the medium response on the spectral amplitudes. The relationship (4.10) gives a calibration of spectral amplitudes corrected for instrument, geometric spreading and attenuation (Y_o) against seismic moment found by the complete correction process including the medium response. The random error (i.e. a standard deviation) is only increased from ± 0.10 in log M_o to ± 0.15 in log Y_o, or equivalently from 25% in M_o to 40% in Y_o. The small random error (standard deviation) in M_o of table 4.8 indicates

a fairly flat spectral shape within about 25% after all of the corrections, since M_o is an average over seven frequencies in the range 30-70s.

North (1977) estimated the total uncertainty in M_o by this method as a factor 3 or so, including systematic errors in the earth model, so the error introduced by the calibration procedure is almost negligible here. An error of a factor 3 in M_o leads to a combination of systematic and random errors in the A parameter of the moment magnitude relation of $\pm \log 3$ or ± 0.47, and similarly a random error of 40% introduced by the calibration procedure gives $\delta A = \pm \log (0.4) = \pm 0.15$.

4.4 Source parameters from P-waves

4.4.1 Introduction

Having evaluated the seismic moments and collected the typical stress drops of published events in the previous two sections for the large events, this section now considers the smaller events picked up by the VOLNET array. The object here is to evaluate the source parameters of the smaller events in mainland Greece and some in the Aegean and to investigate the scaling properties between the smaller and larger events with a view towards testing the assumptions behind the derivation and interpretation of the distribution (3.9). If these assumptions are valid, and some properties of the numerous small events do relate in a specific way to those of the rare larger events, then this has very relevant implications for estimates of the seismogenic slip rate and the seismic hazard.

The VOLNET array data are reduced to a library of digital velocity seismograms on magnetic tape, a small sample of which is

the basic data for this section. The arrival time of the P-wave for each event-station pair is given in the appropriate monthly station bulletin. The design of the overall system means that it is a fairly routine matter to find events and extract them directly off the tapes.

In the first instance 40 events in the magnitude range 1.8-4.5 M_L were chosen for investigation (table 4.9). Eventually 28 of these in the range 1.8-3.5 M_L were found to be suitable for analysis (i.e. having a sufficient signal/noise ratio on at least 6 of the available recording stations and avoiding saturated records). A map of the epicentres of these events is given in fig 4.9.

4.4.2 Theory

The seismic moment of an earthquake is proportional to the long period spectral level Ω_o of a displacement seismogram (i.e. its Fourier transform). The theoretical shape of a P-wave displacement spectrum for an earthquake is much simpler than the surface wave portion. In general it is a flat portion from zero frequency up to a 'corner' frequency f_c, and then a power law tail $f^{-\gamma}$ beyond this value (see fig 4.10c for example). The corner frequency is inversely proportional to the fault length. By making the 'far field' approximation i.e. the epicentral distance R >> r, the source radius, the following relationships between the spectral parameters (Ω_o, f_c) and various source parameters (M_o, r, $\Delta\sigma$, s) can be deduced:-

$$M_o = 4\pi \rho\alpha^3 R\Omega_o/(\Psi_{\phi\theta} 2\sqrt{2}) \quad , \qquad (4.11)$$

Table 4. 9 Hypocentral coordinates and magnitudes of 40 sample earthquakes recorded by VOLNET 1 Jan - 30 Jun 1983.

Event Number	Origin time (Y M D H m sec)	Lat N (deg min)	Lon E (deg min)	Dep (km)	M_L
1	83 1 8 626 5.16	38 13.44	23 18.06	9.21	3.1
2	83 112 1616 53.95	38 0.50	23 7.61	5.48	2.9
3	83 114 224 33.06	39 11.05	24 26.17	5.00	3.2
4	83 120 242 36.84	38 29.16	24 43.40	0.95	2.7
5	83 123 12 6 6.70	38 47.10	25 2.96	1.07	3.5
6	83 2 1 15 9 47.63	38 36.10	23 33.16	14.09	2.7
7	83 2 4 1143 0.71	38 12.39	23 17.39	6.55	3.1
8	83 216 1256 19.29	38 49.00	24 18.72	7.87	3.0
9	83 227 146 21.12	39 1.77	24 57.06	0.94	3.3
10	83 318 1725 42.32	38 8.61	23 15.62	8.48	3.1
11	83 321 746 24.16	36 26.07	22 2.42	0.09	3.7
12	83 325 2323 34.74	38 28.85	21 40.00	0.21	3.2 *
13	83 4 5 2112 21.90	38 39.64	22 6.77	9.81	3.1Z
14	83 4 7 151 50.91	38 40.68	22 18.48	9.99	3.2Z
15	83 4 7 12 1 30.51	38 40.90	22 14.91	10.47	2.9
16	83 4 7 17 8 50.18	38 41.11	22 14.61	11.74	2.8
17	83 4 8 133 34.86	38 26.91	23 43.01	11.16	2.5Z
18	83 4 8 1235 12.64	38 39.87	22 9.29	9.97	3.0Z
19	83 4 8 1329 5.47	38 39.88	22 13.32	13.49	2.8Z
20	83 4 8 2147 45.79	38 42.85	22 15.18	11.64	2.8
21	83 411 1723 9.00	38 2.93	22 3.85	2.97	3.4Z
22	83 414 937 7.69	38 11.95	24 18.27	18.98	2.6
23	83 429 318 11.34	38 40.06	22 13.90	11.92	2.5Z
24	83 514 1220 4.15	38 0.38	22 51.00	3.29	3.2
25	83 610 239 36.89	38 7.79	19 50.70	5.00	4.4
26	83 611 2331 33.85	39 17.33	21 47.77	9.81	3.4
27	83 615 026 18.54	39 3.48	25 38.10	9.88	3.6
28	83 618 2324 55.80	38 5.63	23 8.24	3.62	2.5
29	83 625 2055 36.58	38 21.94	22 8.02	0.28	2.8Z
30	83 627 550 14.47	36 8.18	23 45.30	32.59	4.2
31	83 113 3 6 8.13	38 36.60	22 53.10	14.26	3.0
32	83 227 352 23.50	39 29.82	23 26.91	11.14	3.1
33	83 4 7 23 9 19.22	38 41.01	22 17.35	14.19	2.3
34	83 4 8 4 3 27.58	38 41.62	22 14.70	10.83	2.8Z
35	83 4 8 1911 15.62	38 41.01	22 13.21	9.75	2.5Z
36	83 411 2119 45.56	38 40.69	22 14.71	12.87	2.6
37	83 425 4 2 24.78	38 57.24	22 17.75	7.81	2.7Z
38	83 429 440 5.33	38 40.98	22 14.49	11.06	3.2Z
39	83 325 3 0 16.05	38 47.66	23 27.87	14.43	2.1Z
40	83 319 1012 57.30	39 4.94	23 14.03	16.97	1.9

* Magnitudes assigned by a vertical component only

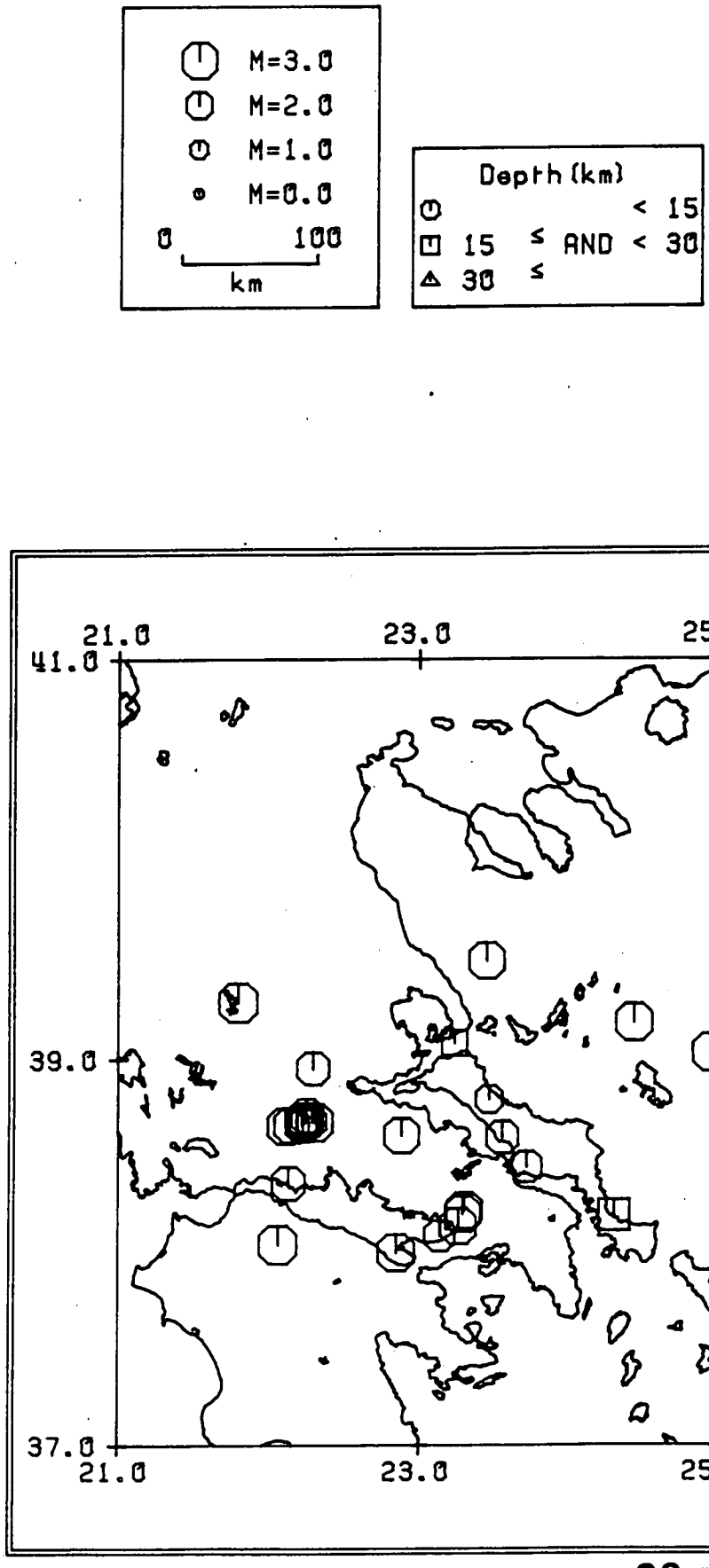

Figure 4.9 Location of sample events for the period 1st Jan 1983 - 30th June, 1983.

$$r = 0.32\,\beta/f_c \quad , \tag{4.12}$$

$$\Delta\sigma = (7/16)\,(M_o/r^3) \quad , \tag{4.13}$$

$$s = M_o/\pi r^2 \mu \quad . \tag{4.14}$$

(4.11) is quoted from Thatcher and Hank's (1973) work on Californian seismic moments, which assumes that small earthquakes can be approximated by circular faults of radius r. Because the VOLNET stations are close to the events in this study, no correction was thought necessary for anelastic attenuation. In support of this Modiano and Hatzfeld (1982) did a similar study to the present one in the Pyrenees, and found that a cylindrical correction for geometric spreading, which consists only of multiplication by source station distance R, accounted for all the observable reduction of the signal amplitude with distance. The factor $\sqrt{2}$ in (4.11) allows for an equal amplitude on the horizontal component of the seismogram, and the factor 2 accounts for losses in energy at the station caused by free surface reflection of SH waves. In the present work the radiation pattern $\Psi_{\phi\theta}$ was taken to be cylindrical, with an average value of 0.6. Since most of the events were shallow, a crustal density $\rho = 2.7$ g cm^{-3} was chosen as in Thatcher and Hanks (1973), and the P wave velocity α was assigned a value according to the event's hypocentral depth (table 4.10, from Makris, 1977). These values for ρ and α have received recent confirmation from Calcagnile et al (1984).

(4.12) is an average formula from Madariaga (1976), which assumes a rupture velocity 0.9 β for propagation of the crack tip with $\beta = (2/3)\alpha$. The last two equations (4.13), (4.14) follow from (4.11), (4.12), (1.4) and (1.18).

Table 4.10 P-wave velocity model for Central Greece*

Velocity (km s^{-1})	Depth to top of layer (km)
4.0	0
6.0	1.07
6.7	24.0
8.16	30.0

* after Makris (1977)

4.4.3 Method of analysis

The basic method of extracting M_o, r, $\Delta\sigma$ and s from the VOLNET seismograms is to fit a theoretical spectral level Ω_o by eye to the Fourier transform of the displacement spectrum, and then judge the corner frequency f_c as the point at which the spectral density begins to fall off. On log-log paper both lines should theoretically be straight (fig 4.10). The data provided from VOLNET are digital velocity seismograms so the first step after applying a Fast Fourier transform is to correct for the instrument response, in this case from a Willmore MkIII seismometer, via the expression

$$\Theta(\omega) = AKD \text{ mod } \frac{\{ -j\omega^3 \}}{\{\omega_o^2 - \omega^2 + 2j\beta\omega\omega_o\}} \quad 10^{-9} \text{ digital units/m}\mu \qquad (4.15)$$

Θ : displacement response

A : amplifier modulator gain = 200

K : seismometer motor constant $\approx$ 500 volt $m^{-1}s^{-1}$

β : seismometer damping = 0.7

f_o : natural frequency = 1/1.5 Hz ($\omega_o = 2\pi f_o$)

D : digitiser gain = 1024 digital units/volt

ω : angular frequency

(see VOLNET Station Bulletin, Jan 1983).

First of all the effect of removing the noise, and then smoothing the resultant spectrum after the instrumental correction (4.15) was investigated (figs 4.10a,b,c). This resulted in an improvement on the basic signal on its own, with a typical random uncertainty in estimating Ω_o and f_c (by eye fitting) of about 40% and 25% respectively. The time 'window' T for these

Figure 4.10 Method of Spectral Analysis: Investigating the effect of (i) removal of noise and smoothing and (ii) different time windows on the spectrum. The following features are common to all of the diagrams; Top line - title; next 3 lines - tape code and station; top diagram - velocity seismogram showing time windows for noise (above left) and signal (right), with 1 sec scale marker (bottom left); bottom diagram - displacement spectrum in 10^{-9} m s units (noise shown as dotted lines). The windows defined by the P arrival time and the theoretical S arrival time from Makris's (1977) earth model are given in percentages below.

a) 75% window: original signal and noise (dotted line)
b) 75% window: signal with noise removed
c) 75% window: smoothed signal with noise removed
d) 25% window: " " " " "
e) 50% window: " " " " "
f) 100% window: " " " " "

The results of fitting two straight lines to estimate Ω_o and f_c as defined in the text are as follows:-

	Ω_o ($\times 10^{-9}$m s)	f_c (Hz)
(a)	7.0	4.0
(b)	6.0	4.2
(c)	5.5	4.0
(d)	4.0	3.6
(e)	4.8	4.2
(f)	6.0	4.1

It can be seen from diagrams (a)-(c) that removing the noise and normalising the resultant spectrum by smoothing greatly assists the eye fit of two straight lines. By inspecting the diagrams (c)-(f) and consulting the above table it can also be seen that procedure (c) covers most of the long period P-wave energy, and has the added benefit of avoiding early S wave energy. Uncertainties in 4(c) are about 40% in Ω_o and approximately 25% in f_c.

(The figures referred to appear on the following six pages).

75% Window. Original signal and noise.
Network: VOLNET=C Tape: VL013 Event: 10200
Start: 14-Jan-83 2:24: 0.0 Corr: 0.88 Length: 2.0 Rate: 50.00 Gain: 1024.
VFI Z original seismogram

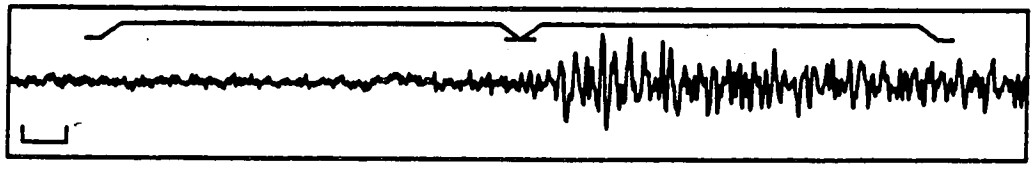

Spectrum of corrected seismogram

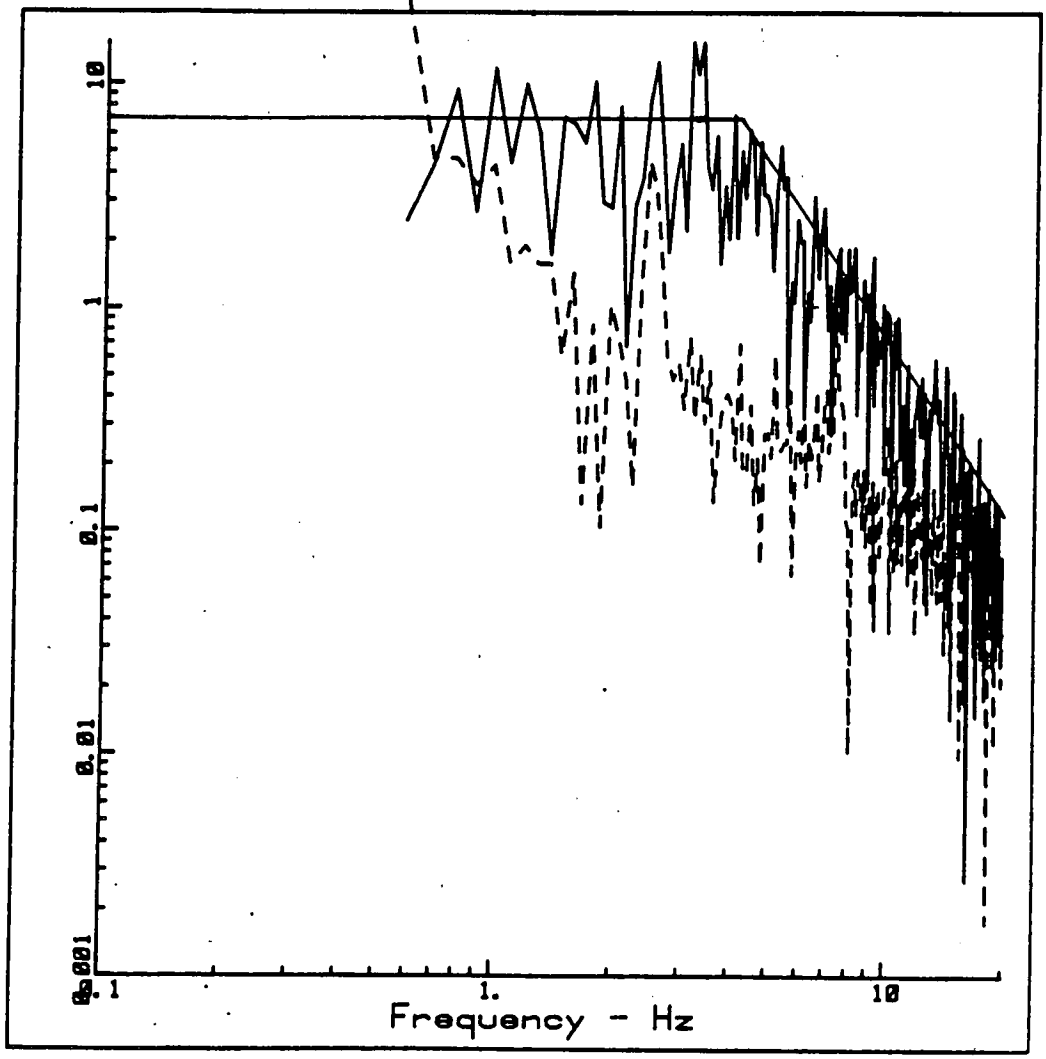

Figure 4.10a

75% Window. Original signal - noise.
Network: VOLNET-C Tape: VL013 Event: 10200
Start: 14-Jan-83 2:24: 0.0 Corr: 0.88 Length: 2.0 Rate: 50.00 Gain: 1024.
VFI Z original seismogram

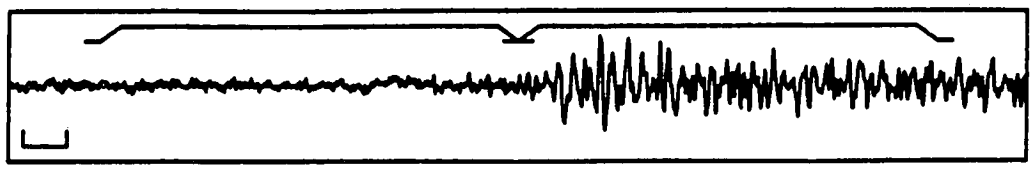

Spectrum of corrected seismogram

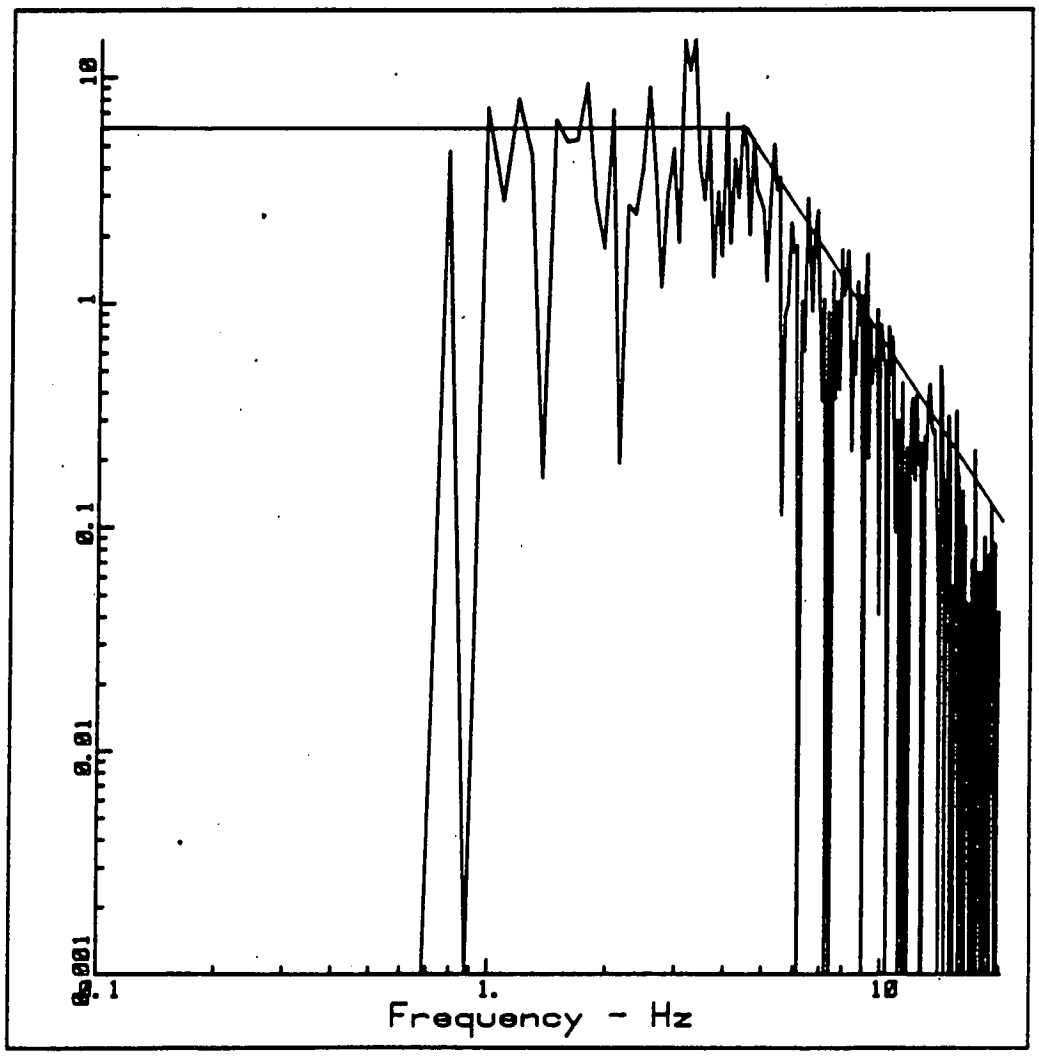

Figure 4.10b

75% Window. Smoothed signal - noise.
Network: VOLNET-C Tape: VL013 Event: 10200
Start: 14-Jan-83 2:24: 0.0 Corr: 0.68 Length: 2.0 Rate: 50.00 Gain: 1024.
VFI Z original seismogram

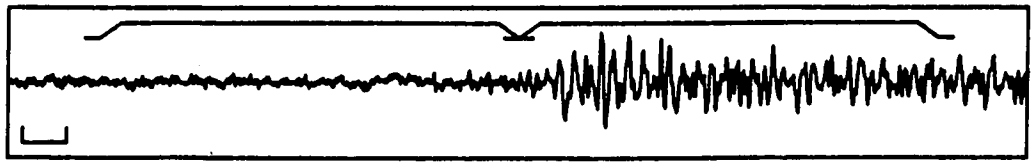

Spectrum of corrected seismogram

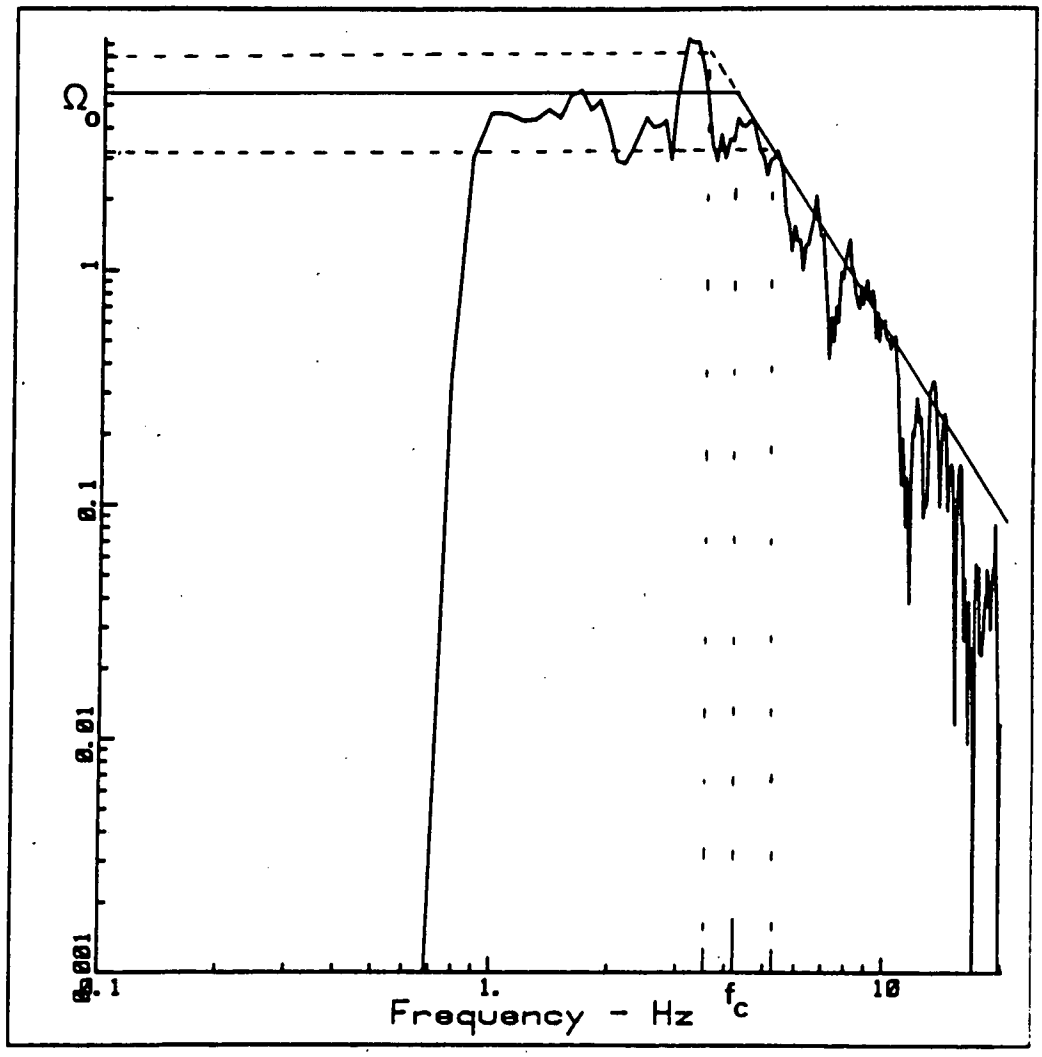

Figure 4.10c

25% Window. Smoothed signal - noise.
Network: VOLNET-C Tape: VL013 Event: 10200
Start: 14-Jan-83 2:24: 0.0 Corr: 0.68 Length: 2.0 Rate: 50.00 Gain: 1024.
VFI Z original seismogram

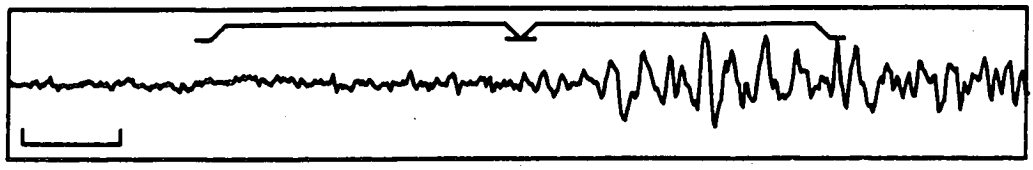

Spectrum of corrected seismogram

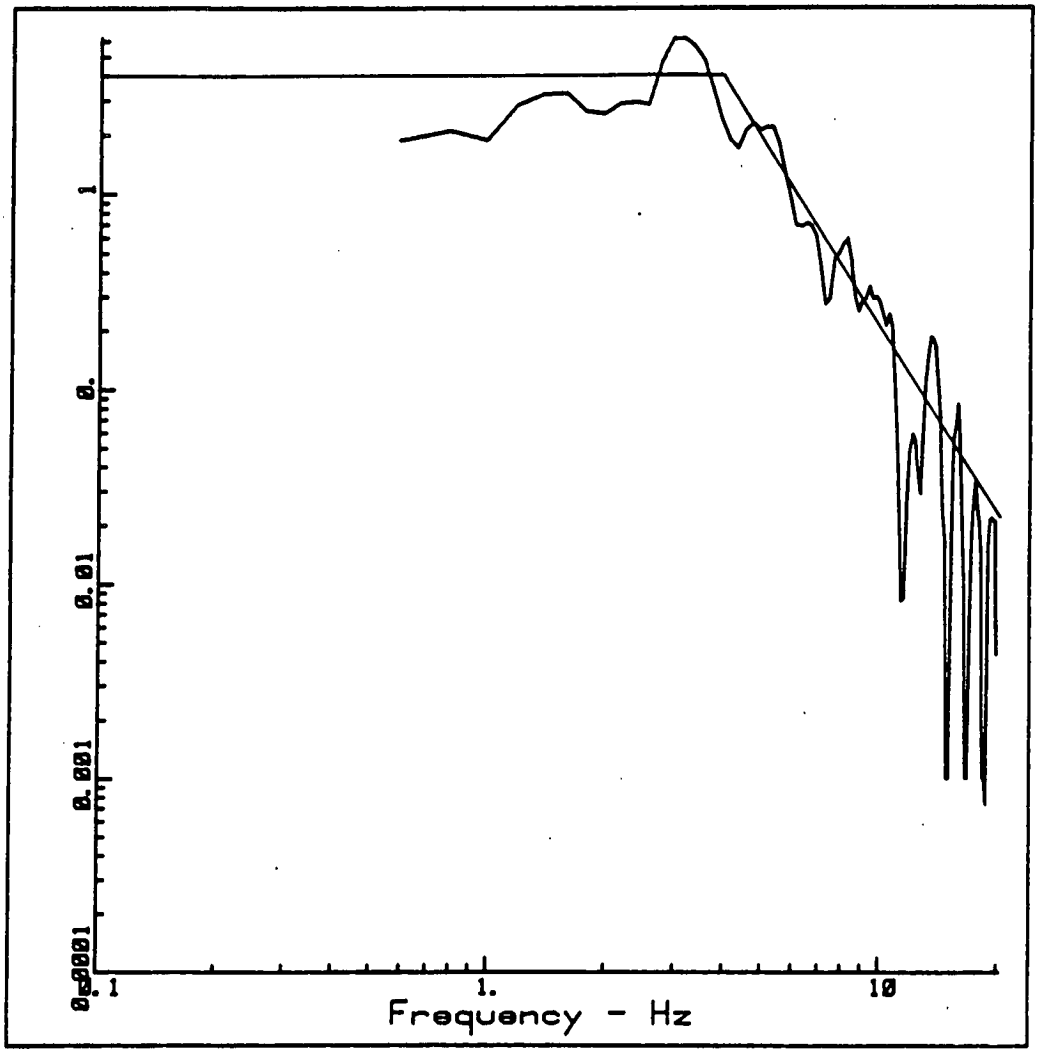

Figure 4.10d

50% Window. Smoothed signal - noise.
Network: VOLNET-C Tape: VL013 Event: 10200
Start: 14-Jan-83 2:24: 0.0 Corr: 0.68 Length: 2.0 Rate: 50.00 Gain: 1024.
VFI Z original seismogram

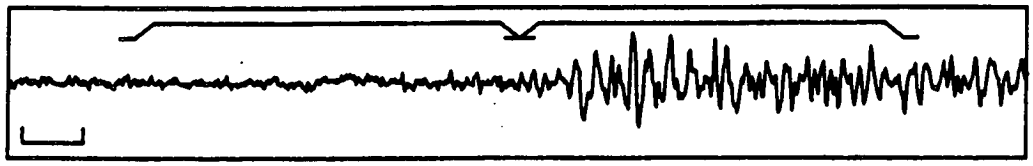

Spectrum of corrected seismogram

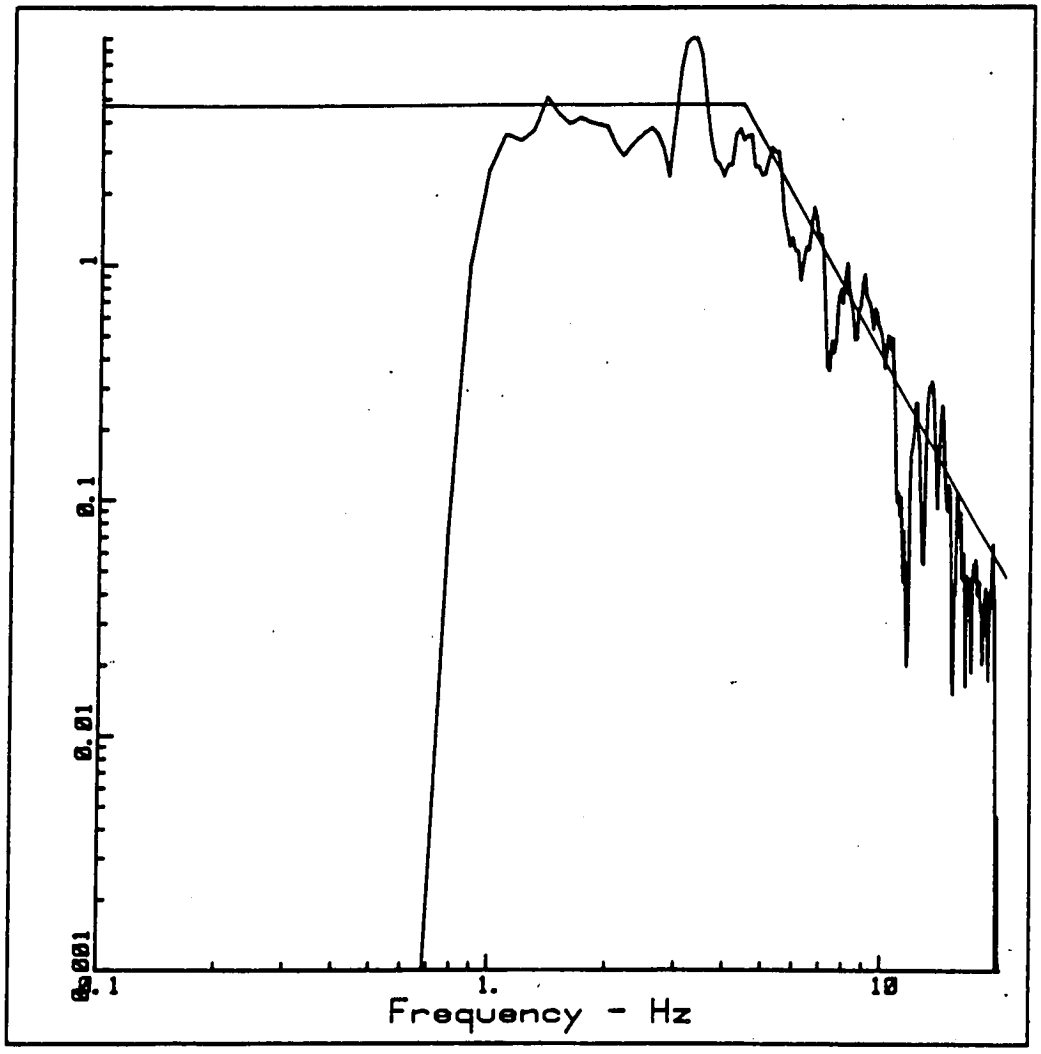

Figure 4.10e

100% Window. Smoothed signal - noise.
Network: VOLNET-C Tape: VL013 Event: 10200
Start: 14-Jan-83 2:24: 0.0 Corr: 0.88 Length: 2.0 Rate: 50.00 Gain: 1024.
VFI Z original seismogram

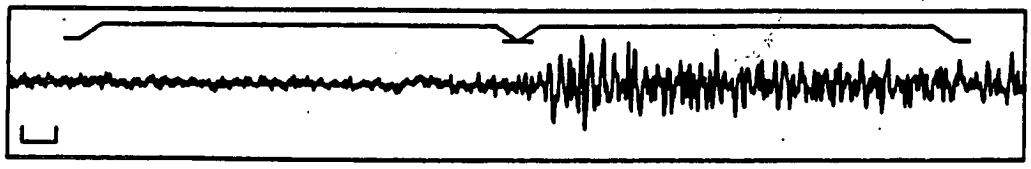

Spectrum of corrected seismogram

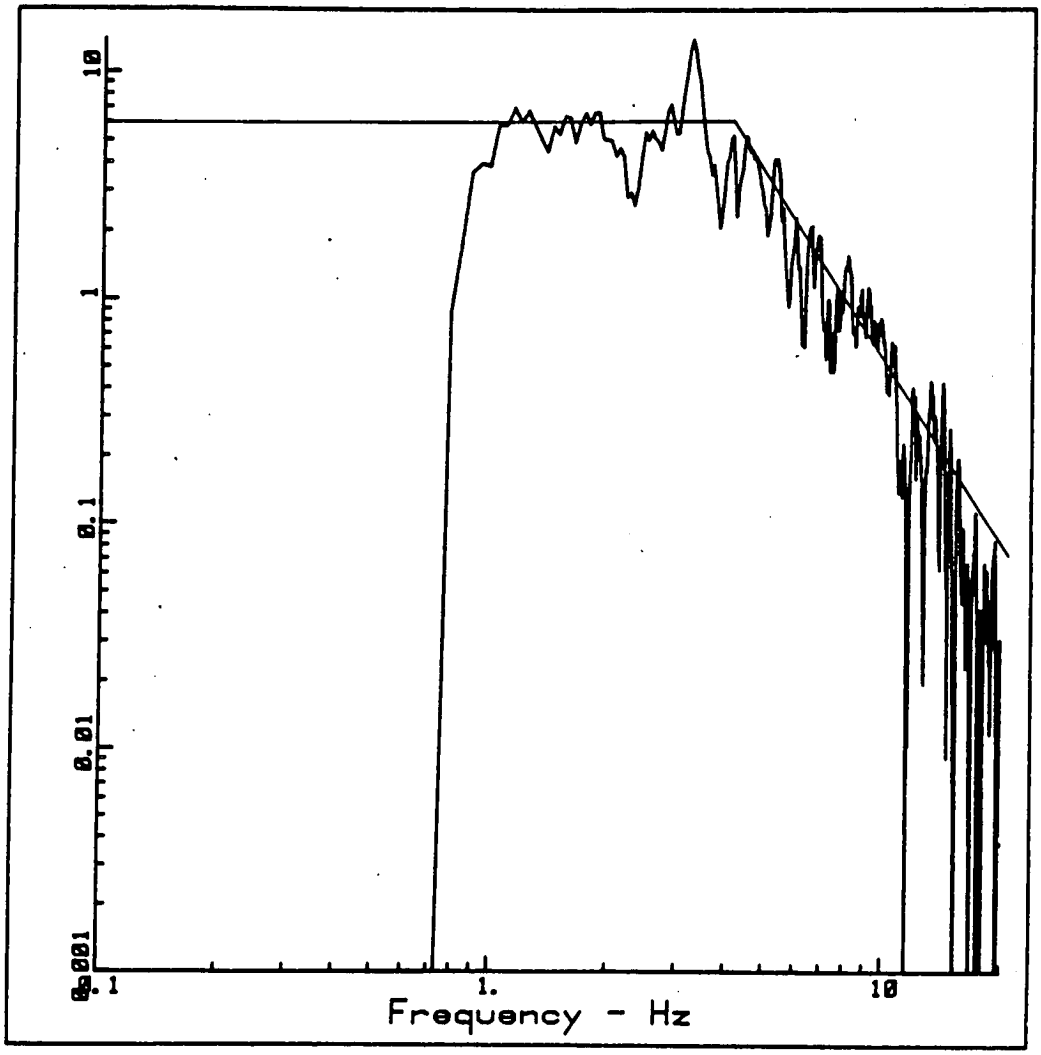

Figure 4.10f

events was initially chosen as 75% of the difference between the theoretical P and S arrival times via

$$T = R/(\alpha-\beta) \quad , \qquad (4.16)$$

where α, β are the P and S wave velocities in the lower layer and R is the source-station distance. By adjusting the time window to 25%, 50% and 100% (figs 4,10d,e,f) it was found that most of the relevant long period signal Ω_o was included by the 75% window (see caption to fig 4.10), while avoiding any possible early S wave energy. This rule of thumb is reasonable except where there was evidence of reflection or refraction. In these cases the recording was not used in the analysis.

The method can be summarised thus:-

1) Copy the digital record of an event's velocity seismogram from a library tape to a working/scratch magnetic tape
2) Copy the event's time and location, its P-wave arrival time t_o, and the location of each station from the VOLNET bulletin
3) Compute R and 75% T by (4.16) to define two time windows at each station (+T for signal, -T for noise)
4) Obtain a Fourier transform of the digital record at each station for the signal and the noise
5) Correct to displacement spectrum via the instrument correction (4.15) at each station
6) Remove noise from signal and smooth to obtain a final spectrum like fig 4.10c
7) Read off Ω_o, f_c from resultant spectrum by eye as in fig 4.10c
8) Convert to source parameters using (4.11)-(4.14)

Steps 1, 2 are routine, 3 is done by VOL-PREP which was written for the present work and computer programmes for carrying out the spectral analysis of steps 4-6 by a Fast Fourier routine were made available (Bob McGonigle, 1984, pers. comm.). Finally Ω_o and f_c were reduced to source parameters by equations (4.11) - (4.14) via VOL-DIST, which uses specific values of α, β for the source layer. This differs from previous studies such as Thatcher and Hanks (1973), who used only one fixed value in their work. Both computer programmes indicated by the prefix VOL- are listed in Appendix 1.

4.4.4 Results

The results of this section are summarised in tables 4.11 and 4.12, the former listing Ω_o, f_c, R for each event-station pair, and the latter the final results for M_o, r, $\Delta\sigma$ and s. The individual parameters are plotted against each other in figs 4.11-4.17.

4.4.5 Error analysis

A typical reading error ±40% in Ω_o and ±25% in f_c (fig 4.10c) has already been noted. Additional random uncertainties lead to standard deviations from the mean value of M_o of 20%-80% and 10%-40% from the mean value of r (see table 4.12). Typical random errors in Ω_o of about ±50% and ±25% in f_c can therefore be estimated. However, there are other sources of uncertainty which are systematic, and these are now considered in turn.

First consider equation (4.11). No measurement of ρ was available for this region at the time of analysis so a value 2.7 g cm^{-3} was assigned (Thatcher and Hanks, 1973). To be conservative

Table 4.11. Intermediary steps in the evaluation of source parameters for 28 sample events recorded on VOLNET.

(a) Station codes and coordinates.

Code	Lat	Lon
1:VSI	38.8793	23.2090
2:VPA	38.7815	22.3400
3:VFI	39.2352	22.5921
4:VGL	39.4456	22.8842
5:VNE	39.3119	23.2322
6:VSK	39.1106	23.6935
7:VMA	38.7059	23.5877
8:VER	38.2005	23.3600
9:VAG	38.3161	22.9003

(b) Epicentral distances R in km calculated from Tables 4.9 & (a)

Event no.	VSI	VPA	VFI	VGL	VNE	VSK	VMA	VER	VAG
1	73.1	104.1	128.0	140.3	120.8	104.1	59.0	5.8	36.5
3	111.4	186.9	159.3	136.9	104.8	64.7	90.7	143.7	164.5
6	42.9	107.3	109.0	110.1	83.5	57.8	12.0	47.6	65.1
7	75.0	104.5	129.2	141.9	122.7	106.3	61.2	6.2	36.2
9	151.8	228.0	205.1	184.2	151.7	109.1	123.6	166.2	195.1
13	98.2	23.9	76.1	109.7	120.9	145.9	128.3	120.2	78.6
14	81.4	11.8	66.5	98.7	106.5	129.4	111.3	106.0	65.4
15	86.2	13.6	68.2	101.0	110.2	134.0	116.5	110.7	69.8
16	86.6	13.6	68.1	100.9	110.3	134.3	116.9	111.3	70.4
17	65.1	125.4	130.9	132.1	104.6	73.5	30.7	41.6	72.8
18	94.6	20.7	73.8	107.2	117.7	142.3	124.7	117.1	75.6
19	89.0	16.5	71.0	103.9	113.2	136.8	118.8	111.9	70.7
20	85.0	10.6	64.8	97.8	107.6	132.4	116.0	112.1	71.6
21	135.9	84.8	139.4	170.5	173.1	184.4	151.7	114.8	79.0
22	121.7	183.1	188.0	185.2	154.6	114.2	84.1	82.7	123.5
23	88.1	15.8	70.3	103.1	112.3	135.9	118.0	111.3	70.1
26	130.3	73.4	68.9	95.3	123.8	165.0	168.0	181.8	144.3
28	87.4	103.2	135.2	151.6	135.4	122.7	78.5	22.8	32.2
29	109.6	49.5	104.4	136.3	141.8	158.7	132.2	108.8	67.2
31	41.0	51.1	73.9	92.7	83.5	89.5	62.0	61.5	32.6
32	71.6	124.4	79.3	48.9	27.7	47.8	88.6	144.0	139.4
33	82.8	11.7	66.6	99.0	107.4	130.6	112.9	107.7	67.1
34	86.2	12.8	67.2	100.1	109.6	133.8	116.7	111.6	70.8
35	88.6	15.1	69.2	102.2	112.0	136.2	118.9	113.0	71.9
36	86.6	14.1	68.7	101.5	110.7	134.4	116.8	110.8	69.8
37	79.6	19.5	40.4	74.5	90.1	122.2	115.4	124.8	88.2
39	24.1	97.6	90.0	88.0	60.8	40.3	14.5	66.5	72.3
40	22.6	84.3	58.0	50.3	25.5	39.9	51.8	98.4	89.8

(cont....)

Table 4.11 (cont.)

(c) Long period spectral level Ω_o in micron s read by eye off diagrams such as fig 4.10c.

No	VSIZ	VSIN	VSIE	VPA	VFI	VGL	VNE	VSK	VMA	VER	VAG
1	0.022			0.015		0.016	0.050	0.035			0.080
3	0.050	0.062	0.045		0.005	0.006	0.010	0.020		0.006	0.007
6		0.012	0.018	0.004	0.004	0.005				0.011	0.003
7	0.065		0.090	0.012	0.020	0.015	0.100	0.120	0.060		
9	0.014	0.018	0.012			0.009	0.006	0.014		0.004	
13		0.180	0.100				0.090	0.020		0.052	0.140
14	0.080	0.120	0.140						0.060	0.060	0.120
15					0.008	0.012	0.006		0.005	0.009	0.028
16	0.014	0.014	0.012		0.010	0.006	0.012		0.010	0.008	0.025
17	0.035	0.060	0.040		0.006	0.028	0.050	0.045	0.095	0.030	0.080
18		0.100	0.085		0.080	0.080	0.180	0.030	0.050	0.100	
19			0.065		0.100		0.250	0.050	0.045	0.040	0.120
20		0.007	0.006		0.009	0.028	0.020		0.004	0.006	0.018
21					0.700	0.800	1.000	0.620	0.700	1.400	1.000
22	0.012	0.015	0.020			0.008	0.012	0.006			
23		0.035	0.025		0.007	0.008	0.010		0.015	0.022	0.030
26	0.110	0.110	0.075	0.030	0.120	0.180	0.180	0.030	0.055	0.028	0.060
28				0.004			0.002	0.005	0.001	0.035	0.007
29	0.054	0.065	0.050	0.160	0.060	0.044	0.040	0.007	0.035	0.045	0.020
31	0.021	0.025	0.030	0.025	0.015		0.022	0.007		0.016	
32	0.200	0.300	0.250	0.032	0.074			0.085	0.050	0.028	0.025
33	0.002	0.003	0.002		0.003	0.002	0.003			0.002	0.007
34	0.015	0.020			0.040	0.040	0.070		0.010	0.009	0.036
35	0.018	0.018	0.023		0.015	0.085	0.070	0.009	0.010	0.012	0.020
36	0.006	0.006	0.004		0.015	0.015	0.012			0.007	0.014
37		0.045	0.056			0.066	0.110	0.026	0.050	0.028	0.020
39					0.005	0.010	0.030	0.013	0.016	0.007	0.004
40					0.012	0.022	0.100	0.010	0.016		0.010

(cont...)

Table 4.11 (cont.)

(d) f_c in Hz read in similar fashion to (c).

No	VSIZ	VSIN	VSIE	VPA	VFI	VGL	VNE	VSK	VMA	VER	VAG
1	2.200			3.400		3.000	2.800	4.500			2.800
3	4.200	4.200	5.400		4.000	9.500	8.000	3.600		5.200	3.400
6		5.200	3.800	4.000	4.500	6.400				4.500	8.000
7	1.400		1.600	2.400	1.400	2.500	2.200	2.900	1.600		
9	4.200	4.200	4.200			3.200	4.500	3.200		6.200	
13		3.000	3.000				4.000	3.800		4.500	4.000
14	5.000	4.800	3.800						3.800	3.500	3.800
15					5.200	5.400	6.500		7.000	6.000	4.100
16	5.200	4.800	5.000		5.200	7.200	4.500		5.000	5.200	4.500
17	3.000	3.000	3.200		3.500	3.200	3.200	3.200	3.000	2.500	3.500
18		3.000	3.000		4.800	5.000	3.600	3.000	3.800	3.200	
19			5.900		4.000		4.000	3.000	5.100	5.400	3.000
20		2.100	3.400		4.800	4.800	4.000		3.200	3.600	4.100
21					2.000	2.100	1.900	1.800	2.000	1.500	1.800
22	2.400	2.200	2.200			3.200	2.500	2.500			
23		2.100	3.100		5.000	5.500	4.000		2.500	2.500	4.500
26	2.200	2.800	3.000	4.000	3.100	1.800	2.200	3.200	1.800	2.800	3.400
28				4.200			4.000	3.500	7.000	3.300	6.400
29	2.800	3.600	3.300	4.200	3.200	3.500	3.500	4.600	3.000	3.100	4.000
31	3.500	2.500	3.100	3.500	3.600		5.200	5.000		5.200	
32	2.200	3.200	2.800	1.800	3.200			4.800	2.500	3.200	3.400
33	12.000	5.000	5.200		7.000	9.000	7.600			6.500	7.000
34	10.000	4.500			6.800	8.200	5.000		3.600	8.000	9.000
35	9.000	6.000	4.000		3.500	1.800	3.500	2.700	3.200	3.100	4.900
36	4.500	4.500	5.700		4.800	5.000	5.000			4.200	4.000
37		3.000	3.000			3.500	5.100	3.200	2.500	1.600	6.000
39					6.000	11.000	7.500	9.000	6.500	6.100	6.000
40					3.000	5.100	4.900	3.900	6.000		5.900

Table 4.12 Source parameters of 28 small earthquakes in Central Greece.

Units : M_o is in 10^{12}Nm, r in m, $\Delta\sigma$ in bars, s in mm.
Standard deviations are given below in %, N=No of stations.

No	M_L	M_o	r	$\Delta\sigma$	s	N
1	3.1	25.9	429.9	1.4	1.49	6
		51.3	20.9	62.8	59.2	
3	3.2	22.6	270.6	5.0	3.28	9
		88.3	29.0	101.6	97.3	
6	2.7	4.4	261.3	1.1	0.68	7
		31.3	22.6	50.1	44.7	
7	3.1	49.9	686.1	0.7	1.12	8
		72.6	26.0	85.4	81.3	
9	3.3	4.2	209.7	2.0	1.02	7
		38.9	19.9	51.9	48.0	
13	3.1	84.1	351.9	8.4	7.21	6
		46.7	15.5	53.9	51.6	
14	3.2	69.7	316.0	9.7	7.41	6
		23.3	12.8	32.1	29.4	
15	2.9	8.7	231.1	3.1	1.73	6
		47.3	18.2	56.8	53.8	
16	2.8	9.5	251.1	2.6	1.59	9
		30.1	11.8	36.4	34.4	
17	2.5	27.4	411.7	1.7	1.72	10
		47.2	9.5	50.0	49.1	
18	3.0	81.2	361.3	7.5	6.60	8
		52.5	18.3	61.3	58.5	
19	2.8	81.6	313.6	11.6	8.81	7
		82.1	25.5	93.2	89.6	
20	2.8	9.9	362.8	0.9	0.80	8
		69.7	28.4	85.3	80.4	
21	3.4	1067.7	690.2	14.2	23.78	7
		25.6	10.8	31.7	29.8	
22	2.6	14.0	519.3	0.4	0.55	6
		32.6	11.7	38.4	36.5	
23	2.5	15.1	391.8	1.1	1.05	8
		46.9	33.4	74.4	66.5	

(cont...)

Table 4.12(cont.)

No	M_L	M_o	r	$\Delta\sigma$	s	N
26	3.4	91.1	493.4	3.3	3.97	11
		53.5	25.6	69.5	64.6	
28	2.5	3.6	293.1	0.6	0.44	6
		55.5	26.4	71.9	66.8	
29	2.8	13.1	246.5	3.8	2.29	11
		39.4	13.9	46.2	44.1	
31	3.0	9.6	344.5	1.0	0.86	8
		29.8	25.3	53.0	46.5	
32	3.1	76.2	455.4	3.5	3.90	9
		75.3	26.9	88.5	84.3	
33	2.3	2.2	185.0	1.5	0.69	8
		43.4	25.0	61.3	56.0	
34	2.8	23.8	208.5	11.5	5.81	8
		75.2	36.3	98.1	91.1	
35	2.5	24.1	366.1	2.2	1.91	10
		98.2	40.5	120.7	113.7	
36	2.6	7.6	274.2	1.6	1.07	8
		43.5	10.3	47.0	45.9	
37	2.7	39.9	423.8	2.3	2.36	8
		49.5	39.7	84.7	74.9	
39	2.1	5.8	180.1	4.4	1.90	7
		75.2	19.8	82.6	80.2	
40	1.9	9.3	282.5	1.8	1.24	6
		64.0	26.4	78.6	74.1	

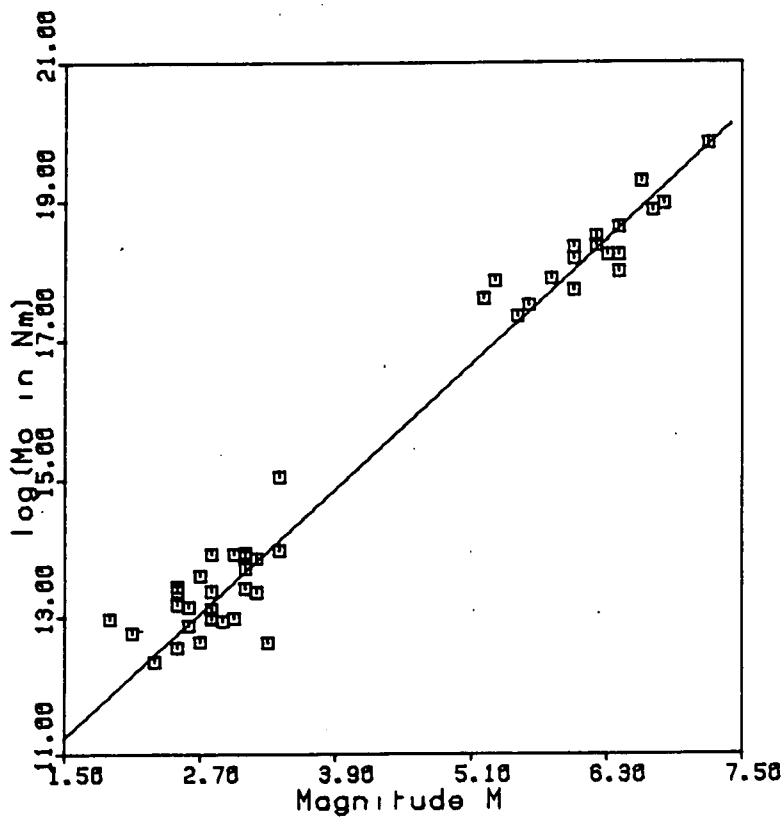

Figure 4.11 Moment-magnitude calibration for Central Greece.

There are two data sets of seismic moment vs magnitude. These are:

(a) M_L/M_O from table 4.12 for the small earthquakes analysed in this chapter ($1.8 < M_L < 3.5$)

(b) M_S/M_O from the tables 4.2 and 4.3 for the teleseismic events analysed by North (1977) and Jackson et al (1982) in the area ($5.3 < M_S < 7.5$)

The straight line drawn corresponds to A = 16.0 in (1.5), or $\Delta\sigma$ = 38 bars, with B = 1.5. Empirically, at least, the two data sets are described by the same equation.

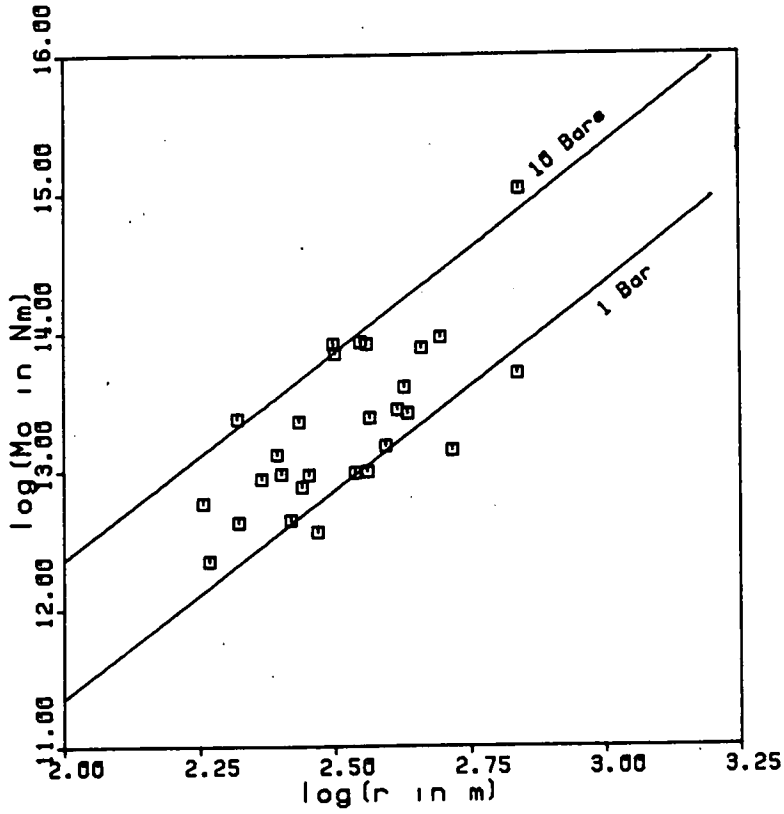

Figure 4.12 Seismic moment vs source radius.
The straight lines are drawn for given stress drops of 1 bar and 10 bars using (4.13). Since $M_o \alpha r^3$ for $\Delta\sigma$ = const, the slope of the lines on this logarithmic plot is 3. Data points come from table 4.12.

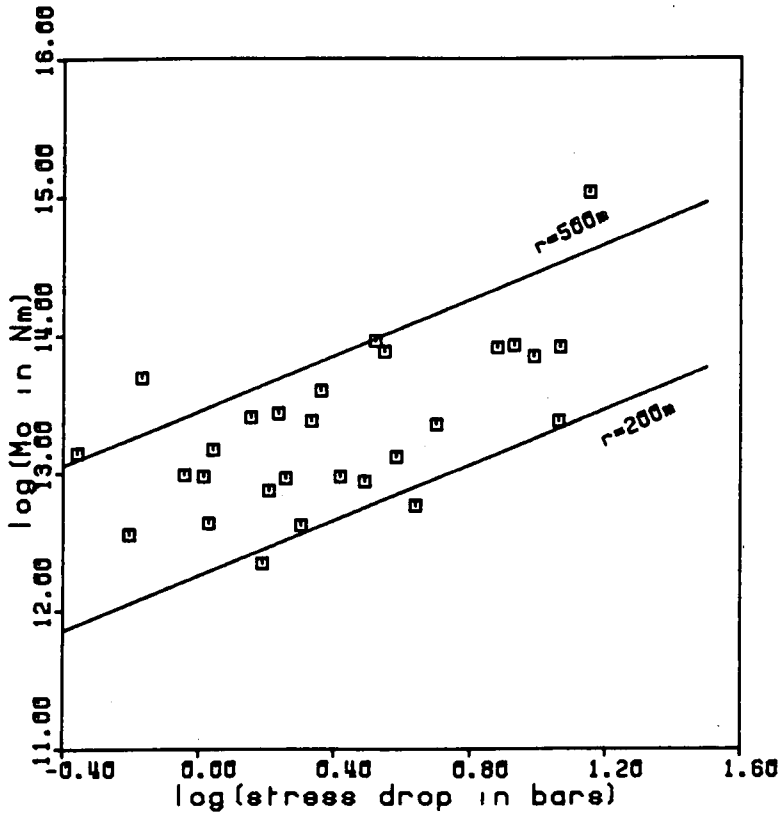

Figure 4.13 Seismic moment vs stress drop.
The straight lines are drawn for given source radii of 200m and 500m using (4.13). Since $M_o \alpha \Delta\sigma$ the slope of the lines is 1 for r = const. Data points come from table 4.12.

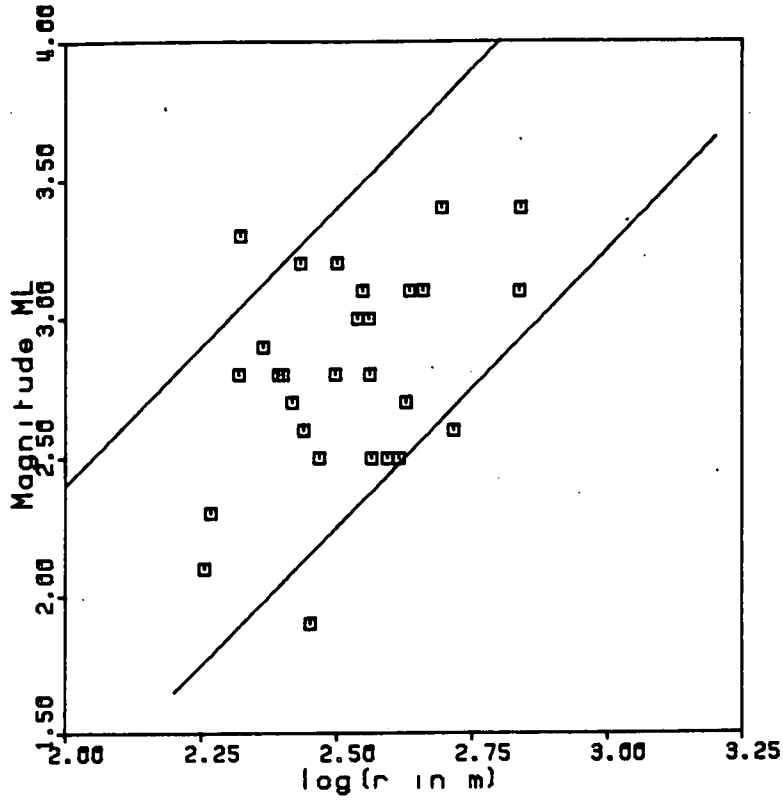

Figure 4.14 Local magnitude vs source radius.
The straight lines drawn are for arbitrary constant $\Delta\sigma$. Since $M_o \propto r^3 \propto 10^{BM}$ a slope of 2 is expected for B = 3/2. Data points come from table 4.12. Note the increased scatter compared with the diagram for M_o vs r (fig 4.12).

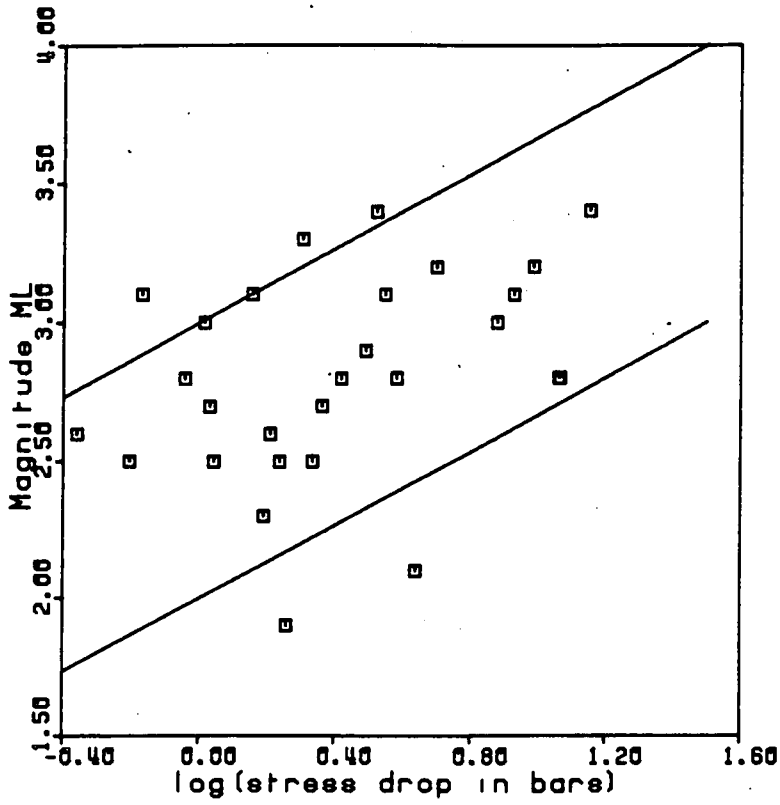

Figure 4.15 Local magnitude vs stress drop.
The straight lines drawn are for arbitrary constant r. Since $M_o \alpha \Delta\sigma \alpha 10^{BM}$ we expect a slope of 2/3 for B = 3/2. Data points come from table 4.12.

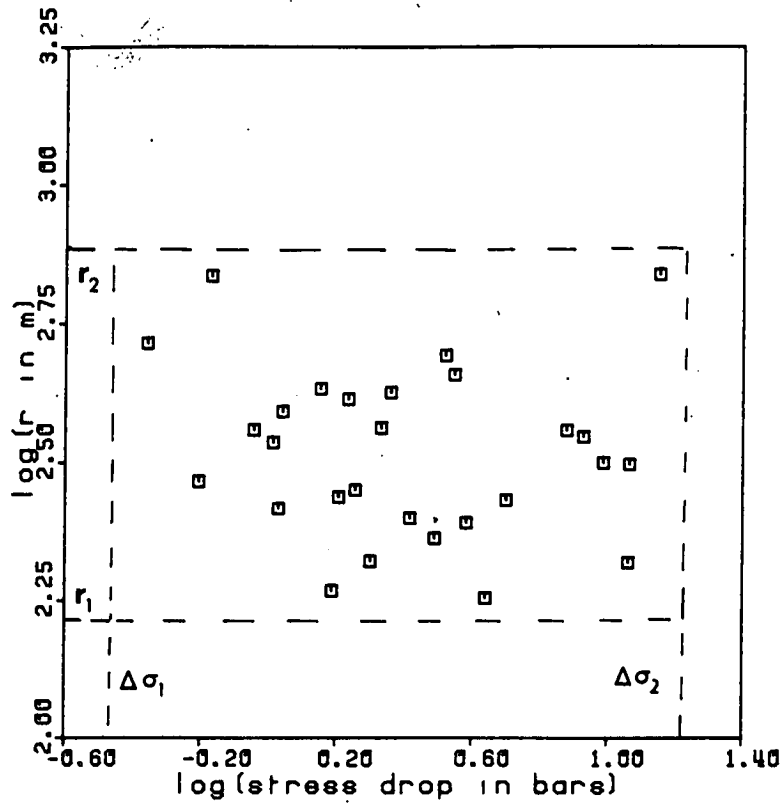

Figure 4.16 Source radius vs stress drop.
These two parameters are confined within limits ($\Delta\sigma_1$, $\Delta\sigma_2$) and (r_1, r_2) as expected by Caputo (1976), but there are not enough points to investigate their internal distribution. Data points come from table 4.12.

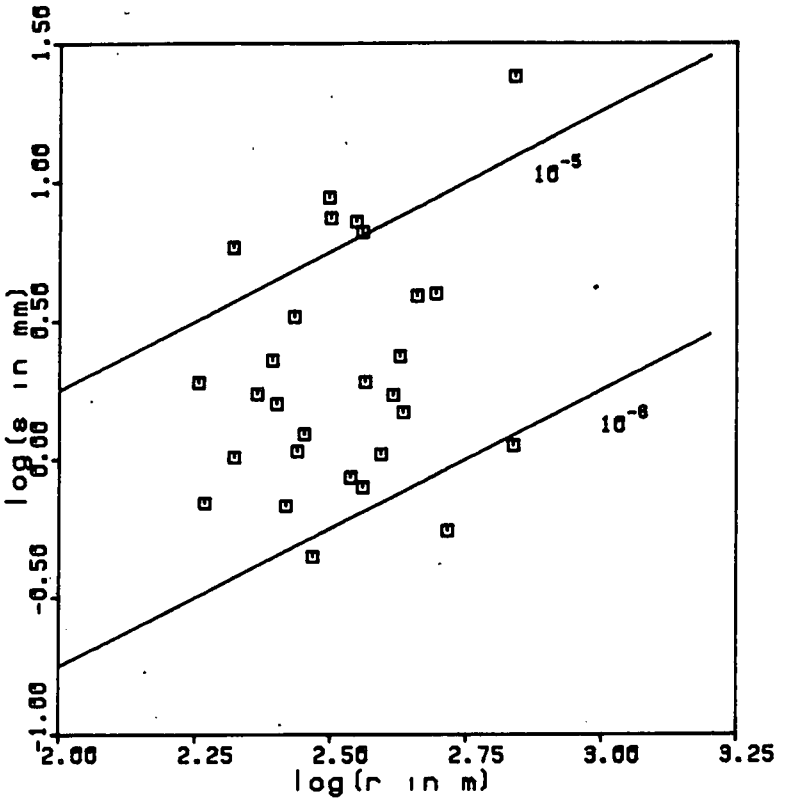

Figure 4.17 Fault slip vs source radius.
This graph shows that typical strain drops (defined by $s/(r\sqrt{\pi})$ for a circular fault) are in the range 10^{-6} to 10^{-5}. Data points come from table 4.12.

an uncertainty of 30% in this parameter may be estimated. Due to uncertainties in focal depth and in the velocity model of table 4.6 α may only be correct to 30% or so. Systematic uncertainties in the radiation pattern will be much smaller than the random error already accounted for by taking a standard deviation, so their contribution can be neglected. Thus the total systematic uncertainty in M_o from equation (4.11) is given approximately by

$$\left\{\frac{\delta M_o}{M_o}\right\}^2 = \left\{\frac{\delta \rho}{\rho}\right\}^2 + 3\left\{\frac{\delta \alpha}{\alpha}\right\}^2 , \qquad (4.17)$$

or 60%. Adding a typical random uncertainty in Ω_o of 50% gives a total error of ±80% in M_o.

A 30% uncertainty in α leads to a 30% systematic error in r via (4.12). After adding the random error, the total error in r is of the order 40%. From (4.13) and (4.14) it follows that the total uncertainty in $\Delta\sigma$ is around 106% and (allowing a conservative 30% error in μ) that in s is 102%.

These uncertainties may seem very small at first glance, but this is a reflection of the quality of the digital network and a consequence of using known local values for the various parameters. Of course the source parameters are highly model dependent, and this could also effect how the errors are quantified.

4.4.6 Discussion of results

The moment magnitude relation (1.5) with A = 16.0, B = 1.5 describes the data from table 4.12 and that of North (1977) and

Jackson et al (1982) quite well (fig 4.11). This empirical observation should not be pushed too far because of the unknown M_S/M_L relationship over the magnitude range 1.8-7.5. However, Kiratzi and Papazachos (1984) showed that $M_S - M_L = 0.5$ for the Athens observatory.

Fig 4.12 shows the range of typical stress drops is quite low (in the range 1-10 bars), but this matches the typical stress drop of about 7-12 bars for the large events near Thessaloniki (1978) and in the Gulf of Corinth (1981) (table 4.3). It may be that the extensional regime which operates in the VOLNET area (including the Gulf of Corinth) leads to lower stress drops. This relatively constant stress drop is an important suggestion that the hypothesis of geometric similarity is applicable to this region.

Fig 4.13 shows the comparatively small variation in source radii 200-500m (a factor 2 or so). This could imply that the characteristic size of the elementary blocks postulated in fig 3.1 are quite large - about 500m. These macroscopic characteristic fault lengths may be yet another example of the crustal geometry behind the characteristic peaks in the frequency magnitude distribution found for the New Madrid area in fig 2.7 at 10km and 100km.

Fig 4.14 shows the increased scatter in the data caused by uncertainties in the local magnitude M_L. (Moment is a better description of the size of the seismic source, both intuitively and as evidenced by the reduced scatter of fig 4.12). A theoretical slope on the diagram of 2 does not describe the data as well as the theoretical slopes of the previous two figures.

Fig 4.15 also shows an increased scatter compared with fig 4.7 caused by uncertainties in M_L. A theoretical slope of 2/3 on

this diagram of magnitude vs stress drop describes the data reasonably well.

Fig 4.16 shows that Caputo's (1976) postulated shape of the boundary of possible stress drops and source lengths (a rectangle) is consistent with the data set of table 4.12. However there is insufficient data to discern the internal form of the distribution within this box.

Figure 4.17 shows that the typical strain drops are in the range 10^{-6} to 10^{-5} corresponding to the observed stress drop of 1-10 bars found on fig 4.6. Only one study of strain drops in the area has been done for events of $M_o > 10^{18}$ Nm. Kim et al (1984) found strain drops of (0.9-1.4) x 10^{-5} corresponding to stress drops of 7-10 bars (table 3 of their paper) for three events in the Corinth sequence of February and March, 1981. Therefore it is reasonable to infer that the assumption of relatively constant strain drop in deriving (3.18) is applicable to this area.

Since the typical size of the seismic moments of the VOLNET events in table 4.12 is 10^{13} Nm, this observation represents geometric self-similarity over a range of 10^{13}: 10^{18} or 1:10,000! This (at first) surprising self similarity of rock fracture, if confirmed in other studies, could have important implications in scaling up observations from controlled experiments on laboratory samples - particularly those investigating precursory phenomena for earthquake prediction (Allegre et al, 1982).

4.5 Summary

The basic objective of this chapter was to produce fundamental parameters for earthquakes in the Aegean area over a large range in magnitudes. First of all a literature search was done to discover

the available information on parameters such as seismic moment, stress drop, fault area, slip and fault plane solutions. The record on seismic moments was found to have gaps prior to 1963 and 1972-1978.

The next section plugged the gap in the seismic moment record of the larger events (>5.5 M_S), producing a complete list for the period 1972-1978 with only one exception out of seventeen events, from studies of surface waves. Three events were analysed by a calibration method because no fault plane solutions were available. This calibration showed that ignoring the medium response calculation only increased the random uncertainty in M_o from 25% to 40% - negligible when compared to the overall error in M_o of a factor ± 3 or so.

By adding these results to a similar study by North (1977), a relatively homogeneous catalogue of seismic moments for events of $M_S > 5.5$, for the period 1963-1978 was produced. These events dominate the total crustal deformation in this period for this area.

(It was hoped to analyse some seismograms for the period prior to 1963, but delays in obtaining somewhat rare records and the necessary scaling parameters postponed this to a future project.)

The final section dealt with the extraction of (M_o, r, $\Delta\sigma$, s) from P-wave spectra characterised by (Ω_o, f_c) of seismograms for small earthquakes (1.8 - 4.5 M_L) in Central Greece recorded on the VOLNET array. This was carried out in order to investigate the scaling properties of faulting over a wide range of earthquake magnitudes. Some 28 records out of 40 produced the required source parameters with seismic moments of about 10^{13} Nm. The main conclusions in this section were:-

(i) The moment-magnitude relation with A = 9.0 used in Chapter 2 for the Eastern Mediterranean also holds for these small events, although with a fairly large scatter;

(ii) Typical stress drops are consistently low in the range 1-10 bars with associated strain drops of 10^{-6} to 10^{-5}. These compare very well with the published data for the events at Thessaloniki (Jul 1978) and the Corinth (Feb, Mar 1981) sequence - representing self similarity of this aspect of the seismic process over an average energy range of 1:10,000! from the typical moment range of 10^{13} Nm to 10^{18} Nm for the region. This observation strongly supports two of the crucial assumptions in deriving the distribution (3.9) i.e. the relative constancy of $A(\Delta\sigma)$ and the assumption of constant strain drop via $e = s/\ell$ = const.;

(iii) Typical fault radii are 200-500m, so they are all roughly similar in extent (within a factor 2). This macroscopic quantisation could be another example of the pattern of characteristic fault lengths seen in the previous two chapters, but on a much smaller scale.

This chapter has laid the groundwork for a more detailed study of seismotectonics and seismic hazard in Greece and the Aegean in the next chapter, by providing moment magnitude data, and by justifying the use of the distribution (3.9) to assess the seismic hazard.

CHAPTER 5

A seismotectonic analysis of the Aegean area II: The seismotectonic model and associated earthquake hazard

5.1 Introduction

The preceeding two chapters have, in turn, developed a general model for the earthquake frequency magnitude relation, and then tested some of the assumptions on which the resulting distribution rests. In particular the assumption of self-similarity was found to hold over a wide range of magnitudes for the Greek seismicity catalogue of Makropoulos and Burton (1981) and for the results of a sample of events recorded by the VOLNET array. The last chapter also produced several new measurements of seismic moment, giving a homogeneous (though not perfectly complete) catalogue of surface wave moments for $M_s > 5.5$ for the time period 1963-1978. In this final chapter the intention is to apply the distribution developed in Chapter 3 to a particular area - the Aegean, by way of a more detailed case study, and also to attempt to shed some further light on an interesting and somewhat controversial problem - the details of the observed spreading of the Aegean.

First of all the available tectonic model is described and this is used to estimate a long-term moment release rate. Next an artificial moment catalogue is constructed by applying a moment magnitude relation to the events above 5.5 M_s which have no seismic moment assigned to them (principally those which occurred before 1963). The individual moments are then summed to give a short-term seismological moment release rate.

Both of these models are then compared and applied to the

frequency-magnitude distribution in the Aegean, in order to test the stationarity of the process of seismic energy release and to further investigate the distribution of Chapter 3. Note that for the purpose of this chapter the 'Aegean area' includes mainland Greece and the western edge of Turkey. (It will be shown that the Aegean area cannot be described as a simple plate).

5.2 A tectonic model of Aegean spreading

The basic problem with describing the tectonics of the Aegean area is that it does not seem to behave as if it were a rigid plate, or even the rigid edge of a larger Eurasian plate. Since plate tectonics requires such rigidity a modified, or second order, theory is needed to account for the observed spreading and concurrent thinning of the earth's crust in mainland Greece and under the Aegean sea.

McKenzie (1972) at first tried to preserve the notion of rigid plates by dividing the whole area into microplates as in fig 5.1, but abandoned this idea (McKenzie, 1978) when it became obvious that there was no evidence for the transform fault cutting through Central Greece on the diagram (fig 5.2), and that the Aegean was actually being thinned rather than moving as a block (Makris, 1976). Makris interpreted the deformation of the area as attenuation due to the surface expression of a mantle plume, and McKenzie (1978) to a convection cell set up by a slab sinking under the Hellenic arc and a sinking blob of cold crust off Western Greece. McKenzie, with the added knowledge of the available fault plane solutions, interpreted the thin crust as being due to stretching rather than attenuation by a mantle plume.

Le Pichon and Angelier (1979, 1981) also interpreted the

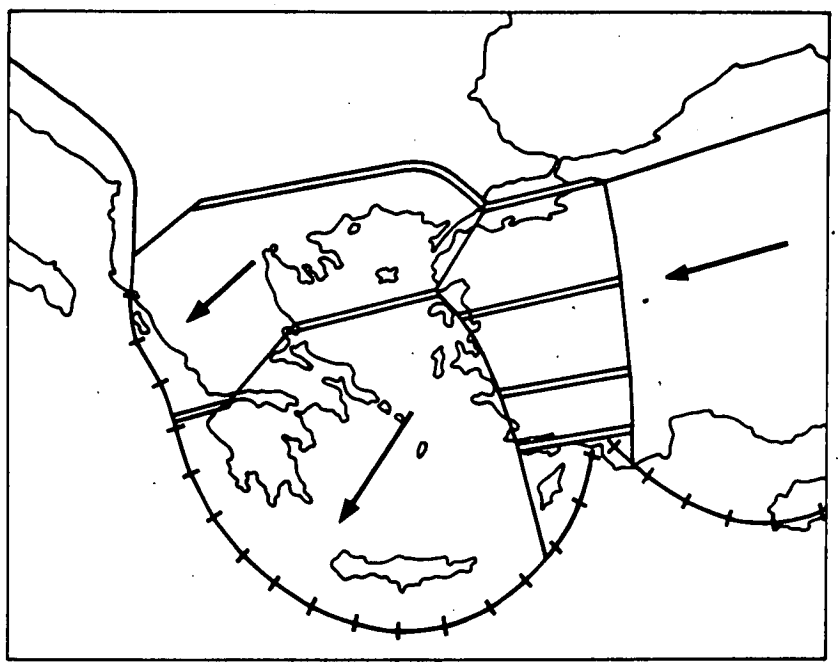

Figure 5.1 A plate tectonic model of the Aegean area after McKenzie (1972). McKenzie envisaged a series of microplates as delineated in the diagram. A single line indicates transcurrent faulting, a double line represents normal faulting and thrusting is represented by a single line with bars. This model was later abandoned when observations of surface fault traces and fault plane solutions contradicted the model.

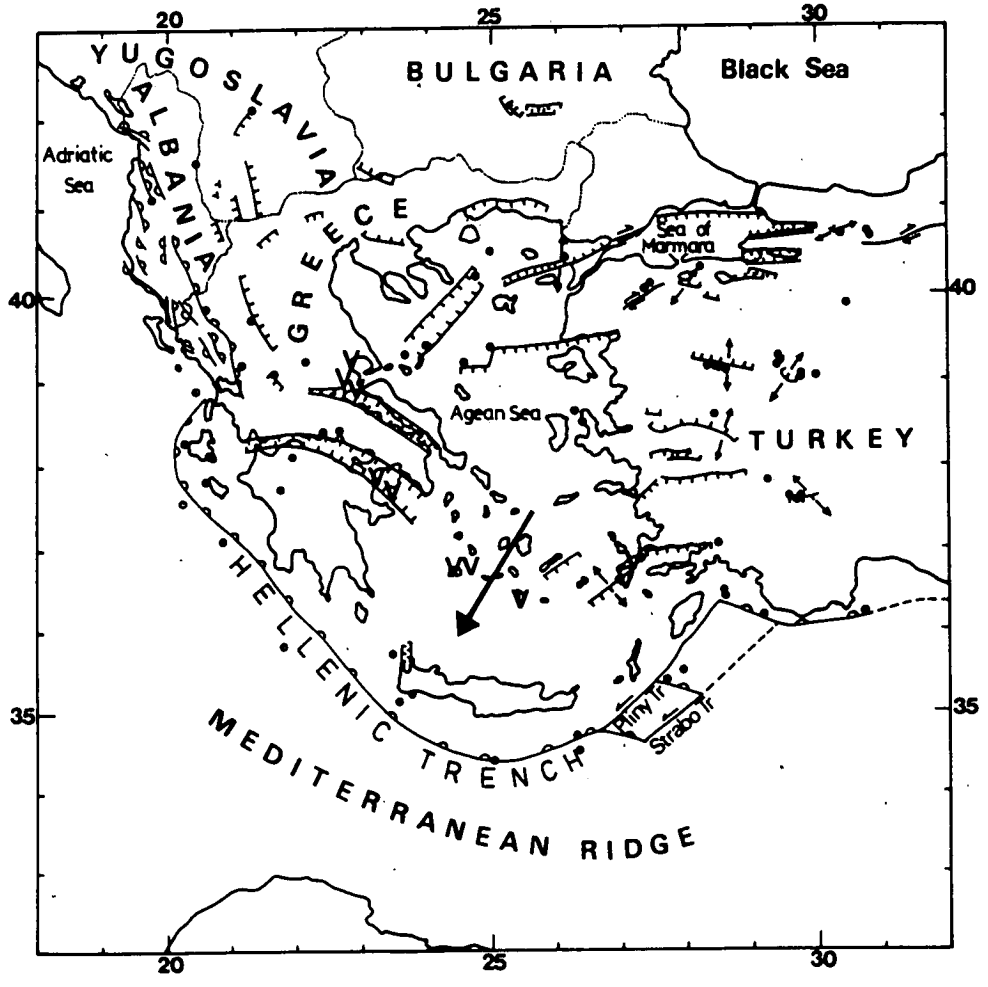

Figure 5.2 A tectonic model of the Aegean area after McKenzie (1978). Evidence from fault plane solutions, field observation and satellite pictures delineated the fault lines as shown. Normal faults are shown as lines with small bars in the direction of slip, thrust with semicircles in the slip direction and transcurrent faults as lines with arrows giving the sense of motion. In this model the Aegean is not rigid or split up into rigid blocks, but is subject to stretching.

geophysical observations of high heat flow and thin crust under the Aegean as being caused by crustal stretching. However they modelled the deformation with a subducting slab sinking vertically under the Hellenic arc rather than as part of a local convection cell (fig 5.3). In this model the cold (presumably remnant) oceanic crust sinks below the Aegean and the hinge of this subducting slab at the Hellenic arc retreats at a rate determined by the velocity of sinking. This retreat allows extension of the Aegean by gravitational instability because the compressive force due to the African Eurasian collision is not great enough to compensate for the hinge retreat. The process is similar to the reduction in height (thickness) of a basin of water if one of the dimensions of the basin is increased. Thus Le Pichon and Angelier (1981) refer to extension as resulting from a 'hydrostatic head' caused by the change in boundary conditions by hinge retreat at the Hellenic arc. In their interpretation the African-Eurasian collision proceeds at about 1 cm yr^{-1}, whereas the Aegean extension goes at a maximum rate of 4 cm yr^{-1} if the motion over time has been constant. Of course this two dimensional stretching looks rather different on the surface of the earth (fig 5.4), where it is consistent with rotation of 30° about a pole near 40°N, 18°E since the Upper-Middle Miocene transition (13M years before the present). The major problem with this model is the mass transfer which is required between mantle material behind and in front of the sinking slab due to the oblique angle of a vertically sinking slab. It has even been suggested that the curve of the Hellenic arc is actually caused by this mass transfer (Brooks, 1984, oral comm.), but it is evident that the mechanism of mass transfer is not well understood.

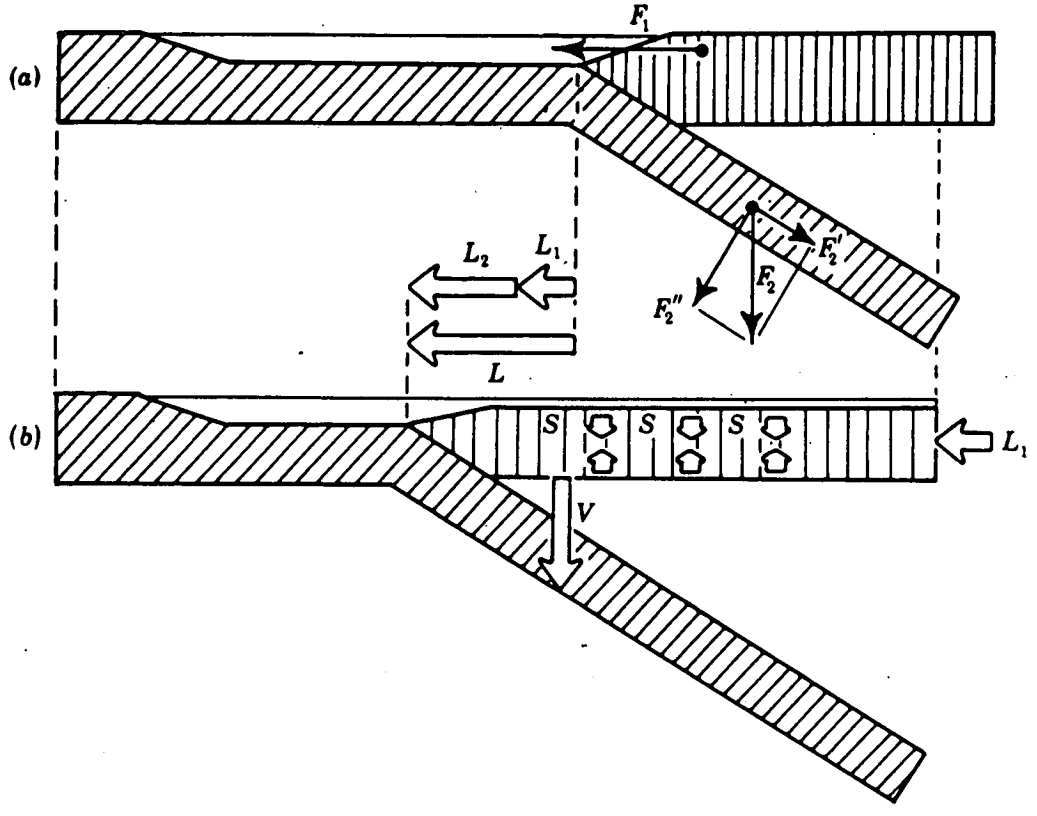

Figure 5.3 A section of the tectonic model of the Aegean area by Le Pichon and Angelier (1981). This is a schematic section of the Hellenic subduction zone with relative motions and gravitational forces.

(a) F_1, outward component of the gravitational force acting on the Aegean region, owing to its hydrostatic head with respect to adjacent Mediterranean sea crust. F_2, negative bouyancy force acting on the sinking slab, with components F_2' and F_2'', parallel and perpendicular to the slab, respectively.

(b) L_1, displacement of Eurasia relative to Africa: L_2, displacement of the Hellenic arc relative to Eurasia due to the Aegean expansion (L_2 is approximately 3 to 4 times larger than L_1); L, total displacement of the Helenic arc relative to Africa; S, subsidence of the Aegean region due to lithospheric thinning (double arrows), and subsequent transgressions; V, vertical motion of the sinking slab.

The vertical disappearance of the sinking slab creates a 'vacuum' which allows the hinge point at the Hellenic arc to retreat.

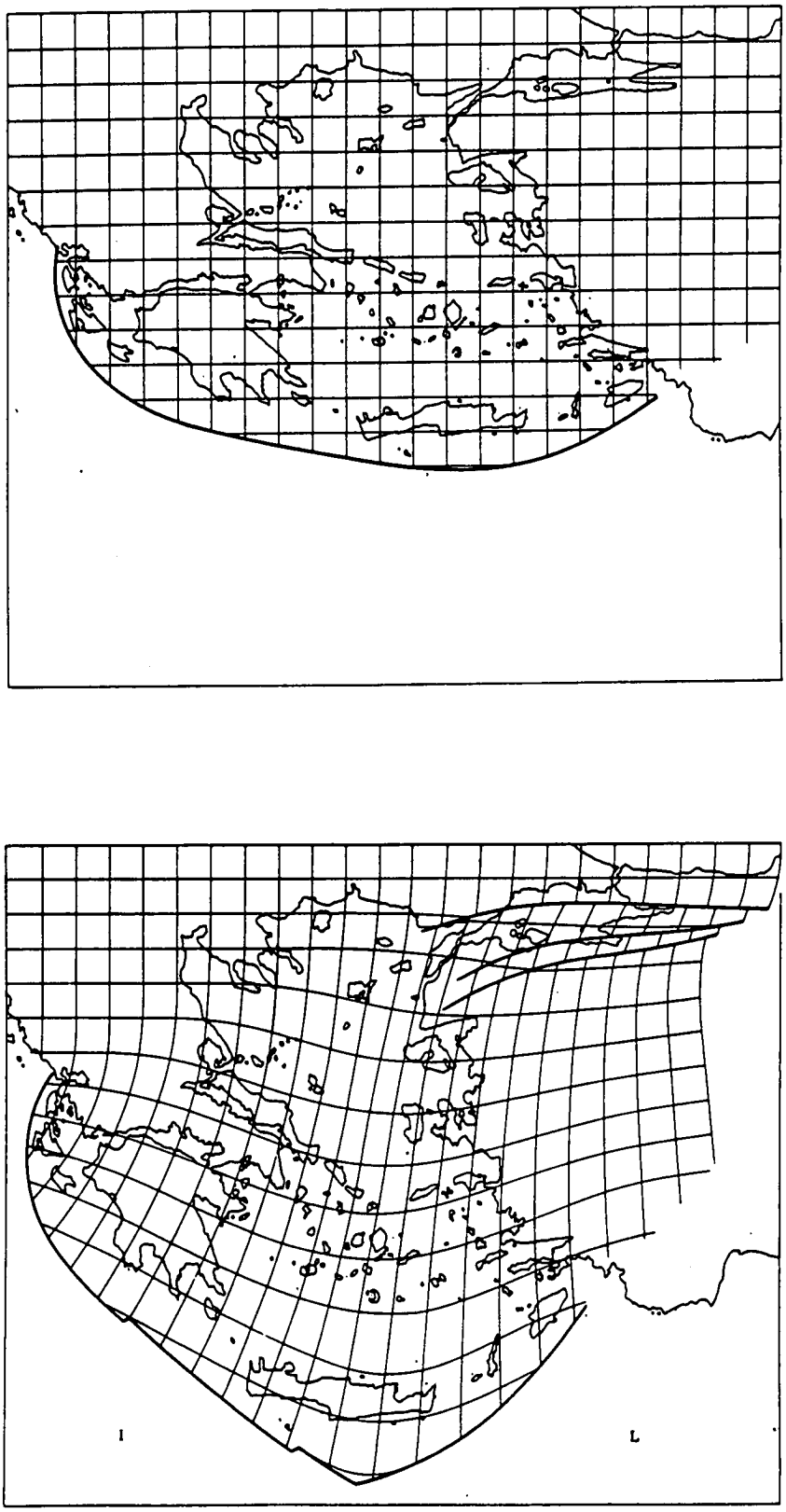

Figure 5.4 The tectonic model of the Le Pichon and Angelier (1981) in plan. The lower figure is the present configuration of the Aegean region. The deformation is shown by the grid which was originally square at the onset of stretching (upper figure). I,L: Ionian, Levantine basins respectively.

The details of the stretching are also interesting. At first the crust necked under tension primarily in a relatively narrow belt in the sea north of Crete. This can be seen from the length of the grid squares on fig 5.4, and from the depth of the sea and the relative thinness of the crust under it (Le Pichon and Angelier, 1981). However this area between the present Hellenic arc and the volcanic arc is currently locked and relatively aseismic. For some reason extension is currently taking place along a belt to the north of the volcanic arc, in Central Greece and around the islands to the east. This activity has been well mapped seismically and by investigations of surface faults, and is even reflected in the topography in features such as the Gulf of Corinth and the bay south of Volos.

In the present chapter the model of Le Pichon and Angelier (1979, 1981) will be adopted because the stretching factor 1.3 compared with of the original length from their model is more compatible with the observed fieldwork data and evidence of subsidence (a factor 1.4) compared with McKenzie's (1978) model, which requires stretching of a factor two or so. In addition the preferred model also explains the shallow angle of the subducting slab below the Aegean found by the earthquake hypocentres of Makropoulos and Burton (1984). Previously Comninakis and Papazachos (1980) showed a more steeply dipping slab at an angle of about 35°, which agrees with the geometric construction of fig 5.5. The dip angle of the slab $\theta = \cos^{-1}\{4/(4+1)\} = 36.8°$ from the horizontal results from relative stretching rates of 4 cm yr^{-1} for the Aegean within an overall compression between Africa and Eurasia of 1 cm yr^{-1}. This construction follows from the simple vertical sinking of the subducting slab with zero horizontal motion

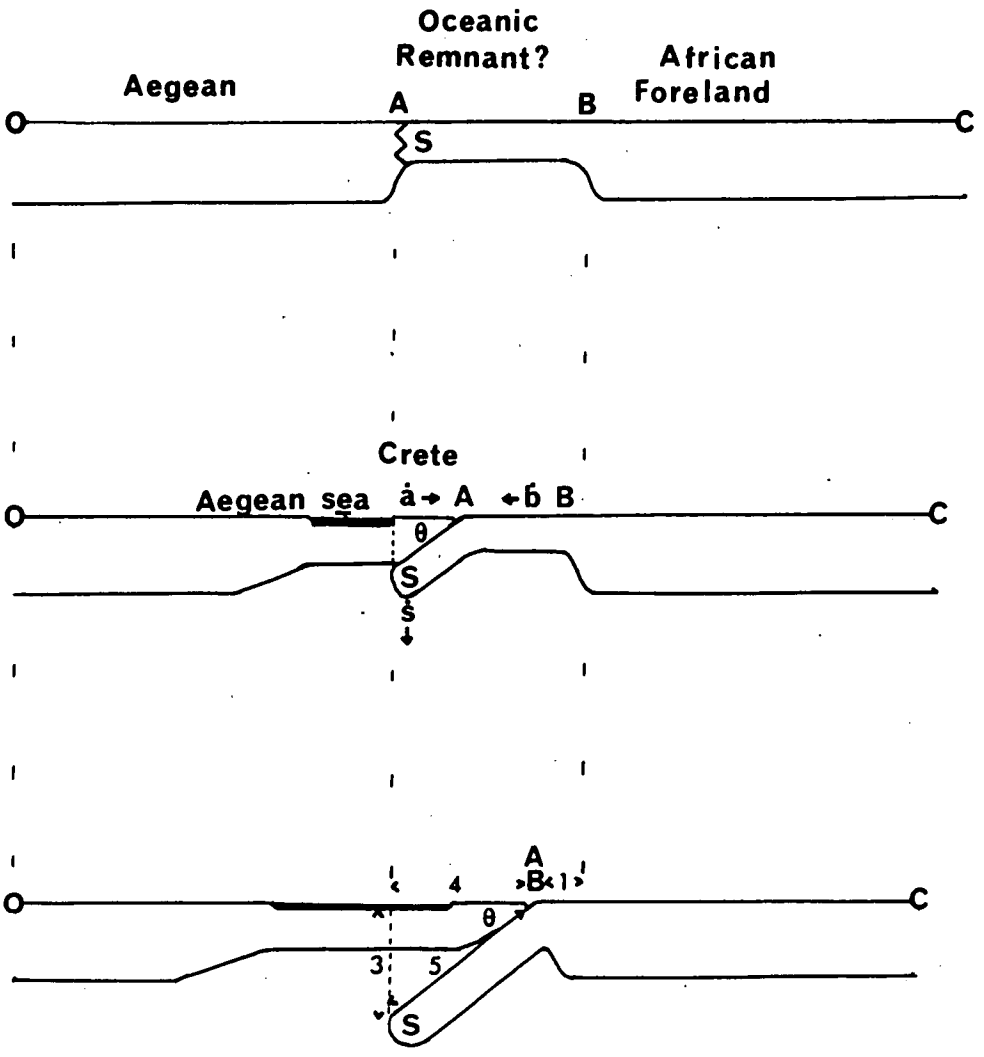

Figure 5.5 A geometric model of the Aegean subduction angle. This simple geometrical construction shows how the sinking slab (now almost totally consumed) could form an angle of $\theta \cos^{-1}(4/5)$ or 36.8°. This occurs if the slab sinks vertically with respect to the Eurasian continent to the North with $\dot{a} = 4$, $\dot{b} = 1$ cm yr^{-1}. $\dot{a}$ and $\dot{b}$ depend on the definition of the coordinate frame in which the slab sinks completely vertically. However $\dot{a}T + \dot{b}T$ = const. is the length of the original remnant ocean. The general expression for θ is $\theta = \cos^{-1}\{\dot{a}/(\dot{a} + \dot{b})\}$.

relative to the Eurasian continent, implying a sinking velocity due to negative buoyancy of about 3 cm yr^{-1}. However, this average sinking rate implies a maximum depth of 3 cm x 13 x 10^6 yrs or 390 km which is about double the maximum focal depth of 200 km or so found in Makropoulos and Burton (1984), fig 5.

At the other extreme, if the slab is sinking in the coordinate frame of the African plate, no stretching motion of the Aegean is possible under the geometric construction of fig 5.5, since $\Theta = \cos^{-1}(5/4+1) = 0$, with the further requirement that the sinking slab must undergo stretching for a non-zero subducting angle. There is no evidence for such stretching, and in fact many of the fault plane solutions for deeper earthquakes show high angle reverse faults (Drakopoulos and Delibasis, 1982), indicating that if any minor changes are occurring in the slab length beyond the geometrical rigidity of fig 5.5, then they are probably compressional.

In summary neither of these two extreme interpretations agree fully with the observations, so it may be that sinking probably takes place approximately vertically in the frame of the original slab, with relative movements towards that position of $\frac{1}{2}$ cm year from both the African and Eurasian plates. This would give an angle of subduction $\theta = \cos^{-1}\{(4+\frac{1}{2})/(5)\} = 25.8^{\circ}$; a sinking velocity $\dot{s} = 4.5 \tan\theta = 2.2$ cm yr^{-1}; and a depth to the slab tip of 280 km. In order to match perfectly the observed maximum seismogenic depth of 200 km or so Europe and Africa would be required to be moving towards a reference plane at velocities of about 8mm and 2 mm yr^{-1} respectively.

At the moment this most recent phase of the movement seems to be almost complete, with the African foreland now right up against

the edge of the Hellenic arc. Once the two continental masses converge the final stages of the Aegean evolution may be seen as being very similar to that currently observed in the Pannonian basin further north (see fig 5.6 from Horvath et al, 1981).

This figure shows that many other Mediterranean basins have developed or are currently active - all of which require some stretching or rotation similar to the current activity in the Aegean. This basin activity could also have resulted from boundary forces, similar to those presently existing at the Hellenic arc, and relying ultimately on the geometry of the African-Eurasian collision. McKenzie's (1978) model would require a very complex internal convection pattern under the Mediterranean to account for the activity, and it is perhaps easier to envisage a complex surface geography giving rise to complex boundary conditions, since there is so much evidence for this elsewhere in nature.

In short it can be seen that no model accounts perfectly for all the observations in the Aegean, far less the Mediterranean, but Le Pichon and Angelier's model is currently the most consistent with those data for the present area of interest.

In order to estimate a moment release rate from the preferred model, normal faulting typically at an angle of 45° is assumed (from the published fault plane solutions - fig. 7 of Drakopoulos and Delibasis, 1982) which cuts through a brittle crust which is about W = 30 ± 5 km thick in Central Greece (Makris, 1976). The length of the seismic zone (E-W extent with some curvature) is approximately 8 ± 1° of longitude, or L = 890 km. This gives a total fault area of $\sqrt{2}WL$ or 37.8×10^3 km^2, and with $\mu = 3.0 \times 10^{10}$ Nm^{-2}, $\dot{s}$ = 2 cm yr^{-1} the moment release rate is $\dot{M}_o = 2.27 \times 10^{19}$ Nm yr^{-1}. The value of $\dot{s}$ here is an average value, assuming a maximum

Figure 5.6 Geotectonic setting of the Meditteranean back-arc basins, after Horvath et al (1981) and Channel et al (1979). The complexity of the collision is evident. Several cycles of opening and closing of an ocean or ocean remnants has left a sinuous chain of deformation, including the Alpine mountains and the ophiolite sequences. This complexity is not easy to explain by internal convection forces as proposed by McKenzie (1978), but may be explained by boundary forces resulting from the geometric shape of oceanic remnants as proposed by Le Pichon and Angelier (1981). The boot of Italy swings anticlockwise to close up the Adriatic, just as the Hellenic arc swings clockwise to cover the last remnants of ocean floor under the Aegean arc. Both processes result in the formation of back-arc basins, and will probably end up in the final stages of the African-Eurasian collision as land-locked basins similar to the Pannonian.

(The figure referred to appears on the following page).

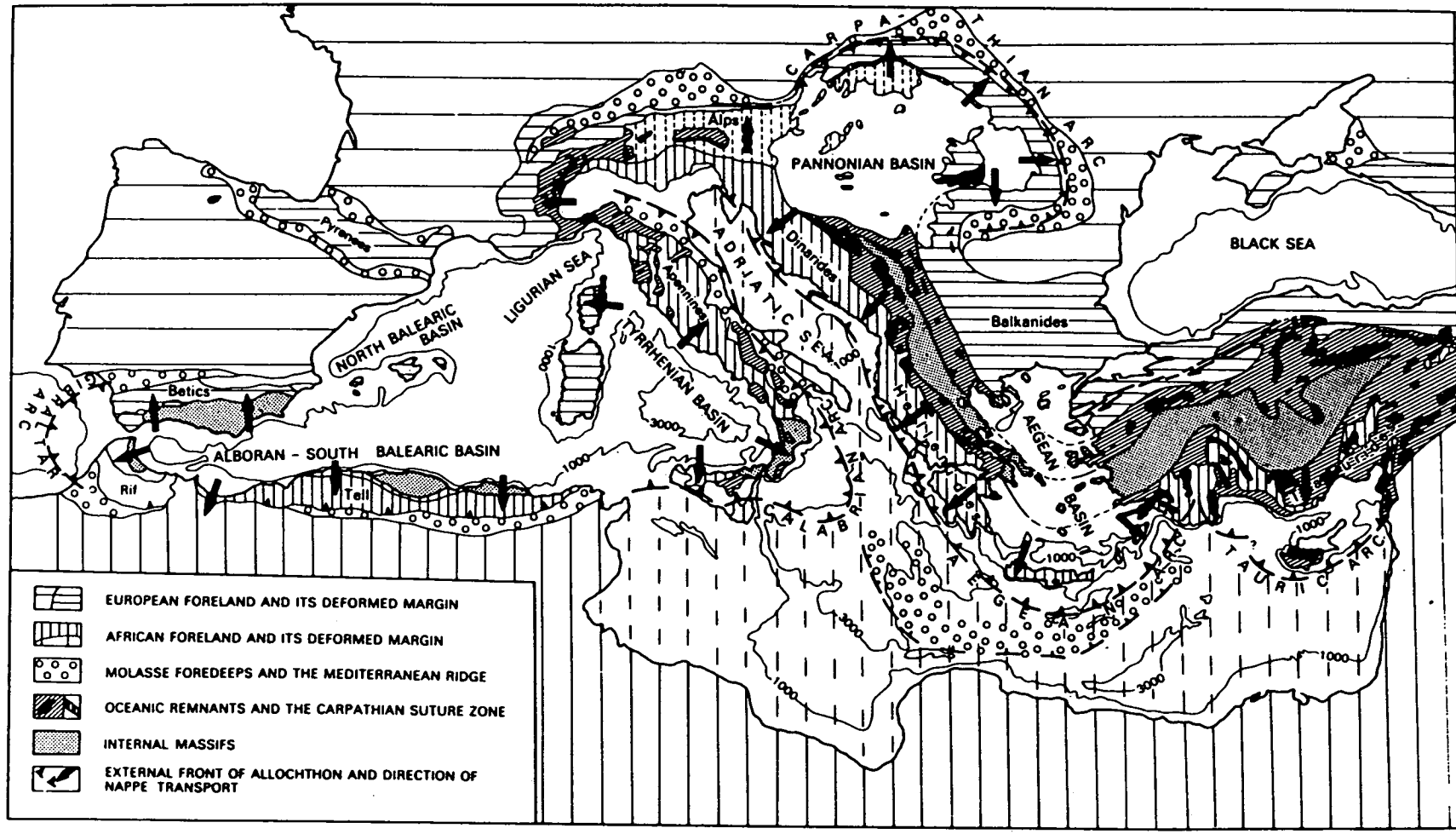

Figure 5.6 Geotectonic setting of the Mediterranean back-arc basins. (Full caption on previous page).

of 4 cm yr^{-1} extension southward in the Central Aegean sea and Crete, and a minimum of zero at the pole of rotation. Of course the Aegean area is much more complex than this gross first order approximation, but it should be reasonably representative of the total resulting from several faults distributed throughout the region. A conservative 50% error in $\dot{M}_o$ was assigned to account for this, and to allow for uncertainties in the assumed average angle of the normal faults.

5.3 The moment-magnitude relation for Greek earthquakes

Most of the events in the catalogue of Makropoulos and Burton (1981) do not yet have seismic moments assigned to them. This means that, in order to estimate a total seismic moment release rate from the events in the catalogue a moment-magnitude relation must first be constructed for the area. Fig 5.7 shows the moment-magnitude plot from tables 4.1-4.4, compared to reference lines for stress drops of 5-50 bars and best lines obtained by assuming B = 1.5. Fig 5.7a plots North's (1977) results from surface waves for 1963-1971, fig 5.7b plots the new results of the last chapter also for surface waves, and fig 5.7c plots the miscellaneous results from body waves. One field observation is shown in fig 5.7c for reference only. It is immediately obvious from the diagrams that the body waves produce systematically lower values for $\dot{M}_o$, given that all of the magnitude have been taken from the same homogeneous earthquake catalogue, because $\dot{M}_o$ for a given magnitude plots systematically lower in the diagram for the body wave results. This is expressed more rigorously in the values of A found in fig 5.7 for the two types of data (surface and body-waves).

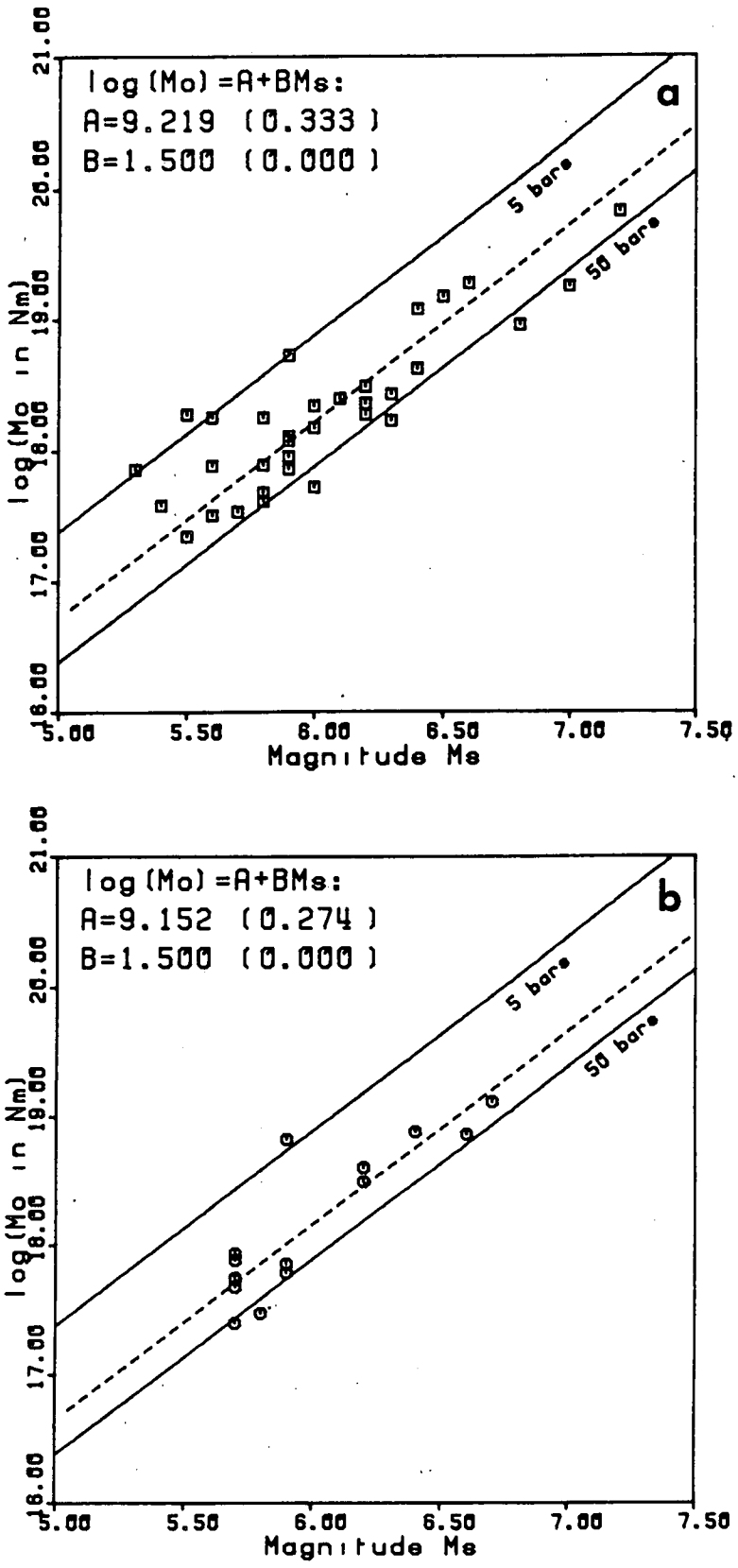

Figure 5.7 Moment-magnitude plots for Greek Earthquakes. These diagrams plot the moment magnitude data for the studies of (a) North (1977) and table 4.2; (b) this thesis, table 4.4; (c) various published (mainly) body-wave determinations, tables 4.1, 4.3; (d) a combination of the two surface wave studies (a) and (b). In (c) one measurement from field measurement is plotted for reference only, with a symbol A (for Ambraseys, 1970).

Solid lines correspond to values of stress drop of 5 and 50 bars, and dotted lines indicate the best fit to the data assuming B = 3/2, with standard deviation errors in brackets.

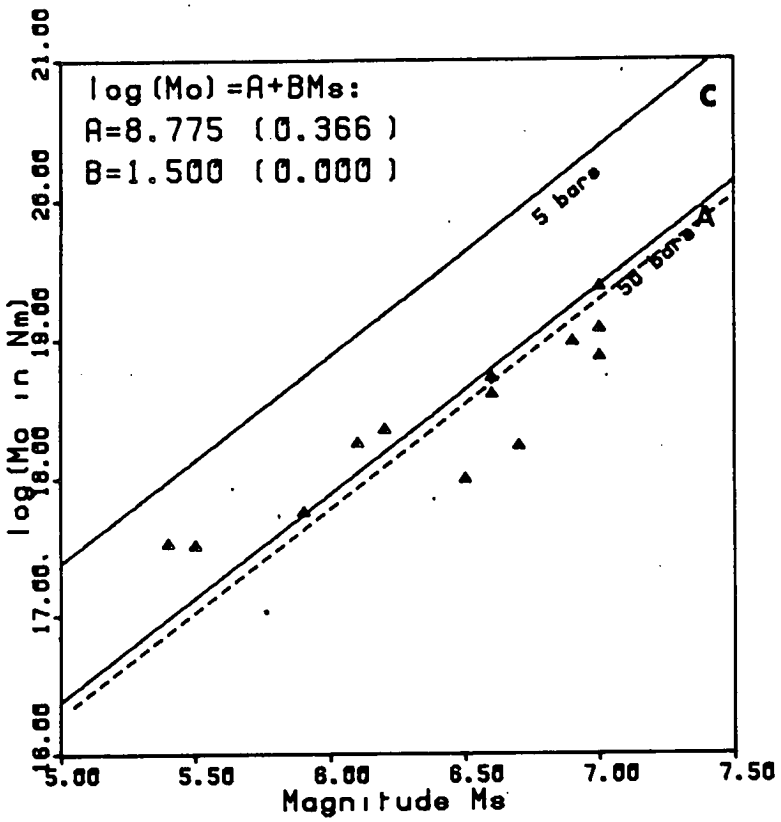

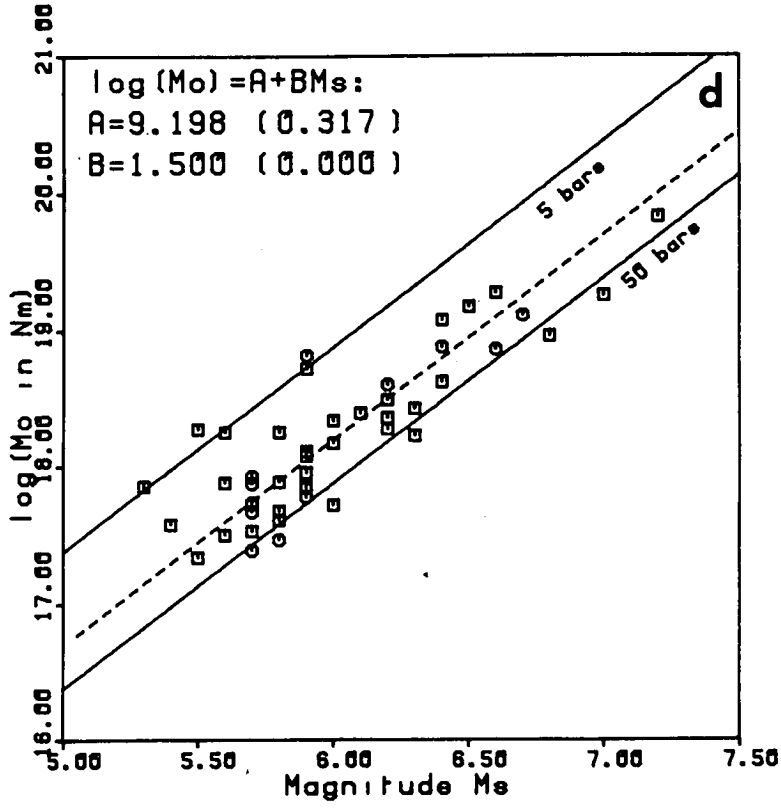

Figure 5.7 (cont.) The body wave results (c) show a marked systematic difference from the surface waves (d). The size of this difference, assuming B = 3/2 is $\delta A = \{A(c)-A(b)\} = 9.196 - 8.775 = 0.394$. This implies that the body wave moments are lower than the surface wave moments by a factor $10^{\delta A}$ or 2.5.

The question then remains to decide which set of results are correct. This was done by reference to the one event which has been assigned a moment and a stress drop from field study (Ambraseys, 1970). This particular point plots almost exactly where it might be expected to on fig 5.7c for a stress drop of 65 bars, but the events in the sequences at Thessaloniki and the Gulf of Corinth plot at much higher stress drops in fig 5.7c than they actually had (100 bars cf about 10 bars). Assuming that the formulation of Kanamori (1977) and Singh and Havskov (1980) used to draw the lines of constant stress drop is not almost an order of magnitude out, it must be concluded that the body wave moments are on average too low by a factor 2.5.

This either represents a major error in the theoretical derivation of the equations for the extraction of seismic moment, or significant errors in the earth parameters being used in the model, although the latter explanation seems very unlikely.. Either way this marked discrepancy is a very significant result of this thesis as a whole. It should be noted, however, that Scott and Kanamori (1985) found no significant difference between moment tensors found from first motion P-waves and phases R_2 and R_3 of the Rayleigh wave at 256 s, so this discrepancy may be a result of unusual conditions in the Aegean or the analysis of the period range 30-70s in North (1977) and the previous chapter. However, perhaps the most likely explanation is that the events analysed in fig 5.7 are typically multiple events caused by segmented faults with two or three elements separated by a few barriers. This was certainly true for the El Asnam event (Algeria) in 1980 (Yielding, 1985). First motion P-waves only gave about 1/3 of the total moment for this event from surface wave studies, and it is known

that this was due to segmented rupture.

A variable B can be allowed for as expected by Kanamori and Anderson (1975), which gives A_s = 10.970 (0.632) B_s = 1.206 (0.105); and A_b = 12.106 (0.871), B_b = 0.981 (0.135) by least squares (see fig 5.8 subscripts refer to s-surface or b-body wave studies). In order to estimate δA given the least squares values for A_s, B_s a standard deviation $\delta A_s = \pm 0.294$ was found assuming $\delta B_s = 0$. In order to retain compatibility with (3.24) in consideration of errors in the frequency magnitude distribution, only these latter values of A_s, δA_s, B_s are used subsequently in this chapter.

5.4 The moment release caused by Aegean spreading

The seismic moment release rate from the tectonic model of section 5.2 has been estimated at a rate $2.3 \pm 1.2 \times 10^{19}$ Nm yr^{-1}. In this section the magnitude catalogue of Makropoulos and Burton (1981) for $M_s > 5.5$ and the moments of tables 4.1-4.4 are used to estimate a seismogenic release rate for the Aegean spreading. First of all the catalogue was reduced to the area north of the Hellenic trench (fig 5.9), with shallow crustal depths ($h < 40$ km) and $M_s > 5.5$. Allowing for uncertainties in the seismogenic depth, this volume corresponds to that used for the tectonic model of Aegean spreading developed in section 5.2.

After this seismic moments were assigned to all of the events which had none given by using the moment magnitude relation and the final values of A_s, δA_s, B_s quoted in the previous section. Makropoulos and Burton (1981) found their catalogue to be complete for $M_s > 5.5$ since 1918, so the time period of interest was taken to be 1918-1981. The sum of the individual moments for this range

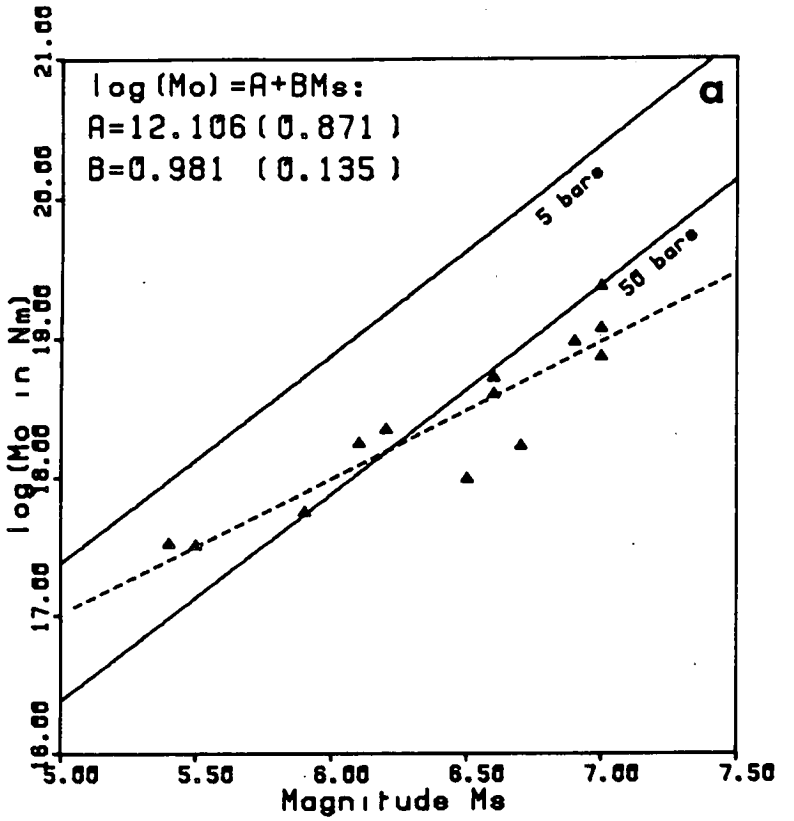

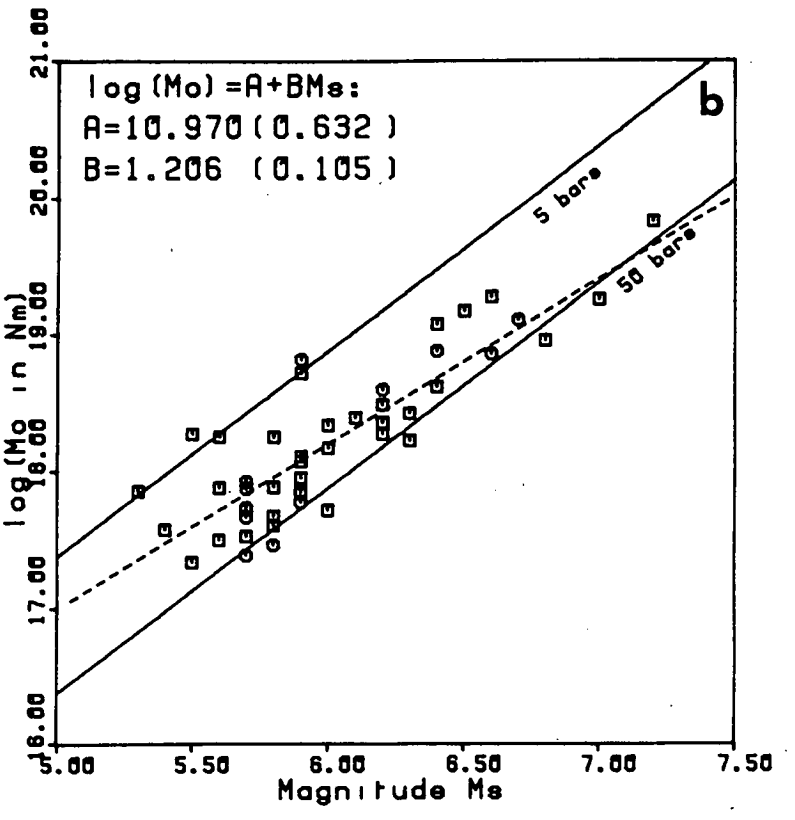

Figure 5.8 The moment-magnitude relation by least squares. Here the data from fig 5.7(c) and fig 5.7(d) are plotted. This is the data for (a) the body wave studies and (b) the two surface wave studies, 1963-1978, tables 4.2, 4.4. The least squares fit gives the values of A, B shown with standard errors in brackets. It is obvious that a systematic trend away from the theoretical lines exists.

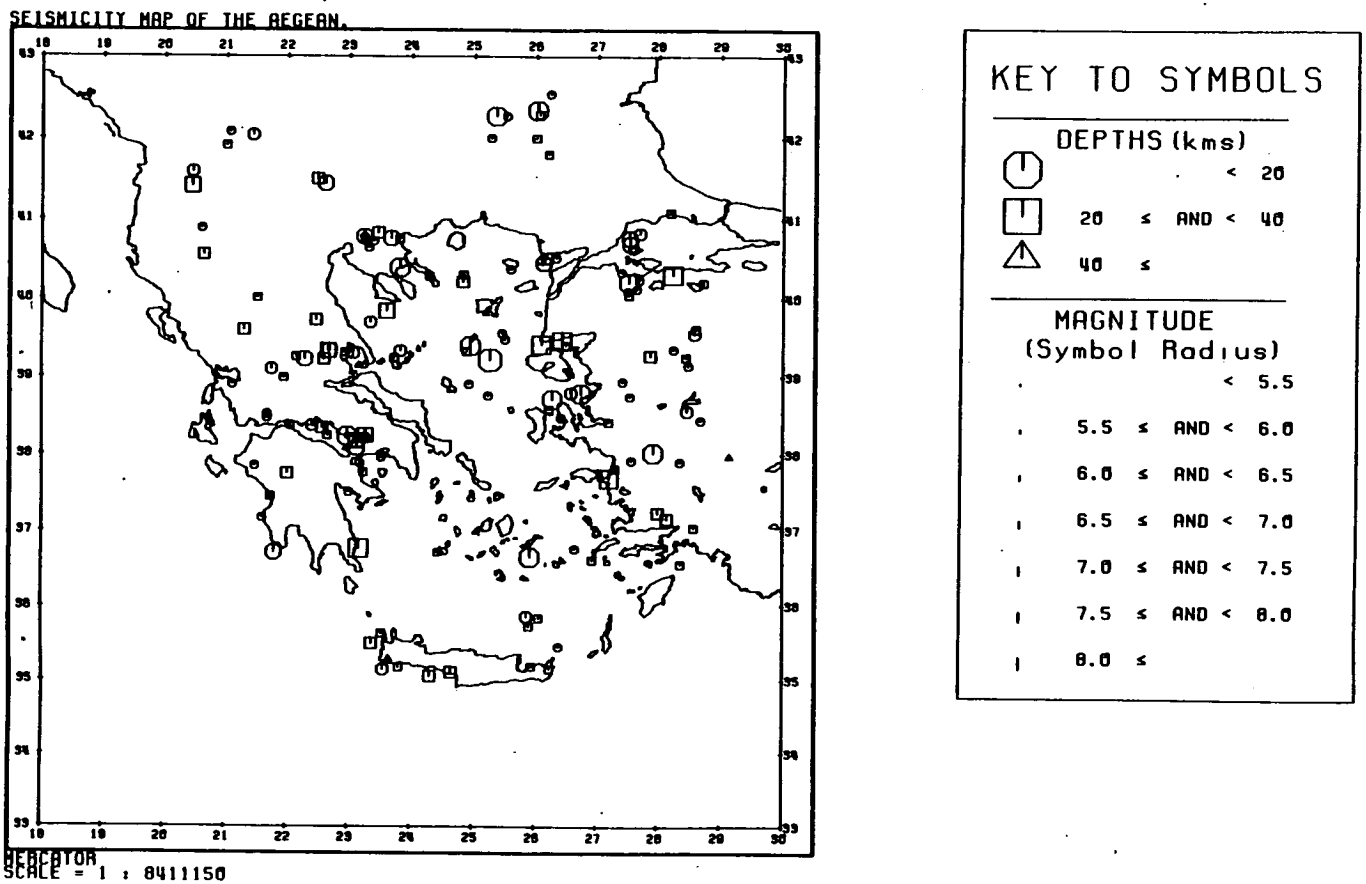

Figure 5.9 Seismicity map of Aegean spreading. All events of $M_S > 5.5$ in the extended catalogue of Makropoulos and Burton (1981) for 1918-1981 are plotted. In addition the catalogue was reduced to the spreading Aegean plate by limiting the listing to events at crustal depths ($h < 40$ km) and to those to the North of the Hellenic arc.

is 102 x 10^{19} Nm, or a rate of 1.59 ± 0.79 x 10^{19} Nm yr^{-1} allowing for a standard error in A_s. Allowing for its error this value agrees very well with the one found from the tectonic model of 2.3 ± 1.2 x 10^{19} Nm yr^{-1}. These correspond to slip rates of 1.4 and 2 cm yr^{-1} respectively by assuming the length, depth and fault orienations of the tectonic model discussed in section 5.2. The remaining difference may be taken up by aseismic creep on faults, but the large uncertainty in both of these values (about 50%) precludes a more detailed discussion.

What can be said, however, is that, to an accuracy of about 50%, the crustal deformation due to the spreading of the Aegean is mostly seismic and relatively stationary (i.e. the average moment release rate is fairly stable over short and long time periods).

5.5 The frequency magnitude distribution due to the spreading of the Aegean

In this section the information obtained from the earthquake catalogue and the seismotectonic model is applied to the problem of evaluating recurrence rates due to shallow events associated with Aegean spreading. The method will be to use the distribution (3.9) developed in Chapter 3. However, in this case there are some advantages over previous use of this distribution, because of the more detailed investigation which was undertaken in these final two chapters of one particular area. These are: (i) a good test of the validity of the assumption of geometric self-similarity from the relatively constant strain (or stress) drops found on figs 4.12 and 4.17; (ii) a good fit to the local moment magnitude relation from a homogeneous data set of 50 points; (iii) a rough test of the overall stationarity of the process from comparison of the moment

release rate over 6 decades compared to 13 million years.

The approach derived in Chapter 3 allows for deviations from these assumptions or for random fluctuations within given uncertainty bounds. Assumptions (i) and (ii) are covered by uncertainties in the stress drop via $\delta A(\Delta\sigma)$, and (iii) by uncertainties $\sigma_{\langle M_o \rangle}$ and δN_T.

Table 5.1 contains the parameters and the predictions of the distribution (3.9) found for this area by methods outlined in Chapter 3, and the theoretical line is compared with the earthquake frequency data in fig 5.10. The value of moment release rate found by summing the moments was used here to constrain the distribution, because of its good agreement with the tectonic model. A value of $\omega = 7.65 \pm 0.3$ M_s was chosen as the upper bound, since the largest catalogue entry (which happened to occur in 1981) is 7.6 M_s for this area.

First consider the discrete frequency diagram fig 5.10a. The most striking feature of this diagram is the number of events with magnitude 7.0 M_s. Only 5.6, 5.7̄ and 5.8 M_s have more. This is less easy to put down to magnitude uncertainty than was done for the Californian data in Chapter 3, because many of the earthquakes here are quite recent and are therefore more accurately determined. This feature also affects the cumulative frequency data in fig 5.10b, which once again show a bimodal seismicity distribution which is, this time, associated with the characteristic peak at about 7.0 M_s. The line (but not its error bound) does not fit the second curve in the distribution above 7.0 M_s too well, because most of the seismic moment release at $M_s > 6.9$ is taken up by the events of $M_s = 7.0$ (see fig 5.10c). However, it may be that this characteristic peak will flatten as

Table 5.1 Parameters and predictions from the distribution (3.9) applied to Aegean spreading

(a) Input parameters/constraints:

m_c, ω : 5.55, 7.65 (0.3)

A, B : 10.970 (0.294), 1.206 (0.0)

$\langle m \rangle$: 6.178 (0.049)

N_T : 1.687 (0.218) yr^{-1}

$\dot{M}_o$: 1.59 (0.79) x 10^{19} Nm yr^{-1}

(b) Resulting distribution:

λ_1, λ_2 : 1.285 (0.956); 0.000 (2.703) x $10^{-20}(Nm)^{-1}$

b : 0.558 (0.415)

$\sigma^2_{\lambda_1}, \sigma^2_{\lambda_2}, \sigma^2_{\lambda_1\lambda_2}$: 0.914, 7.304, -2.538

(c) Predictions: Magnitudes associated with average repeat times T

T in years	m(T)	$\sigma_{m(T)}$
1.0	5.921	(0.100)
2.0	6.380	(0.264)
5.0	6.892	(0.339)
10.0	7.182	(0.152)
20.0	7.381	(0.516)
50.0	7.531	(1.200)
100.00	7.588	(1.566)
200.00	7.619	(1.786)

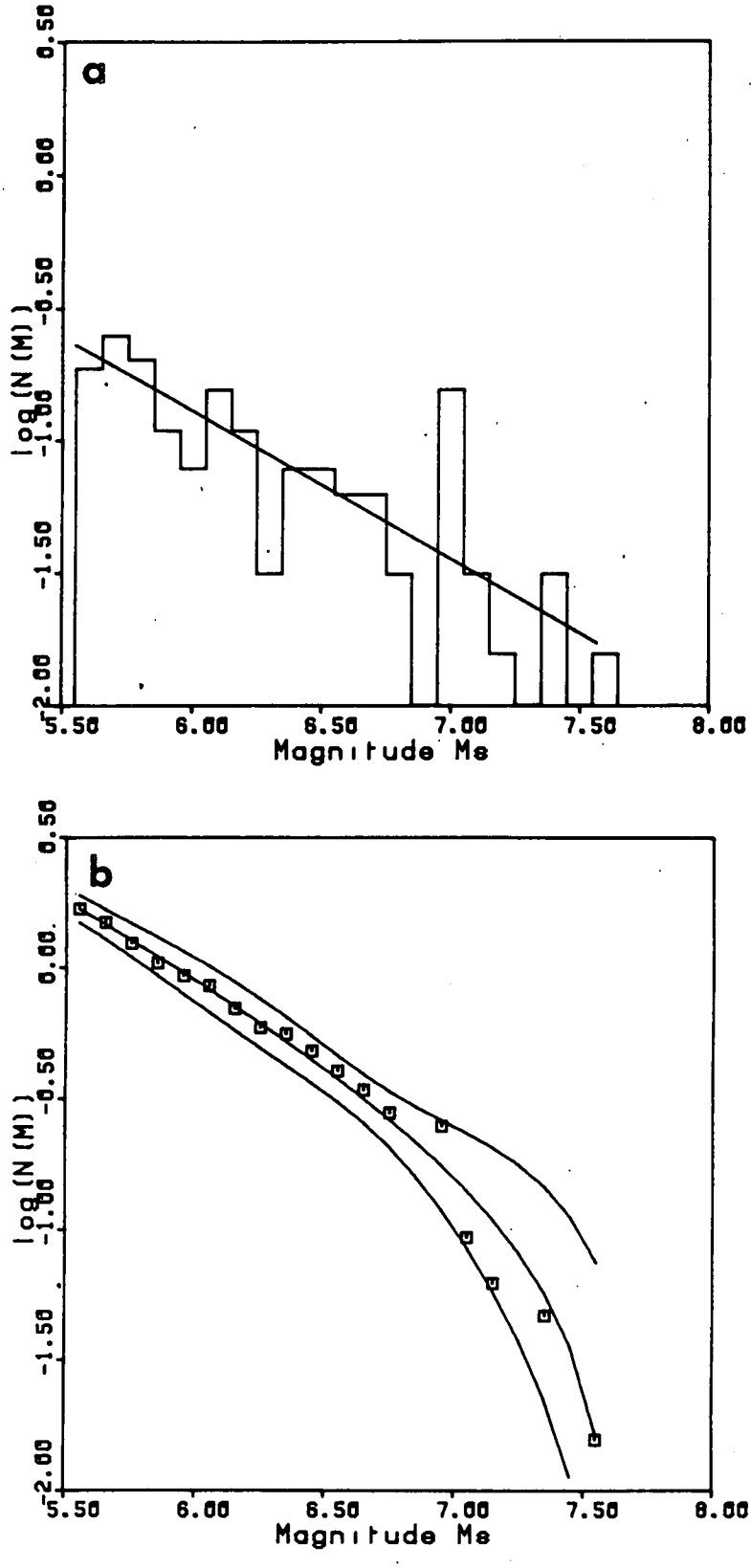

Figure 5.10 Frequency magnitude statistics for Aegean spreading. (a) Discrete frequency, (b) cumulative frequency, (c) discrete and cumulative frequency superposed. The most notable observation from this data set is the prevalence of events with magnitude 7 M_s. The lines are drawn by using the parameters of table 5.1 in the distribution of equation (3.9).

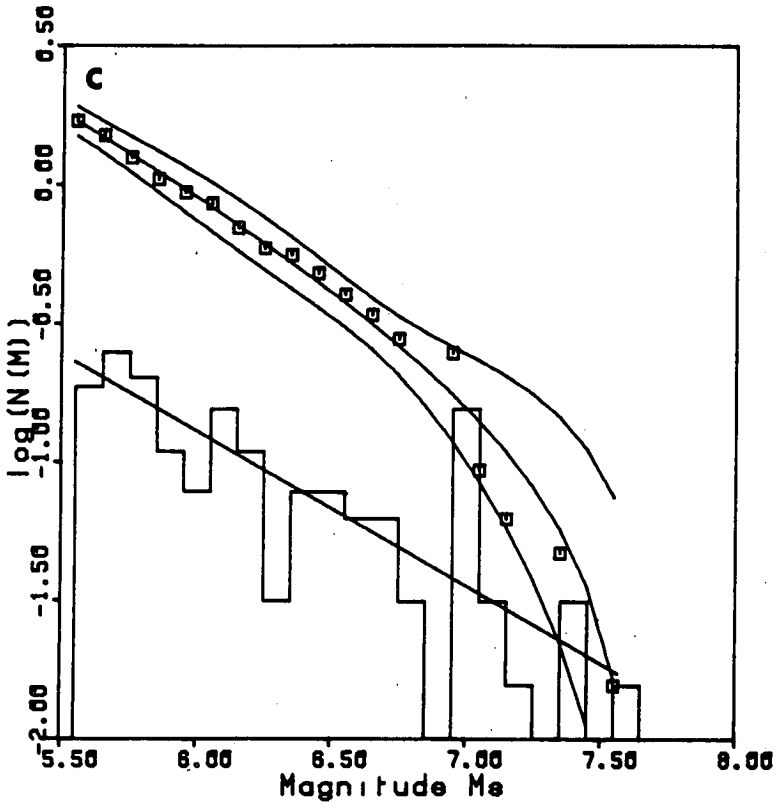

Figure 5.10 (cont.)

more data become available. It was decided not to fit a double Weibull distribution to the data because of the sparse number of points (only four) at the very largest magnitudes corresponding to a second bump in the distribution.

In conclusion the Information theory line fits the data within its error bounds up to magnitude 7 M_s, but does not model the effects of a characteristic peak in the discrete frequency at this value. This happens because the information represented by this peak is simply not present in the model. At least one more parameter would be required as an additional constraint.

5.6 Characteristic earthquake models: discussion

There is one class of model which describes behaviour as seen in fig 5.10a. This is the 'characteristic earthquake' model of Schwartz and Coppersmith (1984), which adequately describes the qualitative form of the bimodal distributions observed in the cumulative frequency diagrams of nearly all of the areas investigated in this thesis. They have applied this distribution to the Wasatch zone and the San Andreas fault in the Western U.S., using geological data on slip rates and recurrence times. In addition Lomnitz-Adler (in press) has developed a similar form of the distribution by considering an asperity model based on percolation theory, and applied it successfully to the earthquakes associated with Mexican subduction. A recent summary of the effect of discrete-sized asperities and barriers is given by Aki (1984). However, the result of all of these models is a relative enhancement of some of the higher magnitudes exactly as seen on fig 5.10a.

Information theory can also be used to study the form of this

distribution. For example Lomnitz-Adler used this theory to give the shape of the characteristic peak of high magnitudes as a Gaussian. By using the principle of superposition the treatment of the data on fig 5.10a could be done in two segments - above and below 6.8 M_s - with a Gaussian and the distribution (3.9) respectively. This could be done by using only one extra constraint - ie the choice of the critical magnitude at $M_s \approx$ 6.8, since the other parameters would follow from the specified forms of the distributions above and below this value, given m_c, ω, $\dot{M}_o$ etc.

Fig 5.11a shows the effect of treating the range 6.85, 7.25 simply as an anomalous Gaussian. The increase in the moment release rate for this range above the Information theory line would require a reduction of probabilities at $M_s > 7.25$ to compensate, as shown by the schematic dotted line in fig 5.11b. This approach is not quantified further here, but it is hoped this line of enquiry may prove fruitful in subsequent investigations.

5.7 The positioning of the characteristic earthquake peak

The average magnitude for $M_s > 6.9$ used to define the Gaussian curve in fig 5.11 was found to be 7.03 M_s, with $\sigma = 0.0625$. This corresponds to a seismic moment of 2.81×10^{19} Nm. If a constant strain drop Δe of 10^{-5} as in the sequence of events at Corinth, 1981 (Kim et al, 1984) is assumed then $s = \Delta eW$ since movement is normal and therefore parallel to the fault width (depth in this case), and the fault length is $L = M_o/\mu W^2 \Delta e$. If a constant aspect ratio L/W = 2 is assumed (Geller, 1976; Purcaru and Berckhemer, 1982), then the magnitude 7.03 corresponds to a fault width of 36km. Assuming an average dip angle of 45^o implies a

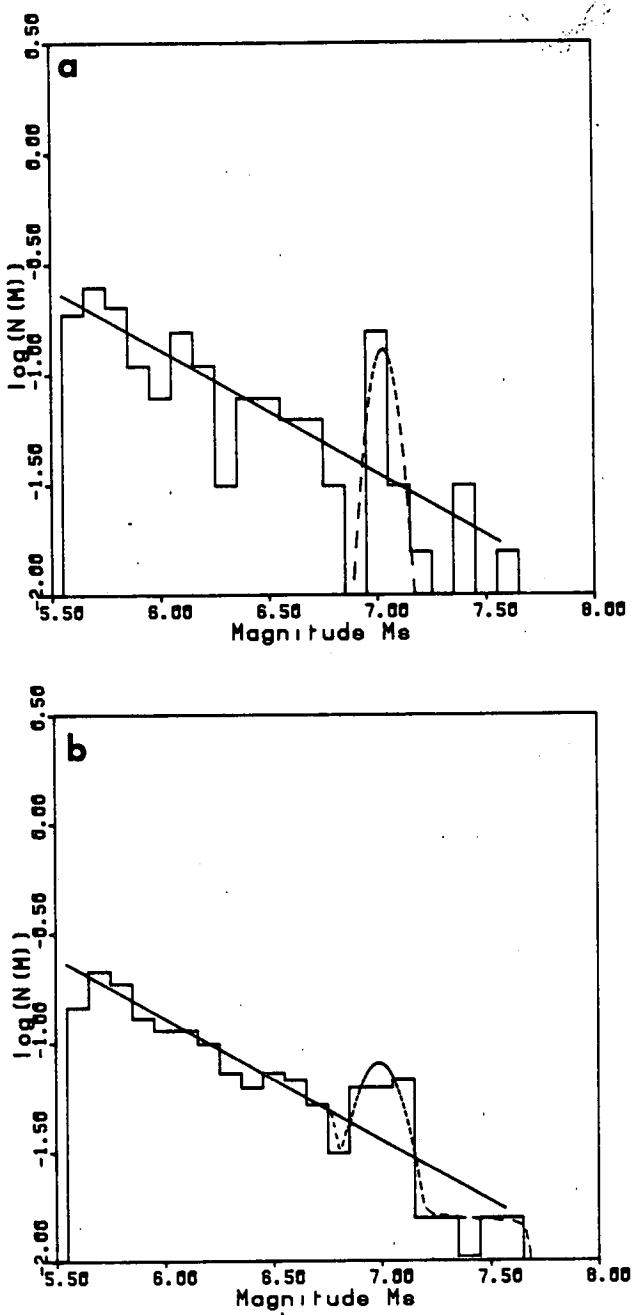

Figure 5.11 Frequency-magnitude statistics for Aegean spreading: a characteristic earthquake model.
(a) A Gaussian is fit to the magnitude data, giving a characteristic peak at magnitude m = 7.031, σ = 0.0625 in the magnitude range (6.85, 7.35). The moment in this range above the solid Information theory line leads to a lowering of the probability of occurrence above magniutude 7.35.
(b) In this diagram the frequency data F_i is smoothed over neighbouring ranges, e.g. $\bar{F}_i = (F_{i-1} + F_i + F_{i+1})/3$. This broadends the Gaussian peak without eliminating it. Here the dotted line represents the reinterpretation in terms of the characteristic earthquake model discussed in the text, with a schematic interpretation of its shape at high magnitude.

seismogenic depth of 25km, which is remarkably similar to that observed in Central Greece (i.e. ≈30km). This macroscopic block like structure of the earth is remarkably similar to observations over a huge range of earth materials noted by Allegre et al (1982), Sadovskii et al (1982) and most recently by Fukao and Furumoto (1985).

5.8 Subduction under the Hellenic arc

The Hellenic arc, which forms a curve south of mainland Greece and Crete, is the point at which the Eurasian and African plates meet. Le Pichon and Angelier (1981) showed that this arc is the junction of two continental masses from isodepth contours of the earth surface under the Mediterranean. If a remnant oceanic mass has initiated and maintained the spreading of the Aegean by its vertical subduction, then it has all but disappeared at present, to form a very rough 'amphitheatre' shape under the present surface features of the area. From the hypocentral maps in Makropoulos and Burton (1984) it can be seen that subduction has not taken place in the form of a neat slab, but that the subsumed material has probably been subject to internal buckling as well as vertical pull due to negative buouancy. The internal buckling may be caused, for example, by thermal expansion as the cold slab slowly heats up without changing its size, or by phase changes in the mantle (Goto et al, 1985).

It is also interesting to note that an earlier phase of continental collision between Africa and Eurasia was responsible for the closure of an old ocean, but this phase of deformation left a characteristic signature in the form of oceanic remnants and ophiolite sequences in a broad swathe from Eastern Turkey to the

Pannonian basin, and then again into the Alps (fig 5.6). However, in this figure, there is no suggestion of the logical continuation of such sequences in the Dinarides west of the Pannonian basin. It is therefore tempting to suggest that the mechanism for the formation of this basin was exactly similar to that of the present Aegean basin, i.e. the complete disappearance by vertical sinking of a fragment of old ocean crust, with concomitant stretching of the adjoining continental crust. Horvath (1984) also comes to this conclusion by mapping areas of active extension and compression.

Fig 5.12 shows the present-day seismicity associated with this subduction, including the deeper events underneath the spreading Aegean, and fig 5.13 shows the frequency-magnitude distribution of these earthquakes for the time period 1918-1981 from the catalogue of Makropoulos and Burton (1981). The total seismic moment release rate of the present day is 72.9×10^{17} Nm yr^{-1} from the earthquake catalogue and using the known moments or those inferred from the moment-magnitude relation of section 5.3. This agrees very well with previous studies by North (1973) of 88.2×10^{17} Nm yr^{-1} over a similar time period and Ambraseys (1981) of 78×10^{17} Nm yr^{-1} over two centuries using historical data. All of these studies show that only a tiny fraction of the total moment which would be due to the plate tectonic disappearance of the slab is seismogenic. North (1973), in his table 5.19, suggested a total value of 1370×10^{17} Nm yr^{-1} based on the African-Eurasian collision rates and the length of the arc, so the seismogenic moment release of these three studies is only about 5.7 - 7.2% of the total. These figures imply that the slab must be sinking almost completely aseismically, just like a slab of cool concrete in wet cement. The second order deformation caused by buckling of the slab may well be enough to

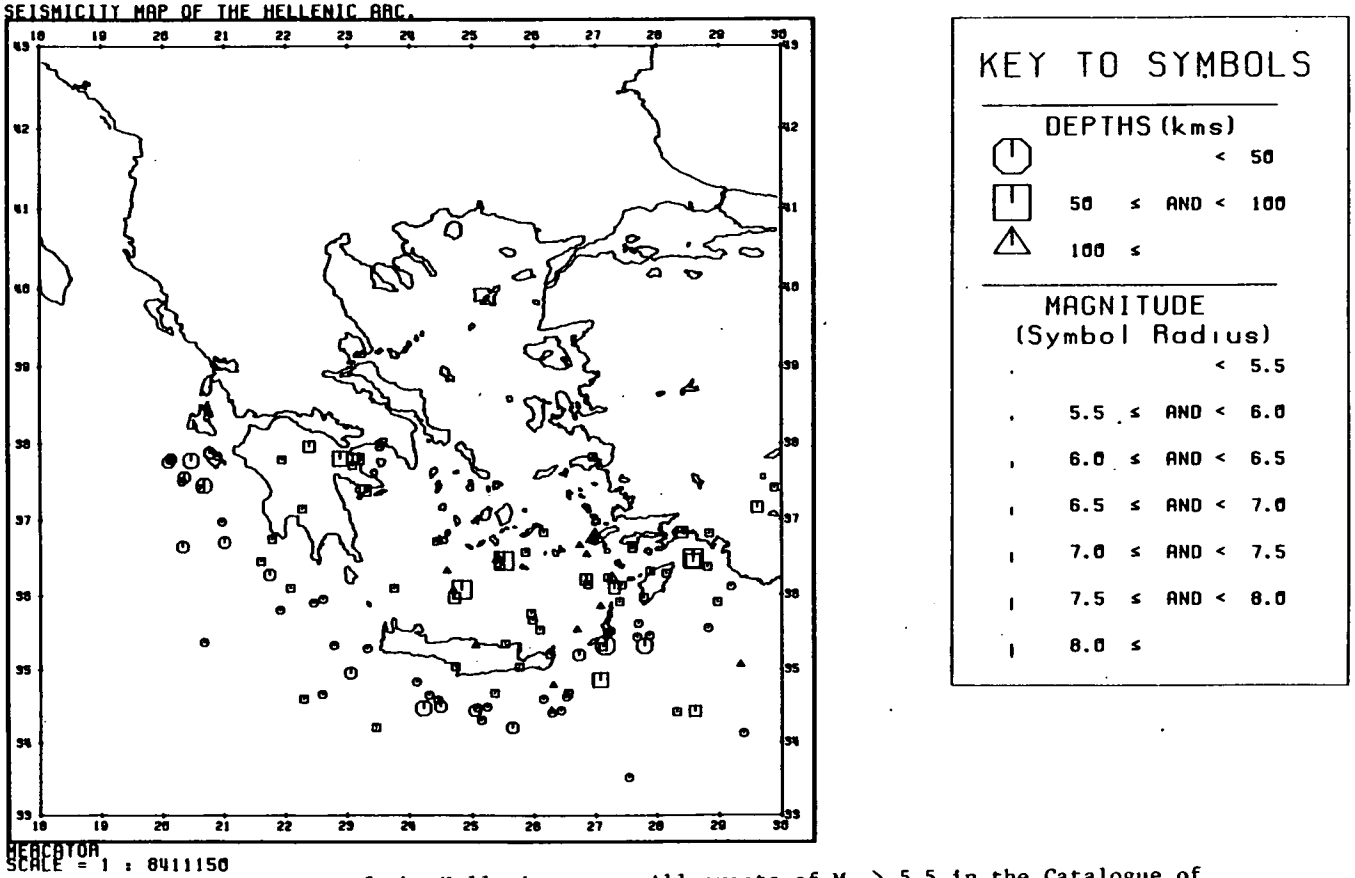

Figure 5.12 Seismicity map of the Hellenic arc. All events of $M_S > 5.5$ in the Catalogue of Makropoulos and Burton (1981), for 1918-1981 are plotted. All shallow events south of the boundary of Aegean spreading, or deep events south of 38°N are plotted.

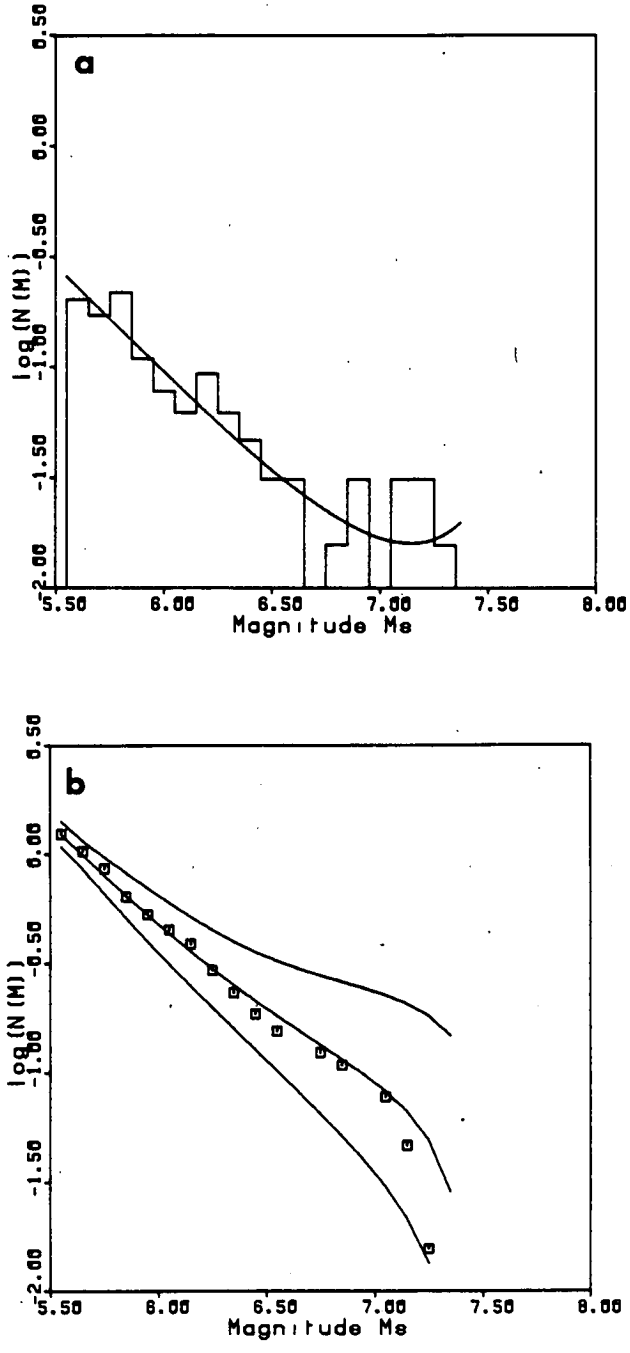

Figure 5.13 Frequency magnitude statistics for subduction of the arc.
(a) Discrete frequency, (b) Cumulative frequency. The most notable observation here is the break in slope at M_S 6.6. The b value reduces above this value, corresponding to a sudden reduction in the similarity dimension at a magnitude coresponding to a slab width of 12 km (see text). Above M_S 6.6 faults can only enlarge in one dimension - along their length. This is very similar to the observation of Californian recurrence statistics in fig 3.5. The lines are drawn by the Information theory parameters of table 5.2.

explain almost all of the observed seismicity. In support of this Goto et al (1985) recently showed that thermal expansion and phase changes within a sinking slab contribute more to earthquake generation than stick-slip sliding at its boundaries. In this case the former explanation seems the more likely.

One final point is that the frequency magnitude statistics of fig 5.13 for the subducting slab show a marked break of slope at a magnitude 6.5 M_s. This corresponds to a seismic moment of 6.4 x 10^{18} Nm, and with a typical strain drop $\Delta e = s/W$ of 10^{-5}, using L≈2W for thrust or normal faults (Geller, 1976; Purcaru and Berckhemer, 1982), a typical fault width of about 17.5 km is found if $\mu \approx 6 \times 10^{10}$ Nm^{-2} for deep earthquakes (North, 1973). As in section 5.7, W does not automatically correspond to the seismogenic width because the faulting may not always be at right angles to the crust or the slab edge. If a typical angle of 45° is assumed for faults caused by this internal buckling of an old ocean floor, the fault width implies a seismogenic depth of 17.5/√2 or 12.4 km for the original slab width. This somewhat speculative analysis in sections 5.7 and here has identified two characteristic dimensions above which the discrete frequency data take on new forms. For the shallow events in the Aegean basin this dimension (25 km) corresponds very well with the known seismogenic depth of 30 km, and in the case of the earthquakes associated with subduction the dimension (12 km) indicates an original crustal depth more like that of a typical ocean (10 km) than a continent (30km).

Finally the parameters and predictions associated with subduction by using the frequency-magnitude data and the inferred short term moment release rate are given in table 5.2.

Table 5.2 Parameters and predictions from the distribution (3.9) applied to subduction at the Hellenic arc

(a) Input parameters/constraints:

m_c, ω : 5.55, 7.45 (0.3)

A, B : 10.970 (0.294), 1.206 (0.0)

$\langle m \rangle$: 6.034 (0.050)

N_T : 1.234 (0.175) yr^{-1}

$\dot{M}_o$: 7.29 (3.64) x 10^{18} Nm yr^{-1}

(b) Resulting distribution

λ_1, λ_2 : 2.251 (1.269), -0.212 (0.468) x 10^{-19} $(Nm)^{-1}$

$\sigma^2_{\lambda_1}$, $\sigma^2_{\lambda_2}$, $\sigma^2_{\lambda_1\lambda_2}$: 1.609, 0.219, -0.585

b : 0.978 (0.551)

(c) Predictions: Magnitudes associated with average repeat times T

T in years	m(T)	$\sigma_{m(T)}$
1.0	5.651	(0.131)
2.0	5.995	(0.103)
5.0	6.489	(0.264)
10.0	6.879	(0.244)
20.0	7.178	(0.216)
50.0	7.355	(0.636)
100.00	7.405	(0.822)
200.00	7.428	(0.919)

5.9 Summary

In this final chapter a detailed case study of the seismotectonics and seismic hazard due to the extension and concomitant thinning of the Aegean area behind the curve of the Hellenic arc was undertaken. The tectonic model of Le Pichon and Angelier (1981) was found to be the most consistent with all of the available geophysical evidence, although it is still not perfectly compatible with all observations. This tectonic model gave a moment release rate of $2.3 \pm 1.2 \times 10^{19}$ Nm yr^{-1} over 13×10^{6} yrs if stretching is due to slip on a series of normal faults dipping at 45^{o}. By applying the magnitude-moment relation found from surface wave studies ($A = 10.970 \pm 0.294$, $B = 1.206$) to the catalogue magnitudes of Makropoulos and Burton (1981), a total catalogue moment of $1.6 \pm 0.8 \times 10^{19}$ Nm yr^{-1} was found for the period 1918-1981. Thus the two moment release rates are in good agreement within their error bounds, although the catalogue moment is smaller. This implies that the process of Aegean stretching is seismotectonically stationary to the accuracy of the model, i.e. about 50%.

A significant result emerged from comparison of the seismic moment magnitude relation for body waves and surface waves. The body wave moments for the Aegean were found to be systematically lower than the surface wave studies of North (1977) and Chapter 4, by a factor two or three on average. This is compatible with multiple ruptures on faults with two or three segments separated by barriers or asperities, since many P-wave moments are evaluated from first motions only.

The frequency magnitude relation of Chapter 3 was then applied to the magnitude data on Aegean spreading. Although once again the distribution modelled the empirical distribution within its error

bounds, there was a strong anomaly at magnitude 7 M_s. This anomaly could be interpreted with the characteristic earthquake models of Schwartz and Coppersmith (1984) and Lomnitz-Adler (in press). The peak magnitude 7 M_s implies a characteristic block-like earth structure in the area, of elements roughly 72 km long by 36 km, just as a characteristic block size of 30-100 x 22 km was found for the New Madrid area in Chapter 2.

A similar analysis of the moment release rate of the Hellenic arc showed that the slab is currently sinking almost perfectly aseismically, and that internal buckling caused by thermal expansion may well be the cause of the observed seismicity. A break in slope at 6.5 M_s is consistent with an original slab width of 12 km, giving another characteristic block dimension. The implied seismogenic depths of 25km for the spreading Aegean crust and 12 km for the depth of the original sinking slab agree well with the known values for typical continental and oceanic seismic depths (30km and 10km respectively).

CONCLUSION

Several conclusions have already been noted in each of the chapters, all of which have turned out to be self-contained enquiries as well as part of the overall investigation. In this final section the main conclusions are brought together in a common theme in order to summarise the overall progress which has been made.

First of all the empirical Weibull distribution and its extreme value equivalent, Gumbel's third distribution, were found to be adequate descriptions both of the frequency magnitude data and the geologically observed seismic moment release rate. The error bounds in the seismogenic moment release rate of a factor 2-3 up to as much as 10 reflect the sparsity of information at low frequencies of occurrence. Several different tectonic zones were investigated: the Eastern Mediterranean gave a good match with short term moment release rates culled from a moment catalogue to prove the internal consistency of the method; the New Madrid seismic zone in the Eastern U.S. showed a bimodal distribution which could be matched to slip rates and fault areas on two separate characteristic fault sizes prevalent in the area (of 10 and 100km lengths); Southern Californian data gave a good match with the observed slip rate of the San Andreas fault at the expense of underestimating the known earthquake hazard at the highest magnitudes; the mainland U.K. showed that only a fraction of the observed crustal rebound following glaciation is taken up seismogenically - exactly as one might expect from an elastic rebound mechanism. All of the zones studied (with the exception of the UK) showed a bimodal distribution, although with insufficient

data to investigate the detail as in New Madrid. An autocorrelation effect observed in Southern California (overestimate of the maximum magnitude, underestimate in the hazard just below this value) can be accounted for by the covariance error in the Weibull parameters, but showed that this empirical distribution is not necessarily the best one to choose.

Because of these observations, a direct method of including the observed maximum fault area and the slip rate was subsequently developed from Shannon's Information theory. By constraining the frequency magnitude distribution using the moment release rate observed over geological time, and the average magnitude from a short-term catalogue, the resulting distribution is automatically made consistent with estimates of the geological parameters. This led to an improvement over the Weibull distribution that was most evident in the discrete frequency statistics of the Eastern Mediterranean. Using statistical mechanics the distribution that was obtained could be interpreted as reflecting two processes: the input of tectonic strain energy, and the release of that energy in a given fault geometry. The Gutenberg-Richter b-value was related to the geometric similarity dimension of the fault system D by $b \approx 2D$, explaining the empirical observation $0.5 < b < 1.5$ as due to the release of tectonic strain energy in a system with finite volume $D < 3$. This observation would also explain why foreshocks ($b < 1$) have a lower b value than aftershocks ($b > 1$). As the stress concentrates on the asperity whose failure results in a large earthquake the seismogenic similarity dimension decreases below two. However once the main event occurs smaller strains are suddenly released in the volume surrounding the fault and the dimension increases above two. This is one reason why the author

believes that aftershock areas should only be treated only as an upper bound to the overall seismogenic fault area of the mainshock, since it is possible that changes in the stress field around the fault after the mainshock could trigger off events away from the primary fault area.

The distribution obtained gives an average repeat time of the largest Californian events ($M_s > 7.9$) of once every 156 years, within error bounds of 87-251 years. This is in good agreement with direct trenching studies into the San Andreas fault: 163 years on average, but between 55-275 years. This result indicates that the method would be useful for evaluating long-term earthquake recurrence intervals in areas where direct trenching is impossible but the slip rate is known. Another application would be in using this average repeat time to define a local time constant to indicate when a seismic gap is likely to be reactivated. (Originally an arbitrary time of 30 years since the occurrence of a plate-rupturing large earthquake was assigned, by way of definition).

Having developed and applied the new distribution the remainder of the thesis was dedicated to a case study of the Aegean area. This region already had a homogeneous magnitude catalogue and a much less complete catalogue of seismic moments. Source parameters over a huge magnitude range of 1.8 M_L-6.7 M_s were obtained from P-waves from the VOLNET array in Central Greece, and from surface waves digitised from WWSSN records. The conclusions from this study of fundamental source parameters were as follows: the moment-magnitude relation with A = 16.0, B = 1.5 holds for both the large teleseismic events $M_s > 5.5$ and the small local earthquakes $1.8 < M_L < 4.5$; typical stress drops of 1-10 bars

and associated strain drops of 10^{-6} to 10^{-5} of the small earthquakes scale very well with known values of large events at Thessaloniki (1978) and the Gulf of Corinth (1981), representing dimensional self-similarity over a moment or energy range of 1:10,000(!); a calibration procedure which ignored the effects of the orientation of the seismic source only increased the standard deviation in the surface wave seismic moments from 25% to 40%.

Having proven the validity of the assumption of self-similarity in the Aegean and produced a homogeneous catalogue of seismic moments for the area, a more detailed seismotectonic evaluation of the spreading of the Aegean area could be undertaken. First of all the moment magnitude relation showed that the body wave moments are lower than the surface wave moments by, on average, a factor two to three or so for the region. If this is shown to be the case on a global scale this has serious implications either for the theoretical models used. One likely explanation for this observation is the occurrence of multiple ruptures of two or three fault segments, since many P-wave studies only use first motions.

By applying the moment magnitude relation to the earthquake catalogue a seismogenic Aegean extension rate of 1.4 cm yr^{-1} was found for the period 1918-1981 using magnitudes above 5.5 M_s. This compares reasonably well with one tectonic model (Le Pichon and Angelier, 1981) with an average extension rate of 2 cm yr^{-1}, especially when large errors of about 50% exist in these parameters. The tectonic model is based on an extension of the idea of plate tectonics, allowing stretching to occur behind a retreating subduction hinge. The reasonable agreement of tectonic and seismogenic slip rates here and throughout this thesis

indicates that the methods used have an important role to play in investigating other second order effects of plate tectonics.

Although the Information theory distribution models the Aegean frequency-magnitude distribution adequately within its error bounds, there is a systematic offset caused by a prevalence of magnitudes around 7 M_s. This characteristic magnitude corresponds to a block like structure of large-scale fractures of about 36 x 72 km, which implies a seismogenic depth of the stretching part of the Aegean area of 25km, which is near the observed 30km depth. The indications are that this characteristic peak could also be modelled by Information theory, and it is hoped that some future project will quantify this characteristic earthquake model further.

By contrast with the Aegean basin, the seismic moment release rate due to the subducting slab under the Hellenic arc is only a fraction (about 6%) of the tectonic release expected from stick-slip at the slab's boundaries. This is consistent with a slab sinking aseismically, but being subject to second order internal buckling due to thermal expansion or phase changes in the mantle. The thickness of the original remnant oceanic crust is estimated at 12 km by a break in slope in the frequency-magnitude statistics.

All of the above discussion has focussed on the academic implications of the thesis, but there are also some immediate practical results in the form of earthquake recurrence probabilities in all of the areas studied. These quantitative estimates of the seismic hazard in the diverse areas studied will be of immediate use to those assessing seismic risk for particular structures, land use and design criteria for engineers in these

earthquake-prone areas. By using the methods developed in this thesis these decision-makers can be a little more confident of the seismic design loadings of buildings and communication systems whose working lifetimes are expected to be longer than the current length of the instrumental or historical earthquake catalogue.

REFERENCES

Abe, K., and Noguchi, S., 1983. Revision of the magnitudes of large shallow earthquakes, 1897-1912, Phys. Earth Planet. Inter., 33, 1-11.

Aki, K., and Richards, P.G., 1980. Quantitative Seismology, Freeman press, San Francisco.

Aki, K., 1981. A probabilistic synthesis of precursory phenomena, in Earthquake prediction - an international review, Maurice Ewing series 4, Am. Geophys. Union, 556-574.

Aki, K., 1984. Asperities, characteristic earthquakes and strong motion prediction, J. Geophys. Res., 89, 5867-5872.

Algermissen, S.T., and Perkins, D.M., 1976. A probabilistic estimate of maximum acceleration in rock in the contiguous United States, U.S. Geol. Surv. Open File Rep., 76-416, 45 pp.

Allegre, C.J., Le Mouel, J.L., and Provost A., 1982. Scaling rules in rock fracture and possible implications for earthquake prediction, Nature, 297, 47-49.

Ambraseys, N.N., 1970. Some characteristic features of the Anatolian fault zone, Tectonophys., 9, 143-165.

Ambraseys, N.N, 1971. Value of historical records of earthquakes, Nature, 232, 375-379.

Ambraseys, N.N., 1981. On the long term seismicity of the Hellenic arc, Boll. di Geofisica Teorica ed Applicata, XXIII, No 92, 355-359.

Anderson, D.L., Ben-Menahem, A., and Archambeau, C.B., 1965. Attenuation of seismic energy in the upper mantle, J. Geophys. Res., 70, 1441-1448.

Anderson, J.G., 1979. Estimating the seismicity from geological structure for seismic-risk studies, Bull. Seism. Soc. Am., 69, 135-158.

Anderson, J.G., and Luco, J.E., 1983. Consequences of slip rate constraints on earthquake occurrence relations, Bull. Seism. Soc. Am., 73, 471-496.

Applied Technology Council, 1978. Tentative provisions for the development of seismic regulations for buildings, ATC-3-06, 514 pp.

Assumcao, M., 1981. The NW Scotland swarm of 1974, Geophys. J. R. astr. Soc., 67, 577-586.

Båth, M., 1981a. Earthquake magnitude - recent research and current trends, Earth Sci. Rev., 17, 315-398.

Bäth, M., 1981b. Earthquake recurrence of a particular type, Pageoph., 119, 1063-1076.

Bäth, M., 1983. Earthquake frequency and energy in Greece, Tectonophys., 95, 233-252.

Berrill, J.B., and Davis, R.O., 1980. Maximum entropy and the magnitude distribution, Bull. Seism. Soc. Am., 70, 1823-1831.

Bevington, P.R., 1969. Data Reduction and error analysis for the physical sciences, McGraw-Hill, New York.

Botti, L.G., Pasquale, V., and Anghinolfi, M., 1980. A new general frequency-magnitude relationship, Pageoph., 119, 196-206.

Burridge, R., and Knopoff, L., 1967. Model and theoretical seismicity, Bull. Seism. Soc. Am., 57, 341-371.

Burton, P.W., 1973. Estimations of Q from seismic Rayleigh waves, Ph.D. Thesis, Durham University.

Burton, P.W., 1978. The IGS file of seismic activity and its use for hazard assessment, Inst. Geol. Sci., Seism. Bull. No. 6, HMSO.

Burton, P.W., 1979. Seismic risk in southern Europe through to India examined using Gumbel's third distribution of extreme values, Geophys. J. R. astr. Soc., 59, 249-280.

Burton, P.W., 1981. Variation in seismic risk parameters in Britain,

Proc. 2nd Int. Symp. on Anal. Seismicity and Seismic Hazard, Liblice, Czechoslovakia, May 18-23, 1981, Vol 2, pp 495-530, Academica, Prague.

Burton, P.W., and Blamey, C., 1972. A computer program to determine the spectrum and a dispersion characteristic of a transient signal, UKAEA AWRE Report No. 0/48/72, HMSO.

Burton, P.W., McGonigle, R.W., Makropoulos, K.C., and Ücer, S.B., 1982. Preliminary studies of seismic risk in Turkey, and the occurrence of upper bounded and other large earthquake magnitudes, Proc. Int. Symp. on Earthquake Prediction in the North Anatolian Fault Zone, Istanbul, Turkey, March 31-April 5 1980, in: A. Mete Isikara & Andreas Vogel (Editors), Multidisciplinary Approach to Earthquake Prediction, Braunschweig/Wiesbaden, Vieweg, pp143-172.

Burton, P.W., McGonigle, R., Makropoulos, K.C., and Ucer, S.B., 1984. Seismic risk in Turkey, the Aegean and the eastern Mediterranean: the occurrence of large magnitude earthquakes, Geophys. J. R. astr. Soc., 78, 475-506.

Burton, P.W. et al (1985). Contemporary seismicity in Eastern Greece from the Volos network (VOLNET): fault parameters of major and minor earthquakes, (in prep.).

Calcagnile, G., Mascia, U., Del Gaudio, V., and Panza, G.F. 1984. Deep structure of Southeastern Europe from Rayleigh waves, Tectonophys., 110, 189-200.

Caputo, M., 1976. Model and observed seismicity represented in a two dimensional space, Ann. Geophys. (Rome), 4, 277-288.

Caputo, M., 1977. A mechanical model for the statistics of earthquakes, magnitude, moment, and fault distribution, Bull. Seism. Soc. Am., 67, 849-861.

Caputo, M., 1982. On the reddening of the spectra of earthquake

parameters, Earthq. Pred. Res., 1, 173-181.

Channell, J.E.T., D'Argenio, B., and Horvath, F., 1979. Adria, the African promontory, in Mesozoic Mediterranean Paleogeography, Earth. Sci. Rev., 15, 213-292.

Chinnery, M.A., and North, R.G., 1975. The frequency of very large earthquakes, Science, 190, 1197-1198.

Comninakis, P.E., and Papazachos, B.C., 1980. Space and time distribution of the intermediate focal depth earthquakes in the Hellenic arc, Tectonophys., 70, T35-T47.

Correig, A.M., Susagna, M.T., and Lana, X., 1982. Lateral variations of attenuation coefficients, group and phase velocities of Rayleigh waves in Europe, Tectonophys., 90, 179-194.

Cosentino, P., and Luzio, D., 1976. A generalisation of the frequency magnitude relation in the hypothesis of a maximum regional magnitude, Ann. Geophys. (Rome), 4, 3-8.

Davies, G.F., and Brune, J.N., 1971. Regional and global fault slip rates from seismicity, Nature, 229, 101-107.

Dong, W.M., Bao, A.B., and Shah, H.C., 1984. Use of maximum entropy principle in earthquake recurrence relationships, Bull. Seism. Soc. Am., 74, 725-737.

Douglas, A., Hudson, J.A., and Blamey, C., 1972. A quantitative evaluation of seismic signals at teleseismic distances-III: computed P and Rayleigh wave seismograms, Geophys. J. R. astr. Soc., 28, 385-410.

Drakopoulos, J., and Delibasis, N., 1982. The focal mechanism of earthquakes in the major area of Greece for the period 1947-1981, Univ. of Athens Seismol. Lab. publ. no. 2., Athens.

Dziewonski, A.M., Franzen, J.E., and Woodhouse, J.H., 1984. Centroid-moment tensor solutions for January-March, 1984, Phys. Earth

Planet. Inter., 34, 209-219.

Epstein, B., and Lomnitz, C., 1966. A model for the occurrence of large earthquakes, Nature, 211, 954-956.

Espinosa, A.F., Sutton, G.H., and Miller, H.J., 1962. A transient technique for seismograph calibration, Bull. Seism. Soc. Am., 52, 4, 767-779.

Espinosa, A.F., Sutton, G.H., and Miller, H.J., 1965. A transient technique for seismograph calibration - Manual and standard set of theoretical transient responses, Geophysics Laboratory, Inst. of Sci. and Tech., University of Michigan.

Esteva, L., 1968. Bases par la formulacion de decisiones de diseno sismico, Natl. Univ. Mexico, Inst. Eng. Rep. 182.

Fukao, Y., and Furumoto, H., 1985. Hierarchy in earthquake size distribution, Phys. Earth Planet. Int., 37, 149-168.

Geller, R.J., 1976. Scaling relations for earthquake source parameters and magnitudes, Bull. Seism. Soc. Am., 66, 1501-1523.

Gill, P.E., and Miller, G.F., 1972. An algorithm for the integration of unequally spaced data, Comp. J., 15, 80-83.

Goto, K., Hamaguchi, H., and Suzuki, Z., 1985. Earthquake generating stresses in a descending slab, Tectonophys., 112, 111-128.

Gringorten, I.I., 1963. A plotting rule for extreme probability paper, J. Geophys. Res., 68, 813-814.

Gumbel, E., 1958. Statistics of Extremes, Columbia University Press, New York.

Hanks, T.C., Hileman, J.A., and Thatcher, W., 1975. Seismic moments of the larger earthquakes of the Southern California region, Geol. Soc. Am. Bull., 86, 1131-1139.

Haskell, N.A., 1964. Radiation pattern of surface waves from point sources in a multi-layered medium, Bull. Seism. Soc. Am., 54,

377-393.

Hays, W.W., 1984. Technical problems in the construction of a map to zone the earthquake ground-shaking hazard in the United States, Eng. Geol., 20, 13-23.

Hileman, J.A., Allen, C.R., and Nordquist, J.M., 1973. Seismicity of the Southern California region 1st Jan. 1932 to 31st Dec. 1972, Div. of Geol. and Planetary Sciences, Calif. Inst. of Technology, Contribution No. 2385.

Horvath, F., 1984. Neotectonics of the Pannonian basin and the surrounding mountain belts: Alps, Carpathians and Dinarides, Ann. Geophys., 2, 147-154.

Horvath, F., and Berckhemer, H., 1982. Mediterranean back-arc basins, in Berckhemer and Hsu (Eds), Alp. Med. Geol. Ser., 7, AGU and GSA publ., 141-173.

Horvath, F., Berckhemer, H., and Stenega, L., 1981. Models of Mediterranean back-arc basin formation, Phil. Trans. R. Soc. Lond., A300, 383-402.

Howell, B.F. Jr., 1981. On the saturation of earthquake magnitudes, Bull. Seism. Soc. Am., 71, 1401-1422.

Jackson, J.A., Gagnepain, J., Houseman, G., King, G.C.P., Papadimitriou, P., Soufleris, C., and Virieux, J., 1982. Seismicity, normal faulting, and the geomorphological development of the Gulf of Corinth (Greece): the Corinth earthquakes of February and March 1981, Earth Planet. Sci. Letts., 57, 377-397.

Jaynes, E.T., 1957. Information theory and statistical mechanics, Phys. Rev., 106, 620-630.

Jenkinson, A.F., 1955. The frequency distribution of the annual maximum (or minimum) values of meteorological elements, Q. Jour. Roy. Meteor. Soc., 87, 158-171.

Johnston, A.C., 1981. On the use of the frequency-magnitude relation in earthquake risk assessment, Proc. Conference on Earthquakes and Earthquake Engineering - the Eastern U.S. J. Beavers, Editor Publ. Ann Arbor Science Ltd., the Butterworth group; Vol. I, 161-181.

Kanamori, H., 1977. The energy release in great earthquakes, J. Geophys. Res., 82, 2981-2987.

Kanamori, H., 1978. Quantification of earthquakes, Nature, 271, 411-414.

Kanamori, H., and Anderson, D.L., 1975. Theoretical bases of some empirical relations in seismology, Bull. Seism. Soc. Am., 65, 1073-1095.

King, C., 1975. Model seismicity and faulting parameters, Bull. Seism. Soc. Am., 65, 245-259.

King, G., 1980. A fault plane solution for the Carlisle earthquake, 26 December 1979, Nature, 286, 142-143.

Kim, W., Kulhanek, O., and Meyer, K., 1984. Source processes of the 1981 Gulf of Corinth earthquake sequence from body-wave analysis, Bull. Seism. Soc. Am., 74, 459-477.

Kiratzi, A. A., and Papazachos, B.C., 1984. Magnitude scales for earthquakes in Greece, Bull. Seism. Soc. Am., 74, 969-985.

Knopoff, L., and Kagan, Y., 1977. Analysis of the theory of extremes as applied to earthquake problems, J. Geophys. Res., 82, 5647-5657.

Knopoff, L., and Chang, F.S., 1977. The inversion of surface wave dispersion data with random errors, J. Geophys., 43, 299-310.

Kuznetsova, K.I., Shumilina, L.S., and Zavialov, A.D., 1981. The physical sense of the magnitude-frequency relation, Proc. 2nd International Symposium on the Analysis of Seismicity and on Seismic Hazard, Liblice, Czechoslovakia, May 18-29, 1981, Vol. 1,

pp 27-46, Academia, Prague.

Lawson, A.C., and others 1908. Atlas of maps and seismograms from the report of the State Earthquake Investigation Commision upon the Californa Earthquake of April 18, 1906, Carnegie Inst., Washington, D.C.

Le Pichon, X., and Angelier, J., 1979. The Hellenic arc and trench system: a key to the neotectonic evolution of the Eastern Mediterranean area, Tectonophys., 60, 1-42.

Le Pichon, X., and Angelier, J., 1981. The Aegean Sea, Phil. Trans. R. Soc. Lond., A 300, 357-372.

Lisowski, M., and Prescott, W.H., 1981. Short-range distance measurements along the San Andreas fault system in Central California, 1975 to 1979, Bull. Seism. Soc. Am., 71, 1607-1624.

Lomnitz-Adler, J., 1985. Asperity models and characteristic earthquakes, In press, Geophys. J. R. astr. Soc.

MacBeth, C., 1983. Propagation and attenuation of seismic Rayleigh waves along single paths in Scotland, Ph.D. Thesis, Edinburgh University.

Madariaga, R., 1976. Dynamics of an expanding circular fault, Bull. Seism. Soc. Am., 66, 639-666.

Main, I.G., 1980. Most perceptible earthquakes in the Eastern United States, M. Sc. Dissertation, Durham University.

Main, I.G., and Burton, P.W., 1984. Physical links between crustal deformation, seismic moment and seismic hazard for regions of varying seismicity, Geophys. J. R. astr. Soc., 79, 469-488.

Makris, J., 1976. A dynamical model of the Hellenic Arc deduced from geophysical data, Tectonophys., 36, 339-346.

Makris, J., 1977. Geophysical investigations of the Hellenides, Hamburger Geophysikalische Einzelschriften, Reiche A:

Wissenschaftliche Abhandlungen, Heft 34, pp 124, GML Wittenborne Sohne, (Hamburg).

Makjanic, B., 1982. On the frequency distribution of earthquake intensity and magnitude, Bull. Seism. Soc. Am., 70, 2253-2260.

Makropoulos, K.C., 1978. The statistics of large earthquake magnitude and an evaluation of Greek seismicity, Ph.D. Thesis, Edinburgh University.

Makropoulos, K.C., and Burton, P.W., 1981. A catalogue of seismicity in Greece and adjacent areas, Geophys. J. R. astr. Soc., 65, 741-762.

Makropoulos, K.C., and Burton, P.W., 1984. Greek tectonics and seismicity, Tectonophys., 106, 275-304.

Mandelbrot, B.B., 1982. The fractal geometry of nature, Freeman press, San Francisco.

Marquardt, D.W., 1963. An algorithm for the least squares estimation of non-linear parameters, J. Soc. Ind. App. Math., 11, 2, 431-441.

Marshall, P.D., 1970. Aspects of the spectral differences between earthquakes and underground explosions, Geophys. J. R. astr. Soc., 20, 397-416.

McCann, W.R., Nishenko, S.P., Sykes, L.R., and Krause, J., 1979. Seismic gaps and plate tectonics: Seismic potential for major plate boundaries, Pageoph., 117, 1082-1147.

McKenzie, D., 1972. Active tectonics of the Mediterranean region, Geophys. J. R. astr. Soc., 30, 109-185.

McKenzie, D., 1978. Active tectonics of the Alpine-Himalayan belt: the Aegean Sea and surrounding regions, Geophys. J. R. astr. Soc., 55, 217-254.

Modiano, T., and Hatzfeld, D., 1982. Experimental study of the spectral content for shallow earthquakes, Bull. Seism. Soc. Am., 72, 1739-1758.

North, R.G., 1973. Seismic source parameters, Ph.D. Thesis, Cambridge University.

North, R.G., 1974. Seismic slip rates in the Mediterranean and Middle East, Nature, 252, 560-563.

North, R.G., 1977. Seismic moment, source dimensions, and stresses associated with earthquakes in the Mediterranean and Middle East, Geophys. J. R. astr. Soc., 48, 137-161.

Nuttli, O.W., 1979. Seismicity of the Central United States, Geol. Soc. Am. Rev. Eng. Geol., IV, 67-93.

Nuttli, O.W., and Herrmann, R.B., 1978. Creditable earthquakes for the Central U.S., State-of-the-art for assessing earthquake hazards in the U.S., U.S. Army Engineering Waterways Experiment Station, Report 12, Paper S-73-1.

Papastamatiou, D., 1980. Incorporation of crustal deformation to seismic hazard analysis, Bull. Seism. Soc. Am., 70, 1321-1335.

Petrov, V.A., 1981. Theory of the law of earthquake recurrence, Izvestia, Earth Phys., 17, 623-624.

Purcaru, G., and Berckhemer, H., 1982. Quantitative relations of seismic source parameters and a classification of earthquakes, Tectonophys., 84, 57-128.

Qamar, A., St Lawrence, W., Moore, J.N., and Kendrick, G., 1983. Seismic signals preceeding the explosive eruption of Mount St Helens, Washington, on 18 May 1980, Bull. Seism. Soc. Am., 73, 1797-1813.

Richter, C.F., 1958. Elementary Seismology, Freeman press, San Francisco.

Rikitake, T., 1976. Earthquake Prediction, Developments in Solid Earth Geophysics 9, Elsevier, Amsterdam.

Rossiter, J.R., 1972. Sea-level observations and their secular

variation, Phil. Trans. R. Soc. Lond., 272, 131-139.

Russ, D.P., 1981. Model for assessing earthquake potential and fault activity in the New Madrid seismic zone, Proc. Conference on Earthquakes and Earthquake Engineering - the Eastern U.S. J. Beavers, Editor, Publ. by Ann Arbor Science Ltd., The Butterworth Group; Vol. 1, 309-335.

Sadovskii, M.A., Bolkhovitinov, L.G., and Pisarenko, V.F., 1982. Discreteness of rocks, Izvestiya, Earth Phys., 18, 919-929.

Schilt, F.S., and Reilinger, R.E., 1981. Evidence for contemporary vertical fault displacement from precise levelling data near the New Madrid seismic zone, Western Kentucky, Bull. Seism. Soc. Am., 71, 1933-1942.

Scholz, C.H., 1968. The frequency-magnitude relation of microfracturing in rock and its relation to earthquakes, Bull. Seism. Soc. Am., 58, 399-415.

Scholz, C.H., 1982. Scaling laws for large earthquakes: consequences for physical models, Bull. Seism. Soc. Am., 72, 1-14.

Schwartz, D.P., and Coppersmith, K.J. 1984. Fault behaviour and characteristic earthquakes: Examples from the Wasatch and the San Andreas fault zones, J. Geophys. Res., 89, 5681-5698.

Scott, P.R., and Kanamori, H., 1985. On the consistency of moment tensor source mechanisms with first-motion data, Phys. Earth Planet. Int., 37, 97-107.

Shannon, C.E., 1948. The mathematical theory of communication, Bell System Tech. J., 27, 379-623.

Shimazaki, K., and Nakata, T., 1980. Time-predictable recurrence model for large earthquakes, Geophys. Res. Letts., 7, 279-282.

Sieh, K.E., 1978. Prehistoric large earthquakes produced by slip on the San Andreas fault at Pallet Creek, California, J. Geophys. Res.,

83, 3907-3939.

Singh, S.K., and Havskov, J., 1980. On moment-magnitude scale, Bull. Seism. Soc. Am., 70, 379-383.

Singh, S.K., Rodriguez, M., and Esteva, L., 1983. Statistics of small earthquakes and frequency of occurrence of large earthquakes along the Mexican subduction zone, Bull. Seism. Soc. Am., 73, 1779-1796.

Sissons, J.B., and Cornish, R., 1982. Rapid localised glacio-isostatic uplift at Glen Roy, Scotland,. Nature, 297, 213-214.

Soufleris, C., and Stewart, G.S., 1981. A source study of the Thessaloniki (northern Greece) 1978 earthquake sequence, Geophys. J. R. astr. Soc., 67, 343-358.

Soufleris, C., Jackson, J.A., King, G.C.P., Spencer, C.P., and Scholz, C.H., 1982. The 1978 earthquake sequence near Thessaloniki (northern Greece), Geophys. J. R. astr. Soc., 68, 429-458.

Street, R., and Lacroix, A., 1979. An empirical study of New England seismicity: 1727-1977, Bull. Seism. Soc. Am., 69, 159-175.

Thatcher, W., and Hanks, T.C., 1973. Source parameters of Southern California earthquakes, J. Geophys. Res., 78, 8547-8576.

Tsai, Y.B., and Aki, K., 1970. Precise focal depth determination from amplitude spectra of surface waves, J. Geophys. Res., 75, 5729-5743.

Vere-Jones, D., 1976. A branching model for crack propagation, Pageoph., 114, 711-725.

Walker, B., 1982. Earthquake (Planet Earth Series no. 1), Time-Life Books.

Weibull, W., 1951. A statistical distribution function of wide applicability, J. Appl. Mech., 18, 293-297.

Wyss, M., 1979. Estimating maximum expectable magnitude of earthquakes from fault dimensions, Geology, 7, 336-340.

Yielding, G., 1985. Control of rupture by fault geometry during the 1980 El Asnam (Algeria) earthquake, Geophys. J. R. astr. Soc., 81 641-670.

Yegulalp, T.M., and Kuo, J.T., 1974. Statistical prediction of the occurrence of maximum magnitude earthquakes, Bull. Seism. Soc. Am., 64, 393-414.

Zoback, M.D., Hamilton, R.M., Crone, A.J., Russ, D.P., McKeown, F.A., and Brockman, S.R., 1980. Recurrent intraplate tectonism in the New Madrid seismic zone, Science, 209, 971-976.

Zoback, M.L., and Zoback, M., 1980. State of stress in the conterminous United States, J. Geophys. Res., 85, 6113-6159.

APPENDIX 1

COMPUTER PROGRAMMES

1(i) Programme summary

This section tabulates the programmes in the order they appear in the main text of the thesis.

Chapter 2

1A : RISK-FF7 - Weibull curve fit

1B : MOMENT-FF2 - Seismic moment release from a Weibull distribution

Chapter 3

1C : MAXENT-FF1 - Preparation of discrete frequency data points and evaluation of the average magnitude

1D : MAXENT-FF2 - The Information theory distribution of equation (3.9)

1E : MAXENT-FF3 - Evaluation of the error bounds of equation (3.9)

1F : MAXENT-FF4 - Magnitudes associated with a given average repeat time for (3.9)

1G : MAXENT-FF5 - Long term prediction of recurrence times from (3.9)

1H : MAXENT-G - Graph file for (3.9)

Chapter 4

1I : VOL-PREP - Preparation file for spectral analysis of VOLNET seismograms

1J : VOL-DIST - Evaluates epicentral distances and source parameters from the VOLNET spectra

1(ii) Programme notes

Most of the programmes developed for the thesis have been kept short, and have been well annotated in order to make them easier to operate and understand. This has meant that the methods chosen are not necessarily the most efficient in terms of computer time, and it is hoped to produce a cost efficient, user friendly package at some future point, especially for all the numerical calculations involved in obtaining the parameters and predictions of the Information theory distribution of equation (3.9). The following notes relate the notation of the thesis (see text referring to each programme or the glossary) to the FORTRAN names used in the programmes for all the variables. Some descriptions of the algorithms used is also given where necessary.

1A

This program, which solves for the Weibull and Gumbel parameters (ω, u, λ) and ε was modified from a listing by Makropoulos (1978). The subroutine CURFIT, originally taken from Bevington (1969), is the basic routine used to fit a Weibull curve to the frequency-magnitude data. Alterations from Makropoulos' (1978) listing are (a) the inclusion of a return period of the large events from geological evidence (RT), and (b) using cumulative frequency data rather than extreme values. This also requires alteration of the form of the derivatives given in subroutine FDERIV. The notation of the important parameters are as follows.

Text Symbol	Programme parameter	Notes
(ω,u,λ)	G3PAR(1,2,3)	
ε	COV(I,J)	
m_i	VAR (I)	the i^{th} magnitude read in from the catalogue

$N = \left(\frac{\omega-m}{\omega-u}\right)^{1/\lambda}$	Z1	in subroutine FDERIV
$\frac{\partial N}{\partial \omega}, \frac{\partial N}{\partial u}, \frac{\partial N}{\partial \lambda}$	DERIV(1,2,3)	
$m = \omega - (\omega-u)N^{\lambda}$	FUNCTN	in function FUNCTN

1B

This program calculates $\dot{\bar{M}}_o$ and $\langle \dot{M}_o \rangle$ as defined in Chapter 2 from the parameters of a Weibull curve fit and an extreme value curve fit respectively, using an analytical form for the former, but relying on a numerical routine for the latter. The numerical integration was done by accessing an algorithm by Gill and Miller (1972) through a call to a standard routine CALL D01GAF (X,Y,N,ANS,ER,IFAIL) available on the EMAS system at Edinburgh. First of all two arrays X,Y of N points each are set up, and then this routine is called by this one line only, giving the integration of $Y = f(X)$ as $ANS = \int_{X_1}^{X_N} f(X)dX$ and an error estimate ER. IFAIL is an error flag, so that any error in running the routine makes IFAIL ≠ 0. For a more complete description see the NAG FORTRAN Library manual (mark 9), Numerical algorithms group, Oxford (1982).

Other parameters are

(ω, u, λ)	W, U, RL
A, B, β	A, B, BETA
$M_{o\omega}$	RMOW
$\langle \dot{M}_o \rangle$	RMO
$\partial \langle \dot{M}_o \rangle / \partial u$	DMOU etc

1C

This is a standard calculation of an average magnitude value $\langle m \rangle$ and its standard error $\sigma_{\langle m \rangle}$ given a catalogue of magnitudes m_i, i=1,N. In addition the frequency magnitude data are also counted from the catalogue entries. The notation is

m_i	VAR(I)	
m_c, ω	RMAG1, RMAGMAX	
$F(m_j)$	X(J)	Discrete Frequency
$N(m_j)$	CF (J)	Cumulative Frequency
$\langle m \rangle$, $\sigma_{\langle m \rangle}$	AVMAG, SIGMAG	
N_T, σ_{N_T}	RNT, SIGNT	

1D

This programme solves for λ_1 and λ_2 in (3.9). This was done by simple iteration from starting values of λ_1(RL1) and λ_2 (RL2) of RL1 = 0.5, RL2 = 0, first by setting a value of λ_1 consistent with $\langle m \rangle$ (RMBAR) within $\pm \sigma_{\langle m \rangle}/10$ (SIG = SIGMA/10). There is no need to solve more accurately at this stage, since the programme subsequently allows for $\pm \sigma_{\langle m \rangle}$ in the covariance error calculation. The first order iteration

RL1 = RL1 (1 + C1 * DELTAM)

is used with constant RL2 to reduce the difference between the calculated value of $\langle m \rangle$ from equation (3.7) given RL1 and RL2 (RM), and the actual value (DELTAM = RM - RMBAR).

Once DELTAM < SIG the routine adjusts RL2 by the iteration

RL2 = RL2 + C2 * DELTAMO

and this time compares the calculated value of $\langle M_o \rangle$ (RMOBAR1) given equation (3.7) and RL1 and RL2 (RMO) with the known value (RMOBAR), via DELTAMO = RMO - RMOBAR1. If at any time during this iteration with constant RL1 the value of DELTAM exceeds SIG, then the procedure is followed once more with these new starting values of RL1 and RL2. Finally a result is produced when DELTAM < SIG and DELTAMO < SIGMO, SIGMO = $\sigma_{\langle M_o \rangle}/10$.

At every step the calculated values of $\langle m \rangle$, $\langle M_o \rangle$ and Z in equation (3.7) are done by the numerical integration routine D01GAF discussed in the notes to 1B, and held in the subroutine INTEGRATE.

The only control on the speed of convergence to a solution are the variables C1 and C2 read in on channel 3 with the data on $\langle M_o \rangle$. Typical values of 1 and 5 respectively give reasonable convergence, but some trial and error is required to avoid convergence which is too slow (ie more than 20 iterations in the program listing) or even a diverging iteration.

1E

Having found λ_1 and λ_2 the next step is to solve for their standard errors, using (3.23). This was done by real brute force - very high precision (REAL * 16) and by back-substitution after diagonalising the (3x3) matrix A, with B the (1x3) covariance error matrix in $\langle m \rangle$ and $\langle M_o \rangle$. By comparison with (3.23), the matrix equation

A C = B ,

is defined, where C is the covariance error matrix $(\sigma^2_{\lambda_1}, \sigma^2_{\lambda_2}, \sigma^2_{\lambda_1\lambda_2})^T$. First of all the coefficients of A are calculated from (3.20) and (3.23) by the subroutine EXPECTATIONS, and then A and C are combined into a 4 x 3 matrix by making C the fourth column of A in the subroutine SOLVE. SOLVE then goes on to diagonalise the matrix A in two stages: first by making the first column entries below A_{11} zero and then those under A_{22}, and writing out the intermediate stages. Finally C is solved for by back substitution.

1F

Here $m_T \pm \sigma_{m_T}$ are calculated, being defined by equation (3.9), with T = 1/N, and the covariance error equation for σ_{m_T} given below. The notation is

A, B, σ_A	A, B, SIGA
ω, σ_ω	W, SIGW
m_c	RMIN
$\langle m \rangle$, $\sigma_{\langle m \rangle}$	RMBAR, SIGMA
N_T, δN_T	RNT, SIGRNT
λ_1, λ_2, Z	RL1, RL2, Z
$\sigma^2_{\lambda_1}$, $\sigma^2_{\lambda_2}$, $\sigma^2_{\lambda_1\lambda_2}$	SL1, SL2, SL3
$\langle M_o \rangle$, $\sigma_{\langle M_o \rangle}$	RMOBAR, SIGMOBAR

The subroutine SOLVE solves (3.9) for λ_1, λ_2 given all the other parameters, and ERROR calculates σ_{m_T} using partial derivatives, e.g.

$$\frac{\partial m_T}{\partial \lambda_1} = \text{DMDL1} \ .$$

The covariance error in m_T,

$$\delta_{m_T} = \left\{\frac{\partial m_T}{\partial \lambda_1}\right\}^2 \sigma^2_{\lambda_1} + \left\{\frac{\partial m_T}{\partial \lambda_2}\right\}^2 \sigma^2_{\lambda_2} + \left\{\frac{\partial m_T}{\partial \lambda_1}\right\} \left\{\frac{\partial m_T}{\partial \lambda_2}\right\} 2\sigma_{\lambda_1\lambda_2} +$$
$$\left\{\frac{\partial m_T}{\partial A}\right\}^2 \delta A^2 + \left\{\frac{\partial m_T}{\partial N_T}\right\}^2 \delta N_T{}^2 + \left\{\frac{\partial m_T}{\partial \omega}\right\}^2 \delta\omega^2 \quad ,$$

called SIG is calculated partly in this routine, and partly in the main program.

1G

This program is similar to 1F except for the use of equation (3.24) rather than the above equation. The notation is similar, except for

N	RN
$\frac{\partial N}{\partial \lambda_1}$	DNDL1 etc

in the subroutine ERROR. Once again INTEGRATE performs the numerical integration. Then the error in the long-term average repeat time is calculated for a given magnitude X read in on channel 5.

$T(m) = 1/N$	T
$+\delta T = \frac{1}{N^2} \delta N$	TP
$-\delta T$	TM

1H

This is a simple graph routine which plots the frequency data against the Information theory curve, made complicated by the form of the distribution. The subroutines INTEGRATE, ERROR etc all have similar functions to those already described.

1I

This programme prepares a control file for spectral analysis from the phase data (P wave arrival times T_o) in the VOLNET bulletins and the velocity model of Makris (1977). The subroutine FDIST calculates the distance R between the epicentre of the I^{th} event at the J^{th} station - DIST (I,J). This is then converted to a time by using $\delta T = (\alpha-\beta)/R$ using given values of α and β, the P and S wave velocities. $T_o \pm \delta T$ now specify two windows for the frequency analysis.

1J

This programme calculates the final source parameters from Ω_o and f_c, using (4.11)-(4.14). The notation is as follows

$\Omega_{o_{ij}}$	OMEGA(I,J)	LP spectral level of i^{th} event at j^{th} station
$f_{c_{ij}}$	FC (I,J)	Corner frequency
R_{ij}	R (I,J)	Source-station distance

with

$M_{o_{ij}}$ = CK * OMEGA (I,J) * R (I,J)

F_{i_j} = C/FC (I,J)

C and CK depend on α, β in the source layer and hence on the depth (DEP(I)). These values are assigned in the subroutine CONSTS, and R is calculated by FDIST.

1(iii) Programme listings

There follows a listing of the actual programs used.

1A

RISK-FF7

```
C
C This program produces estimates and uncertainties of the parameters
C of a cumulative frequency distribution from an earthquake catalogue
C
C   the form is ((w-m)/(w-u))**k
C
C  This version introduces geologically estimated
C  average repeat times.
C
C
C Streams 1:earthquake catalogue
C         5:terminal or control file
C        11:output parameter file
C        12:output file of extremes and plotting points
C
C  Ian Main Dec. 82 (Modified from the extreme value
C  program riskff5 by R.McGonigle)
C
      DIMENSION VAR(3000),X(199),Y(199),SIGY(199),G3PAR(3),G3UN(3)
     -         ,COV(3,3),WK(199),WRK(199),WRKY(199),RINT(2,5)
     -         ,RKA(5),MINTIM(5)
      DATA RAD/57.29577951/,RT/163.0/,RM/8.0/
C
C (RT is the return period of the 'Big ones')
C
C Set up options; initialise variables
C
      CALL FPRMPT('Lat limits:',11)
      READ(5,*)RLAT1,RLAT2
      CALL FPRMPT('Lon limits:',11)
      READ(5,*)RLON1,RLON2
      CALL FPRMPT('Time limits:',12)
      READ(5,*)MINT,MAXT
      CALL FPRMPT('Min mag:',8)
      READ(5,*)RMAG1,RMAGMAX
      CALL FPRMPT('Var option:',11)
      READ(5,*)IVAR
      CALL FPRMPT('Unit time:',10)
      READ (5,*) TUNIT
      CALL FPRMPT('No. of Intervals:',17)
      READ(5,*) NCOMP
      DO 1 J=1,NCOMP
      CALL FPRMPT('Int, time:',10)
    1 READ (5,*) RINT(1,J),RINT(2,J),MINTIM(J)
      RLATM=RLAT1+(RLAT2-RLAT1)/2.
      RLONM=RLON1+(RLON2-RLON1)/2.
      DO 2 I=1,NCOMP
      TIME=MAXT-MINTIM(I)+1
    2 RKA(I)=TIME/TUNIT
      G3PAR(1)=7.0
      G3PAR(2)=5.
      G3PAR(3)=0.7
```

```
C
C Read in magnitudes; assign to VAR the correct variable
C
      RMAG2=RMAG1
      NO=0
   10 READ(11)IYEAR,RLAT,RLON,IDEPTH,RMAG
      IF(IYEAR.EQ.0)GO TO 17
      IF(IYEAR.LT.MINT.OR.IYEAR.GT.MAXT)GO TO 10
      IF(RMAG.LT.RMAG1)GO TO 10
      IF(RMAG.GT.RMAGMAX) GO TO 10
      IF(RLON.GT.RLON2.OR.RLON.LT.RLON1)GO TO 10
      IF(RLAT.GT.RLAT2.OR.RLAT.LT.RLAT1)GO TO 10
      DO 4 K=1,NCOMP
    4 IF(RMAG.GE.RINT(1,K).AND.RMAG.LT.RINT(2,K)) L=K
      IF(IYEAR.LT.MINTIM(L)) GOTO 10
      NO=NO+1
      IF(IVAR.EQ.4)GO TO 14
      GO TO (11,12,13),IVAR
C Acceleration
   11 V=2164.*EXP(EM*0.7)*(R+20.)**(-1.80)
      GO TO 15
C Velocity
   12 V=0.725*10.**(0.52*EM)*(R**(-1.34))
      GO TO 15
C Displacement
   13 V=0.0471*10.**(EM*0.57)*(R**(-1.18))
      GO TO 15
C Magnitude
   14 V=RMAG
      VAR(NO)=V
      IF(V.GT.RMAG2) GOTO 16
   15 GOTO 10
   16 RMAG2=VAR(NO)
      GOTO 10
C
C  Count the frequencies
C
   17 M1=RMAG1*10.0
      M2=RMAG2*10.0
      NPTS=M2-M1+1
   19 DO 20 I=1,NPTS
      Y(I)=(RMAG2-FLOAT(I)/10.0)+0.1
   20 X(I)=0.0
      DO 21 I=1,NO
      J=IFIX((RMAG2-VAR(I))*10.0)+1
      DO 3 K=1,NCOMP
      IF(Y(J).GE.RINT(1,K).AND.Y(J).LT.RINT(2,K)) L=K
    3 CONTINUE
   21 X(J)=X(J)+1.0/RKA(L)
      GOTO 28
C
C  Optional adjustment of large events
C  where there is geological evidence
C  for recurrence rates
C
      WK(1)=1./RT
      NPTS=NPTS+1
      DO 26 I=2,NPTS
      WK(I)=X(I-1)
   26 CONTINUE
      DO 27 I=1,NPTS
   27 X(I)=WK(I)
   28 CONTINUE
C
C  Add up the cumulative frequency
C
      DO 22 I=2,NPTS
   22 X(I)=X(I)+X(I-1)
C
C   Remove zero entries
C
      J=1
      SIGY(1)=0.5
      DO 24 I=2,NPTS
      Z=X(I)-X(I-1)
      IF (Z.EQ.0) GOTO 24
      J=J+1
      WRK(J)=X(I)
      WRKY(J)=Y(I)
   24 CONTINUE
      NPTS=J
      DO 25 I=2,NPTS
      SIGY(I)=0.5
      Y(I)=WRKY(I)
   25 X(I)=WRK(I)
C
C Solve equations and output
C
      FLAMDA=0.01
      CHISQP=10.0**10
   30 CALL CURFIT(X,Y,SIGY,NPTS,3,+1,FLAMDA,G3PAR,COV,CHISQ)
      IF(ABS(CHISQ-CHISQP).LT.0.01)GO TO 31
      CHISQP=CHISQ
      GO TO 30
   31 DO 32 K=1,3
   32 G3UN(K)=SQRT(COV(K,K))
      PRINT 100,RLAT1,RLAT2,RLON1,RLON2,MINT,MAXT,TUNIT,
     -          RMAG1,IVAR,(G3PAR(K),G3UN(K),K=1,3),
     -          COV,(RINT(1,J),RINT(2,J),MINTIM(J),J=1,NCOMP)
      WRITE(11,101)RLATM,RLONM
      WRITE(11,102)G3PAR,G3UN,COV(1,2),COV(1,3),COV(2,3),NPTS
      WRITE(11,102)RLAT1,RLAT2,RLON1,RLON2
      WRITE(12,103)RLATM,RLONM,G3PAR,NPTS
      WRITE(12,104)(X(K),Y(K),K=1,NPTS)
  100 FORMAT(' **Gumbel type 3 distribution program**'/
     -       1X,'The area is',2(F10.4,' to',F10.4,1X)/
```

```
     _      1X,'The time period is ',I4,'-',I4/
     _      1X,'and the unit time interval is',I4,'yrs.'/
     _      1X,'The magnitude cut-off is',F10.4/
     _      1X,'and the variable is',I4/
     _      1X,'the parameters are ',3(F10.4,'(',F10.4,')')/
     _      1X,'The covariance matrix is:',3(/1X,3F10.4)
     _      1X,//'The  intervals are:',5(/1X,F6.2,F6.2,I6))
  101 FORMAT('CELL ',3F10.4)
  102 FORMAT(1X,9E14.6,I4)
  103 FORMAT(5E14.6,I4)
  104 FORMAT(1X,9E14.6)
      STOP
      END
      SUBROUTINE CURFIT(X,Y,SIGMAY,NPTS,NTERMS,MODE,FLAMDA,
     _                  A,COV,CHISQR)
C
C Makes a least squares fit to a non-linear function
C
      REAL*8 ARRAY(10,10),ALPHA(10,10),BETA(10)
      DIMENSION X(199),Y(199),SIGMAY(199),YFIT(199),WEIGHT(199)
      DIMENSION A(3),B(3),DELTAA(3),COV(3,3),DERIV(3)
C
   11 NFREE=NPTS-NTERMS
      IF(NFREE) 13,13,20
   13 CHISQR=0.
      GO TO 110
C
C  Evaluate weights
C
   20 DO 30 I=1,NPTS
   21 IF (MODE) 22,27,29
   22 IF (Y(I)) 25,27,23
   23 WEIGHT(I)=1./Y(I)
      GO TO 30
   25 WEIGHT(I)=1./(-Y(I))
      GO TO 30
   27 WEIGHT(I)=1.
      GO TO 30
   29 WEIGHT(I)=1./SIGMAY(I)**2
   30 CONTINUE
C
C    Evaluate alpha and beta matrices
C
   31 DO 34 J=1,NTERMS
      BETA(J)=0.D0
      DO 34 K=1,J
   34 ALPHA(J,K)=0.D0
   41 DO 50 I=1,NPTS
      CALL FDERIV (X,I,A,DELTAA,NTERMS,DERIV)
      DO 46 J=1,NTERMS
      BETA(J)=BETA(J)+WEIGHT(I)*(Y(I)-FUNCTN(X,I,A))*DERIV(J)
      DO 45 K=1,J
   46 ALPHA(J,K)=ALPHA(J,K)+WEIGHT(I)*DERIV(J)*DERIV(K)
   50 CONTINUE
   51 DO 53 J=1,NTERMS
      DO 53 K=1,J
   53 ALPHA(K,J)=ALPHA(J,K)
C
C    Evaluate chi square at starting point
C
   61 DO 62 I=1,NPTS
   62 YFIT(I)=FUNCTN(X,I,A)
   63 CHISQ1=FCHISQ(Y,SIGMAY,NPTS,NFREE,MODE,YFIT)
C
C  Invert modified curvature matrix to find new parameters
C
   71 DO 74 J=1,NTERMS
      DO 73 K=1,NTERMS
   73 ARRAY(J,K)=ALPHA(J,K)/DSQRT(ALPHA(J,J)*ALPHA(K,K))
   74 ARRAY(J,J)=1.+FLAMDA
   80 CALL MATINV (ARRAY,NTERMS,DET)
   81 DO 84 J=1,NTERMS
      B(J)=A(J)
      DO 84 K=1,NTERMS
   84 B(J)=B(J)+BETA(K)*ARRAY(J,K)/DSQRT(ALPHA(J,J)*ALPHA(K,K))
C
C  If Chi square, increase flambda and try again
C
   91 DO 92 I=1,NPTS
   92 YFIT(I)=FUNCTN(X,I,B)
   93 CHISQR=FCHISQ(Y,SIGMAY,NPTS,NFREE,MODE,YFIT)
      IF (CHISQ1-CHISQR) 95,101,101
   95 FLAMDA=10.*FLAMDA
      GO TO 71
C
C Evaluate parameters and uncertainties
C
  101 DO 102 I=1,NTERMS
      DO 102 J=1,NTERMS
  102 ALPHA(I,J)=0.D0
      DO 103 I=1,NPTS
      CALL FDERIV(X,I,B,DELTAA,NTERMS,DERIV)
      DO 104 J=1,NTERMS
      DO 104 K=1,J
  104 ALPHA(J,K)=ALPHA(J,K)+WEIGHT(I)*DERIV(J)*DERIV(K)
  103 CONTINUE
      DO 105 J=1,NTERMS
      DO 105 K=1,J
  105 ALPHA(K,J)=ALPHA(J,K)
      DO 106 J=1,NTERMS
      DO 106 K=1,NTERMS
  106 ARRAY(J,K)=ALPHA(J,K)/DSQRT(ALPHA(J,J)*ALPHA(K,K))
      CALL MATINV(ARRAY,NTERMS,DET)
      DO 107 J=1,NTERMS
      A(J)=B(J)
      DO 107 K=1,NTERMS
```

```
  107 COV(J,K)=ARRAY(J,K)/DSQRT(ALPHA(J,J)*ALPHA(K,K))
      FLAMDA=FLAMDA/10.
  110 RETURN
      END
      FUNCTION FUNCTN(X,I,A)
C
C Returns the magnitude associated with the probability X(I)
C
      DIMENSION X(199),A(3)
      FUNCTN=A(1)-(A(1)-A(2))*(X(I))**A(3)
      END
C
      FUNCTION FCHISQ(Y,SIGMAY,NPTS,NFREE,MODE,YFIT)
C
C Returns the value of reduced chi-square
C
      DOUBLE PRECISION CHISQ,WEIGHT
      DIMENSION Y(199),SIGMAY(199),YFIT(199)
   11 CHISQ=0.
   12 IF (NFREE) 13,13,20
   13 FCHISQ=0.
      GO TO 40
C
C Accumulate chi square
C
   20 DO 30 I=1,NPTS
   21 IF (MODE)  22,27,29
   22 IF(Y(I)) 25,27,23
   23 WEIGHT=1./Y(I)
      GO TO 30
   25 WEIGHT=1./(-Y(I))
      GO TO 30
   27 WEIGHT=1.
      GO TO 30
   29 WEIGHT=1./SIGMAY(I)**2
   30 CHISQ=CHISQ+WEIGHT*(Y(I)-YFIT(I))**2
C
C  Divide by no. of degrees of freedom
C
   31 FREE=NFREE
   32 FCHISQ=CHISQ/FREE
   40 RETURN
      END
      SUBROUTINE FDERIV (X,I,A,DELTAA,NTERMS,DERIV)
C
C Returns the partial derivatives DERIV
C
      DIMENSION X(199),A(3),DELTAA(3),DERIV(3)
      Z1=X(I)
      Z2=Z1**A(3)
      DERIV(1)=1.-Z2
      DERIV(2)=Z2
      DERIV(3)=-(A(1)-A(2))*Z2*ALOG(Z1)
      RETURN
      END
      SUBROUTINE MATINV (ARRAY,NORDER,DET)
C
C Returns the inverse of ARRAY in place and its determinant DET
C
      DOUBLE PRECISION ARRAY,AMAX,SAVE
      DIMENSION ARRAY(10,10),IK(10),JK(10)
      DET=1.
      DO 100 K=1,NORDER
C
C  Find largest element ARRAY(I,J) in rest of matrix
C
      AMAX=0.
   21 DO 30 I=K,NORDER
      DO 30 J=K,NORDER
   23 IF (DABS(AMAX)-DABS(ARRAY(I,J))) 24,24,30
   24 AMAX=ARRAY(I,J)
      IK(K)=I
      JK(K)=J
   30 CONTINUE
C
C  Interchange rows and columns to put AMAX in ARRAY(K,K)
C
   31 IF (AMAX) 41,32,41
   32 DET=0.
      GO TO 140
   41 I=IK(K)
      IF (I-K) 21,51,43
   43 DO 50 J=1,NORDER
      SAVE=ARRAY(K,J)
      ARRAY(K,J)=ARRAY(I,J)
   50 ARRAY(I,J)=-SAVE
   51 J=JK(K)
      IF (J-K) 21,61,53
   53 DO 60 I=1,NORDER
      SAVE=ARRAY(I,K)
      ARRAY(I,K)=ARRAY(I,J)
   60 ARRAY(I,J)=-SAVE
C
C  Accumulate elements of inverse matrix
C
   61 DO 70 I=1,NORDER
      IF (I-K) 63,70,63
   63 ARRAY(I,K)=-ARRAY(I,K)/AMAX
   70 CONTINUE
   71 DO 80 I=1,NORDER
      DO 80 J=1,NORDER
      IF (I-K) 74 ,80 ,74
   74 IF (J-K) 75,80,75
   75 ARRAY(I,J)=ARRAY(I,J)+ARRAY(I,K)*ARRAY(K,J)
   80 CONTINUE
   81 DO 90 J=1,NORDER
```

```
      IF (J-K) 83,90,83
   83 ARRAY(K,J)=ARRAY(K,J)/AMAX
   90 CONTINUE
      ARRAY(K,K)=1./AMAX
  100 DET=DET*AMAX
C
C  Restore ordering of matrix
C
  101 DO 130 L=1,NORDER
      K=NORDER-L+1
      J=IK(K)
      IF (J-K) 111,111,105
  105 DO 110 I=1,NORDER
      SAVE=ARRAY(I,K)
      ARRAY(I,K)=-ARRAY(I ,J)
  110 ARRAY(I,J)=SAVE
  111 I=JK(K)
      IF (I-K) 130,130,113
  113 DO 120 J=1,NORDER
      SAVE=ARRAY(K ,J)
      ARRAY(K,J)=-ARRAY(I,J)
  120 ARRAY(I,J)=SAVE
  130 CONTINUE
  140 RETURN
      END
```

1B

```
                    MOMENT-FF2
C
C   This program computes Mo(w,u,lambda,A,B) for model
C   I (Weibull frequency distribution) and
C   II (Gumbel's third distribution)
C
C   Input streams
C
C    11 : w,u,lambda set from risk-ff5 or -ff7
c
C   Output stream
C
C    6 : Mo for both models
C
C   Ian Main Jan. 83
C
C   ***********************************************
C
      DATA A/15.58/,B/1.5/
      DATA C/1.59/,D/3.97/
      READ (11,1) W,U,RL,SW,SU,SL,SWU,SWL,SUL
    1 FORMAT (/,1X,9E14.6)
C
C   Optional change Mb-Ms
C
      A1=A-B*D
      B1=B*C
C*      A1=A1
C*      B1=B
      A1=A1-25.
      W1=W
      U1=U
      RL1=RL
      SU1=SU
      SW1=SW
      SL1=SL
C
C   ***********************************************
C
C   (A) <MO> FROM GUMBEL THREE
C
C   EVALUATE MO IN UNITS OF 10**25 DYN CM YR(-1)
C
      RMOW=10.0**(A1+B1*W)
      BETA=B1*ALOG(10.0)
      C1=BETA*(W-U)
C
C  EVALUATE THE INTEGRALS FI,F2,F3
C
      REAL*8 X(1001),Y1(1001),Y2(1001),Y3(1001)
      REAL*8 F1,F2,F3,E1,E2,E3
      DO 10 I=1,1000
      X(I)=0.5+FLOAT(I)/2000.0
```

```
      ARG=(-ALOG(X(I)))**RL
      Y1(I)=EXP(-C1*ARG)
   10 Y2(I)=Y1(I)*ARG
      DO 20 I=1,999
   20 Y3(I)=Y2(I)*ALOG(-ALOG(X(I)))
      CALL DOIGAP(X,Y1,1000,F1,E1,0)
      CALL DOIGAP(X,Y2,1000,F2,E2,0)
      CALL DOIGAP(X,Y3,999,F3,E3,0)
C
C  EVALUATE MO AND ITS PARTIAL DERIVATIVES
C
      RMO=RMOW*F1
      DMOU=RMOW*BETA*F2
      DMOW=RMO*BETA-DMOU
      DMOL=(-C1)*RMOW*F3
C
C  EVALUATE TOTAL COVARIANCE ERROR  INCLUDING SIGMA(W,U,RL)
C
      SMOU=DMOU*SU
      SMOW=DMOW*SW
      SMOL=DMOL*SL
      SMO=(SMOU**2+SMOW**2+SMOL**2)
      SMOUW=DMOW*DMOU*SWU
      SMOLW=DMOW*DMOL*SWL
      SMOLU=DMOU*DMOL*SUL
      SMOCOV=SMO+2*(SMOUW+SMOLW+SMOLU)
      SMO=SMO**0.5
      SMOCOV=SMOCOV**0.5
      SMONEG=RMO*(1.-1./(1.+SMOCOV/RMO))
C
C
C  ************************************
C
C  (B)  MO(BAR) FROM N(M)
C
C
C  EVALUATE MO(BAR) AND ITS PARTIAL DERIVATIVES
C
      RMOW1=10.**(A1+B1*W1)
      C2=BETA*(W1-U1)
      RK1=1.0/RL1
      SK1=-SL1/(RL1**2)
      RKP=RK1+1.0
      G=GAMMA(RKP)
      AK=C2**RK1
      RMOBAR=G*(RMOW1/AK)
      DMDU=RMOBAR*(RK1/(W1-U1))
      DMDW=RMOBAR*(BETA-RK1/(W1-U1))
      DMDK=RMOBAR*(1.0-ALOG(C2))
C
C  EVALUATE THE COVARIANCE ERROR IN MO(BAR) AND
C   DETERMINE THE RATIO  <MO>/MO(BAR)
C
      SMU=DMDU*SU1
      SMW=DMDW*SW1
      SMK=DMDK*SK1
      SMOBAR=(SMU**2+SMW**2+SMK**2)
      SMUW=DMDW*DMDU*SWU
      SMLW=-DMDW*DMDK*SWL*(RL1**2)
      SMUL=-DMDU*DMDK*SUL*(RL1**2)
      SIGCOV=SMOBAR+2*(SMUW+SMLW+SMUL)
      SMOBAR=SMOBAR**0.5
      SIGCOV=SIGCOV**0.5
      SIGNEG=RMOBAR*(1.-1./(1.+SIGCOV/RMOBAR))
      RATIO=RMO/RMOBAR
C
C    *********************************
C
C  WRITE OUT RESULTS
C
      WRITE (6,100)
      WRITE (6,101) W,U,RL
      WRITE (6,110) A,B
      WRITE (6,111) C,D
      WRITE (6,103) RMO,SMOCOV
      WRITE (6,104) SMONEG
      WRITE (6,105) RMOBAR,SIGCOV
      WRITE (6,109) SIGNEG
      WRITE (6,106) RATIO
      WRITE (6,107) DMOW,DMOU,DMOL
      WRITE (6,108) SMOW,SMOU,SMOL
  100 FORMAT(1X,'Eastern U.S. (Stress drop 100 Bars)'/)
  101 FORMAT(2X,' W=',F8.3,' U=',F8.3,' L=',F8.3/)
  102 FORMAT(2X,'W1=',F8.3,'U1=',F8.3,'L1=',F8.3/)
  103 FORMAT(2X,'<MO>=',F8.3,' SIGMA= +',F8.3,' *10**25 DYN CM YR(-1)')
  104 FORMAT (25X,'-',F8.3)
  105 FORMAT(2X,'(MO)=',F8.3,' SIGMA= +',F8.3)
  106 FORMAT(/' <MO>/MO(BAR)=',F10.4)
  107 FORMAT(/'dMo/dw:dMo/du:dMo/dl=',F10.4,':',F10.4,':',F10.4)
  108 FORMAT(/'sMo(w):sMo(u):sMo(l)=',F10.4,':',F10.4,':',F10.4)
  109 FORMAT(25X,'-',F8.3)
  110 FORMAT (1X,'A=',F5.2,' B=',F4.2//)
  111 FORMAT (1X,'C=',F5.2,' D=',F4.2//)
C
      STOP
      END
```

1C

MAXENT-FF1

```
C
C  This program computes the single frequency
C  data points, the total no. of events/year Nt +/- sigma, and the
C  average magnitude <m> +/- sigma.
C
C  Sigma is the Standard error in the mean.
C
C   Input streams
C
C  1 : Risk catalogue
C
C
C  Output streams
C
C  2 : <m>, Nt data
C 12 : Cumulative frequency data
C
C  Ian Main January 1983
C
      DIMENSION IYR(5000),VAR(5000),X(199),Y(199),XC(199),YC(199)
      DATA RAD/57.29577951/,RT/650.0/,RMT/10./,ETA/0.00001/
C
C Set up options; initialise variables
C
      CALL FPRMPT('Lat limits:',11)
      READ(5,*)RLAT1,RLAT2
      CALL FPRMPT('Lon limits:',11)
      READ(5,*)RLON1,RLON2
      CALL FPRMPT('Time limits:',12)
      READ(5,*)MINT,MAXT
      CALL FPRMPT('Min mag:',8)
      READ(5,*)RMAG1,RMAGMAX
      CALL FPRMPT('Var option:',11)
      READ(5,*)IVAR
      RLATM=RLAT1+(RLAT2-RLAT1)/2.
      RLONM=RLON1+(RLON2-RLON1)/2.
      NYR=MAXT-MINT+1
C
C  change unit time to 1yrs.
C
      RKA=FLOAT(NYR)/1.
C
C Read in magnitudes; assign to VAR the correct variable
C
      RMAG2=RMAG1
      NO=0
   10 READ(1)IYEAR,RLAT,RLON,IDEPTH,RMAG
      IF(IYEAR.EQ.0)GO TO 17
      IF(IYEAR.LT.MINT.OR.IYEAR.GT.MAXT)GO TO 10
      IF(RMAG.LT.RMAG1)GO TO 10
      IF(RMAG.GT.RMAGMAX) GO TO 10
```

```
      IF(RLON.GT.RLON2.OR.RLON.LT.RLON1)GO TO 10
      IF(RLAT.GT.RLAT2.OR.RLAT.LT.RLAT1)GO TO 10
      NO=NO+1
      IF(IVAR.EQ.4)GO TO 14
      GO TO (11,12,13),IVAR
C Acceleration
   11 V=2164.*EXP(EM*0.7)*(R+20.)**(-1.80)
      GO TO 15
C Velocity
   12 V=0.726*10.**(0.52*EM)*(R**(-1.34))
      GO TO 15
C Displacement
   13 V=0.0471*10.**(EM*0.57)*(R**(-1.18))
      GO TO 15
C Magnitude
   14 V=RMAG
      VAR(NO)=V
      IYR(NO)=IYEAR
      IF(V.GT.RMAG2) GOTO 16
   15 GOTO 10
   16 RMAG2=VAR(NO)
      GOTO 10
C
C   Count the no. of magnitudes
C
   17 M1=IFIX(RMAG1*10.0+0.05+ETA)
      M2=IFIX(RMAG2*10.0 +ETA)
      NPTS=M2-M1+1
   19 DO 20 I=1,NPTS
      Y(I)=(RMAG2-FLOAT(I)/10.0)+0.1
   20 X(I)=0.0
      DO 21 I=1,NO
      J=IFIX((RMAG2-VAR(I)+ETA)*10.0)+1
   21 X(J)=X(J)+1.0
C
C  Add up cumulative frequencies
C  and normalise to unit time
C
      J=1
      XC(1)=X(1)
      YC(1)=Y(1)
      DO 22 I=2,NPTS
      IF(X(I).LE.ETA) GOTO 22
      J=J+1
      XC(J)=X(I)+XC(J-1)
      YC(J)=Y(I)
   22 CONTINUE
      DO 23 I=1,J
   23 XC(I)=XC(I)/RKA
      DO 24 I=1,NPTS
   24 X(I)=X(I)/RKA
C
C Output 12
C
      WRITE (12,1) J
    1 FORMAT(70X,I4)
      WRITE (12,2) (XC(I),YC(I),I=1,J)
    2 FORMAT (1X,9X14.6)
      WRITE(12,1) NPTS
      WRITE(12,2) (X(I),Y(I),I=1,NPTS)
C
C  Optional adjustment of large events (m>RMT)
C  where there is geological evidence
C  for recurrence rates
C
      DO 26 I=1,NPTS
      IF(Y(I).LT.RMT) GOTO 26
      X(I)=X(I)*FLOAT(NYR)/RT
   25 CONTINUE
      RNT1=FLOAT(NO)/RKA
C
C  evaluate <m> and Nt with standard errors
C
      CALL SIGNT(IYR,NYR,NO,RNT,SIGRNT)
      IF(RNT.GT.RNT1+ETA.OR.RNT.LT.RNT1-ETA) WRITE (6,27)
   27 FORMAT( ' ERROR IN NT  ')
      CALL SIGMA(VAR,NO,AVMAG,SIGMAG)
C
C  Print results
C
      WRITE (6,99) NO
   99 FORMAT(1X,'Total no. of events : ',I4/)
      WRITE (6,100) RMAG1,AVMAG,SIGMAG
  100 FORMAT (1X,'Min mag:',F5.2,' Ave mag:',F6.3,' sigma:',F6.3)
      WRITE (6,101) RNT,SIGRNT
  101 FORMAT(/1X,'Nt:',F8.4,' sigma=',F8.4,' per yr')
      WRITE (2,*)RMAG1,RMAGMAX,AVMAG,SIGMAG,RNT,SIGRNT
      STOP
      END
C
      SUBROUTINE SIGNT(IYR,NYR,NO,RNT,SIGRNT)
C
      DIMENSION SUM(200),NSUM(200),WRK(200),IYR(5000)
      DO 1 I=1,NYR
    1 SUM(I)=0.
      J=1
      NSUM(1)=1
C
      DO 10 I=2,NO
      IF(IYR(I).NE.IYR(I-1)) GOTO 2
      SUM(J)=SUM(J)+1.
      NSUM(J)=I
      GOTO 10
    2 J=J+1
   10 CONTINUE
      WRK(1)=NSUM(1)
```

```
      DO 20 J=2,NYR
   20 WRK(J)=NSUM(J)-NSUM(J-1)
      CALL SIGMA(WRK,NYR,RNT,SIGRNT)
      RETURN
      END
C
      SUBROUTINE SIGMA (X,N,XBAR,SX)
C
      DIMENSION X(5000)
      XSUM=0.
      DO 1 I=1,N
    1 XSUM=XSUM+X(I)
      XBAR=XSUM/N
C
      SUMD=0.
      DO 2 I=1,N
      DEV=(X(I)-XBAR)**2
    2 SUMD=SUMD+DEV
      SX=SUMD/N/(N-1)
      SX=SQRT(SX)
      RETURN
      END
C
      SUBROUTINE ERR1(RM,SM,RN,SN,SMO)
C
      E1=SM/RM
      E2=SN/RN
      E3=E1**2+E2**2
      SMO=RM*SQRT(E3)
      RETURN
      END
```

1D

MAXENT-FF2

```
C
C  This program evaluates l1 and 12 from starting
C   parameters of mmin,mmax,<m>,<Mo> for the distribution
C
C   p(m)=exp(-l1 m-12Mo(m))
C
C   where Mo(m)=10**(A+Bm)
C
C
C  Input streams:
C
C  2 : magnitude data from maxent-ff1
C  3 : moment data from maxent-dat
C
C  Output streams:
C
C  4 : l1,12,Z
C  6 : Output viewing file
C
C  Ian Main July 1983
C
      REAL*8 Z
      READ (2,*) RMIN,RMAX,RMBAR,SIGMA,RNT
      SIG=SIGMA/10.
      READ (3,*) A,B,RMOBAR,SIGMOBAR,POWER,C1,C2
      SIGMO=SIGMOBAR/(10.*RNT)
C
C  Set initial values of l1 and12
C   Set A to the same units as <Mo>
C
C
      A=A-POWER
      RL=.5*ALOG(10.)
      RL2=0.
      RMOBAR1=RMOBAR/RNT
C
C   Iterate 20 times
C
      WRITE (6,11)
   11 FORMAT(7X,'<m>',8X,'<Mo>',10X,'Z',10X,'b',12X,'L2'/)
      DO 100 I=1,20
      CALL INTEGRATE(RMIN,RMAX,A,B,RL,RL2,Z,RMO,RM)
      RL1=RL/ALOG(10.)
      RMOB1=RMO*RNT
      WRITE(6,150) RM,RMOB1,Z,RL1,RL2
  150 FORMAT(1X,5F12.8)
      RATM=RM/RMBAR
      RATMO=RMO/RMOBAR1
      DELTAM=RM-RMBAR
      DELTAMO=RMO-RMOBAR1
      DEL=DELTAMO/RMO
      DRATMO=ABS(RATMO-1.)
```

```
      IF(ABS(DELTAM).LT.SIG.AND.ABS(DELTAMO).LT.SIGMO) GOTO 200
      IF (ABS(DELTAM).LT.SIG) GOTO 2
    1 RL=RL*(1.+C1*DELTAM)
      GOTO 100
    2 RL2=RL2+C2*DELTAMO
  100 CONTINUE
      WRITE (6,20)
   20 FORMAT(/1X,'Iteration unsuccessful to required accuracy')
      GOTO 300
C
  200 WRITE (6,30) RL1,RL,RL2
   30 FORMAT(/1X,'The answer is b=',F12.6,
     ' l1=',F12.6,' l2=',F12.6)
      WRITE (6,15)
   15 FORMAT(/,38(,'.')
      WRITE (6,12) RMIN,RMBAR,SIGMA,RMAX,RMOBAR,SIGMOBAR
      IPOW=IFIX(POWER+0.001)
      WRITE (6,16)
   16 FORMAT(/1X,'.')
      WRITE(6,14) IPOW
   14 FORMAT(1X,'Mo in units of 10**',I2,' dyn cm yr(-1)')
      A=A+POWER
      WRITE (6,13) A,B,RNT
   12 FORMAT (1X,' mo=',F4.2,' <m>=',F5.3,'+/-',F5.3,
     ' mmax=',F4.2,' Mo=',F5.3,'+/-',F5.3)
   13 FORMAT(/1X,'A=',F6.2,' B=',F6.2,' Nt=',F6.2)
      WRITE (4,*) RL,RL2,Z
  300 CONTINUE
      STOP
      END
C
      SUBROUTINE INTEGRATE (RMIN,RMAX,A,B,RL,RL2,F1,RMO,RM)
C
      REAL*8 X(101),Y1(101)
      REAL*8 Y2(101),Y3(101)
      REAL*8 F1,F2,F3,E1,E2,E3,RMOM
C
      ETA=0.001
      DO 5 J=1,100
      X(J)=RMIN+FLOAT(J-1)*(RMAX-RMIN)/100.
      RMOM=10.0**(A+B*X(J))
      Y1(J)=EXP(-RL*X(J)-RL2*RMOM)
      Y2(J)=X(J)*Y1(J)
    5 Y3(J)=RMOM*Y1(J)
C
      CALL DOIGAF(X,Y1,100,F1,E1,0)
      CALL DOIGAF(X,Y2,100,F2,E2,0)
      CALL DOIGAF(X,Y3,100,F3,E3,0)
      RM=F2/F1
      RMO=F3/F1
      IF(E1/F1.LT.ETA) GOTO 6
      WRITE (6,20)
   20 FORMAT( 1X,'ERROR IN Z > .1%')
    6 IF (E2/F2.LT.ETA) GOTO 7
      WRITE (6,60)
   60 FORMAT ( 1X,'ERROR IN <M> > .1%')
    7 IF(E3/F3.LT.ETA)GOTO 400
      WRITE (6,40)
   40 FORMAT(/1X,'Error in Mo integration > .1%')
  400 CONTINUE
      RETURN
      END
```

1E

MAXENT-FF3

```
C
C  This program evaluates the covariance error
C  in l1 and l2
C
C  Input streams:
C
C   2 : data file from maxent-ff1 (magnitude info)
C   3 : data file for moment info
C   4 : l1,l2,Z
C
C  Output streams:
C
C  6 : output viewing file
C  7 : covariance error
C
C   Ian Main November 1983
C
      REAL*16 A(5,5),B(5),C(5)
      READ (2,*) RMIN,RMAX,RMBAR,SIGM,RNT
      READ (3,*) A1,B1,RMOBAR,SIGMO,POWER
      SIGMO=SIGMO/RNT
      READ (4,*)RL1,RL2,Z
      A1=A1-POWER
      CALL EXPECTATIONS(RL1,RL2,RMIN,RMAX,A1,B1,EXM,EXM2,
     EXMO,EXMO2,EXMOM)
      P=EXM**2-EXM2
      Q=EXM*EXMO-EXMOM
      R=EXMO**2-EXMO2
C
C  Set up array A(3,3)
C
      A(3,1)=P**2
      A(3,2)=Q**2
      A(3,3)=2*P*Q
      A(2,1)=Q**2
      A(2,2)=R**2
      A(2,3)=2*R*Q
      A(1,1)=P*Q
      A(1,2)=Q*R
      A(1,3)=P*R+Q*Q
C
C  Set up array B(3)
C
      B(3)=SIGM**2
      B(2)=SIGMO**2
      B(1)=0.
      WRITE (6,9)
    9 FORMAT(/,' Matrix coefficients:'/)
      DO 4 I=1,3
    4 WRITE (6,10) ((A(I,J),J=1,3),B(I))
   10 FORMAT (/,4F11.7)
C
```

```
C  Solve for covariance array C(3)
C
      CALL SOLVE(A,B,C)
      WRITE (6,11) (C(I),I=1,3)
   11 FORMAT (//,' Covariance error: s11,s12,s112',//,3F11.7)
      WRITE(7,*) (C(I),I=1,3)
      STOP
      END
C
      SUBROUTINE EXPECTATIONS(RL1,RL2,RMIN,RMAX,A,B,EXM,
     _EXM2,EXMO,EXMO2,EXMOM)
C
      REAL*8 X(101),Y1(101),Y2(101),Y3(101)
      REAL*8 Y4(101),Y5(101),Y6(101)
      REAL*8 F1,F2,F3,F4,F5,F6
      REAL*8 E1,E2,E3,E4,E5,E6
      DO 5 J=1,100
      X(J)=RMIN+FLOAT(J)*(RMAX-RMIN)/100.
      RMOM=10.**(A+B*X(J))
      Y1(J)=EXP(-RL1*X(J)-RL2*RMOM)
      Y2(J)=X(J)*Y1(J)
      Y3(J)=X(J)*Y2(J)
      Y4(J)=RMOM*Y1(J)
      Y5(J)=RMOM*Y4(J)
    5 Y6(J)=RMOM*Y2(J)
C

      CALL DOIGAF(X,Y1,100,F1,E1,0)
      CALL DOIGAF(X,Y2,100,F2,E2,0)
      CALL DOIGAF(X,Y3,100,F3,E3,0)
      CALL DOIGAF(X,Y4,100,F4,E4,0)
      CALL DOIGAF(X,Y5,100,F5,E5,0)
      CALL DOIGAF(X,Y6,100,F6,E6,0)
C
      Z=F1
      EXM=F2/Z
      EXM2=F3/Z
      EXMO=F4/Z
      EXMO2=F5/Z
      EXMOM=F6/Z
      RETURN
      END
C
      SUBROUTINE SOLVE(A,B,C)
C
      REAL*16 A(5,5),B(5),C(5)
      A(1,4)=B(1)
      A(2,4)=B(2)
      A(3,4)=B(3)
C
C  ZERO 1ST COLUMN
C
      C1=A(1,1)/A(2,1)
      C2=A(1,1)/A(3,1)
      A(2,1)=0.
      A(2,2)=A(2,2)*C1-A(1,2)
      A(2,3)=A(2,3)*C1-A(1,3)
      A(2,4)=A(2,4)*C1-A(1,4)
      A(3,1)=0.
      A(3,2)=A(3,2)*C2-A(1,2)
      A(3,3)=A(3,3)*C2-A(1,3)
      A(3,4)=A(3,4)*C2-A(1,4)
      WRITE (6,9)
    9 FORMAT(/,' Zero first column:'//)
      DO 1 I=1,3
    1 WRITE(6,10) (A(I,J),J=1,4)
   10 FORMAT(/,4F11.7)
C
C  SECOND COLUMN
C
      C3=A(2,2)/A(3,2)
      A(3,2)=0.
      A(3,3)=A(3,3)*C3-A(2,3)
      A(3,4)=A(3,4)*C3-A(2,4)
      WRITE (6,8)
    8 FORMAT (/,' Zero second column',//)
      DO 2 I=1,3
    2 WRITE(6,10) (A(I,J),J=1,4)
C
C  SOLVE FOR C BY BACK SUBSTITUTION
C
      C(3)=A(3,4)/A(3,3)
      C(2)=(A(2,4)-A(2,3)*C(3))/A(2,2)
      C(1)=(A(1,4)-A(1,3)*C(3)-A(1,2)*C(2))/A(1,1)
      RETURN
      END
```

1F

MAXENT-FF4

```
C
C   Magnitudes associated with given
C   return Periods for the frequency distribution
C   F(m)=Sn(m)dm where n(m)=Nt.exp(-RL1*m-RL2*Mo)/Z
C
C
C   Input streams:
C
C   2 : magnitude range and <m>
C   3 : A,B and <Mo>
C   4 : RL1,RL2,Z
C   7 : SL1,SL2,SL12
C
C
C  Output streams:
C
C    6 : All parameters + m(T)
C
C   Ian Main February 1984
C
      SIGA=0.2*ALOG(10.)
      SIGW=0.3
      READ (2,*) RMIN,RMAX,RMBAR,SIGMA,RNT,SIGRNT
      READ (3,*) A,B,RMOBAR,SIGMOBAR,POWER
      READ (4,*) RL1,RL2,Z
      READ (7,*) SL1,SL2,SL12
C
      S1=SQRT(SL1)
      S2=SQRT(SL2)
      BV=RL1/ALOG(10.)
      SBV=S1/ALOG(10.)
      IP=IFIX(POWER+0.001)
      WRITE (6,100)
100   FORMAT(/,' Information theory distribution parameters:')
      WRITE (6,101) RMIN,RMAX,SIGW
101   FORMAT(/,' mmin=',F6.3,' w=',F6.3,' (',F6.3,')')
      WRITE (6,102) RMBAR,SIGMA
102   FORMAT(/,' <m>=',F6.3,'(',F6.3,')',)
      WRITE (6,103)RMOBAR,SIGMOBAR,IP
103   FORMAT(' .',/,' Mo=',F6.3,'(',F6.3') *10**',I2,' dyn.cm/yr')
      SIGA=SIGA/ALOG(10.)
      WRITE (6,104)RNT,SIGRNT,A,SIGA,B
104   FORMAT(/,' NT=',F6.3,'(',F6.3,') /yr A=',F6.3,' (',F6.3,')
       B=',F6.3)
      WRITE (6,105)
105   FORMAT(/,'**********************************')
      WRITE (6,106) RL1,S1,RL2,S2,IP,BV,SBV
106   FORMAT(/,' l1=',F6.3,' (',F6.3,')  :l2=',F6.3,
      ' (',F6.3,')*10**(-',I2,')/dyn.cm',
     -/, ' b=', F6.3,'(',F6.3,')',)
      WRITE (6,107) SL1,SL2,SL12
107   FORMAT(/,' The covariance terms are : ',3F9.5)
```

```
      SIGMOBAR=SIGMOBAR/RNT
      RMOBAR=RMOBAR/RNT
      A=A-POWER
      WRITE (6,10)
   10 FORMAT (/,' Magnitudes associated with ave. rpt. times T',
     _//,'  T in yrs    m(T)  sigma(m)')
C
      DO 1 I=1,8
      IF (I.EQ.1) T=1.
      IF (I.EQ.2) T=2.
      IF (I.EQ.3) T=5.
      IF (I.EQ.4) T=10.
      IF (I.EQ.5) T=20.
      IF (I.EQ.6) T=50.
      IF (I.EQ.7) T=100.
      IF (I.EQ.8) T=200.
C
      RN=1./T
      P=RN/RNT
      CALL SOLVE(P,RL1,RL2,Z,RMIN,RMAX,A,B,RMAG)
C
C  (SOLVES FOR M AS A FN. OF P)
C
      CALL ERROR (SL1,SL2,SL12,RL1,RL2,Z,A,B,RMBAR,RMOBAR,RMAG,SIG)
      RMOX=10.**(A+B*RMAG)
      DENS=EXP(-RL1*RMAG-RL2*RMOX)/Z
      CALL ERRW ( RMAX,A,B,Z,RL1,RL2,SIGW,SW)
      CALL ERRNA(T,P,DENS,SIGRNT,RL1,RL2,RMOX,SIGA,SIGNA)
      SIG=SQRT(SIG**2+SIGNA**2+SW**2)
C
C  (SOLVES FOR SIGMA(M)
C
      WRITE (6,108) T,RMAG,SIG
108   FORMAT(1X,F6.1,3X,F6.3,2X'(',F6.3,')')
1     CONTINUE
      STOP
      END
C
      SUBROUTINE INTEGRATE (Z1,Z2,RL1,RL2,A,B,RNMDM)
C
      REAL*8 X(101),Y(101),Y1(101),Y2(101)
      REAL*8 F,F1,F2,E,E1,E2
C
      DO 5 I=1,100
      X(I)=Z1+FLOAT(I-1)*(Z2-Z1)/100.
      RMO=10.0**(A+B*X(I))
    5 Y(I)=EXP(-RL1*X(I)-RL2*RMO)
      CALL DQ1GAF(X,Y,100,F,E,0)
      IF (E/F.GT.0.01) WRITE (6,40)
   40 FORMAT (1X,'Error in integration in INTEGRATE >1%')
      RNMDM=F
      RETURN
      END
C
      SUBROUTINE SOLVE(P,RL1,RL2,Z,RMIN,RMAX,A,B,RM)
C
      ETA=0.001
      RL=RMIN
      RR=RMAX-0.001
      TL=ROOT(P,RL1,RL2,Z,A,B,RL,RMAX)
      TR=ROOT(P,RL1,RL2,Z,A,B,RR,RMAX)
   10 RM=RL+(RR-RL)/2.
      IF((RR-RL).LT.ETA) GOTO 99
      TEM=ROOT(P,RL1,RL2,Z,A,B,RM,RMAX)
      IF (TEM*TR.GT.0.) GOTO 20
      RL=RM
      TL=TEM
      GOTO 10
   20 RR=RM
      TR=TEM
      GOTO 10
   99 CONTINUE
      RETURN
      END
C
      FUNCTION ROOT(P,RL1,RL2,Z,A,B,R,RMAX)
C
      CALL INTEGRATE(R,RMAX,RL1,RL2,A,B,PROB)
      PROB=PROB/Z
      ROOT=PROB-P
      RETURN
      END
C
      SUBROUTINE ERROR (SL1,SL2,SL12,RL1,RL2,Z,A,B,RMB,RMOB,RM,SIG)
C
      RMO=10.**(A+B*RM)
      DMDL1=(RMB-RM)/RL1
      DMDL2=(RMOB-RMO)/RL1
      ER1=SL1*DMDL1**2
      ER2=SL2*DMDL2**2
      ER3=SL12*DMDL1*DMDL2
      SIG=SQRT(ER1+ER2+2.*ER3)
      RETURN
      END
C
      SUBROUTINE ERRNA(T,P,D,SNT,RL1,RL2,RMO,SA,SNA)
C
      DMDNT=T*P*P/D
      DMDA=RL2*RMO*(1+D)/RL1
      E1=DMDNT*SNT
      E2=DMDA*SA
      SNA=SQRT(E1**2+E2**2)
      RETURN
      END
C
      SUBROUTINE ERRW(W,A,B,Z,RL1,RL2,SIGW,SW)
```

```
C
      RMOW=10.**(A+B*W)
      PW=EXP(-RL1*W-RL2*RMOW)/Z
      DMDW=PW/RL1
      SW=DMDW*SIGW
      RETURN
      END
```

1G

MAXENT-FF5

```
C
C  This program gives long-term predictions T+dT
C  of the average repeat times of magnitudes
C  larger than or equal to M.
C
C  The error is expressed as a fn. of sigma(N(m>m).
C
C  Input streams:
C
C  2 : data on <m> from maxent-ff1
C  3 : data on Mo from maxent-dat
C  4 : l1,l2,Z
C  7 : covariance error matrix
C
C  Output stream:
C
C  6 : T+dt
C
C  Ian Main 07:03:84
C
      SIGW=0.3
      SIGA=0.2*ALOG(10.)
C
C  Read in input data
C
      READ (2,*) RMIN,RMAX,RMBAR,SIGRM,RNT,SIGRNT
      READ (3,*) A,B,RMOBAR,SIGMOBAR,POWER
      READ (4,*) RL1,RL2,Z
      READ (7,*) SL1,SL2,SL12
      CALL FPRMPT ( ' Magnitude :',12)
      READ (5,*) X
      RMOBAR=RMOBAR/RNT
      A=A-POWER
      CALL INTEGRATE (X,RMAX,RL1,RL2,A,B,RN,RM,RMO)
      RN=RN*RNT/Z
      RM=RM/Z
      RMO=RMO/Z
      CALL ERROR(SL1,SL2,SL12,RL1,RL2,RMBAR,RMOBAR,X,
     _RN,RNT,RM,RMO,SIGRNT,SIGA,RMAX,SIGW,A,B,Z,ERN)
      T=1./RN
      RNP=RN+ERN
      TM=1./RNP
      RNM=RN*RN/RNP
      TP=1./RNM
      WRITE (6,1) T,TM,TP
    1 FORMAT (1X, ' The average repeat time is',F8.3,
     _/,' The range considering errors is from',F8.3,' to',F8.3,' yrs')
      STOP
      END
C
      SUBROUTINE INTEGRATE (Z1,Z2,RL1,RL2,A,B,RN,RM,RMO)
C
```

```
      REAL*8 X1(101),YO(101),Y1(101),Y2(101)
      REAL*8 F,E,F1,F2,E1,E2
C
      DO 5 I=1,100
      X1(I)=Z1+FLOAT(I-1)*(Z2-Z1)/100.
      RMOX=10.0**(A+B*X1(I))
      YO(I)=EXP(-RL1*X1(I)-RL2*RMOX)
      Y1(I)=X1(I)*YO(I)
    5 Y2(I)=RMOX*YO(I)
      CALL DO1GAF(X1,YO,100,F,E,0)
      CALL DO1GAF(X1,Y1,100,F1,E1,0)
      CALL DO1GAF(X1,Y2,100,F2,E2,0)
      IF (E/F.LT.0.001) GOTO 400
  399 WRITE (6,40)
   40 FORMAT (1X,'Error in integration >.1%')
      STOP
  400 CONTINUE
      IF(E1/F1.GT.0.001) GOTO 399
      IF (E2/F2.GT.0.001) GOTO 399
      RN=F
      RM=F1
      RMO=F2
      RETURN
      END
C
      SUBROUTINE ERROR(SL1,SL2,SL12,RL1,RL2,RMB,RMOB,X,
     _RN,RNT,RM,RMO,SIGRNT,SIGA,W,SIGW,A,B,Z,ERN)
C
C
      DNDL1=RMB*RN-RM*RNT
      DNDL2=RMOB*RN-RMO*RNT
      RMOW=10.**(A+B*W)
      PW=EXP(-RL1*W-RL2*RMOW)/Z
      DNDW=PW*(RNT-RN)
      DNDA=RL2*DNDL2
      DNDNT=RN/RNT
C
      E1=SL1*DNDL1**2
      E2=SL2*DNDL2**2
      E3=2.*SL12*DNDL1*DNDL2
      E4=(SIGA*DNDA)**2
      E5=(SIGRNT*DNDNT)**2
      E6=(SIGW*DNDW)**2
C
      ERN=E1+E2+E3+E4+E5+E6
      ERN=SQRT(ERN)
      RETURN
      END
C
```

1H

MAXENT-G

```
C
C  Plotting program for the cumulative frequency distribution
C  computed in maxent-ff2 ,with optional Weibull
C  plot for comparison.
C
C  The error is expressed as sigma(N(m>m).
C
C  Input streams:
C
C  2 : data on <m> from maxent-ff1
C  3 : data on Mo from maxent-dat
C  4 : l1,l2,Z from maxent-ff2
C  7 : covariance error matrix from maxent-ff3
C 11 : w,u,lambda from gwul (Weibull option) from maxent-ff7
C 12 : cumulative frequency data from maxent-ff1
C
C  Output stream:
C
C 70 : graph file
C
C  Options are:-
C
C   1 : Cum + Single freq.
C   2 : Cum
C   3 : Single
C   4 : Single + Weibull plot
C
C  Ian Main 25:10:83
C
      DIMENSION RMAG(50),RMAGF(50)
      DIMENSION CF(50),CFG(50),F(50)
      DATA RT/163/,DRT/27/,RMN/7.94/,DRM/0.05/
      SIGW=0.35
      SIGA=0.2
      SIGA=SIGA*ALOG(10.)
      DATA RMF/8.04/,DRMF/0.15/,ETA/0.0001/
      DELTAM=0.1
C
C  Read in cum. frequency data and Gumbel parameters
C
      READ (2,*) RMIN,RMAX,RMBAR,SIGMA,RNT,SIGRNT
      READ (3,*) A,B,RMOBAR,SIGMOBAR,POWER,C1,C2,IOPT
      READ (4,*) RL1,RL2,Z
      READ (7,*) SL1,SL2,SL12
      RMOBAR=RMOBAR/RNT
      A=A-POWER
      IF (IOPT.NE.4) GOTO 500
      READ(11,501)W,U,RL
  501 FORMAT(/,1X,3E14.6)
  500 READ (12,1) RLAT,RLONG,DUM1,DUM2,DUM3,NPTS
      READ(12,2)(CF(I),RMAG(I),I=1,NPTS)
      READ(12,1) D1,D2,D3,D4,D5,NINCS
```

```
      READ(12,2) (F(I),RMAGF(I),I=1,NINCS)
    1 FORMAT(5E14.6,I4)
    2 FORMAT(1X,9E14.6)
      DO 8 I=1,NPTS
    8 CF(I)=ALOG10(CF(I))
      XST=4.
      XSC=1.
      YST=-3.
      YSC=1.
      CALL PLOTS('Ian Main ,Murchseis.',20,70)
C
C  Compute Gumbel distribution points
C
      IF (IOPT.NE.4) GOTO 3
      RK=1./RL
      C3=(W-U)**RK
      DO 6 I=1,NINCS
      C1=(W-RMAGF(I)+DELTAM/2.)**RK
      C2=(W-RMAGF(I)-DELTAM/2.)**RK
      CFG(I)=(C1-C2)/C3
    6 CFG(I)=ALOG10(CFG(I))
      CFG(NINCS+1)=YST
      CFG(NINCS+2)=YSC
      RMAGF(NINCS+1)=XST
      RMAGF(NINCS+2)=XSC
    3 CONTINUE
C
C  Plot graphs
C
      CALL FACTOR(0.7)
      CALL PLOT(1.,1.,-3)
      CALL AXIS(0.,0.,'Magnitude Mw',-12,5.0,0.0,XST,XSC)
      CALL AXIS(0.,0.,'log(N(M))',9,5.,90.,YST,YSC)
      CALL PLOT(5.,0.,+3)
      CALL PLOT(5.,5.,+2)
      CALL PLOT(0.,5.,+2)
C*      CALL SYMBOL(1.25,3.75,0.1,'b=0.89',0.0,6)
C*      CALL SYMBOL(1.5,2.,0.1,'b=0.51',0.0,6)
C*      CALL SYMBOL(2.75,1.,0.1,'(I)',0.0,3)
C*      CALL SYMBOL(4.1,1.,0.1,'(L)',0.,3)
      RMAG(NPTS+1)=XST
      RMAG(NPTS+2)=XSC
      CF(NPTS+1)=YST
      CF(NPTS+2)=YSC
C
C  Cumulative frequency option
C
      IF (IOPT.EQ.3.OR.IOPT.EQ.4) GOTO 9
      CALL LINE(RMAG,CF,NPTS,1,-1,240)
      SIGN=0.
      XR=XST+5.*XSC
      RMOMIN=10.**(A+B*RMIN)
      PMIN=EXP(-RL1*RMIN-RL2*RMOMIN)/Z
      DO 7 N=1,3
      IPEN=3
      DO 10 I=1,50
      X=FLOAT(I)/10.0+RMIN-0.1
C
C     X is m and Y is log10(CF(m))
C
      IF(X.GE.RMAX-0.1) GOTO 100
      CALL INTEGRATE (X,RMAX,RL1,RL2,A,B,RN,RM,RMO)
      RN=RN*RNT/Z
      RM=RM/Z
      RMO=RMO/Z
      CALL ERROR(SL1,SL2,SL12,RL1,RL2,PMIN,RMBAR,RMOBAR,X,
     _RN,RNT,RM,RMO,SIGRNT,Z,A,B,SIGA,RMAX,SIGW,ERN)
      Y=ALOG10(RN)
      YP=ALOG10(RN+ERN)
      YM=2.*Y-YP
      IF(N.EQ.2) Y=YP
      IF(N.EQ.3) Y=YM
      IF(Y.LE.YST) GOTO 100
      IF(X.LT.XST-0.3.OR.X.GT.XR) GOTO 100
      X=(X-XST)/XSC
      Y=(Y-YST)/YSC
      CALL PLOT(X,Y,IPEN)
   10 IPEN=2
C
  100 CONTINUE
    7 CONTINUE
C
C  Plot geologically derived frequencies for largest events
C
C*      CALL GEOLPLOT(RMN,DRM,RT,DRT,XST,XSC,YST,YSC)
      IF (IOPT.EQ.2) GOTO 14
    9 RT=RT*3.
C*      CALL GEOLS(RMF,DRMF,RT,XST,XSC,YST,YSC)
C
C  Set up and plot frequency data
C
      IPEN=3
      X=(RMAGF(1)+0.05-XST)/XSC
      CALL PLOT(X,0.,IPEN)
      IPEN=2
C
      DO 11 J=1,50
      IF (J.GT.NINCS) GOTO 12
      X=RMAGF(1)+0.05-FLOAT(J-1)/10.
      XM=X-DELTAM
      Y=F(J)
      IF(Y.LE.ETA) Y=10.**YST
      Y=ALOG10(Y)
      X=(X-XST)/XSC
      XM=(XM-XST)/XSC
      Y=(Y-YST)/YSC
```

```
      CALL PLOT(X,Y,IPEN)
   11 CALL PLOT(XM,Y,IPEN)
   12 CALL PLOT(XM,0.,IPEN)
      IPEN=3
C
C  Compute and plot theoretical frequencies
C
      DO 13 J=1,50
      X1=RMIN-0.05+FLOAT(J-1)*(RMAX-RMIN)/50.
      X2=X1+DELTAM
      IF(X2.GE.RMAX) GOTO 14
      X=(X1+X2)/2.
      CALL INTEGRATE(X1,X2,RL1,RL2,A,B,RN,RM,RMO)
      RN=RN*RNT/(Z*10.*DELTAM)
      Y=ALOG10(RN)
      IF(Y.LT.YST) GOTO 14
      X=(X-XST)/XSC
      Y=(Y-YST)/YSC
      CALL PLOT(X,Y,IPEN)
   13 IPEN=2
   14 IF (IOPT.EQ.4) CALL LINE(RMAGF,CFG,NINCS,1,-1,154)
      CALL PLOT(0.,0.,999)
      STOP
      END
C
      SUBROUTINE GEOLPLOT(RM,DRM,RT,DRT,XST,XSC,YST,YSC)
      RMPLUS=RM+DRM
      RMMIN=RM-DRM
      RTPLUS=RT+DRT
      RTMIN=RT-DRT
      RTPLUS=ALOG10(1./RTPLUS)
      RTMIN=ALOG10(1./RTMIN)
C
      X1=(RMPLUS-XST)/XSC
      X2=(RMMIN-XST)/XSC
      Y1=(RTPLUS-YST)/YSC
      Y2=(RTMIN-YST)/YSC
      CALL PLOT (X1,Y1,3)
      CALL PLOT (X1,Y2,2)
      CALL PLOT (X2,Y2,2)
      CALL PLOT (X2,Y1,2)
      CALL PLOT (X1,Y1,2)
C
      RTY=ALOG10(1./RT)
      XM=(RM-XST)/XSC
      YM=(RTY-YST)/YSC
      CALL PLOT (XM,Y1,3)
      CALL PLOT (XM,Y2,2)
      CALL PLOT (X1,YM,3)
      CALL PLOT (X2,YM,2)
C
      RETURN
      END
C
      SUBROUTINE INTEGRATE (Z1,Z2,RL1,RL2,A,B,RN,RM,RMO)
C
      REAL*8 X1(101),YO(101),Y1(101),Y2(101)
      REAL*8 F,E,F1,F2,E1,E2
C
      DO 5 I=1,100
      X1(I)=Z1+FLOAT(I-1)*(Z2-Z1)/100.
      RMOX=10.0**(A+B*X1(I))
      YO(I)=EXP(-RL1*X1(I)-RL2*RMOX)
      Y1(I)=X1(I)*YO(I)
    5 Y2(I)=RMOX*YO(I)
      CALL D01GAF(X1,YO,100,F,E,0)
      CALL D01GAF(X1,Y1,100,F1,E1,0)
      CALL D01GAF(X1,Y2,100,F2,E2,0)
      IF (E/F.LT.0.001) GOTO 400
  399 WRITE (6,40)
   40 FORMAT (1X,'Error in integration >.1%')
      STOP
  400 CONTINUE
      IF(E1/F1.GT.0.001) GOTO 399
      IF (E2/F2.GT.0.001) GOTO 399
      RN=F
      RM=F1
      RMO=F2
      RETURN
      END
C
      SUBROUTINE ERROR(SL1,SL2,SL12,RL1,RL2,PMIN,RMB,RMOB,X,
     _RN,RNT,RM,RMO,SIGRNT,Z,A,B,SIGA,W,SIGW,ERN)
C
C
      DNDL1=RMB*RN-RM*RNT
      DNDL2=RMOB*RN-RMO*RNT
      DNDA=RL2*DNDL2
      DNDNT=RN/RNT
      RMOW=10.**(A+B*W)
      PW=EXP(-RL1*W-RL2*RMOW)/Z
      DNDW=PW*(RNT-RN)
C
      E1=SL1*DNDL1**2
      E2=SL2*DNDL2**2
      E3=2.*SL12*DNDL1*DNDL2
      E4=(SIGA*DNDA)**2
      E5=(SIGRNT*DNDNT)**2
      E6=(SIGW*DNDW)**2
C
      ERN=E1+E2+E3+E4+E5+E6
      ERN=SQRT(ERN)
      RETURN
      END
C
      SUBROUTINE GEOLS(RMF,DRMF,RT,XST,XSC,YST,YSC)
```

```
C
      X1=RMF-DRMF
      X2=RMF+DRMF
      Y=ALOG10(1./RT)
      Y=(Y-YST)/YSC
      X1=(X1-XST)/XSC
      X2=(X2-XST)/XSC
      CALL PLOT(X1,0.,3)
      CALL PLOT (X1,Y,2)
      CALL PLOT (X2,Y,2)
      CALL PLOT(X2,0.,2)
      RETURN
      END
```

1I

VOL_PREP

```
C
C This program computes the source-station distance R and the
C P wave time window T=(alpha-beta)/R. Ti is read in from
C entries in the VOLNET bulletin as the P wave onset at the ith
C station. A file is output on channel 6 whis is used as a control
C file for Frequency analysis on an LSI computer using programs
C developed by Bob McGonigle of BGS, Edinburgh.
C
C
C streams 1:station file
C         2:event file
C         3:listing of delays
C         5:Input file of P arrival times
C         6:Output listing
C
C  Ian Main Jul 84 (adapted from a preliminary version by Bob McGonigle)
C
      CHARACTER CODE(100)*3,A*11
      DIMENSION SLAT(100),SLON(100),DIST(40,12)
      DIMENSION T(12,4),WIN(12),ST(12),FILE(3)
      DATA ALPHA/6.7/,BETA/4.4/,E/'END'/
      FAC=(1./BETA-1./ALPHA)
      PIMU=3.*3.14159
C read the station list
      READ(1,*)NS
      DO 1 I=1,NS
      READ(1,*)CODE(I),SLAT(I),SLON(I)
    1 CONTINUE
      WRITE(3,*)'Station list'
      WRITE(3,2)(I,CODE(I),SLAT(I),SLON(I),I=1,NS)
    2 FORMAT(1X,I2,':',A3,2F10.4)
      WRITE(3,5)(CODE(I),I=1,NS)
    5 FORMAT(/,1X,' S-P delay times in s',/,'Site  Code',12(2X,A3,1X))
C read epicentre list and find distances
      I=1
   10 READ(2,3,END=99)A,I1,R1,I2,R2
    3 FORMAT(A11,7X,I2,F6.0,2X,I2,F6.0)
      ELAT=I1+R1/60.
      ELON=I2+R2/60.
      DO 11 J=1,NS
      DIST(I,J)=FDIST(ELAT,ELON,SLAT(J),SLON(J))
   11 DIST(I,J)=DIST(I,J)*FAC
      WRITE(3,6)A,(DIST(I,J),J=1,NS)
    6 FORMAT(1X,A11,12F6.1)
      I=I+1
      GO TO 10
C
   99 CONTINUE
C
C Input
C
      DO 300 NEV=1,40
      IF(NEV.EQ.4.OR.NEV.EQ.12) NEV=NEV+1
      IF(NEV.EQ.8) NEV=NEV+1
```

```
      CALL FPRMPT('File:',5)
      READ (5,100) (FILE(I),I=1,3)
  100 FORMAT(3A4)
      CALL FPRMPT('Event no:',9)
      READ (5,101) NEVENT
  101 FORMAT(I2)
      CALL FPRMPT('Time correction:',16)
      READ(5,*)COR
  102 FORMAT(F3.1)
C
      I=1
    7 CALL FPRMPT('Station code:',13)
      READ (5,103) ST(I)
  103 FORMAT(A4)
      IF (ST(I).EQ.E) GOTO 98
      CALL FPRMPT('Time of onset:',14)
      READ (5,*) T(I,2)
      CALL RECOG(ST(I),NCH)
   12 CALL CON(NCH,J)
      W=DIST(NEV,J)
      WIN(I)=W*1.
      I=I+1
      GOTO 7
   98 NSTS=I-1
C
      DO 8 I=1,NSTS
      T(I,2)=T(I,2)-COR
      T(I,3)=T(I,2)
      T(I,1)=T(I,2)-WIN(I)
    8 T(I,4)=T(I,2)+WIN(I)
C
C  Output file
C
      WRITE (6,201) (FILE(I),I=1,3)
  201 FORMAT('FILE ',3A4)
      WRITE (6,202) NEVENT
  202 FORMAT ('TITL EVENT NO ',I2)
      DO 9 I=1,NSTS
      CALL RECOG(ST(I),NCH)
      WRITE(6,203) NCH,T(I,1),T(I,2),T(I,3),T(I,4)
    9 IF(NCH.EQ.2) CALL ADD(NCH,T(I,1),T(I,2),T(I,3),T(I,4))
  203 FORMAT('CHNL ',I4,4F6.2)
  300 CONTINUE
      STOP
      END
C
      SUBROUTINE RECOG(S,N)
C
      DATA CH2/'VSIZ'/,CH3/'VSIN'/,CH4/'VSIE'/,
     * CH5/'VPA '/,CH6/'VFI '/,CH7/'VGL '/,
     * CH8/'VNE '/,CH9/'VSK '/,CH10/'VMA '/,
     * CH11/'VER '/,CH12/'VAG '/
C
      IF(S.EQ.CH2)N=2
      IF(S.EQ.CH3)N=3
      IF(S.EQ.CH4)N=4
      IF(S.EQ.CH5)N=5
      IF(S.EQ.CH6)N=6
      IF(S.EQ.CH7)N=7
      IF(S.EQ.CH8)N=8
      IF(S.EQ.CH9)N=9
      IF(S.EQ.CH10)N=10
      IF(S.EQ.CH11)N=11
      IF(S.EQ.CH12)N=12
      RETURN
      END
C
      FUNCTION FDIST(RLAT1,RLON1,RLAT2,RLON2)
C returns the distance FDIST in kilometers
      REAL*8 GEOCN
C
      GSLAT=GEOCN(DBLE(RLAT1))
      SLON=RLON1
      GELAT=GEOCN(DBLE(RLAT2))
      ELON=RLON2
      CALL AZDIST(GELAT,ELON,GSLAT,SLON,AZ,DIST)
      FDIST=111.1*DIST
C
      RETURN
      END
      SUBROUTINE AZDIST(ELAT,ELON,SLAT,SLON,AZ,DIST)
C                                                                       4
      REAL*8 PI,RTOD,DTOR
      REAL*8 SLA,SLO,ELA,ELO,SLAC,SLAS,SLOC,SLOS,ELAC,ELAS,ELOC,ELOS,
     1AS,BS,CS,DS,ES,GS,HS,SK,AE,BE,CE,DE,EE,GE,HE,EK,
     2CDIST,SDIST,CSDIST,CAZ,SAZ
      DATA PI/3.1415927D0/,RTOD/57.29578D0/,DTOR/0.0174533D0/
C                                                                       6
      ELAT=ELAT+1.0E-5
      ELON=ELON+1.0E-5
      SLA=SLAT*DTOR                                                     7
      SLO=SLON*DTOR                                                     8
      ELA=ELAT*DTOR                                                     9
      ELO=ELON*DTOR                                                     10
C                                                                       11
      SLAC=DCOS(SLA)
      SLAS=DSIN(SLA)
      SLOC=DCOS(SLO)
      SLOS=DSIN(SLO)
C                                                                       16
      ELAC=DCOS(ELA)
      ELAS=DSIN(ELA)
      ELOC=DCOS(ELO)
      ELOS=DSIN(ELO)
C                                                                       21
      AS=SLAC*SLOC
      BS=SLAC*SLOS                                                      23
      CS=SLAS                                                           24
      DS=SLOS                                                           25
      ES=-SLOC                                                          26
      GS=SLAS*SLOC                                                      27
      HS=SLAS*SLOS                                                      28
```

```
      SK=-SLAC                                                          29
C                                                                       30

      AE=ELAC*ELOC                                                      31
      BE=ELAC*ELOS                                                      32
      CE=ELAS                                                           33
      DE=ELOS                                                           34
      EE=-ELOC                                                          35
      GE=ELAS*ELOC                                                      36
      HE=ELAS*ELOS                                                      37
      EK=-ELAC                                                          38
C                                                                       39
      CDIST=AE*AS+BE*BS+CE*CS                                           40
      SDIST=DSQRT(1.0-CDIST*CDIST)
      DIST=RTOD*DATAN2(SDIST,CDIST)
      CSDIST=1./SDIST                                                   43
      SAZ=-(AS*DE+BS*EE)*CSDIST                                         44
      CAZ=-(AS*GE+BS*HE+CS*EK)*CSDIST                                   45
C                                                                       46
      AZ=DATAN2(SAZ,CAZ)
      IF(AZ.LT.0.0)AZ=AZ+2.*PI                                          48
      AZ=AZ*RTOD                                                        49
C                                                                       50
      RETURN                                                            51
      END                                                               52
      FUNCTION GEOCN(ALAT)                                               3
C                                                                        4
      REAL*8 PI,RTOD,DTOR,ALAT,GEOCN,GCON
      DATA PI/3.1415927D0/,RTOD/57.29578D0/,DTOR/0.0174533D0/
C                                                                        6
      GCON=0.9932315D0
      GEOCN=RTOD*DATAN(GCON*(DSIN(ALAT*DTOR)/DCOS(ALAT*DTOR)))           7
      RETURN                                                           8
      END                                                              9
C
C
      SUBROUTINE CON(N,J)
      IF(N.LE.4) J=1
      IF(N.GE.5) J=N-3
      RETURN
      END
C
      SUBROUTINE ADD(N,T1,T2,T3,T4)
      DO 1 I=1,2
      N=N+1
    1 WRITE(6,204) N,T1,T2,T3,T4
  204 FORMAT('CHNL ',I4,4F6.2)
      RETURN
      END
```

1J

VOL_DIST

```
C
C Program to produce distance list from epicentres
C and to calculate seismic moments from LP spectral levels
C using these distances. Other source parameters are then
C calculated using the corner frequency Fc.
C
C streams 1:station file
C         2:event file
C         3:Mo,Fc readings for N events
C         6:listing
C
C  Ian Main Jun 84 (adapted from a preliminary version by Bob McGonigle)
C
      CHARACTER CODE(10)*3,TCODE(12)*3,A*11
      DIMENSION SLAT(40),SLON(40),DEP(40),RMAG(40),DIST(40,10)
      DIMENSION OMEGA(40,12),FC(40,12),RMO1(40,12),R(40,12)
      DIMENSION RMO(12),RA(12)
      DATA RO/0./
      PIMU=3.*3.14159
C read the station list
      READ(1,*)NS
      DO 1 I=1,NS
      READ(1,*)CODE(I),SLAT(I),SLON(I)
    1 CONTINUE
      WRITE(6,*)'Station list'
      WRITE(6,2)(I,CODE(I),SLAT(I),SLON(I),I=1,NS)
    2 FORMAT(1X,I2,':',A3,2F10.4)
      WRITE(6,5)(CODE(I),I=1,NS)
    5 FORMAT(/,'  Epicentral distances',/,'  Site  Code',12(2X,A3,1X))
C read epicentre list and find distances
      I=1
   10 READ(2,3,END=99)A,I1,R1,I2,R2,DEP(I),RMAG(I)
    3 FORMAT(A11,7X,I2,F6.0,2X,I2,F6.0,F7.0,F6.0)
      WRITE (6,3) A,I1,R1,I2,R2,DEP(I),RMAG(I)
      ELAT=I1+R1/60.
      ELON=I2+R2/60.
      DO 11 J=1,NS
   11 DIST(I,J)=FDIST(ELAT,ELON,SLAT(J),SLON(J))
      WRITE(6,6)A,(DIST(I,J),J=1,NS)
    6 FORMAT(1X,A11,12F6.1)
      I=I+1
      GO TO 10
C
   99 NEV=I-1
C Add 2 extra channels for VSI Ns and EW
      CALL DECODE (CODE,TCODE,NS)
      NS=NS+2
      WRITE (6,7)
    7 FORMAT(/,'LP spectral level in micron s ')
      WRITE (6,8) (TCODE(I),I=1,NS)
    8 FORMAT(12(2X,A3))
```

```
      DO 40 I=1,NEV
C read in omega in nm secs
      READ(3,4) (OMEGA(I,J),J=1,NS)
      READ(4,55) (FC(I,J),J=1,NS)
C convert to micron secs
      DO 97 J=1,NS
   97 OMEGA(I,J)=OMEGA(I,J)*0.001
    4 FORMAT(11(F5.2))
   55 FORMAT(11(F4.1))
   40 WRITE (6,4) (OMEGA(I,J),J=1,NS)
      WRITE(6,88)
   88 FORMAT(/,'Fc in Hz.')
      DO 89 I=1,NEV
   89 WRITE(6,4) (FC(I,J),J=1,NS)
      WRITE (6,31)
   31 FORMAT(/,'Mo in Nm*10**12, r in m, sdrop in bars, s in mm'/
     1 ,'(Standard devs are given below in %, N=No of stations)'//
     2'No  ML  Mo       r        Sdrop       s     N',/)
C Remove zeros, calculate parameters and standard devs.
      DO 50 I=1,NEV
      K=0
      DO 30 J=1,NS
      IF (FC(I,J).LT.0.01) GOTO 30
      K=K+1
      CALL JL(J,L)
      CALL CONSTS(DEP(I),CK,C)
      RMO1(I,K)=CK*OMEGA(I,J)*DIST(I,L)
      R(I,K)=C/FC(I,J)
      RMO(K)=RMO1(I,K)
      RA(K)=R(I,K)
   30 CONTINUE
      IF(K.EQ.0) GOTO 50
      CALL SIGMA(RMO,K,RMOBAR,ERMO)
      CALL SIGMA(RA,K,RABAR,ERRA)
      SDROP=(7.*RMOBAR)/(16.*RABAR**3)
      SBAR=RMOBAR/(PIMU*RABAR**2)
C
      ERSDR=ERMO**2+3.*ERRA**3
      ERSBAR=ERMO**2+2.*ERRA**2
      ERSDR=SQRT(ERSDR)
      ERSBAR=SQRT(ERSBAR)
C Scale for output units
C omega read in in micron.s, Fc in Hz
C  Output Mo in 10**12 Nm, r in m, sdrop in bars, s in mm
      SDROP=SDROP*10000000.
      SBAR=SBAR*100000.
C
      WRITE(12,43) RMAG(I),RMOBAR,SDROP,RABAR,SBAR
   43 FORMAT (5F10.4)
      WRITE(6,41) I,RMAG(I),RMOBAR,RABAR,SDROP,SBAR,K
      WRITE(6,42) ERMO,ERRA,ERSDR,ERSBAR
   41 FORMAT(I4,F4.1,3F10.1,F10.2,I4)
   42 FORMAT(8X,4F10.1/)
   50 CONTINUE
      STOP
      END
      FUNCTION FDIST(RLAT1,RLON1,RLAT2,RLON2)
C returns the distance FDIST in kilometers
      REAL*8 GEOCN
C
      GSLAT=GEOCN(DBLE(RLAT1))
      SLON=RLON1
      GELAT=GEOCN(DBLE(RLAT2))
      ELON=RLON2
      CALL AZDIST(GELAT,ELON,GSLAT,SLON,AZ,DIST)
      FDIST=111.1*DIST
C
      RETURN
      END
      SUBROUTINE AZDIST(ELAT,ELON,SLAT,SLON,AZ,DIST)
C                                                                       4
      REAL*8 PI,RTOD,DTOR
      REAL*8 SLA,SLO,ELA,ELO,SLAC,SLAS,SLOC,SLOS,ELAC,ELAS,ELOC,ELOS,
     1AS,BS,CS,DS,ES,GS,HS,SK,AE,BE,CE,DE,EE,GE,HE,EK,
     2CDIST,SDIST,CSDIST,CAZ,SAZ
      DATA PI/3.1415927D0/,RTOD/57.29578D0/,DTOR/0.0174533D0/
C                                                                       6
      ELAT=ELAT+1.0E-5
      ELON=ELON+1.0E-5
      SLA=SLAT*DTOR                                                     7
      SLO=SLON*DTOR                                                     8
      ELA=ELAT*DTOR                                                     9
      ELO=ELON*DTOR                                                     10
C                                                                       11
      SLAC=DCOS(SLA)
      SLAS=DSIN(SLA)
      SLOC=DCOS(SLO)
      SLOS=DSIN(SLO)
C                                                                       16
      ELAC=DCOS(ELA)
      ELAS=DSIN(ELA)
      ELOC=DCOS(ELO)
      ELOS=DSIN(ELO)
C                                                                       21
      AS=SLAC*SLOC
      BS=SLAC*SLOS                                                      23
      CS=SLAS                                                           24
      DS=SLOS                                                           25
      ES=-SLOC                                                          26
      GS=SLAS*SLOC                                                      27
      HS=SLAS*SLOS                                                      28
      SK=-SLAC                                                          29
C                                                                       30
      AE=ELAC*ELOC                                                      31
```

```
      BE=ELAC*ELOS                                                      32
      CE=ELAS                                                           33
      DE=ELOS                                                           34
      EE=-ELOC                                                          35
      GE=ELAS*ELOC                                                      36
      HE=ELAS*ELOS                                                      37
      EK=-ELAC                                                          38
C                                                                       39
      CDIST=AE*AS+BE*BS+CE*CS                                           40
      SDIST=DSQRT(1.0-CDIST*CDIST)
      DIST=RTOD*DATAN2(SDIST,CDIST)
      CSDIST=1./SDIST                                                   43
      SAZ=-(AS*DE+BS*EE)*CSDIST                                         44
      CAZ=-(AS*GE+BS*HE+CS*EK)*CSDIST                                   45
C                                                                       46
      AZ=DATAN2(SAZ,CAZ)
      IF(AZ.LT.0.0)AZ=AZ+2.*PI                                          48
      AZ=AZ*RTOD                                                        49
C                                                                       50
      RETURN                                                            51
      END                                                               52
      FUNCTION GEOCN(ALAT)                                               3
C                                                                        4
      REAL*8 PI,RTOD,DTOR,ALAT,GEOCN,GCON
      DATA PI/3.1415927D0/,RTOD/57.29578D0/,DTOR/0.0174533D0/
C                                                                        6
      GCON=0.9932315D0
      GEOCN=RTOD*DATAN(GCON*(DSIN(ALAT*DTOR)/DCOS(ALAT*DTOR)))           7
      RETURN                                                             8
      END                                                                9
C
      SUBROUTINE SIGMA (X,N,XBAR,SX)
C
C  RETURNS THE STANDARD DEVIATION AS A PERCENTAGE
C
      DIMENSION D(12),X(12)
      XSUM=0.
      DO 1 I=1,N
    1 XSUM=XSUM+X(I)
      XBAR=XSUM/N
C
      SUMD=0.
      DO 2 I=1,N
      DEV=(X(I)-XBAR)**2
    2 SUMD=SUMD+DEV
      SX=SUMD/N
      SX=SQRT(SX)
      SX=100.*SX/XBAR
      RETURN
      END
C
      SUBROUTINE DECODE(C,TC,NS)
      CHARACTER TC(12)*3,C(10)*3
      DO 1 I=2,NS
      J=I+2
    1 TC(J)=C(I)
      TC(1)=C(1)
      TC(2)=C(1)
      TC(3)=C(1)
      RETURN
      END
C
      SUBROUTINE JL(J,L)
      IF(J.LE.3) L=1
      IF(J.GE.4) L=J-2
      RETURN
      END
C
C
      SUBROUTINE CONSTS(D,CK,C)
C
C   CK=12*10**15 Kg s(-3)
C   C=1427 m s(-1) both for ALPHA=6.7 Km s(-1)
C
      IF (D.GT.24.) CK=12.
      IF (D.GT.24.) C=1427.
      IF(D.LE.24.0.AND.D.GT.1.07) CK=8.618
      IF(D.LE.24.0.AND.D.GT.1.07) C=1278.
      IF(D.LE.1.07) CK=2.554
      IF(D.LE.1.07) C=851.9
      RETURN
      END
```

APPENDIX 2

MATHEMATICAL DERIVATIONS OF SOME TEXT EQUATIONS

Appendix 2A Derivation of equation 3.5

Differentiating equations (3.1) to (3.4) in turn with respect to the probability density we are trying to find - p(m) - gives

$$\frac{\partial S}{\partial p} = -\int_{m_c}^{\omega} \frac{\partial}{\partial p}\{p\,\ell n(p)\}\,dm = -\int_{m_c}^{\omega} \{\ell n\,(p) + 1\}\,dm = 0 \quad , \qquad \text{(i)}$$

$$\frac{\partial(1)}{\partial p} = 0 \quad , \qquad \text{(ii)}$$

$$\frac{\partial \langle m \rangle}{\partial p} = \int_{m_c}^{\omega} m\,dm = 0 \quad , \qquad \text{(iii)}$$

$$\frac{\partial \langle M_o \rangle}{\partial p} = \int_{m_c}^{\omega} M_o(m)\,dm = 0 \quad . \qquad \text{(iv)}$$

$\langle m \rangle$ and $\langle M_o \rangle$ are constant averages, so their derivatives are zero. Similarly we wish to maximise the entropy S so that $\partial S/\partial p = 0$. Thus we can sum all of the quantities together to give a net zero.

$$\delta S = \delta(1) + \delta\langle m \rangle + \delta\langle M_o \rangle = 0 \quad . \qquad \text{(v)}$$

Since all the individual terms equal zero we can introduce the Lagrangian undetermined multipliers λ_0, λ_1 and λ_2 and the sum will still be zero.

$$-\delta S + \lambda_0\,\delta(1) + \lambda_1\,\delta\langle m \rangle + \lambda_2\,\delta\langle M_0 \rangle = 0 \quad , \qquad \text{(vi)}$$

or alternatively

$$\int_{m_c}^{\omega} \{(\ell n\ p + 1)\ \delta p + \lambda_o \delta p + \lambda_1\, m\ \delta p + \lambda_2\, M_o(m)\ \delta p\}\,dm = 0 \quad . \qquad \text{(vii)}$$

This last equation can only hold where the term under the integral is zero for all m, so

$$(\ell n\ p + 1) + \lambda_o + \lambda_1\ m + \lambda_2\ M_o(m) = 0\ , \qquad \text{(viii)}$$

and finally this can be rearranged to give

$$p(m) = \exp\ \{-1 - \lambda_o - \lambda_1\ m - \lambda_2\ M_o(m)\}\ . \qquad \text{(ix)}$$

This is almost the same as equation (3.5) except for the normalising term $Z = \exp\ (1+\lambda_0)$.

Putting this form of p into the normalising equation (3.2) gives

$$\exp\ \{\ -1 - \lambda_o\} \int_{m_c}^{\omega} \exp\ \{-\lambda_1\ m - \lambda_2\ M_o(m)\}\ dm = 1\ , \qquad \text{(x)}$$

so if $Z = \exp\ \{1 + \lambda_0\}$ as in the denominator of equation (3.5) then Z also has the form of equation (3.6) from (x).

Appendix 2B Derivation of equation (3.7)

By differentiating equation (3.3) and (3.4) wrt. λ_1 and λ_2 respectively we have

$$\int_{m_c}^{\omega} m\ \frac{\partial p}{\partial \lambda_1}\ dm = \frac{\partial \langle m \rangle}{\partial \lambda_1}\ , \qquad \text{(i)}$$

$$\int_{m_c}^{\omega} M_o(m)\ \frac{\partial p}{\partial \lambda_1}\ dm = \frac{\partial \langle M_o \rangle}{\partial \lambda_1}\ , \qquad \text{(ii)}$$

with $p = \exp\{-\lambda_1 m - \lambda_2 M_o(m)\}/Z$, (iii)

$$Z = \int_{m_c}^{\omega} \exp\{-\lambda_1 m - \lambda_2 M_o(m)\}\, dm \quad , \tag{iv}$$

as in the text.

Now consider differentiating Z wrt. λ_1 and λ_2.

$$\frac{\partial Z}{\partial \lambda_1} = \int_{m_c}^{\omega} \frac{\partial}{\partial \lambda_1} \{\exp(-\lambda_1 m)\}.\ \exp\{-\lambda_2 M_o(m)\}\ dm$$

$$= \int_{m_c}^{\omega} -m \exp\{-\lambda_1 m - \lambda_2 M_o(m)\}\, dm \quad ,$$

or

$$\frac{\partial Z}{\partial \lambda_1} = -\langle m \rangle Z \quad , \tag{v}$$

after comparison with (3.3), using (iii) and (iv). Similarly

$$\frac{\partial Z}{\partial \lambda_2} = -\langle M_o \rangle Z \ . \tag{vi}$$

Now consider differentiating $\ell n\ Z(\lambda_1, \lambda_2)$ using the chain rule

$$\frac{\partial(\ell n\ Z)}{\partial \lambda_1} = \frac{1}{Z} \frac{\partial Z}{\partial \lambda_1} \tag{vii}$$

$$\frac{\partial(\ell n\ Z)}{\partial \lambda_2} = \frac{1}{Z} \frac{\partial Z}{\partial \lambda_2} \quad , \tag{viii}$$

and using (v) and (vi) gives equation (3.7) directly.

APPENDIX 3

GREEK LITERATURE SEARCH:

REFERENCE LIST

*ANON.,1971.
SEISMIC MICROZONING OF BANJALUKA-SEISMIC MICROZONING MAP OF THE URBAN AREA OF BANJALUKA.
INST.EARTHQ.ENG.ENG.SEISMOL.,UNIV.KIRIL & METODIJ,SKOPJE
WORK NO.S-21/71.

*ANON.,1979.
THE THESSALONIKI EARTHQUAKE.
U.S.GEOL.SURV.,PROF.PAP.1150,P.243

*ANON.,1981.
INTERNATIONAL SYMPOSIUM ON THE HELLENIC ARC AND TRENCH (H.E.A.T.)-ABSTRACTS. ATHENS 1981.

AGARWAL,N.K.,JACOBY,W.R.,BERCKHEMER,H.,1976
TELESEISMIC P-WAVE TRAVELTIME RESIDUALS AND DEEP STRUCTURE OF THE AEGEAN REGION.
TECTONOPHYS.31,33-57.

ALVAREZ,W.,1973.
THE APPLICATION OF PLATE TECTONICS TO THE MEDITERRANEAN REGION.
IMPLICATIONS OF CONTINENTAL DRIFT TO THE EARTH SCIENCES,2.
ACADEMIC PRESS,LONDON,893-908.

AMBRASEYS,N.N.,1967.
THE EARTHQUAKES OF 1965-66 IN THE PELOPONNESUS,GREECE;A FIELD REPORT.
BULL.SEIS.SOC.AMER.VOL.57,NO.5.1025-1046.

AMBRASEYS,N.N.,1981.
ON THE LONG TERM SEISMICITY IN THE HELLENIC ARC.
BOLL.GEOFIS.TEOR.APPL.23,355-359.

AMBRASEYS,N.N.,JACKSON,J.A.,1982.
EARTHQUAKE HAZARD AND VULNERABILITY IN THE NORTHEASTERN MEDITERRANEAN
THE CORINTH EARTHQUAKE SEQUENCE OF FEBRUARY-MARCH 1981.
DISASTERS INTERNATIONAL JOURNAL,5,NO.3.

ANGELIER,J.,LYBERIS,N.,LE PICHON,X.,BARRIER,E.,HUCHON,P.,1982.
THE TECTONIC DEVELOPMENT OF THE HELLENIC ARC AND THE SEA OF CRETE:
A SYNTHESIS.
TECTONOPHYS.86,159-196.

APPLEGATE,J.K.,1982
THE VARIABILITY OF DYNAMICALLY-DETERMINED POISSON'S RATIOS
AND SOME FACTORS THAT MAY AFFECT THE VARIABILITY.

AUBOUIN,J.,STEPHAN,J.,ROUMP,J.,RENARD,V.,1982.
THE MIDDLE AMERICA TRENCH AS AN EXAMPLE OF A SUBDUCTION ZONE.
TECTONOPHYS.86,113-132.

BOGER,H.,1978.
SEDIMENTARY HISTORY AND TECTONIC MOVEMENTS DURING THE LATE NEOGENE.
ALPS,APENNINES,HELLENIDES.(ED.CLOSS ET AL).1978.

BOSSOLASCO,M,EVA,C.,PASQUALE,V.,1973.
ON THE SEISMICITY OF THE LIGURIAN SEA.
BULL.GEOL.SOCGREECE 10,19-22.

BOTT,M.H.P.,1976.
MECHANISMS OF BASIN SUBSIDENCE-AN INTRODUCTORY REVIEW.
TECTONOPHYS.36,1-4.

BOTT,M.H.P.,1976
FORMATION OF SEDIMENTARY BASINS OF GRABEN TYPE BY EXTENSION
OF THE CONTINENTAL CRUST.
TECTONOPHYS.36,77-86

BOTTARI,A.,FEDERICO,B.,1979.
ESTIMATE OF THE FOCAL DEPTH OF DEEP EARTHQUAKES AND SOME
STRUCTURAL IMPLICATIONS FOR THE DEEP SEISMIC ACTIVITY IN THE
TYRRHENIAN REGION.
BSSA.69,NO.4,1193-1208.

BROOKS,M.,FERENTINOS,G.,1980.
STRUCTURE AND EVOLUTION OF THE SPORADHES BASIN OF THE NORTH
AEGEAN TROUGH,NORTHERN AEGEAN SEA.
TECTONOPHYS.68,15-30.

BUFE,C.G.,MALEY,R.P.,YERKES,R.F.,CARVER,D.L.,1978.
THE MAY-JULY 1978 EARTHQUAKE SEQUENCE NEAR THESSALONIKI,GREECE.
EOS(AM.GEOPHYS.UNION,TRANS.)59,12,1127.

BUTTNER,D.,KOWALCZYK,G.,1978.
LATE CENOZOIC STRATIGRAPHY AND PALEOGEOGRAPHY OF GREECE-A REVIEW.
ALPS,APENNINES;HELLENIDES.(ED.CLOSS ET AL).1978.

CAGNETTI,V.,PASQUALE,V.,POLINARI,S.,1978.
FAULT-PLANE SOLUTIONS AND STRESS REGIME IN ITALY AND ADJACENT REGIONS
TECTONOPHYS.46,239-250.

CARVER,D.,HENRISEY,R.,1978.
PRELIMINARY REPORT ON THE AFTERSHOCKS OF THE JUNE 20,1978,
THESSALONIKI,GREECE,EARTHQUAKE.
U.S.GEOL.SURV.,OPEN-FILE REP.78-1099,P.11.

CARVER,D.,BOLLINGER,G.A.,1981.
AFTERSHOCKS OF THE JUNE 20,1978,GREECE EARTHQUAKE;A MULTIMODE
FAULTING SEQUENCE.
TECTONOPHYS.73,4,343-363.

CARYDIS,P.G.,SBOKOS,J.G.,1976
EVALUATION OF GREEK STRONG MOTION RECORDS.
PROC.INT.SYMPOSIUM EARTHQ.STRUCT.ENG.,
ST.LOUIS,MISSOURI,1976,1079-1093.

CELAL SENGOR,A.M.,CANITEZ,N.,1982.
THE NORTH ANATOLIAN FAULT.
ALP.-MED.GEOD.,GEOD.SER.VOL.7.1982.205-216.

COMNINAKIS,P.E.,PAPAZACHOS,B.C.,1976.
A NOTE ON THE CRUSTAL STRUCTURE STRUCTURE OF EASTERN MEDITERRANEAN.
ANNALI.GEOFIS.29,59-63.

COMNINAKIS,P.E.,PAPAZACHOS,B.C.,1980.
SPACE AND TIME DISTRIBUTION OF THE INTERMEDIATE FOCAL DEPTH EARTHQUAKES IN THE HELLENIC ARC.
TECTONOPHYS.70,3-4,T33-T42.

CONSTANTINESCU,L.,RUPRECHTOVA,L.,ENESCU,D.,1966.
MEDITERRANEAN-ALPINE EARTHQUAKE MECHANISMS AND THEIR SEISMOTECTONIC IMPLICATIONS.
GEOPHYS.J.R.ASTR.SOC.10,347-368.

CRAMPIN,S.,1975.
SEISMIC NOISE MEASUREMENTS IN YUGOSLAVIA AND GREECE;A SURVEY PRIOR TO STATION INSTALLATION.
SEISMOLOGICAL BULLETIN NO.3,I.G.S.,LONDON.

DELIBASIS,N.,DRAKOPOULOS,J.C.,1974.
FOCAL MECHANISM OF EARTHQUAKES IN THE NORTH AEGEAN SEA,1965-1968 AND RELATED PROBLEMS.(13TH ESC ASSEMBLY,BRASOV,1972).
STUDII.TEH.ECON.INST.GEOL.ROM.D.,NO.10,149-167.

DELIBASIS,N.,CARYDIS,P.,1977.
RECENT EARTHQUAKE ACTIVITY IN TRICHONIS REGION AND ITS TECTONIC SIGNIFICANCE.
ANNALI.GEOFIS.30,19-81.

DELIBASIS,N.D.,1982.
SEISMIC WAVE ATTENUATION IN THE UPPER MANTLE BENEATH THE AEGEAN REGION
PURE APPL.GEOPHYS.120/4,820-839.

DEL PEZZO,E.,LUONGO,G.,SCARPA,R.,1979.
SEISMIC WAVE TRANSMISSION IN SOUTHERN TYRRHENIAN SEA.
BOLL.GEOFIS.TEOR.APPL.21,81,53-66.

DERMITZAKIS,M.D.,1973.
RECENT TECTONIC MOVEMENTS AND OLD STRANDLINES ALONG THE COASTS OF CRETE.
BULL.GEOL.SOC.GREECE 10,48-64.

DEWEY,J.F.,SENGOR,A.M.,1979.
AEGEAN AND SURROUNDING REGIONS.COMPLEX MULTIPLATE AND CONTINUUM TECTONICS IN A CONVERGENT ZONE.
GEOL.SOC.AM.BULL.90,84-92.

DRAKOPOULOS,J.C.,1971.
A STATISTICAL MODEL ON THE OCCURRENCE OF AFTERSHOCKS IN THE AREA OF GREECE.
INT.INST.SEISMOL.EARTHQUAKE ENG.,BULL.8,17-39.

DRAKOPOULOS,J.,1973.
GENERAL CONSIDERATIONS ABOUT A MICROZONING STUDY AND THESSALONIKI (GREECE)AS A SITE FOR SUCH A STUDY.
PAGEOPH.104,495-506.

DRAKOPOULOS,J.C.,ROUSSOPOULOS,A.A.,1973.
ANALYSIS OF STRONG MOTION RECORDS OF THE CEPHALORIAN SHOCK OCCURRING ON SEPTEMBER 17,1972 AND OF ITS LARGER AFTERSHOCK.
ANNALI.GEOFIS.26,613-635.

DRAKOPOULOS,J.C.,DELIBASIS,N.,1974.
ON THE MECHANISMS OF SOME EARTHQUAKES IN THE AREA OF WESTERN GREECE AND THE STRESS PRODUCING THEM.(13TH ESC.ASSEMBLY,BRASOV,1972)
STUDII.TEH.ECON.INST.GEOL.ROM.D.,NO.10,169-192.

DRAKOPOULOS,J.C.,1976.
ON SEISMIC ZONING IN THE MAJOR AREA OF GREECE WITH EMPHASIS IN THE AEGEAN REGION.
SOC.GEOL.FR.BULL.18,2,P354.

DRAKOPOULOS,J.C.,1976.
ON THE COMPLETENESS OF MACROSEISMIC DATA (A) IN THE MAJOR AREA OF GREECE (B) IN THE BALKAN AREA.
PROCEEDINGS OF THE SEMINAR ON SEISMIC ZONING MAPS,SKOPJE 27 OCT.-4 NOV.1975,UNESCO,SKOPJE 1976.PP 132-155

DRAKOPOULOS,J.C.,1976.
ON THE SEISMIC ZONING PROBLEMS IN GREECE.
PROCEEDINGS OF THE SEMINAR ON SEISMIC ZONING MAPS,SKOPJE 27 OCT.-4 NOV.1975,UNESCO,SKOPJE 1976.PP 300-335.

DRAKOPOULOS,J.C.,1978.
ATTENUATION OF INTENSITIES WITH DISTANCE FOR SHALLOW EARTHQUAKES IN THE AREA OF GREECE.
BOLL.GEOFIS.TEOR.APPL.20,114-130.

DRAKOPOULOS,J.C.,1978
STATISTICAL SIGNIFICANCE TESTS OF THE DIFFERENCE BETWEEN THE B-VALUES FOR GROUPS OF SHOCKS THAT OCCURRED ON AND AROUND EUBOEA ISLAND(GREECE).
REVUE ROUM.GEOL.GEOPHYS.GEOGR.SER.GEOPHYS.22,25-32.

DRAKOPOULOS,J.,LEVENTAKIS,G.,ROUSSOPOULOS,A.,1978.
MICROZONATION IN THE SEISMIC AREA OF CORINTH-LOUTRAKI.
ANNALI.GEOFIS.31,1,51-93.

FINETTI,I.,1976.
MEDITERRANEAN RIDGE;A YOUNG SUBMERGED CHAIN ASSOCIATED WITH THE HELLENIC ARC.
BOLL.GEOFIS.TEOR.APPL.19,31-65.

FITCH T.J.,MUIRHEAD,K.J.,1974.
DEPTHS TO LARGER EARTHQUAKES ASSOCIATED WITH CRUSTAL LOADING.
GEOPHYS.J.R.ASTR.SOC.37,2,285-296.

FRISCH,W.,1978.
A PLATE TECTONICS MODEL OF THE EASTERN ALPS.
ALPS,APENNINES,HELLENIDES.(ED.CLOSS ET AL).1978.

GALANOPOULOS,A.G.,1955.
SEISMIC GEOGRAPHY OF GREECE.
ANN.GEOL.PAYS HELL.6,81-121.

GALANOPOULOS,A.G.,1960.
A CATALOGUE OF SHOCKS WITH IO>=VI OR M>=5 FOR THE YEARS 1801-1958.
ATHENS UNIVERSITY-EXTRACT FROM CATALOGUE.

GALANOPOULOS,A.G.,1961.
A CATALOGUE OF SHOCKS WITH IO>=VII FOR THE YEARS PRIOR TO 1800.
ATHENS UNIVERSITY.

GALANOPOULOS,A.G.,1963.
ON MAPPING OF SEISMIC ACTIVITY IN GREECE.
ANNALI.GEOFIS.16,37-100.

GALANOPOULOS,A.G.,1967.
THE SEISMOTECTONIC REGIME IN GREECE.
ANNALI.GEOFIS.20,109-119.

GALANOPOULOS,A.G.,1968.
ON QUANTITATIVE DETERMINATION OF EARTHQUAKE RISK.
ANNALI.GEOFIS.21,193-206.

GALANOPOULOS,A.G.,1971.
MINIMUM AND MAXIMUM MAGNITUDE THRESHOLD IN THE AREA OF ATTICA,GREECE.
ANNALI.GEOFIS.24,29-54.

GALANOPOULOS,A.G.,1972.
ANNUAL AND MAXIMUM POSSIBLE STRAIN ACCUMULATION IN THE MAJOR AREA OF GREECE.
ANNLS.GEOL.PAYS.HELL.24,467-480.

GALANOPOULOS,A.G.,1972.
PLATE TECTONICS IN THE AREA OF GREECE AS REFLECTED IN THE DEEP FOCUS SEISMICITY.
BULL.GEOL.SOC.GREECE,9,266-285.

GALANOPOULOS,A.G.,1973.
PLATE TECTONICS IN THE AREA OF GREECE AS REFLECTED IN THE DEEP FOCUS SEISMICITY
BULL.GEOL.SOC.GREECE 10,67-69.

GALANOPOULOS,A.G.,1973.
ON THE DIFFERENCE OF THE STRESS FIELD IN THE TWO CENTRES OF HIGHER EARTHQUAKE ACTIVITY IN THE AREA OF GREECE.
ANNLS.GEOL.PAYS.HELL.25,350-372.

GALANOPOULOS,A.G.,EKONOMIDES,A,1973.
RAPID DIAPIR GROWTH A TRIGGERING AGENT OF A 6.5 MAGNITUDE EARTHQUAKE ON OCTOBER 29 1966 IN AKARNANIA,GREECE.
ANNALI.GEOFIS.26,605-612.

GALANOPOULOS,A.G.,1974.
ON THE TECTONIC PROCESSES ALONG THE HELLENIC ARC.
ANNALI.GEOFIS.27,429-442.

GALANOPOULOS,A.G.,1975.
A NEW MODEL ACCOUNTING FOR THE INTERMEDIATE EARTHQUAKES ON THE CONVEX SIDE OF THE HELLENIC ARC.
ANNLS.GEOL.PAYS.HELL.27,355-370.

GALANOPOULOS,A.,1976.
DATA REQUIRED FOR THE ESTIMATION OF THE MAXIMUM FEASIBLE EARTHQUAKE.
ANN.GEOL.PAYS.HELL.28,465-470.

GALANOPOULOS,A.G.,1979.
GREECE:NATIONAL REPORTS ON SEISMOLOGY 1975-1978.
ATHENS UNIVERSITY.

GERTIG,H.,1973.
FOCAL MECHANISMS AND TECTONICS IN THE AREA OF THE IONIAN ISLANDS KEFALLINIA AND ZAKYNTHOS.
BULL.GEOL.SOC.GREECE 10,1,72.

GIESE,P.,REUTTER,K.-J.,JACOBSHAGEN,V.,NICOLICH,R.,1982.
EXPLOSION SEISMIC CRUSTAL STUDIES IN THE ALPINE MEDITERRANEAN REGION AND THEIR IMPLICATIONS TO TECTONIC PROCESSES.
ALP.-MED.GEOD. GEOD.SER.VOL.7.,1982.39-73.

GREGERSEN,S.,1977.
P-WAVE TRAVEL TIME RESIDUALS CAUSED BY A DIPPING PLATE IN THE AEGEAN ARC IN GREECE.
TECTONOPHYS.37,83-93.

GURPINAR,A.,1981.
IMPORTANCE OF FIELD OBSERVATIONS ON SEISMIC SAFETY OF NUCLEAR POWER PLANTS:TWO RECENT CASE HISTORIES IRPINIA (ITALY) 1980 AND CORINTH (GREECE) 1981.
D´APPOLONIA,S.A.,BRUSSELS,BELGIUM.

HABERMANN,R.E.,1980
PRECURSORY SEISMICITY PATTERNS:STALKING THE MATURE SEISMIC GAP.
EARTHQUAKE PREDICTION:AN INTERNATIONAL REVIEW.
AM.GEOPHYS.UNION,WASHINGTON DC,USA.

HEDERVARI,P.,1979.
THE RELATIONSHIP BETWEEN TECTONIC EARTHQUAKES AND VOLCANIC ERUPTIONS WITH PARTICULAR REFERENCE TO SANTORINI(AEGEAN SEA) AND INDONESIA.
GEOLOGIE MIJNB.58,213-224.

HINZ,K.,1973.
THE RESULTS OF REFRACTION AND REFLECTION SEISMIC SURVEYS OF THE F.S. METEOR IN THE IONIAN SEA.
BULL.GEOL.SOC.GREECE 10,203.

HUCHON,P.,LYBERIS,N.,ANGELIER,J.,LE PICHON,X.,RENARD,V.,1982.
TECTONICS OF THE HELLENIC TRENCH:A SYNTHESIS OF SEA-BEAM AND SUBMERSIBLE OBSERVATIONS.
TECTONOPHYS.86,69-112.

IOSIF,T.,IOSIF,S.,CUCU,G,1979
ERRORS OF THE EARTHQUAKE PARAMETERS DETERMINATION FOR A GIVEN BALKAN NETWORK.
REV.ROUM.GEOL.GEOPHYS.GEOGR.SER.GEOPHYS.23,59-62.

JACKSON,J.A.,GAGNEPAIN,J,HOUSEMAN,G.,KING,G.C.P.,PAPADIMITRIOU,P., SOUFLERIS,C.,VIRIEUX,J.,1982.
SEISMICITY,NORMAL FAULTING,AND THE GEOMORPHOLOGICAL DEVELOPMENT OF THE GULF OF CORINTH(GREECE);THE CORINTH EARTHQUAKES OF FEBRUARY AND MARCH 1981
EARTH.PLAN.SCI.LETTERS 57,1982.

JACOBSHAGEN,V.,KOPP,K.-O.,MARKIS,J.,1978.
INVESTIGATIONS IN THE AEGEAN REGION:AN INTRODUCTION.
ALPS,APENNINES,HELLENIDES.(ED.CLOSS ET AL).1978.

JACOBSHAGEN,V.,SKALA,W.,WALLBRECHER,E.,1978.
ALPINE STRUCTURE AND DEVELOPMENT OF THE SOUTHERN PELION
PENINSULA AND THE NORTH SPORADES.
ALPS,APENNINES,HELLENIDES.(ED.CLOSS ET AL).1978.

JACOBSHAGEN,V.,ST.DURR,KOCKEL,F.,KOPP,K.-O.,KOWALCZYK,G.,
(CONTRIBUTIONS FROM BERCKHEMER,H.,& BUTTNER,D.).1978.
STRUCTURE AND GEODYNAMIC EVOLUTION OF THE AEGEAN REGION.
ALPS,APENNINES,HELLENIDES.(ED.CLOSS ET AL).1978.

JACOBY,W.R.,AGARWAL,N.K.,BERCKHEMER,H.,1978.
CRUSTAL AND UPPER MANTLE STRUCTURE OF THE AEGEAN ARC FROM TRAVEL
TIME RESIDUALS AND GRAVITY.
ALPS,APENNINES,HELLENIDES-INT.COUNC.SCI.UNIONS,INTER UNION COMM.
GEODYNAMICS SCI.,REP.38,401-406.

JONGSMA,D.,1974
HEAT FLOW IN THE AEGEAN SEA.
GEOPHYS.J.R.ASTR.SOC.37,337-346.

JONGSMA,D.,WISSMAN,G.,HINZ,K.,GARDE,S.C.,1975.
RESULTS OF SEISMIC REFLECTION MEASUREMENTS IN THE SOUTHERN AEGEAN
SEA CRUISES OF FS METEOR AND RRS SHACKLETON.
RAPP.COMMN.INT.MER.MEDIT.23,169-171.

JONGSMA,D.,WISSMANN,G.,HINZ,K.,GARDE,S.,1978.
RESULT OF REFLECTION SEISMIC SURVEYS IN THE SOUTHERN
AEGEAN SEA.
ALPS,APENNINES,HELLENIDES.(ED.CLOSS ET AL).1978.

KARNIK,V,1964.
MAGNITUDE-FREQUENCY RELATION AND SEISMIC ACTIVITY IN DIFFERENT
REGIONS OF THE EUROPEAN AREA.
BULL.INT.INST.SEISM.EARTHQ.ENG.1,9-32.

KARNIK,V.,HUBNEROVA,Z.,1968.
THE PROBABILITY OF OCCURRENCE OF LARGEST EARTHQUAKES IN THE
EUROPEAN AREA.
PAGEOPH.70,61-73.

KARNIK,V.,1969.
SEISMICITY OF THE EUROPEAN AREA PART 1.
'D.REIDEL PUBLISHING COMPANY',DORDRECHT-HOLLAND.
EXTRACT FROM BOOK.

KARNIK,V,1971.
SEISMICITY OF THE EUROPEAN AREA PART 2.
'D.REIDEL PUBLISHING COMPANY',DORDRECHT-HOLLAND.
EXTRACT FROM BOOK.

KARNIK,V.,PROCHAZKOVA,D.,1976.
MAGNITUDE-FREQUENCY RELATIONS FOR THE BALKAN EARTHQUAKE PROVINCES
AND SOME RELATED PROBLEMS.
GEOFYS.SB.24,149-184.

KARNIK,V.,PROCHAZKOVA,D.,SCHENKOVA,Z.,1977.
EARTHQUAKE EPICENTRES AND MACROSEISMIC INTENSITY IN THE CARPATHO-BALKAN REGION.
ACTA.GEOL.(ACAD.SCI.HUNG.)21,4,309-324.

KING,G.C.P.,TSELENTIS,A.,GOMBERG,J.,MOLNAR,P.,1983.
MICROEARTHQUAKE SEISMICITY AND ACTIVE TECTONICS OF NORTHWESTERN GREECE
EARTH PLANET.SCI.LETT.,66,279-288

KOPP,K.-O.,1978.
STRATIGRAPHIC AND TECTONIC SEQUENCE OF CRETE.
ALPS,APENNINES,HELLENIDES.(ED.CLOSS ET AL).1978.

KRONBERG,P.,GUNTHER,R.,1978.
CRUSTAL FRACTURE PATTERN OF THE AEGEAN REGION.
ALPS,APENNINES,HELLENIDES.(ED.CLOSS ET AL).1978.

KULHANEK,O.,MEYER,K.,1979.
SOURCE PARAMETERS OF THE VOLVI-LANGADHAS EARTHQUAKE OF JUNE 20,1978 DEDUCED FROM BODY WAVE SPECTRA AT STATIONS UPPSALA AND KIRUNA.
BSSA.69,NO.4,1289-1294.

LANGER,C.J.,1980.
THESSALONICA,GREECE,EARTHQUAKE OF JUNE 1978.
GEOLOGICAL SURVEY PROFESSIONAL PAPER(WASHINGTON D.C.)1175,264-265.

LEITE,O.,MASCLE,J.,1982.
GEOLOGICAL STRUCTURES ON THE SOUTH CREATAN CONTINENTAL MARGIN AND HELLENIC TRENCH (EASTERN MEDITERRANEAN).
MAR.GEOL. 49/3-4,199-223.

LE PICHON,X.,ANGELIER,J.,1979.
THE HELLENIC ARC AND TRENCH SYSTEM;A KEY TO THE NEOTECTONIC EVOLUTION OF THE EASTERN MEDITERRANEAN AREA.
TECTONOPHYS.60,1-42.

LE PICHON,X.,ANGELIER,J.,AUBOUIN,J.,LYBERIS,N.,MONTI,S.,RENARD,V., GOT,H.,HSU,K.,MART,Y.,MASCLE,J.,MATTHEWS,D.,MITROPOULOS,D.,TSOFLIAS,P CHRONIS,G.,1979.
FROM SUBDUCTION TO TRANSFORMATION MOTION;A SEABEAM SURVEY OF THE HELLENIC TRENCH SYSTEM.
EARTH PLAN.SCI.LETTERS 44,3,441-450.

LE PICHON,X.,LYBERIS,N.,ANGELIER,J.,RENARD,V.,1982.
STRAIN DISTRIBUTION OVER THE EAST MEDITERRANEAN RIDGE:A SYNTHESIS INCORPORATING NEW SEA-BEAM DATA.
TECTONOPHYS.86,243-274.

LEYDECKER,G.,BERCKHEMER,H.,DELIBASIS,N.,1978.
A STUDY OF SEISMICITY IN THE PELOPONNESSUS REGION BY PRECISE HYPOCENTER DETERMINATIONS.
ALPS,APPENNINES,HELLENIDES-INT.COUNC.SCI.UNIONS,INTER-UNION COMM. GEODYNAMICS SCI.,REP 38,406-410.

LOGTERS,G.,VOORT,H.,1974.
IN-SITU DETERMINATION OF THE DEFORMATIONAL BEHAVIOUR OF A CUBICLE ROCK-MASS SAMPLE UNDER TRI-AXIAL LOAD.
ROCK MECH.6,2,65-79.

LORT,J.M.,1971.
THE TECTONICS OF THE EASTERN MEDITERRANEAN;A GEOPHYSICAL REVIEW.
REV.GEOPHYS.SPACE PHYS.9,189-216.

LORT,J.M.,1973.
SUMMARY OF SEISMIC STUDIES IN THE EASTERN MEDITERRANEAN.
BULL.GEOL.SOC.GREECE 10,99-108.

LYBERIS,N.,DESCHAMPS,A.,1982.
A SEISMO-TECTONIC STUDY OF THE NORTH AEGEAN TROUGH:RELATION WITH THE NORTH ANATOLIAN FAULT.
C.R.HEBD.SEANCES.ACAD.SCI.SER.2 PHYS.CHIM.SCI.TERRE.SCI.UNIVERS. 295/5

MAKRIS,J.,1973.
SOME GEOPHYSICAL ASPECTS OF THE EVOLUTION OF THE HELLENIDES.
BULL.GEOL.SOC.GREECE,10,206-213.

MAKRIS,J.,1975.
CRUSTAL STRUCTURE OF THE AEGEAN SEA AND THE HELLENIDES OBTAINED FROM GEOPHYSICAL SURVEYS.
Z.GEOPHYS.41,441-443.

MAKRIS,J.,1976.
A DYNAMIC MODEL OF THE HELLENIC ARC DEDUCED FROM GEOPHYSICAL DATA.
TECTONOPHYS.36,339-346.

MAKRIS,J.,1977.
GEOPHYSICAL INVESTIGATIONS OF THE HELLENIDES.
HAMBURGER GEOPHYS.EINZELSCHR.A,NO.34,1-124.

MAKRIS,J.,1977.
A DYNAMICAL MODEL OF GREECE DEDUCED FROM GEOPHYSICAL DATA.
PUBLS.INST.GEOPHYS.POL.ACAD.SCI.A,NO.4,399-412.

MAKRIS,J.,VEES,R.,1977.
CRUSTAL STRUCTURE OF THE CENTRAL AEGEAN SEA AND THE ISLANDS OF EVIA AND CRETE,GREECE,OBTAINED BY REFRACTIONAL SEISMIC EXPERIMENTS
J.GEOPHYS.42,329-341.

MAKRIS,J.,1978.
SOME GEOPHYSICAL CONSIDERATIONS ON THE GEODYNAMIC SITUATION IN GREECE.
TECTONOPHYS.46,251-268.

MAKRIS,J.,1978.
THE CRUST AND UPPER MANTLE OF THE AEGEAN REGION FROM DEEP SEISMIC SOUNDINGS.
TECTONOPHYS.46,269-284.

MAKRIS,J.,1978.
A GEOPHYSICAL STUDY OF GREECE BASED ON:DEEP SEISMIC SOUNDINGS,GRAVITY, AND MAGNETICS.
ALPS,APENNINES,HELLENIDES.(ED. CLOSS ET AL).1978.

MAKROPOULOS,K.C.,BURTON,P.W.,1981.
A CATALOGUE OF SEISMICITY IN GREECE AND ADJACENT AREAS.
GEOPHYS.J.R.ASTR.SOC.65,741-762.

MASCLE,J.,JONGSMA,D.,CAMPREDON,R.,DERCOURT,J.,GLACON,G.,LECLEACH,A.,
LYBERIS,N.,MALOD,J.A.,MITROPOULOS,D.,1982.
THE HELLENIC MARGIN FROM EASTERN CRETE TO RHODES:PRELIMINARY RESULTS.
TECTONOPHYS.86,133-147.

MCKENZIE,D.P.,1970.
PLATE TECTONICS OF THE MEDITERRANEAN REGION.
NATURE 226,239-243.

MCKENZIE,D.,1972
ACTIVE TECTONICS OF THE MEDITERRANEAN REGION.
GEOPHYS.J.R.ASTR.SOC.30,109-185.

MCKENZIE,D.P.,1978.
ACTIVE TECTONICS OF THE ALPINE-HIMALAYAN BELT;THE AEGEAN SEA AND
SURROUNDING REGIONS.
GEOPHYS.J.R.ASTR.SOC.55,217-254.

MEULENKAMP,J.E.,1982.
ON THE PULSATING EVOLUTION OF THE MEDITERRANEAN.
EPISODES,1982,NO.1.

MORELLI,C.,PISANI,M.,GANTAR,C.,WRIGHT,D.,ET.AL.,1975.
GEOPHYSICAL STUDIES IN THE AEGEAN SEA AND IN THE EASTERN MEDITERRANEAN
BOLL.GEOFIS.TEOR.APPL.18,127-168.

MORELLI,C.,1978.
EASTERN MEDITERRANEAN;GEOPHYSICAL RESULTS AND IMPLICATIONS.
TECTONOPHYS.46,333-346.

NUR,A.,BEN-AVRAHAM,Z.,1978.
THE EASTERN MEDITERRANEAN AND THE LEVANT;TECTONICS OF CONTINENTAL
COLLISION.
TECTONOPHYS.46,297-311.

OZELCI,F.,1978.
A SUGGESTION ON THE POSSIBLE SIGNIFICANCE OF VOLCANIC ACTIVITY IN THE
TECTONIC DEVELOPMENT OF THE EASTERN MEDITERRANEAN REGION.
TECTONOPHYS.46,227-237.

PAPAZACHOS,B.,POLATOU,M,MANDALOS,N.,1967.
DISPERSION OF SURFACE WAVES RECORDED IN ATHENS
PAGEOPH.67,95-106.

PAPAZACHOS,B.C.,1969.
PHASE VELOCITIES OF RAYLEIGH WAVES IN SOUTHEASTERN EUROPE AND
EASTERN MEDITERRANEAN SEA.
PAGEOPH.75,47-55.

PAPAZACHOS,B.C.,DELIBASIS,N.D.,1969.
TECTONIC STRESS FIELD AND SEISMIC FAULTING IN THE AREA OF GREECE.
TECTONOPHYS.7,231-255.

PAPAZACHOS,B.C.,1973.
SEISMIC ACTIVITY IN THE ALPINE-MEDITRRANEAN REGION AND THE TECTONIC
MODELS PROPOSED TO INTERPRETE THIS ACTIVITY
BULL.GEOL.SOC.GREECE 10,165-168.

PAPAZACHOS,B.C.,1973
DISTRIBUTION OF SEISMIC FOCI IN THE MEDITERRANEAN AND ITS TECTONIC IMPLICATION.
GEOPHYS.J.R.ASTR.SOC.33,421-430.

PAPAZACHOS,B.C.,1974.
SEISMOTECTONICS OF THE EASTERN MEDITERRANEAN AREA.
ENGINEER,SEISMOL.AND EARTHQUAKE ENGINEER.,NOORDHOFF LEIDEN, ED.J.S.SOLNES,1-31.

PAPAZACHOS,B.C.,1974.
ON THE TIME DISTRIBUTION OF AFTERSHOCKS AND FORESHOCKS IN THE AREA OF GREECE.
PAGEOPH.112,627-631.

PAPAZACHOS,B.C.,1974
ON CERTAIN AFTERSHOCK AND FORESHOCK PARAMETERS IN THE AREA OF GREECE
ANNALI.GEOFIS.27,497-515.

PAPAZACHOS,B.C.,1975.
FORESHOCKS AND EARTHQUAKE PREDICTION.
TECTONOPHYS.28,4,213-226.

PAPAZACHOS,B.C.,1976.
EVIDENCE OF CRUSTAL SHORTENING IN THE NORTHERN AEGEAN REGION.
BOLL.GEOFIS.TEOR.APPL.19,66-71.

PAPAZACHOS,B.C.,1976.
SEISMOTECTONICS OF THE NORTHERN AEGEAN AREA.
TECTONOPHYS.33,199-209.

PAPAZACHOS,B.C.,COMNINAKIS,P.E.,1976.
MODES OF LITHOSPHERIC INTERACTION IN THE AEGEAN AREA.
SYMP.INTERNAT.ON THE STRUCTURAL HISTORY OF THE MEDITERRANEAN BASINS, SPLIT-YUGOSLAVIA,OCT.1976,319-332.

PAPAZACHOS,B.C.,1977.
A LITHOSPHERIC MODEL TO INTERPRET FOCAL PROPERTIES OF INTERMEDIATE AND SHALLOW SHOCKS IN CENTRAL GREECE.
PAGEOPH.115,655-666.

PAPAZACHOS,B.C.,COMNINAKIS,P.E.,1978
DEEP STRUCTURE AND TECTONICS OF THE EASTERN MEDITERRANEAN.
TECTONOPHYS.46,285-296.

PAPAZACHOS,B.C.,MOUNDRAKIS,D.,PSILOVIKOS,A.,LEVENTAKIS,G.,1978.
FOCAL PROPERTIES OF THE 1978 EARTHQUAKES IN THE THESSALONIKI AREA.
BULG.GEOFIZ.SPIS.6,72-80.

PAPAZACHOS,B.,MOUNTRAKIS,D.,PSILOVIKOS,A.,LEVENTAKIS,G.,1979
SURFACE FAULT TRACES AND FAULT PLANE SOLUTIONS OF THE MAY-JUNE 1978 MAJOR SHOCKS IN THE THESSALONIKI AREA,GREECE.
TECTONOPHYS.53,171-183.

PAPAZACHOS,B.C.,COMNINAKIS,P.E.,1982.
LONG-TERM EARTHQUAKE PREDICTION IN THE HELLENIC TRENCH-ARC SYSTEM.
TECTONOPHYS.86,3-16.

PAQUIN,C.,FROIDEVAUX,C.,BLOGET,J.,RICARD,Y.,ANGELIDIS,C.,1982.
TECTONIC STRESSES ON THE MAINLAND OF GREECE:IN-SITU MEASUREMENTS BY OVERCORING.
TECTONOPHYS.86,17-26.

PERISSORATIS,C.,MITROPOULOS,D.,ANGELOPOULOS,I.,1984.
THE ROLE OF EARTHQUAKES IN INDUCING SEDIMENT MASS MOVEMENTS IN THE EASTERN KORINTHIAKOS GULF.AN EXAMPLE FROM THE FEBRUARY 24-MARCH 4, ACTIVITY.
MAR.GEOL.,55/1-2,35-45

PICHLER,H.,SCHIERING,W.,1977.
THE THERA ERUPTION AND LATE MINOAN-IB DESTRUCTIONS ON CRETE.
NATURE,267,819-822.

PROCHAZKOVA,D.,1973.
MIGRATION OF EARTHQUAKE FOCI IN EUROPE.
PAGEOPH.110,2005-2011.

PSYCHARIS,J.,1978.
THE SALONICA(THESSALONIKI)EARTHQUAKE OF JUNE 20 1978.
EERL-78-03,CALTECH,EER LAB,PASADENA,CALIFORNIA.

PUCHER,R.,BANNERT,D.,FROMM,K.,1978.
PALEOMAGNETISM IN GREECE:INDICATIONS FOR RELATIVE BLOCK MOVEMENT.
ALPS,APENNINES,HELLENIDES.(ED.CLOSS ET AL).1978.

RICHTER,I.,STROBACH,K.,1978.
BENIOFF ZONES OF THE AEGEAN ARC.
ALPS,APENNINES,HELLENIDES.(ED.CLOSS ET AL).1978.

RITSEMA,A.R.,DE BILT,K.N.M.I.,1974.
THE EARTHQUAKE MECHANISMS OF THE BALKAN REGION.
UNESCO,SURVEY OF THE SEISMICITY OF THE BALKAN REGION.UNDP PROJECT REM/

RIZHIKOVA,S.,1974
ATTENUATION OF THE SHORT-PERIOD SURFACE WAVES TRAVELLING ACROSS THE RILA-RHODOPE MASSIF.(13TH ESC ASSEMBLY,BRASOV,1972.)
STUDII.TEH.ECON.INST.GEOL.ROM.D.,NO.10,335-338.

ROEDER,D.,BOGEL,H.,1978.
GEODYNAMIC INTERPRETATION OF THE ALPS.
ALPS,APENNINES,HELLENIDES.(ED.CLOSS ET AL).1978.

ROUSSOPOULOS,A.A.,SYRMAKEZIS,C.A.,1973.
APPLICATION OF THE FINITE ELEMENT METHOD TO A MICROZONATION STUDY OF THE SALONICA REGION.
ANNALI.GEOFIS.26,513-523.

RYAN,W.B.F.,KASTENS,K.A.,CITA,M.B.,1982.
GEOLOGICAL EVIDENCE CONCERNING COMPRESSIONAL TECTONICS IN THE EASTERN MEDITERRANEAN.
TECTONOPHYS.86,213-242.

SCHENKOVA,Z.,KARNIK,V.,1974.
COMPARISON OF METHODS OF DETERMINING LARGEST POSSIBLE EARTHQUAKES.
PHYS.SOLID EARTH(ENGL.ED.)NO.11,765-769.

SCHENKOVA,Z.,KARNIK,V.,1976.
APPLICATION OF THE LARGEST VALUES THEORY TO BALKAN EARTHQUAKES.
PROC.OF THE SEMINAR ON SEISM.ZONING MAPS,
SKOPJE,27 OCT.-4 NOV.1975,1,193.

SCHENKOVA,Z.,KARNIK,V.,1978.
THE THIRD ASYMPTOTIC DISTRIBUTION OF LARGEST MAGNITUDES IN THE BALKAN EARTHQUAKE PROVINCES.
PAGEOPH.116,1314-1325.

SCHICK,R.,1978.
SEISMOTECTONIC SURVEY OF THE CENTRAL MEDITERRANEAN.
ALPS,APENNINES,HELLENIDES.(ED.CLOSS ET AL).1978.

SHERIF,M.A.,BOSTROM,R.C.,ISHIBASHI,I.,1974.
MICROZONATION IN RELATION TO PREDOMINANT GROUND FREQUENCY,
AMPLIFICATION AND OTHER ENGINEERING CONSIDERATIONS.
INT.ASSOC.ENG.GEOL.,INT.CONGR.,PROC.,2,VOL.1,II2.1-II2.11.

SMITH,A.G.,WOODCOCK,N.H.,1982.
TECTONIC SYNTHESES OF THE ALPINE-MEDITERRENEAN REGION:A REVIEW.
ALP.-MED.GEOD. GEOD.SER.VOL.7.1982.15-38.

SPOHN,T.,NEUGEBAUER,H.J.,1978.
ON THE MECHANISM OF SUBSIDENCE OF SEDIMENTARY BASINS ADJACENT TO PASSIVE CONTINENTAL MARGINS.
ALPS,APENNINES,HELLENIDES.(ED.CLOSS ET AL).1978.

STEINWACHS,M.,1979.
STUDIES OF INDUCED SEISMICITY USING A MOBILE RADIOTELEMETRIC SEISMIC ARRAY.
BULL.INT.ASSOC.ENG.GEOL.20,128-131.

STEWART,G.S.,1978.
COMPLEXITY OF RUPTURE PROPAGATION IN LARGE EARTHQUAKES.
EOS (AM.GEOPHYS.UNION,TRANS.)59,12,1127.

THERIANOS,A.D.,1974
THE SEISMIC ACTIVITY OF THE KREMASTA AREA,GREECE,BETWEEN 1967 AND 1972.(INT.COLLOQM.SEISMIC EFFECTS OF RESEVOIR IMPOUNDING,LONDON 1973)
ENGNG.GEOL.8,49-52.

UDIAS,A.,1982.
SEISMICITY AND SEISMOTECTONIC STRESS FIELD IN THE ALPINE-MEDITERRANEAN REGION.
ALP.-MED.GEOD.,GEOD.SER.VOL.7.1982.75-82.

VANEK,J.,CHRISTOSKOV,L.,1971.
AMPLITUDE CURVES OF P AND S WAVES AT SHORT EPICENTRAL DISTANCES.
INT.INST.SEISMOL.EARTHQUAKE ENG.,BULL.,8,161-171.

VOGT,P.R.,HIGGS,R.H.,1969.
AN AEROMAGNETIC SURVEY OF THE EASTERN MEDITERRANEAN SEA AND ITS INTERPRETATION.
EARTH & PLANET.SCI.LETTERS,5,439-448.

VROMAN,A.J.,1978.
ON THE ORIGIN OF THE MEDITERRANEAN AND OTHER MARGINAL SEAS.
TECTONOPHYS.46,219-225.

WEIGEL,W.,1978.
A TECTONIC MODEL OF THE NORTHERN IONIAN SEA FROM REFRACTION SEISMIC DATA.
ALPS,APENNINES,HELLENIDES.(ED.CLOSS ET AL).1978.

WYSS,M.,BAER,M.,1980.
EARTHQUAKE HAZARD IN THE HELLENIC ARC.
EXTRACT-EARTHQUAKE PREDICTION;AN INTERNATIONAL REVIEW.
AM.GEOPHYS.UNION,WASHINGTON,DC,USA.

YERKES,R.F.,BUFE,C.G,MALEY,R.P.,1979.
EARTHQUAKE INVESTIGATIONS.
U.S.GEOL.SURV,PROF.PAP.1150,P.251.

APPENDIX 4

DISPERSION CHARACTERISTICS AND THE GROUP VELOCITY WINDOW

Not all of the seismograms were as easy to interpret as the example given in fig 4.4, where the group velocity windows $4 < U < 2.5$ km s^{-1} proved to be compatible with an obvious influx and decay of long period surface wave energy. Consider, for example, the seismogram at the top of fig 4A.

In this part of the diagram the horizontal scale has been changed from time T to group velocity U by $U = R/T$, where R is the epicentral distance. By eye it is not obvious exactly where the energy in the period range 30-70s comes in.

One way of checking this is to draw the diagram in the lower half of the figure, which plots the signal content as contours in decibels on a two dimensional grid with group velocity on the horizontal axis and frequency on the vertical axis. Again this matrix (called the E-matrix) is drawn by the programme TSAP developed in Burton (1973). Note that the signal has been corrected for the instrument response before drawing the diagram.

It is not easy to pick the surface wave arrival too well here by eye, but a time window can be chosen with reference to a ridge in the contours of the signal content picked out by the dotted line. With the exception of using frequency rather than period, this ridge crest corresponds to the dispersion line drawn on the graph of fig 4B, which can be compared to the dispersion curve for southeastern Europe, fig 4.5 in the main text.

Horizontal lines at 14 mHz and 34 mHz correspond to the period range of interest (30-70s), and the vertical lines at 4 kms^{-1} and 2.95 kms^{-1} adequately cover this dispersion ridge without including spurious effects such as the possibility of noise at lower frequencies in this case.

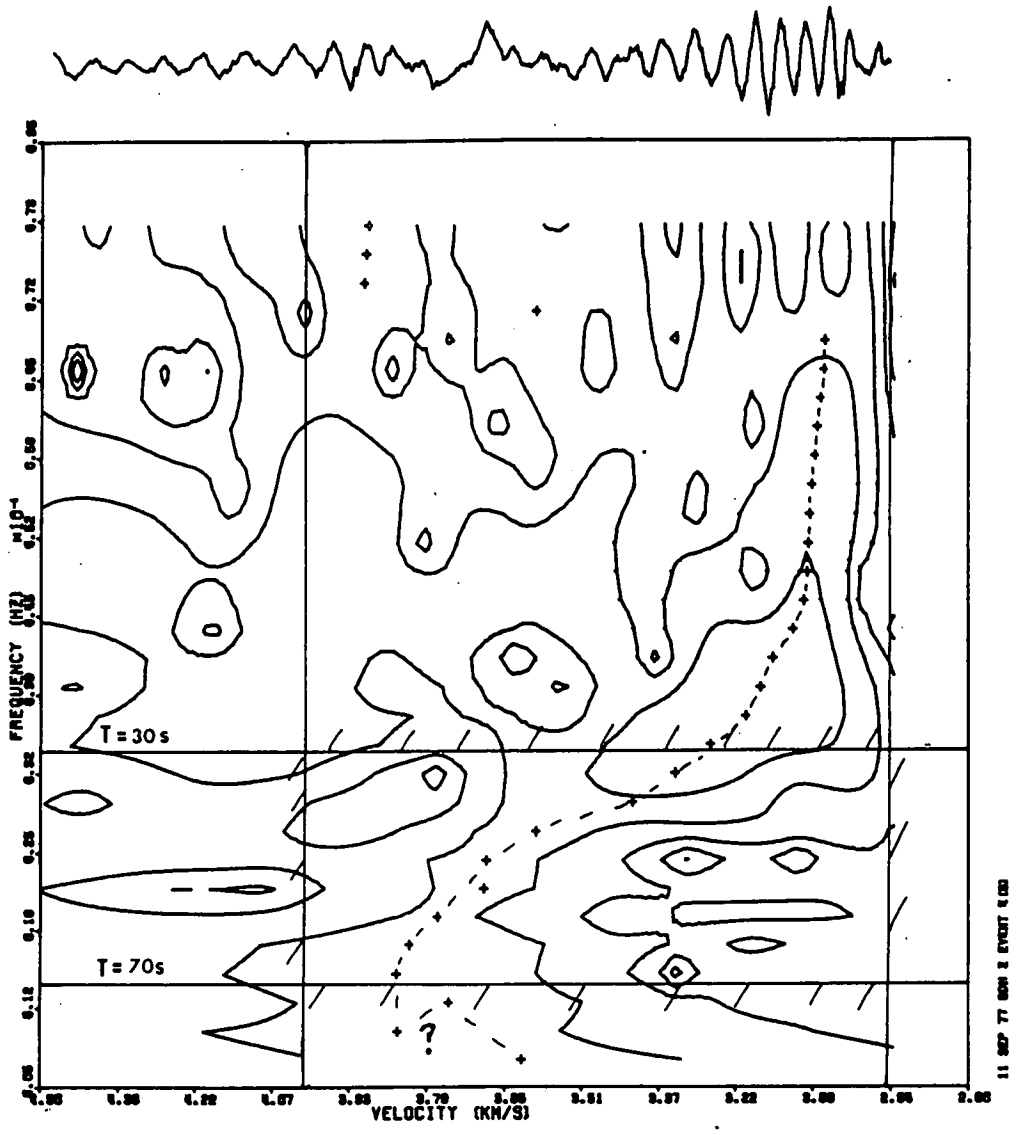

Figure 4A The E matrix for event E, at station GDH (Godhavn, Greenland)

A two dimensional plot of signal content in frequency and velocity space (called the E matrix). The dispersion line is drawn on the crest of a ridge on this contour plot by the dotted line. Because the contours are in decibels nearly all of the signal is close to this ridge. In this case the time window defined by group velocities at 4km s^{-1} and 2.95km s^{-1} adequately cover the periods of interest between 30 and 70s.

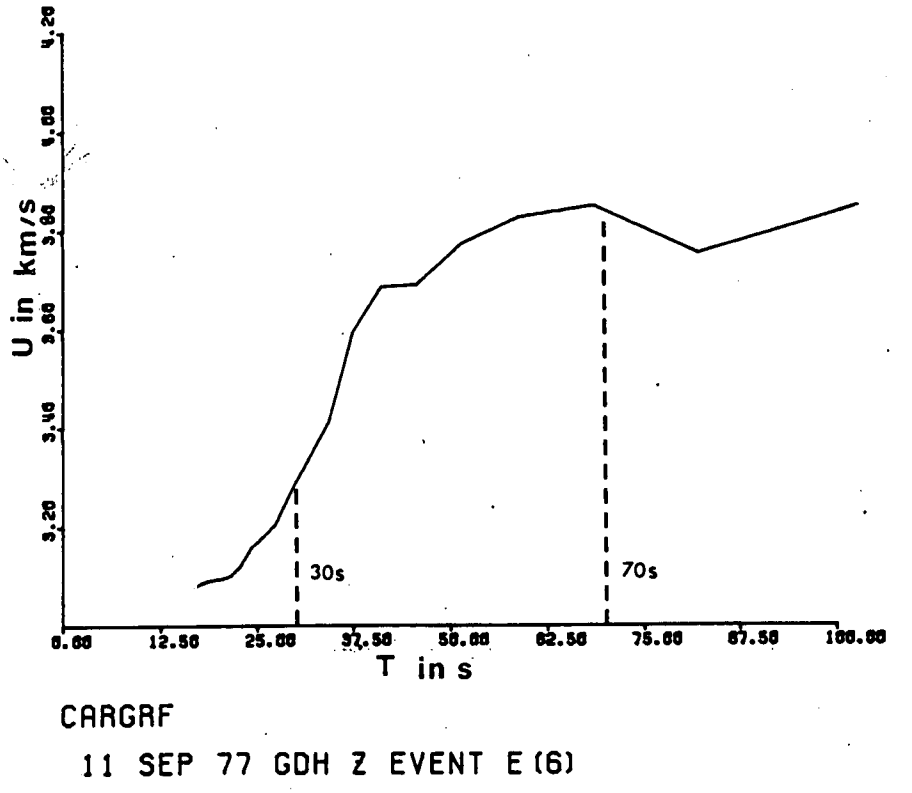

Figure 4B Dispersion characteristics.
This diagram plots the ridge outlined on fig 4A, to allow comparison with a 'typical' dispersion curve such as fig 4.14. The azimuthal path for this recording at southern Greenland is predominantly continental.

Physical links between crustal deformation, seismic moment and seismic hazard for regions of varying seismicity

Ian G. Main and Paul W. Burton

REPRINTED FROM
Geophys. J. R. astr. Soc. (1984) **79:2**, 469–488
PUBLISHED BY
BLACKWELL SCIENTIFIC PUBLICATIONS
OXFORD LONDON EDINBURGH BOSTON PALO ALTO MELBOURNE

Geophys. J. R. astr. Soc. (1984) 79, 469–488

Physical links between crustal deformation, seismic moment and seismic hazard for regions of varying seismicity

Ian G. Main *Natural Environment Research Council, British Geological Survey, Murchison House, West Mains Road, Edinburgh EH9 3LA, and University of Edinburgh, Department of Geophysics, James Clerk Maxwell Building, Mayfield Road, Edinburgh EH9 3JZ, Scotland*

Paul W. Burton *Natural Environment Research Council, British Geological Survey, Murchison House, West Mains Road, Edinburgh EH9 3LA*

Received 1984 March 8; in original form 1984 January 13

Summary. Seismic moment release rates $\dot{M}_0$ inferred from a Weibull frequency–magnitude distribution and its extreme value equivalent are compared with observation. The seismotectonically diverse regions studied all exhibit the curvature of a log-linear frequency magnitude plot associated with applying a maximum magnitude to earthquake recurrence statistics. The inferred seismic moment release rates are consistent with available crustal deformation data within uncertainties resulting from the line fit and in magnitude determination. The uncertainties for the regions studied (Southern California, the New Madrid seismic zone, the Central and Eastern Mediterranean and mainland UK) vary from at worst an order of magnitude down to a factor of 2 or 3.

This agreement can be used to justify the extrapolation of frequency–magnitude statistics beyond the historical and instrumental era in seismic hazard studies as a test of the stationarity of short-term statistics against long-term effects.

A striking example of a bimodal seismicity distribution is observed in the New Madrid zone. This can be interpreted as being due to the superposition of two distinct seismogenic source types observed in the area. A quantitative analysis of the separate orders of seismicity observed in the frequency–magnitude statistics – comparing the different maximum magnitudes and inferred seismic moment release rates with those observed – supports this hypothesis. Superposition of many such seismogenic sources can explain the linearity observed in global frequency versus seismic moment magnitude statistics.

Introduction

The incorporation of crustal deformation into analyses of seismic hazard has given useful insight into probabilities of the largest events associated with long time periods. By linking

the observed statistical magnitude occurrence with a physical parameter – seismic moment – a means is provided to test an extrapolation from short-term historical and instrumental reports against an average of crustal deformation observed over geological time. Examples of observed deformation would come from plate tectonic models, from observed rates of slip along faults which break the surface, or from geodetically determined strain rates in more complex tectonic regions. Some knowledge of the dimensions of the fault zone (extent and depth) and appropriate elastic constants are required to convert slip or strain rates to seismic moment. This information also places deterministic constraints on an important parameter in any seismicity distribution – the largest earthquake consistent with the finite breaking strength of the Earth and the finite extent of the fault zone.

In previous work on this subject (e.g. Anderson 1979; Papastamatiou 1980) this largest earthquake specifies a truncation of the two parametered Gutenberg–Richter frequency relation (equation 2 below) in order to avoid problems such as an infinite rate of strain energy release (Knopoff & Kagan 1977). This effectively introduces a third parameter to the assessment of seismic hazard, and is consistent with the simple geometric seismicity model of Kanamori & Anderson (1975).

A more complex model of seismicity (Caputo 1977), which includes the effect of variable and limited stress drop as well as source dimension shows that such arbitrary and sudden truncation is not physically valid, and rather that we might expect a gradual roll-off both in the number density and the cumulative frequency asymptotic to a maximum earthquake at zero probability. (Incidentally the model also requires a similar roll-off at very small magnitudes.) This roll-off appears as curvature on a log-linear frequency–magnitude plot. For the cumulative form, such curvature has been observed in the laboratory by Burridge & Knopoff (1967) and King (1975) for earthquake models, and also in a theoretical model by Kuznetsova, Shumilana & Zavialov (1981), which considered inhomogeneities along a fault. This behaviour has already been observed in seismicity distributions around the world – for example by Botti, Pasquale & Anghinolfi (1980) in the Western Alps, Burton *et al.* (1982) in Turkey, Makjanik (1980) in Yugoslavia, Makropoulos (1978) in Greece and by Cosentino & Luzio (1976). There is also experimental evidence that the distribution of microfracture events in stressed San Marco gabbro also shows curvature asymptotic to a maximum size at low frequencies (Scholz 1968). Analogous curved distributions have been observed elsewhere in nature, for example in the yield strength and fatigue life of steel (Weibull 1951), and are commonly used in meteorological analysis (Jenkinson 1955).

The Weibull distribution can be usefully extended to analyse preferentially the largest events associated with curvature because of its simple form. The largest events in this case consist of a subset of the frequency distribution – namely the largest value in any unit time interval. This distribution of extreme values has been used in seismic hazard analysis (Burton 1979) and also in order to assign a maximum magnitude to events on a global basis (Yegulalp & Kuo 1974). There follows a discussion on crustal deformation compatible with curvature in both the cumulative frequency distribution and that of the extreme values, with application to different tectonic regimes.

Curved cumulative frequency distributions

The most commonly used seismicity distribution is the log-linear Gutenberg–Richter law

$$\log N(x \geqslant m) = a - bm \tag{1}$$

where N is the number of times a magnitude m is equalled or exceeded and a and b are regionally varying positive constants. (The symbol m is used in the theoretical discussion for

a general magnitude in order to avoid confusion with the seismic moment M_0. Elsewhere M_L, M_s, M_w and m_b have their usual meanings.) b is commonly observed to be close to 1 in accordance with the geometrical model of Kanamori & Anderson (1975). If we define a number density distribution $n = -dN/dm$ and rearrange (1) then

$$n(m) = p \exp(-b'm); \quad \begin{matrix} b' = b \ln 10 \\ p = b' 10^a. \end{matrix} \tag{2}$$

Caputo's (1977) model introduces a third parameter to the distribution at high magnitudes, above m_2 say, and defines a maximum value for m via the relation

$$n(m) = p \exp(-b'm) - q \tag{3}$$

where p, b' and q can be related to constants specifying the distribution of fault dimension and stress drop, and to maximum values of these parameters. The model also indicates that $b \approx 1$. Equation (3) is therefore a simple generalization of (2), or we can regard (2) as the limit in which $q \to 0$ or the equivalent maximum magnitude (ω) tends to infinity, since $q = p \exp(-b'\omega)$.

Jenkinson's (1955) general solution for a cumulative frequency distribution related to the extreme values takes the form

$$N(x \geqslant m) = [(\omega - m)/(\omega - u)]^{1/\lambda}$$

and is equivalent to the Weibull distribution for positive, non-zero λ. ω is the maximum magnitude, $u < \omega$ is a characteristic value associated with unit time, and $\lambda < 1$ is a measure of the curvature of the distribution. As $\lambda \to 0$ (4) reduces to the form (1) (Gumbel 1958). This form of the distribution in (4) is chosen as the most convenient for the present work. In both cases curvature in N and n asymptotic to a maximum value is reflected by three parameters, rather than the two of (1).

An alternative attempt to limit the distribution is to define $N(m) = 0$ at a finite maximum magnitude, given a normalized form of (2). The form, after Cosentino & Luzio (1976) is the truncated Gutenberg–Richter law

$$N(x \geqslant m) = \frac{\exp(-b'm) - \exp(-b'\omega)}{\exp(-b'u) - \exp(-b'\omega)} \tag{5}$$

where ω and u are defined as in the Jenkinson notation and $b' = b \ln 10$. In this case the number density distribution $n(m)$ is *not* curved although the *cumulative* frequency is (Båth 1981a), so there is a philosophical difference between (5) and the forms (3) and (4). Finally, the effects of both a lower and an upper bound to earthquake occurrence can be combined in the single equation

$$P(m) = (1 - K) + K \exp[b'(m - m_0)] \tag{6}$$

where P is the fraction of earthquakes greater than m, K is $\{1 - \exp[-b'(\omega - m_0)]\}^{-1}$ and m_0, ω are lower and upper bounds to the seismicity distribution (Cornell & Vanmarcke 1969). Normally the effects of a lower bound on earthquake statistics are negligible and can be safely ignored. The relationship of this form of the seismicity distribution to crustal deformation rates was analysed by Papastamatiou (1980) directly in terms of seismic moment.

In summary, the inclusion of a third parameter which limits the seismicity distribution gives a more general form than the open-ended Gutenberg–Richter law, and in a form in common use outside seismology. The main parameterizations are outlined above, although

others are possible, but in the present work the form used will be that of (4), because this form allows us to compare both the initial distribution (N) and the extreme value distribution (P) discussed below.

Extreme value distributions

The theory of extreme values has been covered extensively by Gumbel (1958). For our purpose the most important relation is

$$P(x \leqslant m) = \exp[-N(x \geqslant m)] \tag{7}$$

where P is a probability of non-exceedance in unit time of a magnitude m – or alternatively that m is an extreme value. This relation follows from a Poissonian assumption that different events are unrelated, in the limit as the total number of events analysed $\to \infty$. A derivation of the form of N (and hence P) consistent with certain assumptions pertinent to the extreme values gave equation (4). The form of this distribution which reflects an upper bounded magnitude is defined as Gumbel's third distribution of extreme values:

$$P(x \leqslant m) = \exp\{-[(\omega - m)/(\omega - u)]^{1/\lambda}\} \tag{8}$$

where $0 < \lambda < 1$, $u < \omega$ as for the Weibull distribution.

Knopoff & Kagan (1977) have objected to the use of extreme value statistics of the first type (related to equation 1) because methods which analyse the whole data set in this case generally give more accurate results in earthquake statistics. However, the curvature consistent with Caputo's physical model is usually emphasized to a greater degree in the extreme value case for a type three distribution because it deals preferentially with the largest events where such curvature is to be expected. Gumbel's third distribution of extreme values may well be the best available method of extrapolating to earthquake occurrence at low probabilities from an existing catalogue of events, particularly when it is incomplete, although where possible the predictions should be checked against known physical parameters such as slip rate. The theoretical means of carrying this out is derived in the next section.

Crustal deformation

The measure of crustal deformation is taken to be the seismic moment M_0. This can be related to slip rates ($\dot{s}$) on individual faults, or strain rates ($\dot{e}$) over a more diffuse area by the equations

$$\dot{M}_0 = \mu A \dot{s} \tag{9}$$

$$\dot{M}_0 = 2.5 \mu V \dot{e} \tag{10}$$

where μ is the rigidity modulus, A is the area of slip and V is the crustal volume of the zone of deformation. Equation (10) is derived in Papastamatiou (1980).

Two models are used to estimate the rate of crustal deformation, following from (I) the cumulative frequency of occurrence (whole process) and (II) from the extreme value probabilities (part process).

MODEL I

An average value for the rate of release of seismic moment is given by integration over the range $(0, M_{0\omega})$ where $M_{0\omega}$ is the largest moment which might be released in a single event

for a particular region

$$\bar{\dot{M}}_0 = \int_0^{M_0\omega} M_0 n(M_0)\, dM_0 \tag{11}$$

$n(M_0)\, dM_0$ is the number of earthquakes occurring in an interval dM_0 per unit time with $n = -dN/dM_0$. N is given by the cumulative frequency relationship, but is normally expressed in terms of magnitude, since moment is still a fairly rare observational parameter. To convert between the two we may use the relationship

$$M_0(m) = 10^{A+Bm} \tag{12}$$

where $B = 3/2$ for the M_w scale follows from Kanamori & Anderson's (1975) theoretical considerations on fault geometry as well as from empirical fits to available data. The most recent work on this conversion from seismic moment, M_0, to seismic moment magnitude, M_w, indicates the following values for A and related stress drops $\Delta\sigma$:

interplate events = 16.1, $\Delta\sigma$ = 30 bar

intraplate events = 15.7, $\Delta\sigma$ = 76 bar

average value = 15.85, $\Delta\sigma$ = 52 bar

California = 15.83

(from Singh & Havskov 1980).

By an appropriate change of variables, and using (4) to define $n(m) = -dN/dm$, it can be shown from (11) and (12) that

$$\bar{\dot{M}}_0 = \frac{M_{0\omega}\,\Gamma(1 + 1/\lambda)}{[\beta(\omega - u)]^{1/\lambda}} \tag{13}$$

where $\bar{\dot{M}}_0$ and u are expressed per unit time interval, and $\beta = B \ln 10$. Γ is the usual symbol for the Gamma function.

MODEL II

Forming a probabilistic expectation value

$$\langle \dot{M}_0 \rangle = \int_0^{M_0\omega} M_0\, p(M_0)\, dM_0 \tag{14}$$

where

$$P(X \leqslant M_0) = \int_0^{M_0} p(X)\, dX$$

is the extreme value distribution following from the normalized probability density p. After a suitable change of variables involving (8) and (12)

$$\langle \dot{M}_0 \rangle = M_{0\omega} \int_0^1 \exp\,[-\beta(\omega - u)(-\ln x)^{\lambda}]\, dx. \tag{15}$$

In the present work this equation is evaluated numerically.

Thus in both models the seismic moment release per unit time interval is expressed as a fraction of the maximum moment $M_{0\omega}$, for all values of (ω, u, λ) consistent with a

Gumbel's third extreme value distribution and its initial Weibull distribution. We can also show that $\langle \dot{M}_0 \rangle / \bar{\dot{M}}_0 < 1$ for appropriate values of the parameters and if (7) holds.

In evaluating parameters of the distribution (8) the unit time interval must sometimes be taken to be i yr rather than annually, in order to reduce problems associated with intervals devoid of any recorded events. If this is the case u and λ are appropriate for this scale, and we can convert to annual rates via

$$\langle \dot{M}_0 \rangle_i = i \langle \dot{M}_0 \rangle_1 \tag{16}$$

where $\langle \dot{M}_0 \rangle_i$ is the seismic moment released per i yr.

(13) and (15) then define the rate of release of seismic moment in terms of the statistically determined parameters (ω, u, λ) – the link to the physical process of strain or slip rates being represented by the terms $M_{0\omega}$ and β.

UNCERTAINTIES IN $\bar{\dot{M}}_0$, $\langle \dot{M}_0 \rangle$ AND $M_{0\omega}$

Because (ω, u, λ) are subject to (often large) statistical error we have to allow for this in predictions of $\dot{M}_0$. This can be done by the equation

$$\delta(\langle \dot{M}_0 \rangle, \bar{\dot{M}}_0) = \left\{ \sum_{i=1}^{3} \sum_{j=1}^{3} \frac{\partial^2 (\langle \dot{M}_0 \rangle, \bar{\dot{M}}_0)}{\partial p_i \, \partial p_j} \sigma_{ij}^2 \right\}^{1/2} \tag{17}$$

which represents a complete covariance error in $\langle \dot{M}_0 \rangle$ and $\bar{\dot{M}}_0$ respectively. $p_{i,j}$ takes on values (ω, u, λ) and σ_{ij} is the statistically determined covariance error in these parameters. The covariance matrix ϵ is defined by

$$\epsilon = \begin{pmatrix} \sigma_\omega^2 & \sigma_{\omega u}^2 & \sigma_{\omega\lambda}^2 \\ \sigma_{u\omega}^2 & \sigma_u^2 & \sigma_{u\lambda}^2 \\ \sigma_{\lambda\omega}^2 & \sigma_{\lambda u}^2 & \sigma_\lambda^2 \end{pmatrix} \tag{18}$$

as in Burton (1979). This is the most complete method of allowing for error, because in general the parameters ω and λ are dependent on each other. A large ω leads to less curvature (lower λ) and vice versa. This manifests itself in a negative contribution from $\sigma_{\omega\lambda}^2$, or a reduction in the error compared to the variance method (a sum of the diagonal elements σ_i^2).

The uncertainty in ω is often unusually large (Burton 1979), and in many cases may be reduced where limitations on stress drop (usually in the range $1 < \Delta\sigma < 100$ bar), fault dimension and fault type place an upper bound on $M_{0\omega}$ through the general expression

$$M_{0\omega} = C \Delta\sigma_{\max} \, l_{\max}^3 \tag{19}$$

where C is a dimensionless constant which depends on the type of fault, and $l_{\max}$ is the maximum fault dimension (Kanamori & Anderson 1975). Alternatively we may use this value to compare $M_{0\omega}$ obtained by $l_{\max}$ and $\Delta\sigma_{\max}$ with statistically determined values of ω via (12).

Saturation

It is well known that curvature of the form (3), (4) or (5) may be artificially present for magnitudes above $M_S = 7.5$ to 8.0 because of instrumental saturation of the magnitude scale (Howell 1981). Chinnery & North (1975) have shown that when M_S values are

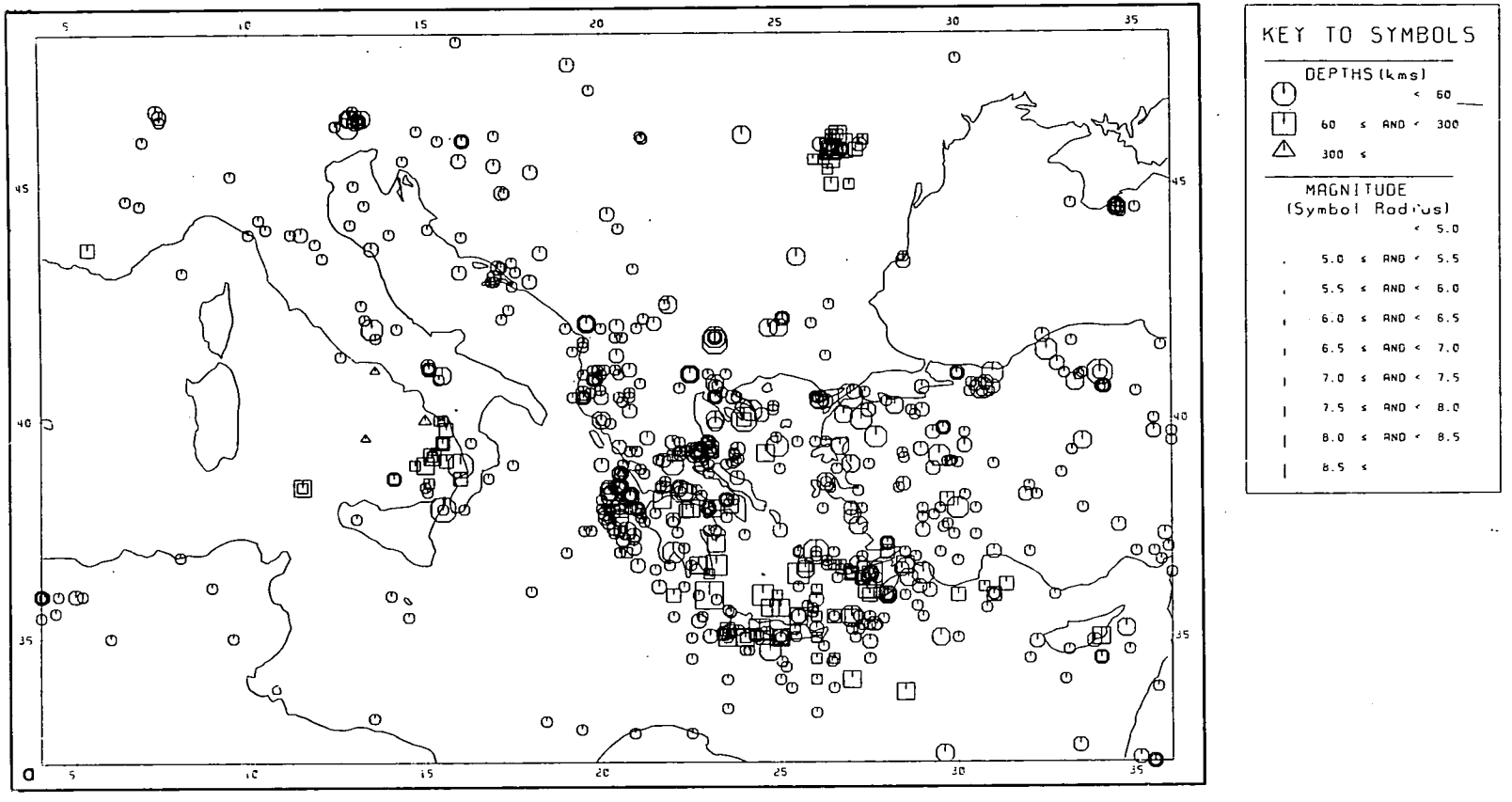

Figure 1. (a) Seismicity of the Central and Eastern Mediterranean area. Only those events of $M_S \geq 5$ are shown for economy of plotting. The tectonic interaction is composed of a collision between Africa and Eurasia, with seismic energy being released mainly along the arcuate trend of the Hellenic arc south and west of Greece.

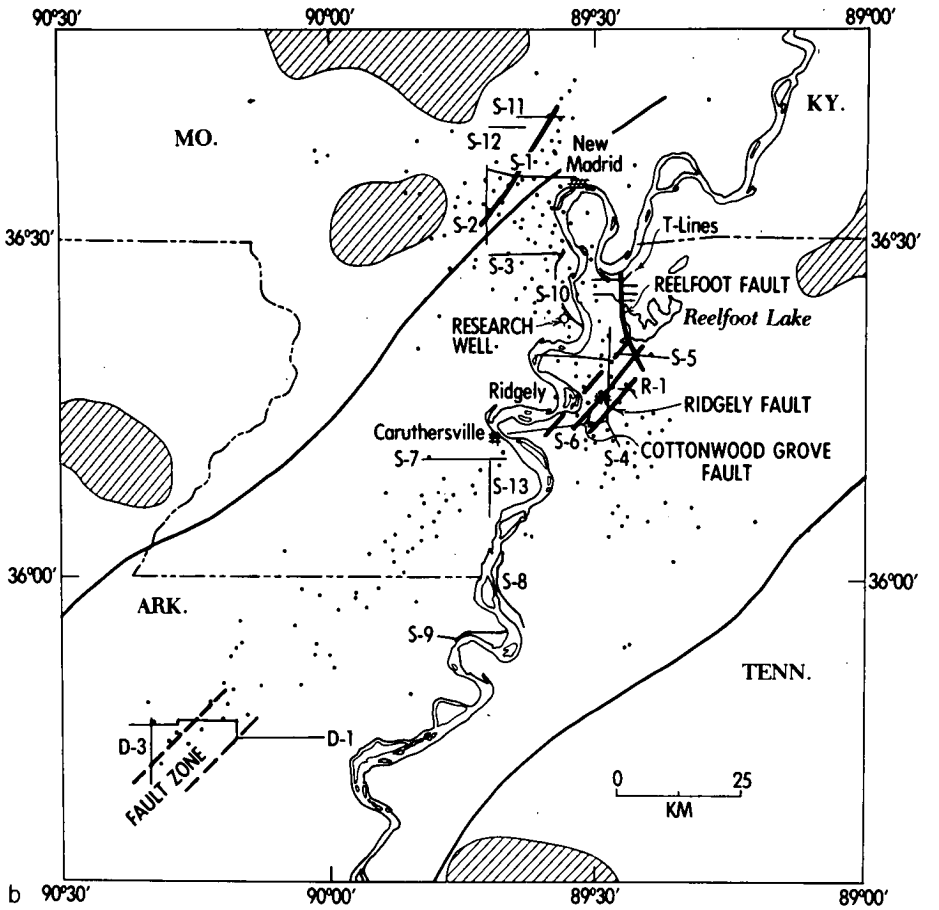

Figure 1. (b) Tectonic setting of the area around the New Madrid seismic zone (after Zoback *et al.* 1980), showing microearthquake epicentres (dots), locations of seismic profiles (e.g. S-7) and principal faults inferred from the data. The continuous heavy black lines are rift boundaries, and igneous plutons are represented by the hatched areas. There are three main seismicity trends: (1) a 100 km long stretch running SW–NE from the SW corner, (2) a section running SSE–NNW at the terminus of (1), and (3) the smallest trend SW–NE near New Madrid. Copyright 1980 by the American Association for the Advancement of Science.

corrected to what is, in effect, Kanamori's (1978) M_w on a global level then (1) is the best description of world seismicity, but concede that there are no convincing theoretical arguments for such linearity. There are, moreover, several examples of non-linearity below the threshold of curvature due to instrumental saturation when events on a more local scale are grouped together as well as a solid body of theoretical and experimental backing for such behaviour (for references see the Introduction). It may well be that the linearity observed on a global scale is due to the *superposition* of many curved distributions. For example Duda (1965) and Makropoulos (1978) found a poor fit to (1) and (8) respectively for the Aleutians–Alaska arc. Båth (1981b) and Singh, Rodriguez & Esteva (1983) have also observed such behaviour in Turkey and Mexico. A further example is cited in this paper. In many cases the superposition of two or more earthquake populations offer a plausible explanation for this apparently anomalous behaviour.

For this reason care has been taken in the following section to investigate any possible curvature which may result from such instrumental saturation. In effect, this would amount

to using Chinnery & North's (1975) empirical method for converting from M_S to a seismic moment magnitude, M_w – a much more meaningful description of the 'size' of the seismic source. For the areas considered in the present work this turns out to be unnecessary.

It is not even clear that such correction is always appropriate, since Kanamori's (1977) tabulation of M_S/M_w for large events shows that M_S is commonly greater than M_w for large events – the opposite effect of that of saturation. This anomaly may be ironed out as more data become available, but can be partially included in the method of line fitting by assuming an uncertainty in each magnitude value of the same order as any saturation

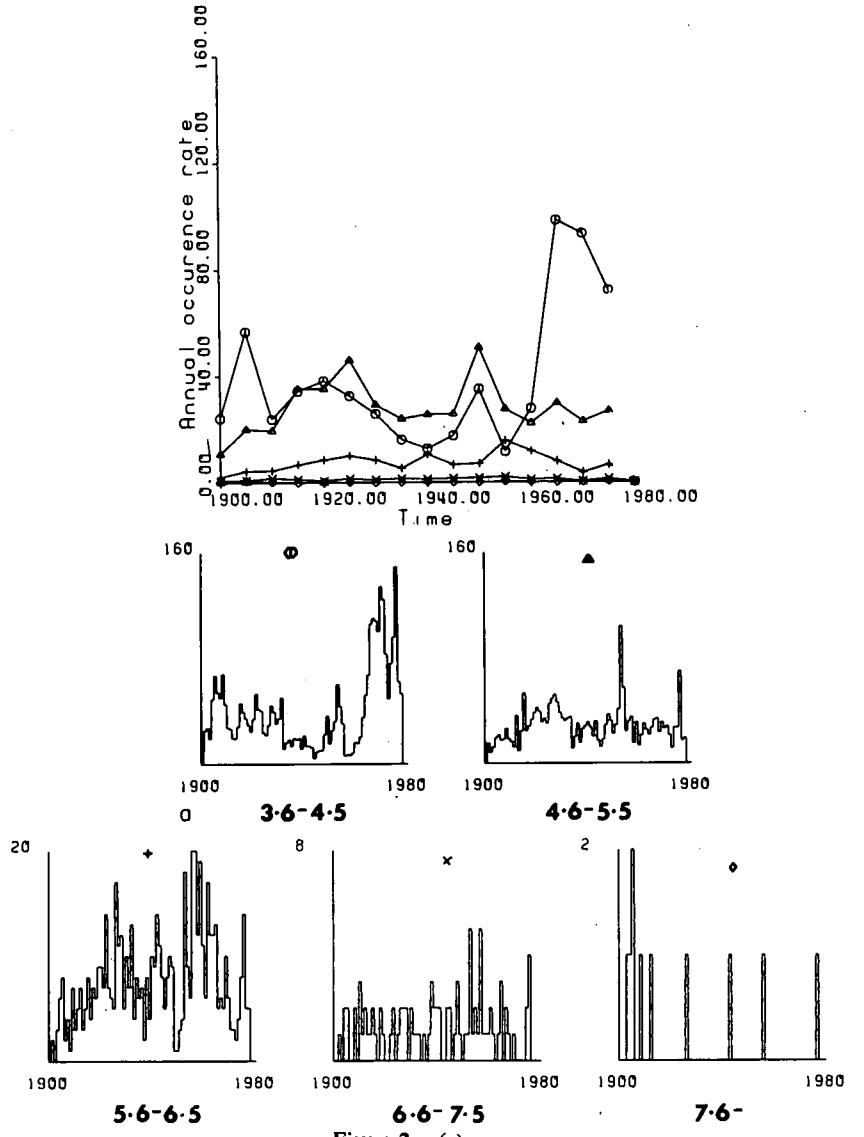

Figure 2 – (a)

Figure 2. Completeness testing. (a) The Central and Eastern Mediterranean. The roughly constant frequency of events in the range (4.6, 5.5) since 1920 or so, compared to the sudden jump in the range (3.6, 4.5) around 1963 indicates that the former is complete for the time span analysed (1943–1971). (b) Southern California. Again the roughly constant frequency of events in (4.0, 4.9) indicates a completeness threshold of 4.0.

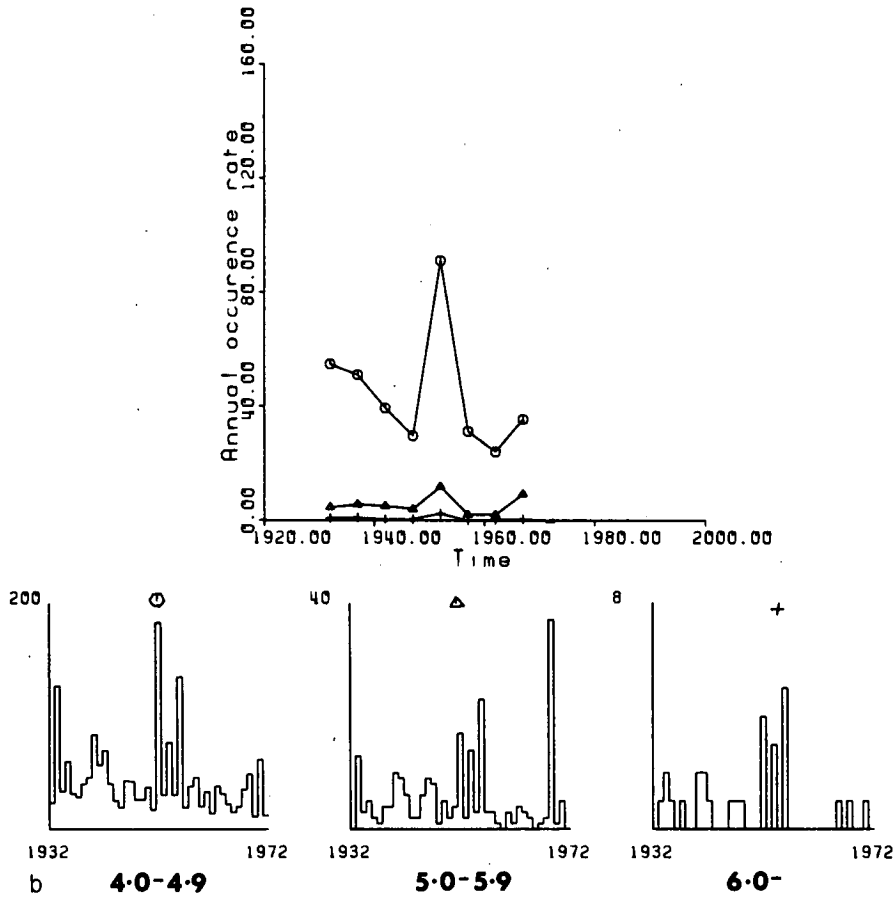

Figure 2 – (b)

correction. In the present work this value is taken to be ±0.5 of a magnitude unit, which includes estimates of measuring uncertainty, conversion to seismic moment as well as possible saturation effects in the final value of $\dot{M}_0$.

Results and discussion

Empirical line fits to establish $\dot{M}_0(\omega, u, \lambda, A, B)$ were attempted for four diverse tectonic regions: (a) the Central and Eastern Mediterranean, (b) the New Madrid seismic zone, (c) Southern California, and (d) mainland UK. The results are summarized in Tables 1 and 2 and in Figs 1–4. This section investigates in detail the areas tentatively assessed in Main & Burton (1981).

(a) THE CENTRAL AND EASTERN MEDITERRANEAN (32°–48°N, 4°–36°E)

North (1977) has tabulated seismic moment values for this area of diffuse, plate boundary seismicity. From his table 4 the total seismic moment released in this area for the period 1943–1971 was 70×10^{26} dyne cm or a rate $\dot{M}_0 = 24 \times 10^{25}$ dyne cm yr^{-1}. A more complete picture from 1963–1970 (his table 1) gives a rate 46×10^{25} dyne cm yr^{-1} which may be regarded as a minimum value.

A seismicity map of the area concerned is given in Fig. 1(a) and an excellent summary of the complex geo-tectonic setting is given in Horvath & Berckhemer (1982). The histograms of Fig. 2(a) show that the catalogue used (Burton 1978) is complete for the time range analysed (1943–1971) above mag 4.5. The range (3.6, 4.5) is not complete – as can be

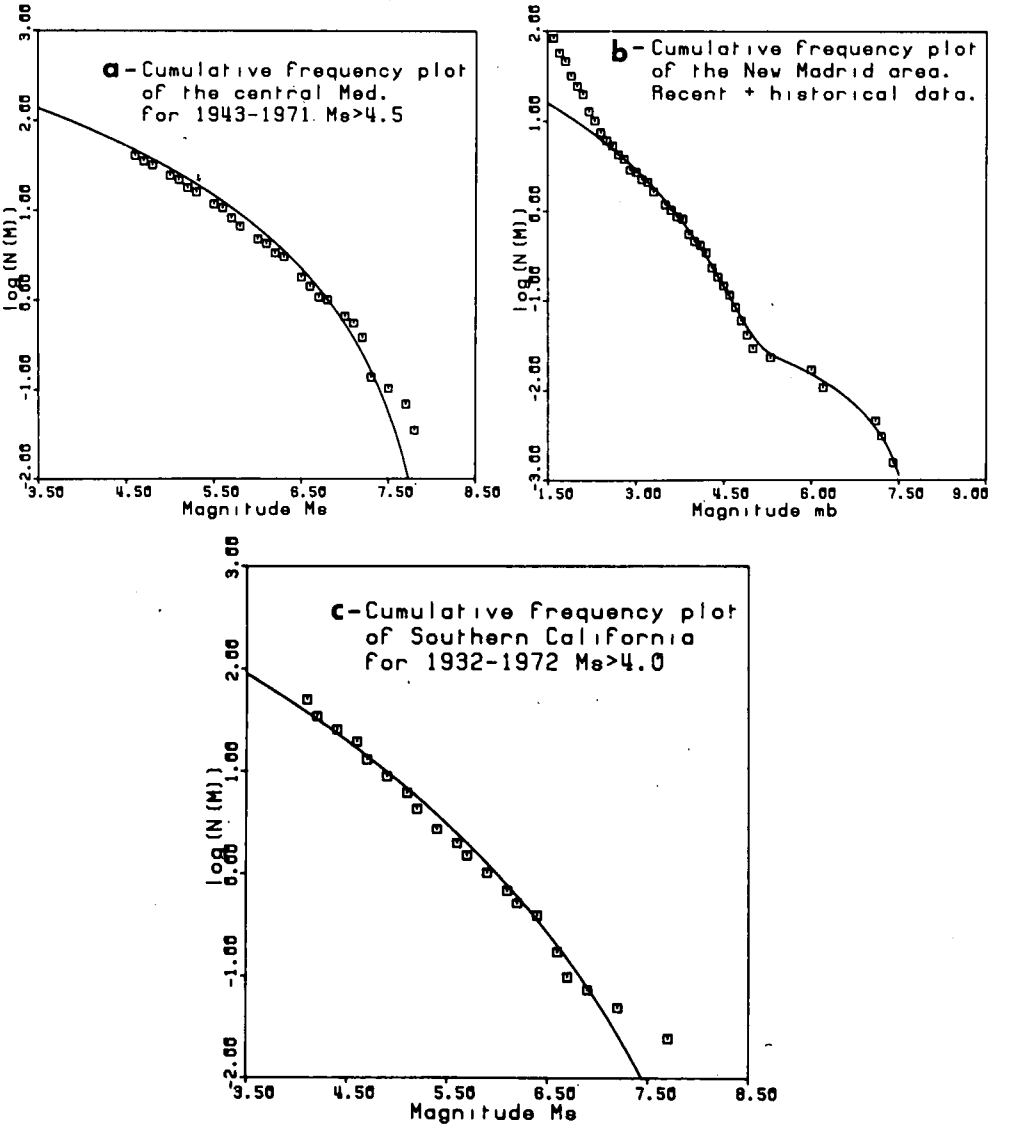

Figure 3. Cumulative frequency line fits to the distribution $N(m) = [(\omega - m)/(\omega - u)]^{1/\lambda}$. The parameters and their covariance error matrices are given in Table 1. (a) The Central and Eastern Mediterranean. In this case there seems to be a high autocorrelation error – there being a systematic trend in the positioning of the data points relative to the line. It would be difficult to justify a linear fit of the form (1) in this case, the curvature being so marked at high magnitudes. (b) The New Madrid area. Here the most successful fit was obtained by splitting the magnitude range into two segments – above and below 5, and fitting the line separately. The New Madrid events were repositioned at average repeat times $T = 650$ years ($N = 1/T$). (c) Southern California. In this case the line fit seriously underestimates the occurrence rate of the largest events which have occurred. A line fit of the form (1) would in this case give a better fit at these magnitudes, but again there seems to be some evidence of a bimodal distribution, the ranges meeting at $M_L \approx 6.7$ or so.

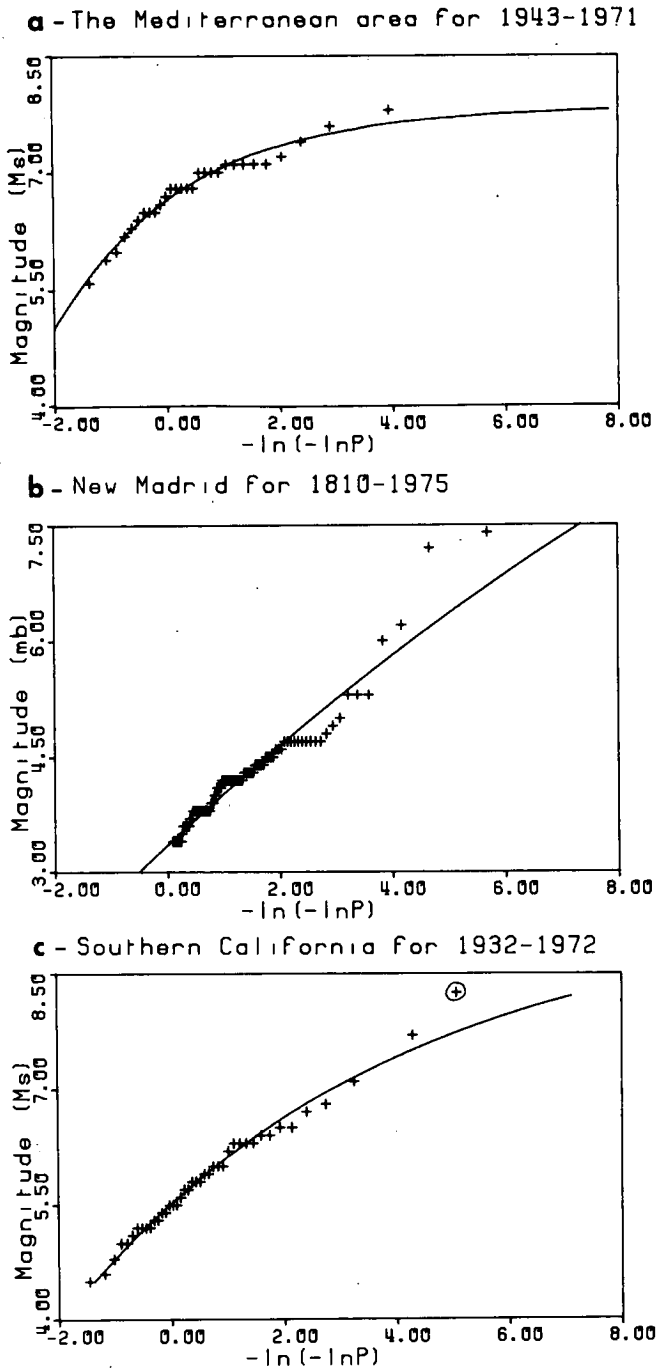

Figure 4. Extreme value line fits to the distribution $P = \exp\{-[(\omega - m)/(\omega - u)]^{\nu\lambda}\}$. The parameters and their covariance error matrices are given in Table 2. (a) The Central and Eastern Mediterranean. Curvature and a maximum magnitude are well established. (b) The New Madrid area. The line fit is effectively straight – implying a moment release rate which is deterministically several orders of magnitude too high. A bimodal distribution as in Fig. 3(b) is apparent, but in this case the data could not be separated into the two portions successfully, because of their scarcity in the higher range. (c) Southern California. The curvature is enhanced compared to Fig. 3(c), but again the occurrence of the largest magnitudes is underestimated. The ringed data point has been inferred from Sieh's (1978) work which indicates $M_S = 8.25$ and $T = 163$ yr, with $P = 1 - 1/T$.

Table 1. Moment release rates predicted by cumulative frequency line fits to $N(m) = [(\omega - m)/(\omega - u)]^{1/\lambda}$ (model I and Fig. 3).

Area*		Parameters (ω, u, λ)	Covariance error matrix ϵ			Local values for A, B		$\dot{\bar{M}}_0(\omega, u, \lambda, A, B)$ $\times 10^{25}$ dyne cm yr^{-1}	$\dot{M}_0$ observed or estimated $\times 10^{25}$ dyne cm yr^{-1}
(a)		(8.16, 6.80, 0.251)	0.855	−0.031	−0.119				
			−0.031	0.018	0.008	16.0	1.5	87 + 110 − 48	≥46
		M_s	−0.119	0.008	0.018				
(b)	Range (5.0, 7.5)	(7.81, −23.4, 0.680)	1.43	71.1	−0.752				
			71.1	4179.0	−42.5	15.58	1.5	1.2 + 12 − 1.1	≈0.6
		$m_b^\dagger$	−0.752	−42.5	0.437				
(b)	Range (2.5, 5.0)	(5.61, 3.63, 0.263)	1.00	−0.084	−0.154				
			−0.084	0.019	0.015	15.58	1.5	4.0 + 23.5 − 3.4 ($\times 10^{-4}$)	$\approx 10^{-4}$–10^{-2}
		$m_b^\dagger$	−0.154	0.015	0.025				
(c)		(9.26, 6.00, 0.126)	9.54	−0.304	−0.340				
			−0.304	0.026	0.012	15.83	1.5	8 + 26 − 6	≈16
		M_s/M_L	−0.340	0.012	0.012				

* Areas are: (a) the Central and Eastern Mediterranean, (b) the New Madrid seismic zone, and (c) Southern California.
† Refer to text for m_b/M_s conversion.

Table 2. Moment release rates predicted by extreme value line fits to $P(m) = \exp[-(\omega - m)/(\omega - u)]^{1/\lambda}$ (model II and Fig. 4).

Area*		Parameters (ω, u, λ)	Covariance error matrix ϵ			Local values for A, B		$\dot{M}_0(\omega, u, \lambda, A, B)$ $\times 10^{25}$ dyne cm yr^{-1}	$\dot{M}_0$ observed or estimated $\times 10^{25}$ dyne cm yr^{-1}
(a)		(7.84, 6.64, 0.435)	0.484	−0.044	−0.200				
			−0.044	0.014	0.021	16.0	1.5	43 + 26 −16	≥46
		M_S	−0.200	0.021	0.093				
(b)	Range (3.0, 7.5)	(19.4, 3.36, 0.042)	1123.00	2.54	−3.20				
			2.54	0.013	−0.007	15.58	1.5	–	≈0.6
		$m_b^\dagger$	−3.20	−0.007	0.009				
(c)		(9.11, 5.46, 0.182)	3.70	−0.062	−0.219				
			−0.062	0.008	0.004	15.83	1.5	8.5 + 16.2 −5.6	≈16
		M_S/M_L	−0.219	0.004	0.013				
(d)		(5.46, 4.58, 0.59)	0.190	−0.026	−0.134				
			−0.026	0.015	0.026	15.7	1.5	2.2 + 1.0 −0.7 ($\times 10^{-3}$)	≈34 ($\times 10^{-3}$)
		$m_b^\dagger$	−0.134	0.026	0.113				

* Areas are: (a) the Central and Eastern Mediterranean, (b) the New Madrid seismic zone, (c) Southern California, and (d) mainland UK.
† Refer to text for m_b/M_S conversion.

inferred from the sudden jump in the number of events reported on introduction of the WWSSN network in 1963. Fig. 3(a) shows the cumulative frequency line fit to these data and Fig. 4(a) the Gumbel plot, both of whose parameters were calculated using the method described in Burton (1979). The parameters and covariance errors (which include an allowance for ±0.5 uncertainty in the magnitude measurement) can be seen in Tables 1 and 2. Note that in some cases the actual values of (ω, u, λ) for N and P differ slightly as expected by Makjanik (1980).

To convert to moment release rates we refer to North's table 4 again, where we find for this area that an average stress drop is 38 bar. This converts to $A = 16.0$ using Singh & Havskov's (1980) formulation, and with $B = 1.5$ leads to a good linear fit to North's (1974) fig. 4, right up to the highest magnitudes. This last point indicates that there appears to be no instrumental saturation effect.

Both predictions of the moment release rates agree with that expected to within a factor 2 or so, which is in both cases within the expected uncertainty. This consistency, where we have reasonable error in (ω, u, λ) and some knowledge of a local stress drop or A value shows that the model proposed is quantitatively adequate well within the limits of statistical uncertainty.

Further inspection of this uncertainty shows the following relative effects of the three Gumbel parameters

$$\frac{\partial\langle\dot{M}_0\rangle}{\partial\omega} : \frac{\partial\langle\dot{M}_0\rangle}{\partial u} : \frac{\partial\langle\dot{M}_0\rangle}{\partial\lambda} = 1.3:1:1.8$$

$$\frac{\partial\langle\dot{M}_0\rangle}{\partial\omega}\sigma_\omega : \frac{\partial\langle\dot{M}_0\rangle}{\partial u}\sigma_u : \frac{\partial\langle\dot{M}_0\rangle}{\partial\lambda}\sigma_\lambda = 7.7:1:14.7.$$

This result shows that u is the best-determined parameter and that ω and λ have a dominant effect on the total uncertainty in this case. This effect is tempered by their interdependence already discussed above, and highlights the need to include the off-diagonal elements of the covariance error matrix in any attempt to quantify an error in $\langle\dot{M}_0\rangle$.

Finally, note from the tables that the error in $\langle\dot{M}_0\rangle$ is less than that for $\bar{\dot{M}}_0$ (60 per cent compared with 126 per cent).

The comments of the last three paragraphs were all found to apply qualitatively to the following areas of study, the actual values being quoted in this subsection for illustration only.

(b) THE NEW MADRID SEISMIC ZONE (35°–37°N, 89°–90.5°W)

This area of mid-plate seismicity has received much attention in recent years for reasons both practical and theoretical. Zoback *et al.* (1980) summarized the available geological and geophysical data, and concluded that the area consists of three main seismic trends (see Fig. 1b), set in a reactivated graben structure. Why the seismicity should largely follow the axis of the graben is not clear.

Practical interest is stimulated by the possibility of a repeat of the 1811–1812 sequence of major events (m_b 7.1–7.4) in an area of relatively low seismic attenuation and high population density, and theoretical interest comes from the breakdown of the classical theory of rigid plate tectonics. Because the seismicity trends are situated in a zone primarily of EW compression (Zoback & Zoback 1980) we would expect right lateral strike-slip motion along the trends (1) and (3) of Fig. 2(b) and thrust on section (2). Russ (1981) showed that this is borne out to a large extent by the few fault plane solutions available, and

that section (2) may result from reactivated dip-slip faulting. Together with Schilt & Reilinger (1981), he also indicates that such evidence as there is favours 5 mm yr^{-1} of uplift occurring in and around the northern part of the active zone. There is some evidence that some of this motion is taken up by aseismic creep since earthquakes in Schilt & Reilinger (1981) did not produce enough movement to account for all of the uplift detected in a later levelling survey.

The catalogues analysed are described by Nuttli (1979) and Johnston (1981) quoting m_b values inferred from macroseismic intensities and recent microseismic data, so there are no problems associated with instrumental saturation. All events from Johnston's (1981) data set for $m_b > 2.5$ were included in the analysis. The most successful line fit came from considering the range (2.5, 5.0) and (5.0, 7.5) separately as in Fig. 3(b), which plots the superposition of these two separate distributions. There may also be a third component in the range of (1.6, 2.5). This superposition can also be seen in the extreme value case (Fig. 4b), but due to the scarcity of data in the higher portion the two ranges cannot be separated. In this case the line fit is effectively straight, even though systematic bimodal curvature is evident from the figure. For this reason no realistic $\dot{M}_0$ could be obtained with the impossibly high value of ω obtained in Table 2(b).

In arriving at the entries in Table 1(b) for $\dot{M}_0$ the magnitude conversions

$$M_s = 1.59\, m_b - 3.97 \qquad 6.5 < M_s < 8.0 \tag{20}$$

$$M_s = 1.93\, m_b - 4.8 \qquad 4.0 < M_s < 6.0 \tag{21}$$

from results summarized in Marshall (1970) were used to match the ranges above and below 5.0 respectively. There is some evidence that the stress drops in this area are relatively high, so a value $\Delta\sigma = 100$ bar was chosen to define A via Singh & Havskov's (1980) formulation. Considering the large error involved in converting from epicentral intensities I_0 to m_b (Burton, Main & Long 1983) and then to M_S it is not surprising that the final error quoted in $\dot{M}_0$ is as high as a factor 10 or so.

In Fig. 3(b) for the range $m_b > 5.0$ the largest events ($m_b > 7$) were moved to positions consistent with average repeat times of 650 years (Russ 1981). This gave agreement within a factor 2 with the estimated moment release rate from three fault areas modelled as one fault 20 km deep (Nuttli & Herrmann 1978) by 200 km long moving at 0.5 cm yr^{-1}, if $\mu = 3 \times 10^{11}$ dyne cm^{-2}.

For the range (2.5, 5.0), using a circular fault model (Kanamori & Anderson 1975) the maximum fault size (for $\omega = 5.6$) was found to be $\approx 150\,km^2$, with $\dot{s} \approx 9 \times 10^{-2}$ mm yr^{-1}. This typical movement on what are supposed to be a collection of several subsidiary faults compares favourably with that observed on one such fault ($\sim 1.2 \times 10^{-2}$ mm yr^{-1} from Zoback *et al.* 1980) on the Cottonwood Grove fault. We can see that the seismicity represented by the range (2.5, 5.0) contributes only a minor fraction of the stress release.

The conclusion here is that bumps in the cumulative frequency distribution have been numerically related to the superposition of two different orders of observed faulting.

(c) SOUTHERN CALIFORNIA (31°–38°N, 114.5°–121°W)

This well-researched area of high seismicity on a plate boundary is very different from the previous example. It includes the site of the 1952 Kern Co event and the 1971 San Fernando earthquake, as well as the 400 km long 'locked zone' which previously ruptured in 1857 with an estimated M_S of 8.25 or greater and an average repeat time of 163 yr (Sieh 1978).

The catalogue used was that of Hileman, Allen & Nordquist (1973), whose publication also gives excellent maps of the seismicity and the tectonic setting. The analysis of Fig. 2(b) shows that for the period concerned (1932–1972) magnitudes above 4.0 or so are completely reported.

Anderson (1979) indicated a moment release rate of 12×10^{25} dyne cm yr^{-1} for a 500 km long fault, but this catalogue contains a 650 km stretch of the San Andreas fault and its offshoots, so $\dot{M}_0 \approx 16 \times 10^{25}$ dyne cm yr^{-1} may be more appropriate. These figures assume a depth of the brittle zone of 15 km and $\mu \approx 3 \times 10^{11}$ dyne cm^{-2}, with a movement from plate tectonic constraints of 5.5 cm yr^{-1}. Since the movement on surface faults is of the order 1–3.7 cm yr^{-1} the deformation must taken place in a broad zone around the main fault trend.

Fitting the Weibull distribution to the data proved to be unsuccessful above magnitude 6.7 (Fig. 3c). The line fit seems to follow curvature apparent in the range (4.0, 6.7) and seriously underestimates the occurrence of the highest magnitudes. It may be that the activity above 6.7 is a separate distribution as in the New Madrid area, but with only three or four data points this cannot be tested from the current catalogue. Singh & Havskov (1980) give $A = 15.83$ for this area, which implies a moment release rate of the right order only at the expense of allowing a value for ω of 9.3 – one magnitude higher than Sieh's (1978) deterministic estimate.

Hanks, Hileman & Thatcher (1975) indicate that M_0 for the Kern Co (1952) event was 200×10^{25} dyne cm and $M_S = 7.7$. Using $A = 15.83$, we find $M_w = 7.65$ so there are no grounds for supposing instrumental saturation is important.

The extreme value line fit (Fig. 4c) gives a similar value for ω, but u is significantly different (even considering its error). Curvature does seem to be enhanced by this method (higher value for λ) but once more there is a poor fit at the highest magnitudes and the possibility of two separate curved distributions is evident. The ringed data point is inferred from Sieh's (1978) estimates of M_S and the average repeat time T, with $T = 1/(1-P)$. As in sections (a) and (b) the moment release rates inferred from the line fit are in agreement with those observed within a factor less than the estimated uncertainty (a factor of 2, cf. 3 or 4) but in this case it is evident that the parameters of the line fit may be significantly improved upon.

(d) MAINLAND UK

This area of relatively low intraplate seismicity differs from the New Madrid area in that no catastrophic events are documented in historical times. Burton (1981) analysed the area in terms of the third distribution of extreme values and produced the (ω, u, λ) set in Table 2(d). The unit time for this set was 6 yr. The m_b/M_s relation (21) is thought appropriate because of the typical range of events.

Using equation (12) $M_{0\omega} = 2.0 \times 10^{24}$ dyne cm for $A = 15.7$ for an intraplate area, and if we model this as a circular fault via (19) the maximum fault area would be ≈ 350 km^2 for a corresponding typical stress drop of 76 bar. Since $\langle \dot{M}_0 \rangle = 2.2 \times 10^{22}$ dyne cm yr^{-1} and $\mu = 3 \times 10^{11}$ dyne cm^{-2}, a typical fault movement of 0.2 mm yr^{-1} is expected.

Unfortunately there is very little direct tectonic information as yet on UK seismicity. However, King's (1980) results showed that the fault area for the Carlisle event of 1979 December 26 was of the order of 40 km^2 for an event of m_b 5.0. Very little information exists on contemporary fault movement rates, although some unconfirmed evidence of surface movement directly following glacial unloading does exist (Sissons & Cornish 1982). The thrust mechanism of the Carlisle event (King 1980), and the strike-slip solution for the

Kintail earthquake swarm of 1974 (Assumçao 1981) are both compatible with compressive intraplate tectonics.

King (1980) assumes $\Delta\sigma = 30$ bar might be appropriate for the UK. In this case $A = 16.1$, $M_{0\omega} = 5.13 \times 10^{24}$ dyne cm, the maximum fault area = 1200 km^2, $\dot{s} = 0.06$ mm yr^{-1}. King's results are consistent in themselves, but if $\Delta\sigma = 30$ bar, we should expect fault planes of an order higher than those which have been observed so far. A more realistic picture might be to interpret the maximum fault area as representing a sum of several smaller faults of the order of tens of km^2, moving at rates ≈ 0.1 mm yr^{-1}. This speculative interpretation is compatible with the spread of UK seismicity around small, localized centres such as at Comrie and in pockets in the north-west of England and South Wales, and the absence of catastrophic events such as in the New Madrid area.

A deterministic estimate of the movement between the sinking south of England and the relative uplift consistent with glacial unloading of the north of England and Scotland is 1.5 mm yr^{-1} (Rossiter 1972). If the depth of the UK seismogenic zone is ~5 km, and its width is modelled as of the order 200 km, then $A \approx 1000$ km^2 and $\dot{M}_0 \approx 3.4 \times 10^{23}$ dyne cm yr^{-1}. This area favours King's choice of $\Delta\sigma$ and comparison of the values of $\dot{M}_0$ and $\langle \dot{M}_0 \rangle$ indicate that over 90 per cent of the observed movement occurs aseismically.

Conclusion

In most cases where moment release rates were available the distributions N and P successfully modelled both the observed curvature at high magnitudes and the predicted moment release rates from models I and II. The exceptions tended to be in areas where there was evidence that the distribution was bimodal – being most striking in the New Madrid area (Fig. 4b).

Careful quantitative comparison of $\dot{M}_0 \pm \delta\dot{M}_0$ can be used as a method of distinguishing areas where the line fit is deficient at the higher magnitudes. Incorporation of deterministic values for the maximum magnitude (from seismicity trends or geological zoning), and geological estimates of their average repeat times will also improve the quality of the line fit at these magnitudes as better quality data become available.

Typical uncertainties in $\dot{M}_0$ were found to be a factor of 2–4 or so, with the Gumbel estimates giving slightly lower uncertainties, and agreement within this range with observed moment release rates from (1) a short-term catalogue for an internal consistency check in the Mediterranean and (2) long-term geological estimates in Southern California is encouraging.

A serious drawback of the distribution used is that $n(\omega) = 0$. For a cyclic input and release of strain energy we might expect $n(\omega)$ to be some non-zero value, implying a repeat time $T = 1/N(m)$ which is not infinite as $m \to \omega$. Work is currently progressing in this area to generalize (2) to allow curvature in the density distribution without requiring $n(\omega) = 0$. This will imply a less severe curvature at magnitudes just below ω, and thereby offset the underestimation of observed occurrence rates to which the Weibull and Gumbel's third distribution seems to be prone.

Acknowledgments

This work was supported by the Natural Environment Research Council and is published with the approval of the Director of the British Geological Survey (NERC). We are also indebted to Dr Arch Johnstone of the Tennessee Earthquake Information Centre for providing the cumulative frequency data used to plot Fig. 3(b).

References

Assumçao, M., 1981. The NW Scotland swarm of 1974, *Geophys. J. R. astr. Soc.*, **67**, 577–586.

Anderson, J. G., 1979. Estimating the seismicity from geological structure for seismic risk studies, *Bull. seism. Soc. Am.*, **69**, 135–158.

Båth, M., 1981a. Earthquake magnitude – recent research and current trends, *Earth Sci. Rev.*, **17**, 315–398.

Båth. M., 1981b. Earthquake recurrence of a particular type, *Pageoph*, **119**, 1063–1076.

Botti, L. G., Pasquale, V. & Anghinolfi, M., 1980. A new general frequency-magnitude relationship, *Pageoph*, **119**, 196–206.

Burridge, R. & Knopoff, L., 1967. Model and theoretical seismicity, *Bull. seism. Soc. Am.*, **57**, 341–371.

Burton, P. W., 1978. The IGS file of seismic activity and its use for hazard assessment, *Seism. Bull. Inst. geol. Sci.*, No. 6, HMSO, London.

Burton, P. W., 1979. Seismic risk in Southern Europe through to India examined using Gumbel's third distribution of extreme values, *Geophys. J. R. astr. Soc.*, **59**, 249–280.

Burton, P. W., 1981. Variation in seismic risk parameters in Britain, *Proc. 2nd int. Symp. Anal. Seismicity and Seismic Hazard*, Vol. 2, pp. 495–530, Liblice, Czechoslovakia, May 18–23, Academia, Prague.

Burton, P. W., McGonigle, R. W., Makropoulos, K. C. & Ucer, S. B., 1982. Preliminary studies of seismic risk in Turkey, and the occurrence of upper bounded and other large earthquake magnitudes, *Proc. int. Symp. Earthquake Prediction in the North Anatolian Fault Zone*, Istanbul, Turkey, 1980 March 31–April 5, in *Multidisciplinary Approach to Earthquake Production*, pp. 143–172, eds Mete Isikara, A. & Vogel, Andreas, Braunschweig, Wiesbaden, Vieweg.

Burton P. W., Main, I. G. & Long, R. E., 1983. Perceptible earthquakes in the central and eastern U.S., *Bull. seism. Soc. Am.*, **73**, 497–518.

Caputo, M., 1977. A mechanical model for the statistics of earthquakes, magnitude, moment and fault distribution, *Bull. seism. Soc. Am.*, **67**, 849–861.

Chinnery, M. A. & North, R. G., 1975. The frequency of very large earthquakes, *Science*, **190**, 1197–1198.

Cornell, A. & Vanmarcke, E., 1969. The major influences on seismic risk, *Proc. 4th W.C.E.E.*, Santiago, Chile.

Cosentino, P. & Luzio, D., 1976. A generalisation of the frequency magnitude relation in the hypothesis of a maximum regional magnitude, *Annali Geophis.*, **4**, 3–8.

Duda, S. J., 1965. Secular seismic energy release in the Circum-Pacific Belt, *Tectonophys.*, **2**, 409–452.

Gumbel, E., 1958. *Statistics of Extremes*, Columbia University Press, New York.

Hanks, T. C., Hileman, J. A. & Thatcher, W., 1975. Seismic moments of the larger earthquakes of the Southern California region, *Bull. geol. Soc. Am.*, **86**, 1131–1139.

Hileman, J. A., Allen, C. R. & Nordquist, J. M., 1973. Seismicity of the Southern California region 1st Jan. 1932 to 31st Dec. 1972, *Contr. Div. Geol. planet. Sci., Calif. Inst. Techn., No. 2385.*

Horvarth, F. & Berckhemer, H., 1982. Mediterranean back-arc basins, *Alp. Med. Geol. Ser.*, **7**, 141–173.

Howell, B. F., (Jr), 1981. On the saturation of earthquake magnitude, *Bull. seism. Soc. Am.*, **71**, 1401–1422.

Jenkinson, A. F., 1955. The frequency distribution of the annual maximum or minimum values of meteorological elements, *Q. Jl R. met. Soc.*, **87**, 158–171.

Johnston, A. C., 1981. On the use of the frequency–magnitude relation in earthquake risk assessment, *Proc. Conf. Earthquakes and Earthquake Engineering – the Eastern U.S.*, pp. 161–181, Vol. I, ed. Beavers, J., Ann Arbor Science Ltd., the Butterworth group.

Kanamori, H., 1977. The energy release in great earthquakes, *J. geophys. Res.*, **82**, 2981–2987.

Kanamori, H., 1978. Quantification of earthquakes, *Nature*, **271**, 411–414.

Kanamori, H. & Anderson, D. L., 1975. Theoretical bases of some empirical relations in seismology, *Bull. seism. Soc. Am.*, **65**, 1073–1095.

King, C., 1975. Model seismicity and faulting parameters, *Bull. seism. Soc. Am.*, **65**, 245–259.

King, G., 1980. A fault plane solution for the Carlisle earthquake, 26 December 1979, *Nature*, **286**, 142–143.

Knopoff, L. & Kagan, Y., 1977. Analysis of the theory of extremes as applied to earthquake problems, *J. geophys. Res.*, **82**, 5647–5657.

Kuznetsova, K. I., Shumilina, L. S. & Zavialov, A. D., 1981. The physical sense of the magnitude–

frequency relation, *Proc. 2nd int. Symp. Analysis of Seismicity and on Seismic Hazard,* Vol. 1, pp. 27–46, Liblice, Czechoslovakia, 1981 May 18–29, Academia, Prague.

Main, I. G. & Burton, P. W., 1981. Rates of crustal deformation inferred from seismic moment and Gumbel's third distribution of extreme values, *Proc. Conf. Earthquakes and Earthquake Engineering – the Eastern U.S.,* Vol. 2, pp. 937–951. ed. Beavers, J., Ann Arbor Science Ltd, the Butterworth group.

Makjanik, B., 1980. On the frequency distribution of earthquake magnitude and intensity, *Bull. seism. Soc. Am.,* **70,** 2253–2260.

Makropoulos, K. C., 1978. The statistics of large earthquake magnitude and an evaluation of Greek Seismicity, *PhD thesis,* University of Edinburgh.

Marshall, P. D., 1970. Aspects of the spectral differences between earthquakes and underground explosions, *Geophys. J. R. astr. Soc.,* **20,** 397–416.

North, R. G., 1974. Seismic slip rates in the Mediterranean and Middle East, *Nature,* **252,** 560–563.

North, R. G., 1977. Seismic moment, source dimensions and stresses associated with earthquakes in the Mediterranean and Middle East, *Geophys. J. R. astr. Soc.,* **48,** 137–162.

Nuttli, O. W., 1979. Seismicity of the Central United States, *Geol. Soc. Am. Rev. Engrg. Geol.,* **IV,** 67–93.

Nuttli, O. W. & Herrmann, B., 1978. Creditable earthquakes for the central U.S, *State of the art for assessing earthquake hazards in the U.S., U.S. Army Engrng. Wat. Ways Exp. Station, Rep. 12, paper S-73-1.*

Papastamatiou, D., 1980. Incorporation of crustal deformation to seismic hazard analysis, *Bull. seism. Soc. Am.,* **70,** 1321–1335.

Rossiter, J. R., 1972. Sea level observations and their secular variation, *Phil. Trans. R. Soc.,* **272,** 131–139.

Russ, D. P., 1981. Model for assessing earthquake potential and fault activity in the New Madrid seismic zone, *Proc. Conf. Earthquakes and Earthquake Engineering – the Eastern U.S.,* Vol. 1, pp. 309–335, ed. Beavers, J., Ann Arbor Science Ltd, the Butterworth group.

Schilt, F. S. & Reilinger, R. E., 1981. Evidence for contemporary vertical fault displacement near the New Madrid zone, *Bull. seism. Soc. Am.,* **71,** 1933–1942.

Scholz, C. H., 1968. The frequency-magnitude relation of microfracturing in rock and its relation to earthquakes, *Bull. seism. Soc. Am.,* **58,** 399–415.

Sieh, K. E., 1978. Prehistoric large earthquakes produced by slip on the San Andreas fault at Pallet Creek, California, *J. geophys. Res.,* **83,** 3907–3939.

Singh, S. K. & Havskov, J., 1980. On moment magnitude scale, *Bull. seism. Soc. Am.,* **70,** 379–383.

Singh, S. K., Rodriguez, M. & Esteva, L., 1983. Statistics of small earthquakes and frequency of occurrence of large earthquakes along the Mexican subduction zone, *Bull. seism. Soc. Am.,* **73,** 1779–1796.

Sissons, J. B. & Cornish, R., 1982. Rapid localised glacio-isostatic uplift at Glen Roy, Scotland, *Nature,* **297,** 213–214.

Weibull, W., 1951. A statistical distribution function of wide applicability, *J. appl. Mech.,* **18,** 293–297.

Yegulalp, T. M. & Kuo, J. T., 1974. Statistical prediction of the occurrence of maximum magnitude earthquakes, *Bull. seism. Soc. Am.,* **64,** 393–414.

Zoback, M. D., Hamilton, R. M., Crone, A. J., Russ, D. P., McKeown, F. A. & Brockman, S. R., 1980. Recurrent intraplate tectonism in the New Madrid seismic zone, *Science,* **209,** 971–976.

Zoback, M. L. & Zoback, M., 1980. State of stress in the conterminous United States, *J. geophys. Res.,* **85,** 6113–6159.

PRINTED IN ENGLAND BY
ADLARD AND SON LTD, DORKING

Bulletin of the Seismological Society of America, Vol. 74, No. 4, pp. 1409–1426, August 1984

INFORMATION THEORY AND THE EARTHQUAKE FREQUENCY-MAGNITUDE DISTRIBUTION

By Ian G. Main and Paul W. Burton

Bulletin of the Seismological Society of America, Vol. 74, No. 4, pp. 1409–1426, August 1984

INFORMATION THEORY AND THE EARTHQUAKE FREQUENCY-MAGNITUDE DISTRIBUTION

BY IAN G. MAIN AND PAUL W. BURTON

ABSTRACT

A new frequency-magnitude relation consistent with an average magnitude $\langle m \rangle$ and an average seismic moment $\langle M_0 \rangle$ in the magnitude range (m_c, ω) is derived using the principles of information theory. The resulting density distribution $n(m)\,dm = C \exp\{-\lambda_1 m - \lambda_2 M_0(m)\}\,dm$ can be interpreted as a Boltzmann distribution of possible energy transitions scaled by a geometric factor, depending on how such transitions may occur on a fault plane. It gives a better fit to available frequency data on the Central Mediterranean area than other distributions which can only successfully model part of the magnitude range. The technique offers a *direct* method of including long-term geological information from plate models or observed fault movement in order to extrapolate seismicity statistics beyond the instrumental and historical eras. This approach is found to be in reasonable agreement with southern Californian frequency data—the resulting distribution being consistent with a geologically estimated recurrence time for the major events on the southern locked portion of the San Andreas fault.

INTRODUCTION

Great interest is currently being expressed in assigning probabilities to the occurrence of the large earthquakes which occur in response to the dynamic motion of the earth's crust over geological time scales. One obvious goal is to predict the time, place, and the size of an event at a given probability level, but the limited amount of data currently available and the lack of detailed understanding of earthquake mechanisms are likely to restrict wide application of reliable prediction to some time in the future.

A second approach is to assess the probability of occurrence of the largest events and to predict their magnitudes in the light of the seismotectonic properties of the area under consideration. Knowledge of the distribution and location of past earthquake magnitudes may be linked to attenuation studies in order to predict maximum, or the most likely, ground motion to be expected at a given site some distance from the likely earthquake source. If there is good control on propagation effects from source to site—e.g., on local soil mechanics and site conditions as well as on attenuation of seismic energy—the study of the distribution of earthquakes can assign probabilities of ground shaking of use to a design engineer.

One recent example of such an approach is to estimate the most probable earthquake which will affect a site within the region of interest. Burton *et al.* (1983) find that the maximum magnitude expected to occur in the Eastern United States is approximately 7.7, while the most likely to be felt at any given site, after inclusion of attenuation effects, is 6.5. These are macroseismic body wave magnitudes, which do not suffer from the instrumental saturation discussed more fully below (Nuttli, 1983, personal communication).

The nondeterministic nature of the latter approach necessitates the use of a probabilistic framework, but currently suffers from a lack of information at low frequencies of earthquake occurrence. The instrumental record of earthquakes only stretches back to the turn of the century, and we are often forced to use a subjective scale of reported earthquake damage in order to extend our knowledge to the

historically documented period before then (Ambraseys, 1971). There is, however, a third source of information which gives direct evidence for the occurrence of the rare large events, on the right time scale. This is the geological field evidence for earthquake-related deformation of the earth's crust. For example, Sieh (1978) dug into the San Andreas fault in California and uncovered field evidence in the recent sedimentation for eight previous major events at irregular spacings averaging 163 yr. More routinely, it is common for field geologists to record slip vectors on surface faults from stratigraphic and other evidence. The quaternary geological record gives direct information on a fault's long-term behavior, which in many cases can be understood in the framework of plate tectonic theory.

This paper will address the problem of incorporating such deterministic studies into the probabilistic assessment of seismic hazard evaluation in a direct way. The method used is the classic approach of information theory (also known as the maximum entropy method), which picks the most objective probability distribution consistent with the currently available data. Even if the distribution thus obtained requires modification as more information becomes available, it remains the best contemporary solution to a problem where our knowledge of the system is incomplete (Jaynes, 1957).

The Magnitude-Seismic Moment Relation

It is well known that instrumental magnitude scales suffer from saturation at high magnitudes. As earthquakes increase in size, more energy shifts towards the long-period end of the ground motion—the direct movement on the fault itself (Howell, 1981). Thus, one reaches the point where an event twice as large in terms of energy produces hardly any increase in the measured magnitude. For M_S, this occurs at approximately 8.0 and so Kanamori (1978) proposed an unsaturated magnitude scale called the "seismic moment magnitude", M_w, which extrapolates M_S beyond the onset of saturation.

The seismic moment M_0 is perhaps the best currently available measure of the size of an event. It is defined by the equation

$$M_0 = \mu A s = (\mu/\bar{\sigma})\Delta W \tag{1}$$

where μ is the rigidity modulus, A is the fault area, s is the movement on the fault, $\bar{\sigma}$ is the average stress level during the earthquake, and ΔW is the change in strain energy. Thus, the seismic moment can be easily related to various source parameters. The seismic moment magnitude M_w is then defined by

$$M_w = (\log_{10} M_0 - A)/B \tag{2}$$

where $B = 1.5$ from theoretical constraints (Kanamori and Anderson, 1975), and A is a function of the average stress drop $\Delta\sigma$, which is assumed to be a constant. Sing and Havskov (1980) have shown that appropriate values for A in interplate, intraplate, and "average" regions are 16.1, 15.7, and 15.85, respectively (in cgs units). The seismic moment of an individual event can be measured from geological field evidence, or from the seismological record of an event, particularly the longer periods.

In the following sections, we shall formulate a distribution in terms of M_w and assume that this is applicable to the M_S or M_L values in the region below instrumental saturation ($M_S \lesssim 8.0$) when we compare this to frequency-magnitude data. This is effected in practice by using locally correct values for A and B, and can be

tested by comparing the theoretical line (M_w) with the available (M_S) data. In order to avoid confusion between seismic moment and magnitude, we shall henceforth adopt the symbol m for "seismic moment magnitude".

The Earthquake Frequency Distribution from Information Theory

Information theory is applicable in a wide class of problems where the average value of a physical parameter can be estimated even though it may deviate significantly from this value from time to time. Its methods have been shown to be mathematically identical to, but are more general than those of statistical mechanics (Jaynes, 1957) and have found recent application in geophysics. Rubincam (1982) has used the method to solve the inverse problem of determining the lateral density distribution of the earth's crust from the current global gravity field, and Berrill and Davis (1980) have previously applied it to the earthquake frequency-magnitude distribution. In this section, we extend their results by directly including the average strain energy release through the seismic moment.

Consider the continuous range of magnitudes (m_c, ω), where ω is the maximum magnitude consistent with the finite breaking strain of the earth and the finite dimensions of the source zone, and m_c is an arbitrarily chosen lower bound. m_c may be physically determined by the minimum dimension which will support seismic rupture, but in practice will usually be the lower bound of complete reporting of events.

For this range, we wish to choose a distribution which is consistent with currently available knowledge but is the least biased with respect to our ignorance of the system—the "missing information". The "missing information" inherent in this probabilistic approach is characterized in information theory by the function

$$S(p) = \int_{m_c}^{\omega} p(m) \ln(p(m))\, dm \tag{3}$$

where $p(m)$ is the probability density function of magnitudes. S is also known as the "information theory entropy", and we look for the distribution of p which maximizes S subject to the constraints

$$\int_{m_c}^{\omega} p(m)\, dm = 1 \tag{4}$$

$$\int_{m_c}^{\omega} mp(m)\, dm = \langle m \rangle \tag{5}$$

$$\int_{m_c}^{\omega} M_0(m)p(m)\, dm = \langle M_0 \rangle. \tag{6}$$

$\langle m \rangle$ and $\langle M_0 \rangle$, respectively, the average magnitude and moment per event in the range (m_c, ω), are the two pieces of information we have about the system. $\langle m \rangle$ is evaluated simply from the earthquake catalog once m_c is specified, and $\langle M_0 \rangle$ may be inferred from a catalog of moments where this is available, from geological or geophysical evidence of long-term fault movement or from current plate tectonic models. Note that $\langle M_0 \rangle$ is proportional to the average release of seismic strain

energy via (1). The quantity normally accessible is $\dot{M}_0$ – the rate of release of seismic moment, but this is related quite simply to $\langle M_0 \rangle$ by $\langle M_0 \rangle = \dot{M}_0/N_T$ where N_T is the total number of events in the catalog above m_c per unit time. In regions where the deformation is more diffuse, $\dot{M}_0$ may be inferred from the geodetically determined strain rate $\dot{\epsilon}$ by

$$\dot{M}_0 = 2.5\mu V\dot{\epsilon} \tag{7}$$

if V is the crustal volume (Papastamatiou, 1980).

The method of Lagrangian undetermined multipliers applied to (3), (4), (5), (6) gives

$$p(m) = \exp\{-\lambda_1 m - \lambda_2 M_0(m)\}/Z \tag{8}$$

where Z is the normalizing integral

$$Z = \int_{m_c}^{\omega} \exp\{-\lambda_1 m - \lambda_2 M_0(m)\}\, dm. \tag{9}$$

It is easy to show that

$$\begin{aligned} \langle m \rangle &= -d\{\ln(Z)\}/d\lambda_1 \\ \langle M_0 \rangle &= -d\{\ln(Z)\}/d\lambda_2. \end{aligned} \tag{10}$$

In principle, we could solve equations (10) and specify the distribution uniquely in terms of the three variables $\langle m \rangle$, $\langle M_0 \rangle$, and ω, once m_c has been chosen. Unfortunately this must be done numerically. The method applied in this paper involves an iteration procedure from starting values of λ_1 and λ_2, using a third order finite-difference formula due to Gill and Miller (1972) to evaluate the complicated integrals $\langle m \rangle$ and $\langle M_0 \rangle$.

The cumulative form of the probability distribution is defined by

$$P(x \geqq m) = \int_m^{\omega} p(x)\, dx = N(x \geqq m)/N_T \tag{11}$$

if N is the cumulative frequency distribution. The number density $n(m) = -dN(x \geqq m)/dm$ is then given by

$$n(m)\, dm = C \exp\{-\lambda_1 m - \lambda_2 M_0(m)\}\, dm \tag{12}$$

where $C = N_T/Z$, and $M_0(m)$ is given by (2).

It will be noted that $\langle m \rangle$, $\langle M_0 \rangle$, Z, and N_T will depend on the range chosen (m_c, ω), but are most sensitively dependent on m_c. For the purpose of the present type of work, this will not matter if: (a) the form of the distribution is self-similar at the lower magnitudes, i.e., the term in λ_1 dominates at low magnitudes and is reasonably constant independent of the choice of m_c, and (b), proper normalization is carried out. It is obvious that (a) can only be effected by considering a range of events where we are sure the catalog is complete.

A Physical Model from Statistical Mechanics

In order to interpret (12), we now consider a physical model of a fault and apply the methods of statistical mechanics to its localized elements. These elements may be as small as the lattice constant of the predominant crystal or may be related to inhomogeneities such as joints or bedding planes. In the following, we assume that the elements A_0 are small enough to warrant a continuous approach.

Consider an arbitrary area $A = l^2$ which ruptures during an event on the fault plane A_{max} (Figure 1). Assuming a constant strain drop (so that the model is self similar), we may take the fault movement $s \propto l$, so that

$$M_0 \propto l^3 \text{ from (1).}$$

If an energy level E is characterized by the symbol r and can be filled in g ways,

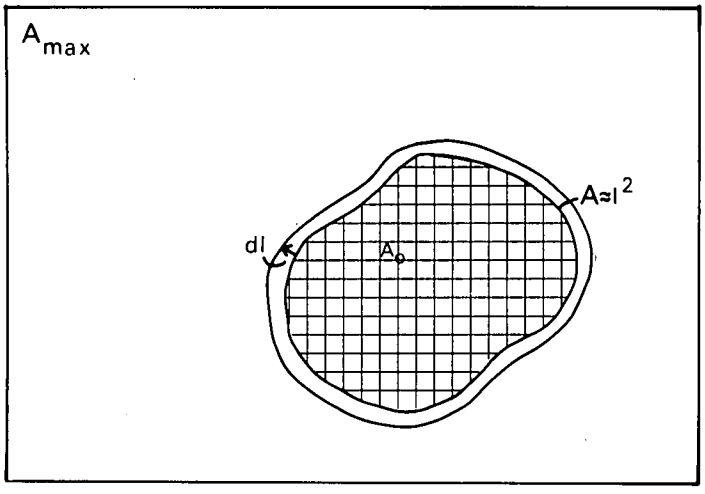

FIG. 1. *A geometric fault model.* The area A can fit into A_{max} in A_{max}/A ways. A_0 represents the physical lower limit to seismic energy release and depends on the spacing of inhomogeneities in the earth. The density of degenerate states if A_0 is assumed to be very small is $D(l)\,dl = \{A_{max}/l^2\} - \{A_{max}/(l + dl)^2\} = 2A_{max}/l^3\,dl$.

then the discrete frequency F of state transition is given by

$$F_r = g_r \exp\{-\beta'(E_r - E_{r'})\}. \tag{13}$$

$\Delta W = (E_r - E_{r'})$ is the change in strain energy which is proportional to M_0 via (1), and β' depends on the average energy $\langle E \rangle$. The degeneracy g is given by a simple geometric constraint on $M_0(l)$. On a planar fault, we take $g(l) = A_{max}/A(l)$ so that for the continuous case, the density $D(l)$ of degenerate states is given by

$$D(l)\,dl = g(l) - g(l + dl) = (2A_{max}/l^3)\,dl \tag{14}$$

after binomial expansion and ignoring terms in dl^2 and higher. The continuous number density $n(l)$ is then given by

$$n(l)\,dl = D(l)\,dl \exp(-\beta M_0(l)) \tag{15}$$

where $\beta M_0 = \beta' \Delta W$ from (1).

Remembering $M_0 \propto l^3$ and incorporating (2) gives

$$n(m)\, dm = \text{const}\ 10^{-bm} e^{-\beta M_0(m)}\, dm \tag{16}$$

with $b = (\frac{2}{3})B$ [see the Appendix for a general derivation of b for $D(l) \propto l^{-\nu}$]. This is identical in form to (12) if $\lambda_1 = b \ln(10)$, $\lambda_2 = \beta$. Since $B = 1.5$, b should be close to unity. If moment is the relevant parameter

$$n(M_0)\, dM_0 = \text{const}\ M_0^{-5/3} e^{-\beta M_0}\, dM_0 \tag{17}$$

where the geometric term $M_0^{-5/3}$ follows from (14) with $M_0 \propto l^3$. The form of this distribution can then be interpreted as a Boltzmann distribution of energy transitions via $\exp(-\beta M_0)$, multiplied by a geometric factor $M_0^{-5/3}$ which results in another exponential if magnitude is the relevant parameter.

A Note on Fractal Dimension

It is interesting to note that data on Californian fault breaks indicate that $D(l) \propto l^{-\nu}$ with $\nu = 2.5$ rather than 3 given previously in (14) (Caputo, 1982). This would imply $b = [(\nu - 1)/3] \times B$ is 0.75, in good agreement with theoretical models developed by Petrov (1981), where $b = 0.75$ results from random statistical fluctuations in microcrack density and Vere-Jones (1976) where $b = 0.75$ results from a critical branching model. The noninteger ν implies by analogy with the normal concept of density, a density distribution of fault lengths which has a *fractal* (i.e., noninteger) dimension (of 1.5 in this case). The fractal dimension of the fault geometry may be modeled by: (a) irregularities along the main fault break or (b) scattered smaller replicas of the original fault (see Mandelbrot, 1977). Caputo's (1982) value for ν only accounts for (b), which may explain why the b value predicted from ν underestimates the empirical value for b of 0.87 (Epstein and Lomnitz, 1966) and 0.86 (this paper).

Comparison with Other Models

Normally, in seismicity statistics, there are insufficient data to observe the contribution of the term in $M_0(m)$ in (12) or (16)—the direct result of incorporating a finite rate of release of strain energy. The most common frequency distribution used has therefore been the Gutenberg-Richter frequency law

$$n(m)\, dm = a\ 10^{-bm}\, dm. \tag{18}$$

This law can be applied as an open distribution in the range (m_c, ∞) (Richter, 1958) or in truncated form in (m_c, ω) (Cosentino *et al.*, 1977). The truncated form is preferable because it leads to finite rates of strain energy release, but the open-ended form often serves as a useful approximation. Figure 2 shows this distribution compared with some of the other truncated distributions mentioned in this section.

By comparison, the effect of the term $\exp\{-\lambda_2 M_0(m)\}$ is to progressively reduce n as ω is approached. Roll-off can also be seen in a physical model by Caputo (1976), which considers the effects of variable stress drop as well as source dimension, and which also includes, directly, an explicit value for the finite release of strain energy as an *a priori* assumption. This model has the form

$$n(m)\, dm = \{a\ 10^{-bm} - c\}\, dm \tag{19}$$

where c is 0 below m_2 and a finite positive constant, $a10^{-b\omega}$, in the range (m_2, ω). The differences between the distributions are only significant just below ω, so in many cases are not yet reliably observable because of the rare occurrence of the large events and the short time coverage of present earthquake catalogs. Perhaps the most important point to note is that inclusion of the long-term information leads us to expect *fewer* events at the largest magnitudes than an extrapolation of (18) would suggest. Additional information, such as the predominance of aftershock sequences (Båth, 1981) may alter this conclusion.

Statistical analyses which preferentially investigate the higher magnitudes by extreme value methods (Gumbel, 1958) generally show curvature similar to that indicated just below ω (Yegulalp and Kuo, 1974; Burton, 1979). The form of this

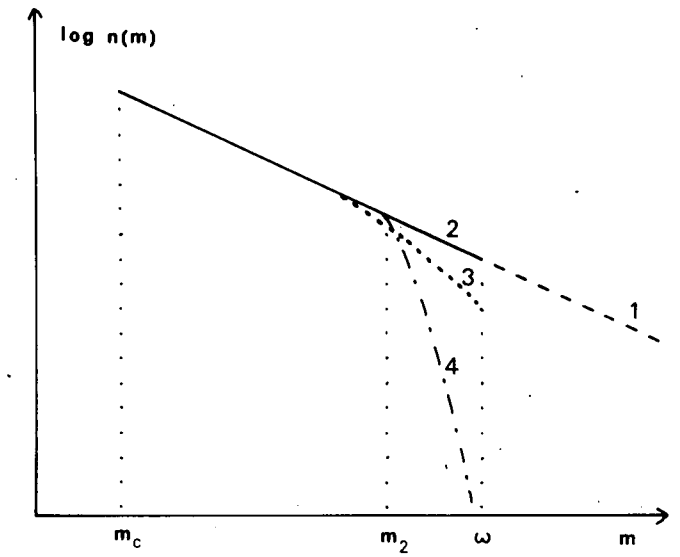

FIG. 2. *Comparison between seismicity models.* The models shown, in increasing order of complexity are: (1) the Gutenberg-Richter law; (2) a truncated form of (1), due to Cosentino *et al.* (1977); (3) the information theory model; and (4) Caputo's model. Model (3) tends simply to (2) if the parameter λ_2 in equation (12) is zero. Caputo's version differs from (3) in having (a) a sudden departure from log-linearity at m_2 rather than more gradually, and (b) an asymptotic limit ω at $n(\omega) = 0$ rather than at finite n. This allows the strain to build up to infinity since $n(m)\, dm = 0$ corresponds to infinite repeat times. Model (3) is, therefore, more compatible with a cyclical input and release of strain energy, since it does not allow such a build up.

curvature is related to the type III Weibull cumulative frequency distribution

$$NIII(x \geqq m) = \{(\omega - m)/(\omega - u)\}^{1/\lambda} \tag{20}$$

(Jenkinson, 1955). As λ approaches 0, this form reduces to that of (18) (a type *I* distribution). The difference is that type *I* is unlimited but type *III* has an upper bound to m. Main and Burton (1981, 1983) have applied this form to the forward problem of predicting crustal deformation rates from available catalogs in such diverse regions as California, the Eastern United States, the United Kingdom, and the Mediterranean. Where there is adequate control on the relation (2) the agreement with the observed deformation is good. The extreme value equivalent to (20) also gives inferred moment rates consistent with available data. This form is especially useful for areas where the data set is severely incomplete.

Equations (19) and (20) both tend continuously to $n(\omega) = 0$, which allows infinite repeat times of the largest events and so is seen as a drawback (see legend to Figure 2 and Main and Burton, 1983).

RESULTS

Example (1): The central Mediterranean. The deformation around the Mediterranean is composed mainly of continental collision and arcuate subduction, and may involve a significant amount of aseismic creep processes such as folding and continuous fault movement (North, 1974). The region encompasses many diverse tectonic features which currently defy complete explanation within the framework of classical plate tectonics. However, it does serve as a good example of the application of earthquake statistics to an arbitrary area with sufficient numbers of events for statistical rigor. A seismicity map is given in Figure 3.

The histograms of Figure 4 show that the catalog used (Burton, 1978) is complete for the time range analyzed (1943, 1971) above magnitude 4.5, so we choose this value of m_c. We can infer this from the roughly constant number of events per year in the range (4.6, 5.5), despite the introduction of the WWSSN network in 1963, which has such a marked effect on the range (3.6, 4.5). The dramatic rise in the number of events in (4.6, 5.5) just before a large event (M_S 7.8) in 1953 is interesting, but is not investigated in further detail here. The frequency $F(m) = \int_{m-\delta m/2}^{m+\delta m/2} n(m)\, dm$, for $\delta m = 0.1$ and equation (12) is plotted in Figure 5, with the solid line being determined by numerical solution of equations (10), the parameters of which are summarized in Table 1. North's (1977) Tables 4 and 1, respectively, indicate $\dot{M}_0 = 2.4 \times 10^{26}$ dyne-cm yr^{-1} for the time period 1943 to 1971 and 4.5×10^{26} dyne-cm yr^{-1} for the more completely analyzed period 1963 to 1970. These may be regarded as minimum values, so the value 8×10^{26} dyne-cm yr^{-1} is a reasonable one. There is some scatter about the theoretical line, but this is of the same order as instrumental errors in measuring magnitude (±0.3 units typically). Some compensation for this has already been incorporated into Figure 5 by averaging the frequency data over neighboring ranges. This smoothing also serves to correct for spurious empty magnitude intervals and serves as a normalizing agent at the highest currently available magnitudes where the data shown on Figures 5 to 7 become effectively discrete. The smoothed discrete data points are then described by $F_2(i) = \sum_{j=i-1}^{i+1} F_1(j)/3$ where $F_1(j)$ represents the original unsmoothed data. Note that $F = F(M_w)$ is the theoretical line and $F_2(M_S)$ is shown for comparison purposes only.

By comparison, the dotted line representing the truncated Gutenberg-Richter law overestimates the occurrence of the largest magnitudes. The departure point from this line indicates that Caputo's m_2 parameter is around 7.0 for this region. The Weibull frequency distribution of Figure 6 is not such a good fit for the intermediate magnitudes, but is similar for the largest ones which dominate the moment release.

A summary of the results are presented in Table 1. $A = 16.0$, $B = 1.5$ are found to be appropriate values for the Mediterranean (North, 1974; Figure 2). The same figure indicates that the highest magnitudes do not suffer from instrumental saturation so the M_S and M_w scales can be regarded as equivalent within their uncertainties. The time period (1943, 1971) and magnitude range (4.6, 7.8) are also common to all of the entries. The parameter $b = \lambda_1/\ln(10)$ is quoted here because it is more commonly used in seismology. The uncertainty in the empirically inferred values for $\dot{M}_0$ results from the covariance errors in (ω, u, λ) as do those of Table 2, which compares estimates of average repeat time. The covariance error matrix as

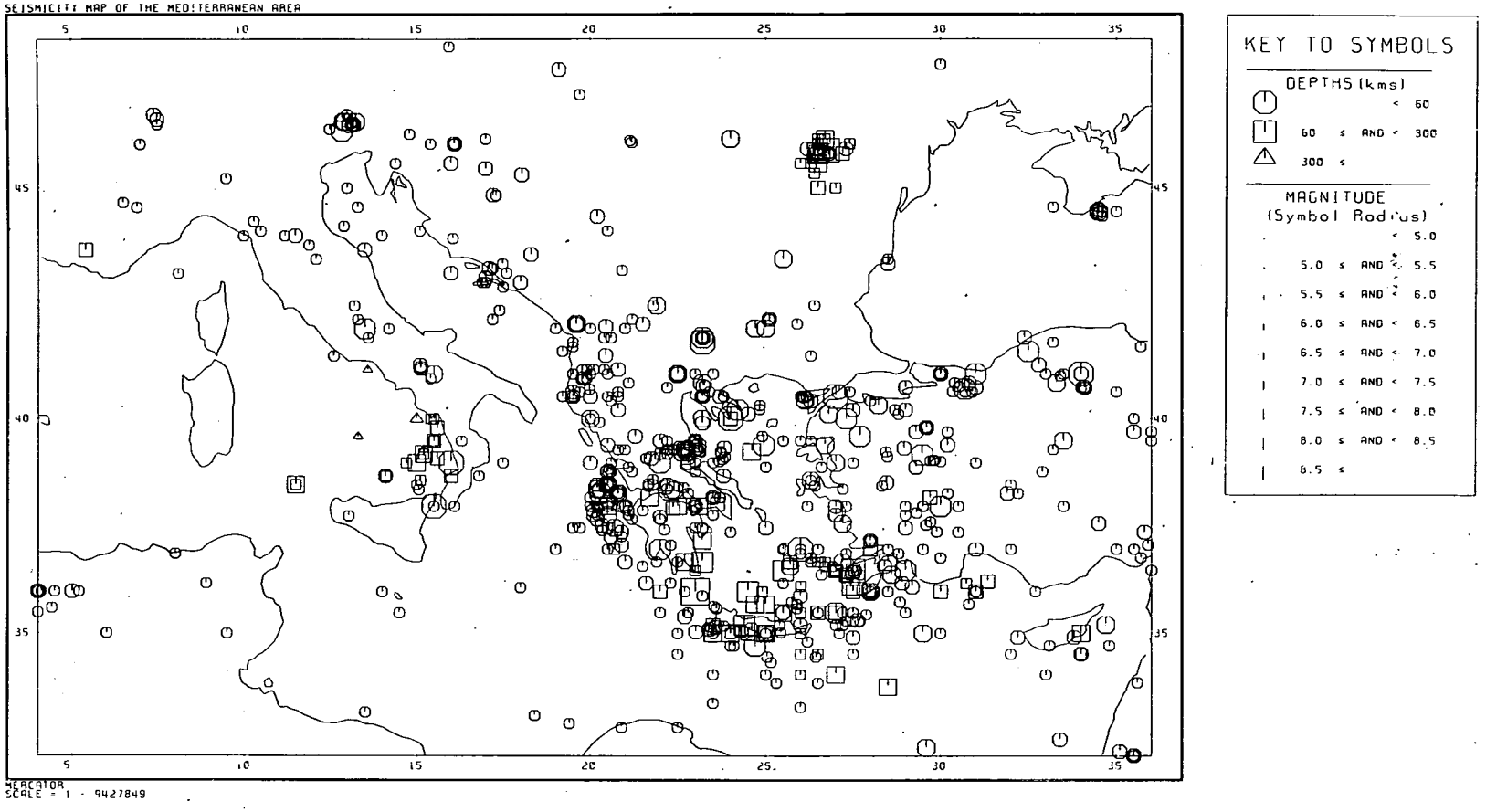

FIG. 3. *Seismicity map of the Central Mediterranean area.* All events of $M_S \geqq 5.0$ are included. Smaller events are too numerous to be plotted economically, but are easily accessible for frequency analysis.

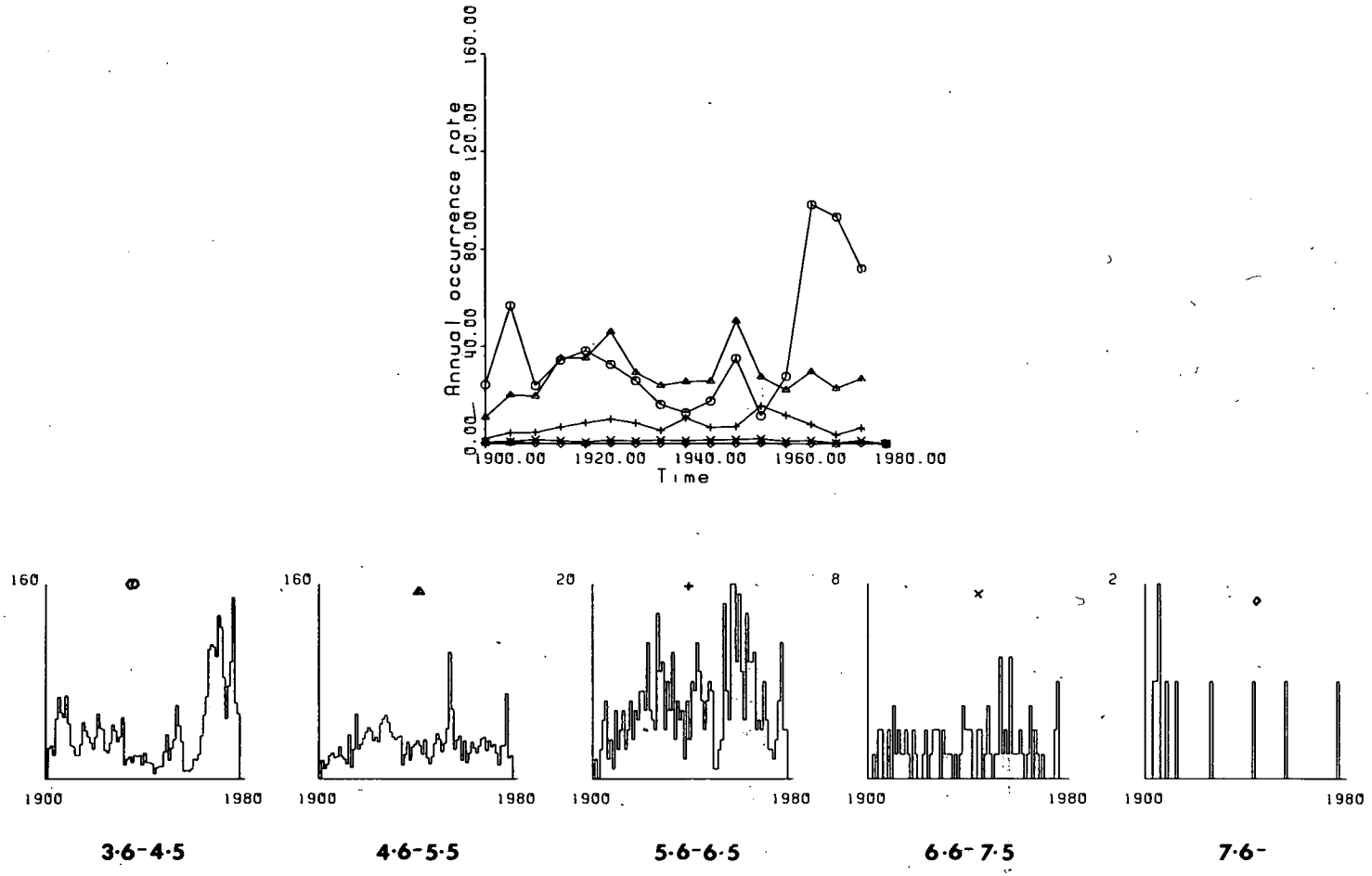

FIG. 4. *Completeness histograms for the earthquake catalog.* The symbols correspond with the magnitude ranges as indicated.

described in Burton (1979) for Figure 6 is

$$\begin{Bmatrix} \sigma_\omega^2 & \sigma_{\omega u}^2 & \sigma_{\omega\lambda}^2 \\ \sigma_{u\omega}^2 & \sigma_u^2 & \sigma_{u\lambda}^2 \\ \sigma_{\lambda\omega}^2 & \sigma_{\lambda u}^2 & \sigma_\lambda^2 \end{Bmatrix} = \begin{Bmatrix} 0.855 & -0.031 & -0.119 \\ -0.031 & 0.018 & 0.008 \\ -0.119 & 0.008 & 0.018 \end{Bmatrix}_{NIII}.$$

In comparing the models, we have already found that the truncated Gutenberg-Richter law overestimates the occurrence of the highest magnitudes. The type *III* cumulative frequency distribution is an improvement in that it is consistent with the curvature observed on log-linear graphs at the highest magnitudes. However

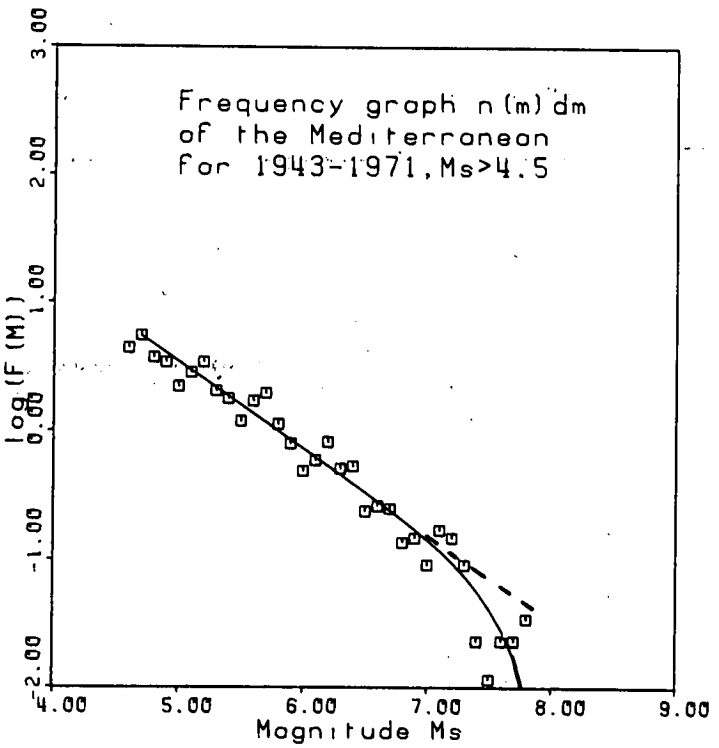

FIG. 5. *The frequency distribution of events in the central Mediterranean.* Comparison of $F_2(i) = \sum_{j=1}^{i+1} F_1(j)/3$ with the information theory prediction from the input values of Table 1. The solid line is the information theory prediction, which falls *below* the extrapolation of the dotted straight line segment corresponding to the truncated Gutenberg-Richter law. Although the data points shown are all M_S, these are regarded as being equivalent within measuring errors to M_w used to produce the theoretical line.

there is some evidence of autocorrelation error in Figure 6, in that the distribution of data points around the theoretical line is not random. There is a tendency for data points in the middle range of magnitudes to fall *below* the best-fitting line. However, because the fit is good at high magnitudes, the moment predictions from (ω, u, λ) (obtained by the method described in Main and Burton, 1981) turn out to be reasonable considering their error.

The information theory distribution has no such apparent autocorrelation error in the low and medium magnitude range, and for this reason is considered to be an improvement on the type III distributions. However, for the high magnitudes, the

TABLE 1

SUMMARY OF RESULTS FOR THE CENTRAL MEDITERRANEAN

Figure	Method	Model	Distribution	Input	Results
5	Information theory	Average of magnitude and short-term moment release	This paper Equation (12)	$\langle m \rangle = 5.216 \pm 0.017$ $\dot{M}_0 = 8 \times 10^{26}$ dyne-cm yr^{-1} $N_T = 41.0$ yr^{-1}	$b = 0.666$ $\lambda_2 = 3.29 \times 10^{-28}$ (dyne-cm)$^{-1}$
6	Cumulative frequency with upper bound to magnitude	Whole process of earthquake magnitude catalog	Jenkinson (1955) Equation (20)	Cumulative frequency data from catalog	$(\omega, u, \lambda) = (8.2, 6.8, 0.2)$ $\dot{M}_0 = \left(8 + \frac{11}{5}\right) \times 10^{26}$ dyne-cm yr^{-1}

fit to the data and the consistency of appropriate seismic moment release rates indicate that both methods can model this range successfully. The advantage here of the information theory distribution is that it models the occurrence in a way which is directly consistent with available knowledge of the highest magnitudes via the extra information represented by $\dot{M}_0$.

Example (2): Southern California. In the first example, we checked for self-consistency of the method with contemporary data and compared the information theory distribution with some commonly used empirical methods. In this section, we test the primary objective of this paper—the direct incorporation of crustal deformation via the terms $\dot{M}_0$ and N_T with a view to extrapolating beyond historical

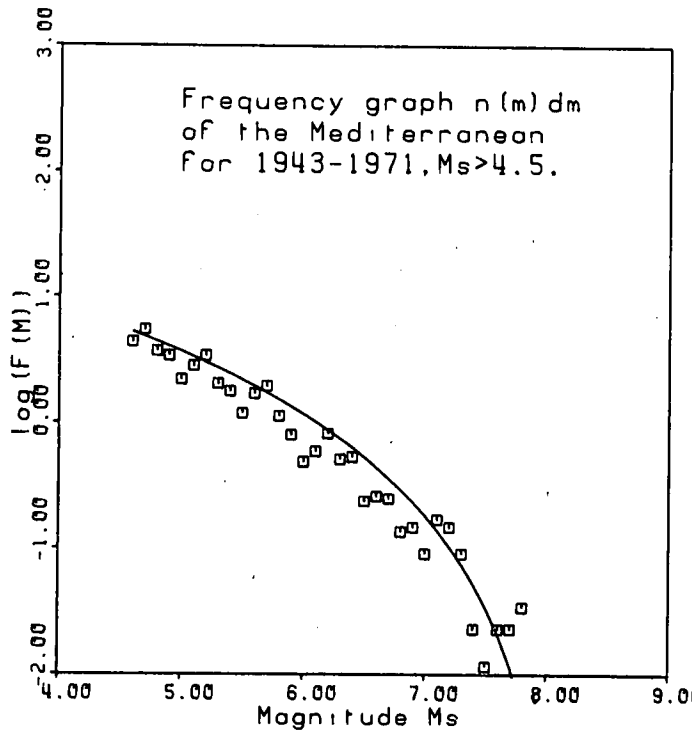

FIG. 6. *Empirical frequency fit.* The type III form of equation (20) is fitted to the data by computer algorithm. The line fits high and low magnitudes well, and predicts a reasonable value for $\dot{M}_0$ [by the method developed in Main and Burton (1981)] but overestimates the occurrence of the intermediate events.

and instrumental time scales. Previously, this has been done indirectly by comparing moment predictions from extrapolation of line fits to contemporary data with quaternary evidence of fault movement. Examples are Anderson (1979) for the (linear) truncated Gutenberg-Richter law, and Main and Burton (1981, 1983) for the more general (curved) type III Weibull frequency distribution and its extreme value equivalent.

The catalog used is that of Hileman *et al.* (1973) which covers the period 1932 to 1972 inclusive. Their magnitudes are taken to be M_S or equivalent M_w, although most of the entries are M_L. The only event which might possibly be subject to saturation effects is the 1952 Kern County event, but this is not found to be the case (Main and Burton, 1983). The area has, however, been subject to occasional

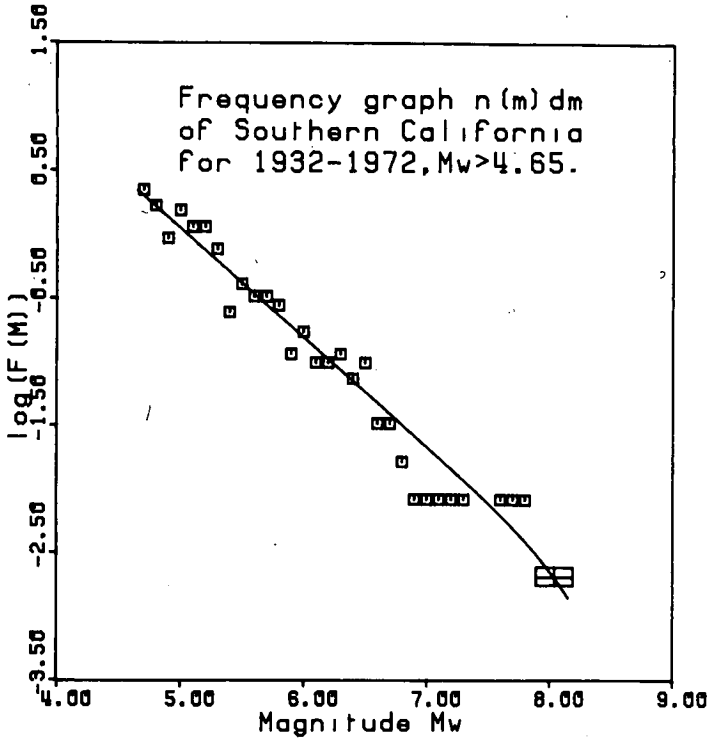

FIG. 7. *Frequency data from Californian instrumental records and Sieh's geologically estimated occurrence time of the largest events, compared with the information theory prediction.* Curvature due to λ_2 is small but significant and leads to a good match at the box representing Sieh's results. The box represents a seismic moment magnitude obtained from Sieh's results, and the catalog data (M_S or M_L) is regarded as equivalent to M_w within their measuring errors. The good fit of the theoretical line (expressed as M_w) with the magnitude data seems to bear this assumption out.

TABLE 2

MAGNITUDES M_T CORRESPONDING TO AVERAGE REPEAT TIME T YEARS FOR THE CENTRAL MEDITERRANEAN USING: (A) INFORMATION THEORY (5) AND (B) CUMULATIVE FREQUENCY (6)

Figure: 5*		6*	
T (yr)	M_T	M_T	(σM_T)†
1.0	6.75	6.80	(0.138)
2.0	7.00	7.03	(0.137)
5.0	7.25	7.27	(0.165)
10.0	7.45	7.42	(0.208)
20.0	7.55	7.55	(0.262)
50.0	7.65	7.68	(0.339)
100.0	7.80	7.84	(0.456)

* $T = 1/N(M \geqq M_T)$.

† Uncertainties follow from the covariance matrix on errors in (ω, u, λ).

major shocks, the last being in 1857 along the currently locked aseismic portion of the San Andreas fault. Sieh (1978) has shown that shocks of this order of magnitude repeat on average every $T = 163 \pm 27$ yr, where the uncertainty is a standard error in the mean. The repeat time has varied from 50 to 275 yr for the eight events regarded as proven without reasonable doubt.

Sieh estimates the size of this event as $M_S > 8.25$, by comparison of macroseismic effects with those for the instrumentally recorded 1906 San Francisco earthquake. Sing and Havskov (1980) find that $A = 15.83$, $B = 1.5$ is most appropriate for southern California, and Anderson (1979) gives M_0 for the 1857 event as 9×10^{27} dyne-cm from the extent of the surface break and fault movement. These two data imply that $M_w = 8.1$, showing that the $M_0 - M_w$ relation cannot account for the relatively high M_S value of the 1906 event.

Further, if we assume an average movement rate at the 1857 fault break of 3.2 cm yr^{-1} and let $s = \dot{s}t$ in (1), then we find $M_w = 8.05 \pm 0.15$ from (2) for appropriate values of t from Sieh's table of recurrence times. The movement rate is consistent within ± 0.5 cm yr^{-1} with: (a) the creep rate over 4 yr in central California – 3.2 cm yr^{-1} (Lisowski and Prescott, 1981); (b) $4\frac{1}{2}$ m of slip repeated every 163 yr for approximately 2000 yrs – 2.8 cm yr^{-1} (Sieh, 1978); and (c) geologically estimated movement rates on the San Andreas fault – 3.7 cm yr^{-1} (Anderson, 1979, Table 1). This good agreement over different time scales also lends support to the stationary

TABLE 3

MAGNITUDES M_T CORRESPONDING TO AVERAGE REPEAT TIMES T FOR THE INFORMATION THEORY DISTRIBUTION IN SOUTHERN CALIFORNIA

T (yr)	M_T*
1	5.85
2	6.20
5	6.65
10	6.95
20	7.25
50	7.60
100	7.80
200	7.95

* $T = 1/N(M \geqq M_T)$.

hypothesis. A higher value for the relative plate motion across the San Andreas transform of 5.5 cm yr^{-1} indicates that a significant amount of movement occurs in a broad deformation zone around the main fault. The calculated value of M_w results from locally appropriate values of A (15.83) and B (1.5), $\mu \approx 3 \times 10^{11}$ dyne-cm^{-2}, length $L \approx 400$ km (Sieh, 1978) and depth 15 km (Anderson, 1979).

Figure 7 shows the information theory line compared with the catalog and quaternary geological data discussed above. The appropriate parameters are $(m_c, \omega) = (4.7, 8.2)$, $\dot{M}_0 = 16.1 \times 10^{27}$ dyne-cm yr^{-1} (for a fault zone 150 km longer than Anderson's (1979) area of study where $\dot{M}_0 = 12.0 \times 10^{25}$ dyne-cm yr^{-1} and $\dot{s} = 5.5$ cm yr^{-1} from plate models). The average magnitude and standard error in this range is found to be $\langle m \rangle = 5.157 \pm 0.021$, with $N_T = 11.15$ yr^{-1}. These imply $b = 0.856$ and $\lambda_2 = 3.0 \times 10^{-29}$ dyne^{-1} cm^{-1} and seem to compare well with the data. The effect of increasing ω progressively is negligible on b even to three figures, but λ_2 increases to 6.0, 7.6, 7.8×10^{-29} for $\omega = 8.4$, 8.6, 8.8, respectively. These solutions all pass through the error confines around this point, but $\omega = 8.2$ gives the best fit. Finally, the average repeat times from the information theory distribution are quoted in Table 3.

The main conclusion from this section is that the information theory distribution can successfully model the extrapolation of current seismicity statistics in the light of quaternary geological data.

Discussion and Conclusions

The method of statistical inference known as information theory can be applied to earthquake statistics in the range (m_c, ω) if the average magnitude $\langle m \rangle$, the seismic moment release rate $\dot{M}_0$, and the number of events per unit time N_T are known. The form of the distribution thus obtained can be interpreted as a Boltzmann distribution of energy transitions multiplied by a geometric term which dominates the high frequencies of occurrence at the lower magnitudes. The geometric term corresponds to the commonly used Gutenberg-Richter law, and the Boltzmann term to the roll-off below this line which is often observed in nature.

The distribution has been tested in a region which has a reasonably complete set of contemporary unsaturated magnitude and seismic moment data, and fits well considering the instrumental errors involved. It also compares favorably with other commonly used distributions in that it accurately reflects the behavior over the entire magnitude range. The method is a general one, and could conceivably be extended to include premonitory effects from earthquake prediction studies. For example Von Seggern (1980) noted that isolated stress measurements along a fault are unreliable for earthquake prediction because of the large random component involved. The *average* stress (or strain) measured on a broader scale over the whole fault may yield information on the increased probability of occurrence of the largest magnitudes as the strain builds up.

For the moment, however, the method does give some hope of extrapolating frequencies of occurrence beyond the instrumental and historical era by including long-term geological movement rates where they are available through the term $\dot{M}_0$. Thus, we might be slightly more confident of estimating design criteria for buildings or communications systems whose life times are expected to be longer than the time scale of the available catalog.

Acknowledgments

This work was supported by the Natural Environmental Research Council and is published with the approval of the Director of the British Geological Survey (NERC).

References

Ambraseys, N. N. (1971). Value of historical records of earthquakes, *Nature* **232**, 375–379.

Anderson, J. G. (1979). Estimating the seismicity from geological structure for seismic risk studies, *Bull. Seism. Soc. Am.* **69**, 135–158.

Båth, M. (1981). Earthquake recurrence of a particular type, *Pure Appl. Geophys.* **119**, 1065–1076.

Berrill, J. B. and R. O. Davis (1980). Maximum entropy and the magnitude distribution, *Bull. Seism. Soc. Am.* **70**, 1823–1831.

Burton, P. W. (1978). The IGS file of seismic activity and its use for hazard assessment, *Inst. Geol. Sci., Seism. Bull.* no. 6, HMSO.

Burton, P. W. (1979). Seismic risk in southern Europe through to India examined using Gumbel's third distribution of extreme values, *Geophys. J. R. Astr. Soc.* **59**, 249–280.

Burton, P. W., I. G. Main, and R. E. Long (1983). Perceptible earthquakes in the eastern United States (examined using Gumbels third distribution of extreme values), *Bull. Seism. Soc. Am.* **73**, 497–518.

Caputo, M. (1976). Model and observed seismicity represented in a two dimensional space, *Ann. Geophys.* **4**, 277–288.

Caputo, M. (1982). On the reddening of the spectra of earthquake parameters, *Earthquake Predict. Res.* **1**, 173–181.

Cosentino, P., V. Ficarra, and D. Luzio (1977). Truncated exponential frequency-magnitude relationship in earthquake statistics, *Bull. Seism. Soc. Am.* **67**, 1615–1623.

Epstein, B. and C. Lomnitz (1966). A model for the occurrence of large earthquakes. *Nature* **211**, 854–856.

Gill, P. E. and G. F. Miller (1972). An algorithm for the integration of unequally spaced data, *Comp. J.* **15**, 80–83.

Gumbel, E. T. (1958). *Statistics of Extremes*, Columbia University Press, New York.

Hileman, J. A., C. R. Allen, and J. M. Nordquist (1973). *Seismicity of the Southern California Region 1932–1972*, Contribution 2385, Div. of Geological and Planetary Sciences, California Institute of Technology, Pasadena, California.

Howell, B. F. (1981). On the saturation of earthquake magnitudes, *Bull. Seism. Soc. Am.* **71**, 1401–1422.

Jaynes, E. T. (1957). Information theory and statistical mechanics, *Phys. Rev.* **106**, 620–630.

Jenkinson, A. F. (1955). The frequency distribution of annual maximum (or minimum) values for meterological elements, *Q. J. Roy. Meteor. Soc.* **87**, 158–171.

Kanamori, H. (1978). Quantification of earthquakes, *Nature* **271**, 411–414.

Kanamori, H. and D. L. Anderson (1975). Theoretical basis of some empirical relations in seismology, *Bull. Seism. Soc. Am.* **65**, 1073–1095.

Lisowski, M. and W. H. Prescott (1981). Short-range distance measurements along the San Andreas fault system in Central California, 1975 to 1979, *Bull. Seism. Soc. Am.* **71**, 1607–1624.

Main, I. G. and P. W. Burton (1981). Rates of crustal deformation inferred from seismic moment and Gumbel's third distribution of extreme values, in *Proc. Conference on Earthquakes and Earthquake Engineering: The Eastern U.S.*, J. Beavers, Editor, Ann Arbor Science Ltd., Ann Arbor, Michigan, **II**, 937–951.

Main, I. G. and P. W. Burton (1983). Physical links between crustal deformation, seismic moment and seismic hazard for regions of varying seismicity, British Geological Survey GSU Report No. 199, *Geophys. J. Roy. Astr. Soc.* (in press).

Mandelbrot, B. B. (1977). *Fractals: Form Chance and Dimension*, W. H. Freeman, San Francisco, California.

North, R. G. (1974). Seismic slip rates in the Mediterranean and the Middle East, *Nature* **252**, 560–563.

North, R. G. (1977). Seismic moment, source dimensions and stresses associated with earthquakes in the Middle East, *Geophys. J. R. Astr. Soc.* **48**, 137–161.

Papastamatiou, D. (1980). Incorporation of crustal deformation into seismic hazard analysis. *Bull. Seism. Soc. Am.* **70**, 1321–1335.

Petrov, V. A. (1981). Theory of the law of earthquake recurrence, *Izvestia Earth Physics* **17**, 623–625.

Richter, C. F. (1958). *Elementary Seismology*, W. H. Freeman, San Francisco, California.

Rubincam, D. G. (1982). Information theory lateral density for earth inferred from global gravity field, *J. Geophys. Res.* **87**, 5541–5552.

Sieh, K. E. (1978). Prehistoric large earthquakes produced by slip on the San Andreas fault at Pallet Creek, California, *J. Geophys. Res.* **83**, 3907–3939.

Sing, S. K. and J. Havskov (1980). On moment-magnitude scale, *Bull. Seism. Soc. Am.* **70**, 379–383.

Vere-Jones, D. (1976). A branching model for crack propagation, *Pure Appl. Geophys.* **114**, 711–725.

Von Seggern, D. (1980). A random stress model for seismicity statistics and earthquake-prediction, *Geophys. Res. Letters* **7**, 637–640.

Yegulalp, T. M. and J. T. Kuo (1974). Statistical prediction of the occurrence of maximum magnitude earthquakes, *Bull. Seism. Soc. Am.* **64**, 393–411.

NATURAL ENVIRONMENT RESEARCH COUNCIL
BRITISH GEOLOGICAL SURVEY
MURCHISON HOUSE
WEST MAINS ROAD
EDINBURGH EH9 3LA,
SCOTLAND (I.G.M., P.W.B.)

UNIVERSITY OF EDINBURGH
DEPARTMENT OF GEOPHYSICS
JAMES CLERK MAXWELL BUILDING
MAYFIELD ROAD
EDINBURGH EH9 3JZ,
SCOTLAND (I.G.M.)

Manuscript received 19 August 1983

APPENDIX: THE RELATIONSHIP BETWEEN ν, B, AND b

We have

$$M_0 = e^{\alpha+\beta m}; \quad dM_0 = \beta M_0\, dm \tag{A1}$$

$$M_0 \propto l^3; \quad dM_0 \propto 3l^2\, dl \tag{A2}$$

$$D(l) \propto l^{-\nu}. \tag{A3}$$

From (A2) we first convert the variable in (A3) from l to $M_0(l)$

$$D(M_0)\, dM_0 = D(l)\, dl$$
$$\propto M_0^{-(\nu+2)/3}\, dM_0 \tag{A4}$$

and then to $m(M_0)$ via (A1)

$$D(m)\, dm = D(M_0)\, dM_0$$
$$\propto \exp\left\{(\propto + \beta m)\left(\frac{1-\nu}{3}\right)\right\} dm. \tag{A5}$$

If we define

$$D(m) \propto 10^{-bm}, \tag{A6}$$

then

$$b = \left(\frac{\nu - 1}{3}\right) \beta/\ln 10 \tag{A7}$$

or

$$b = \left(\frac{\nu - 1}{3}\right) B. \tag{A8}$$

Since $B = \beta/\ln 10$, $A = \propto/\ln 10$ by comparing (2) with (A1).